U.PORTO

FEUP FACULDADE DE ENGENHARIA
UNIVERSIDADE DO PORTO

ANALYSIS OF REINFORCED CONCRETE FRAMES EXPOSED TO FIRE

Based on Advanced Calculation Methods

HÉLDER FRANCISCO BRÁS XAVIER

Dissertation submitted in partial fulfilment of the requirements for the degree of

MASTER IN CIVIL ENGINEERING — STRUCTURAL ENGINEERING BRANCH

Scientific Supervisor:

Associate Professor Doctor Rui Manuel Carvalho Marques de Faria

JULY, 2009

MASTERS IN CIVIL ENGINEERING 2008/2009

DEPARTMENT OF CIVIL ENGINEERING

Tel. +351-22-508 1901

Fax +351-22-508 1446

✉ miec@fe.up.pt

Edited by

FACULTY OF ENGINEERING OF THE UNIVERSITY OF PORTO

Rua Dr. Roberto Frias

4200-465 PORTO

Portugal

Tel. +351-22-508 1400

Fax +351-22-508 1440

✉ feup@fe.up.pt

http://www.fe.up.pt

"… Por mares nunca dantes navegados…"
in Os Lusíadas, I-1

ACKNOWLEDGEMENTS

First of all, I am compelled to express my deepest gratitude towards my scientific supervisor, Professor Rui Faria from the University of Porto, for the invaluable guidance, encouragement and dedication displayed during the course of this work.

I am also extremely grateful to Professor Paulo Vila Real and Professor Nuno Lopes from the University of Aveiro, for kindly providing the access to the software SAFIR as well as for guiding me during the first steps in its application.

A gratitude remark has to be made, regarding my fellow structural engineer João Barbosa, Ph.D. student at the University of Porto, for his relevant role played during the initial stages of this work, especially concerning computer programming aspects.

To structural engineer Márcio Fernandes, MEng, author of the spreadsheet for the application of simplified calculation methods, I have to express my gratitude for the help he has provided, enabling his spreadsheet to deal with the files obtained from SAFIR, thus easing the task of comparing advanced and simplified calculation methods results.

At last, I shall not forget to direct a kind word to my senior grade colleagues at the Masters in Civil Engineering, for the constant support and friendship demonstrated along this last semester, always improving my work through their reviews and recommendations. Among all, the following names ought to be underlined: structural engineer Albano de Castro e Sousa, structural engineer Bruno Vieira and building engineer Bruno Duarte.

ABSTRACT

The structural stability of reinforced concrete buildings exposed to fire is gaining a significant role in the design process, as users and authorities are increasingly demanding for fire safety solutions.

The application of advanced calculation methods constitutes the most accurate numerical procedure to trace the global behaviour of a reinforced concrete structure during the course of the fire, until collapse is achieved. In this work, a reinforced concrete frame subjected to different fire scenarios is investigated applying a Finite Element Code capable of simulating both materials strength deterioration due to temperature and fire induced effects.

It is known that the application of advanced calculation methods demands a great deal of expertise, usually not part of structural engineers training. For this reason, fire safety assessment is often performed by means of simplified cross-sectional calculation methods based in single element verifications, where in accordance to the current version of Eurocode 2, it is possible to neglect fire induced effects.

In this work, a comparison between the results obtained with advanced calculation methods and the application of simplified methods, indicates that applying the last methods ignoring the increase of internal forces may lead to non-conservative results.

A simplified procedure for shear failure assessment of reinforced concrete elements at elevated temperatures is proposed. Applying this procedure it is pointed out that shear may become a critical factor in the frame's columns fire resistance, due to the imposed beams thermal elongation.

The inclusion of short-columns in reinforced concrete frames originates high risk situations related to shear and bending failure during fire exposure.

KEYWORDS: Reinforced concrete, structural fire engineering, advanced calculation method, global behaviour, thermal elongation effects, shear failure at elevated temperatures.

RESUMO

A estabilidade de edifícios de betão armado em situação de incêndio tem ganho um papel de relevo no projecto estrutural, pois os seus ocupantes e as autoridades têm exigido cada vez mais soluções que garantam uma adequada resistência ao fogo.

A aplicação de métodos de cálculo avançados constitui a ferramenta numérica mais rigorosa para avaliar o comportamento global de estruturas de betão armado ao longo da duração de um incêndio, até que o colapso ocorra. Neste trabalho, um pórtico de betão armado exposto a diferente casos de incêndio será investigado através da aplicação de um programa baseado no Método dos Elementos Finitos, capaz de simular a degradação das propriedades dos materiais em função da temperatura, bem como de incluir os esforços induzidos pelo incêndio.

Como é reconhecido, a aplicação de métodos de cálculo avançados exige por parte dos engenheiros de estruturas um conjunto de conhecimentos específicos que geralmente não faz parte da sua formação. Devido a isto, a verificação da resistência ao fogo é em regra avaliada através de métodos de cálculo simplificados, baseada na análise de elementos estruturais isolados para os quais a actual versão do Eurocódigo 2 permite que se desprezem os esforços induzidos pelo fogo.

Neste trabalho foi feita uma comparação entre a resistência ao fogo avaliada considerando o comportamento global da estrutura e a resistência dada pelos métodos simplificados, demonstrando-se que aplicando os últimos métodos e desprezando os esforços induzidos pelo fogo se é por vezes conduzido a verificações não conservativas.

Um método simplificado para verificação da resistência ao corte de elementos de betão armado a elevadas temperaturas é proposto neste trabalho. Aplicando este método constata-se que a resistência ao corte pode ser condicionante na resistência ao fogo dos pilares do pórtico, devido aos esforços induzidos pela dilatação térmica das vigas.

Neste trabalho também se constatou que a existência de pilares-curtos na tipologia da estrutura origina situações de alto risco, relacionadas com roturas por corte e também por flexão destes elementos em situação de incêndio.

PALAVRAS-CHAVE: Betão armado, cálculo estrutural em situação de incêndio, método de cálculo avançado ao fogo, comportamento global, efeitos da dilatação térmica, rotura por corte a altas temperaturas.

CONTENTS

3. Analysis of Reinforced Concrete Frames Exposed to Fire: Part1 – Global Response Compared to Simplified Methods

LIST OF FIGURES

Chapter 1

Chapter 2

Chapter 3

LIST OF TABLES

Chapter 2

Chapter 3

Chapter 4

LIST OF ABBREVIATIONS

FSE – Fire Safety Engineering

SFE – Structural Fire Engineering

NIST – National Institute of Standards and Technology (USA)

WTC – World Trade Centre, twin towers, New York

ATM – Anderberg & Thelandersson Model (concrete model at elevated temperatures)

LITS – Load Induced Thermal Strain

EN 1990 – Eurocode 0

EN 1991 1-2 - Eurocode 1 Part 1-2

EN 1992 1-1 - Eurocode 2 Part 1-1

EN 1992 1-2 – Eurocode 2 Part 1-2

EN 1993 1-2 – Eurocode 3 Part 1-2

EN 1994 1-2 – Eurocode 4 Part 1-2

1
Introduction

1.1. BACKGROUND TO THE THESIS

1.1.1. FOREWORD NOTE

Ever since its earliest applications, reinforced concrete has been used as the main construction material worldwide. From bridges and arch dams to tunnels and skyscrapers, it has allowed mankind to shape the face of the earth, especially because, among all the other construction materials, reinforced concrete outstands for its strength, durability and cost-effectiveness. Besides that, the application of this material enables the construction of irregular and complicated shapes, either in the form of cast-in-situ or pre-cast concrete, making it the appropriate structural constituent for modern buildings, increasingly moving towards aesthetics concerns and integration with the surrounding built environment requirements.

The analysis and design of reinforced concrete stands in more than one century of gained experience, with respect to gravity loads, wind, snow and seismic actions. In this way, the current codes of practice and standards are able to provide structural engineers with the tools for the design of concrete elements regarding the above mentioned loads and considering a performance-based approach, meaning that the loads which concrete elements are expected to withstand depend on the assessment severity level, and are related to the degree of damage acceptable to the limit state in analysis. In other words, the structural design is based on probability risk analysis to evaluate loads and actions at different severity levels.

In spite of this, a different scenario has been observed in the evolution of codes and standards concerned with the behaviour of concrete elements exposed to fire. Although fire represents one of the most severe environmental conditions to which buildings may be subjected in their lifetime, the global safety of reinforced concrete structures with regards to fire scenarios has always been neglected or taken for granted.

Traditionally, fire safety assessment of reinforced concrete has been based on a prescriptive single element analysis, neglecting statically redundancies and restraints to thermal expansions. For a long time, this approach was considered conservative mainly due to the fact that, in one hand, concrete members exhibit a good performance in fire conditions when compared with other constituent materials, and in the other hand, concrete material presents by itself a low thermal diffusivity (slowing down the temperature rise during fire exposure) and a considerable non-combustible property. Nevertheless, even if a structure is labelled as safe when exposed to fire within the scope of these prescriptive rules, structural engineers are not able to assess the real level of fire safety, because the real global structural response is unknown. This is perhaps the reason why the National Institute of Standards and Technology (NIST) report shows that, since 1970, a considerable number of fire induced collapses among conventional buildings belongs to reinforced concrete structures [1].

Recent large scale experiments, such as the ones in Cardington [2], and real events like the Windsor tower's fire in Madrid [3] (see Figure 1.1) and the World Trade Centre (WTC) collapse in New York [1] have shown the real impact of structural continuity in the global response of buildings subjected to fire hazard. Since then a lot of work has been carried out to understand the global fire response, especially of steel and composite structures. For reinforced concrete structures the global behaviour is not yet fully understood, mainly because of the lack of reliable data concerning material's properties at high temperatures. Even so, codes of practice and standards, such the Eurocode 2 Part 1-2 (EN1992-1-2) [4], have drawn the first steps in the pursuit of a comprehensive model that allows structural engineers to assess the real level of buildings' fire safety.

Before listing the objectives of this work and outlining the thesis chapters, an introductory note on structural fire engineering and on concrete behaviour when exposed to fire is presented, to provide the reader with a concise insight about the main features of this branch of structural engineering.

1.1.2. STRUCTURAL FIRE ENGINEERING

1.1.2.1 General overview

Structural fire engineering (SFE) can be considered as a constituent of a general multi-discipline approach to determine safety for buildings subjected to fire, in which structural stability is achieved by providing fire protection (active and/or passive) [2]. This multi-discipline approach is usually referred to as Fire Safety Engineering (FSE). Although there are several definitions to FSE, it can be acceptably defined as " (...)*the application of scientific and engineering principles to the effects of fire in order to reduce the loss of life and damage to property by quantifying the risks and hazards involved and provide an optimal solution to the application of preventive and protective measures (...)"*[5]. Further detailed information about FSE can be found in references [6], [7] and [8].

a) b)

Fig.1.1. – The Windsor Tower's fire, Madrid (2005): a) full developed fire, b) post-fire damaged structure [2].

Considering the above statements, SFE is the branch of engineering concerned with the design and analysis of structures when exposed to fire hazard. Its main goal is to ensure that *the building shall be designed and constructed so that, in the event of a fire, its stability will be maintained for a reasonable period* [9]. In other words, it deals with the analysis of thermal effects of fire on buildings, defining the necessities of specific passive fire protection and structural detail, in order to ensure that the structure presents the required load bearing resistance when subjected to fire.

1.1.2.2 Methods of assessment of fire resistance

There are several methods for assessing the fire resistance of reinforced concrete structures, ranging different levels of complexity and accuracy. The main procedures available are [10]:

1. Standard fire tests;
2. Tabulated data;
3. Simplified calculation methods;
4. Advanced calculation methods;
5. Full-scale fire tests.

Standard fire testing constitutes one of the most expensive assessment procedures, tending to be less used in our days. It is mainly applied to single structural elements, measuring fire resistance as the period of time until the element no more fulfils the function for which it was design (structural or other functions, such as integrity and insulation). When the structural resistance is assessed, failure criteria are usually defined as lack of load-bearing capacity, level of deformation and also rate of deformation [11]. The results of these tests are very limited because it is very difficult to properly reproduce in a furnace the real structural restraint and continuity, and to simulate the realistic load level, meaning that the actual characteristics of the structural system are not accounted for. This is why these tests are not capable of predicting the actual element's behaviour when integrated in the real structure [12]. Even so, fire testing presents some advantages, such as the ability to emphasize construction detailing weaknesses that are poorly assessed with numerical models [13]. Other advantage of fire testing resides in the fact that the concept of fire resistance, associated to standard fire testing, is easily understood by structural engineers and approval authorities worldwide, providing an indication of relative products performance and fire assessment against common criteria [11] [14].

Tabulated data methods are directly attached to a prescriptive approach of fire resistance assessment. Basically, these methods specify minimum geometric sizes of cross-sections and reinforcement cover that ensure fire resistance to standard fire up to some predetermined time of exposure [11]. Although highly conservative, these methods are used for structural engineers because they are very easy to apply, especially in regular building design. Conversely, application of tabulated data constitutes a severe obstacle to innovative engineering and architectural solutions. Tabulated data methods can be found in several codes of practice and standards such as the EN1992-1-2. The latter code of practice refers in its section 5 that tabulated data was developed on an empirical basis confirmed by experience and theoretical evaluation of tests, derived from approximate conservative assumptions for the more common structural elements [4]. Further reading on this method can be found in reference [15].

Simplified calculation methods may be applied within a prescriptive or performance-base approach, depending on the type of design fire chosen to undertake the analysis. In the scope of EN1992-1-2, simplified methods may be used on the analysis of a single structural element or of a part of a structure. When applied to member analysis, simplified methods are able to assess the element resistance in every time-steps based on: i) a reduction of the concrete cross-section affected by fire and accounting for the remaining cross-section considered with its mechanical properties at ambient temperature, or ii) attributing reduced strength properties to the affected cross-section zones as well as ignoring the contribution of fire damage concrete layers. Simplified methods have presented so far a significant accuracy for current structural elements such as beams and columns, when compared against advanced computer methods, as stated by the exhaustive numerical analyses performed in references [15] and [16]. A numerical implementation of the EN1992-1-2's simplified methods is documented in [17].

Advanced calculation methods in SFE are those where a time-dependent thermal and mechanical analysis is performed to assess the resistance of the whole structure, parts of the structure or simple structural elements. Because these methods are within the scope of this work, a detailed analysis of their formulation will be presented in the following chapters.

Full-scale fire testes are rare in SFE, as they are highly time consuming, complex and very expensive [14]. Notwithstanding that, these fire tests have been performed for several times, namely in the United Kingdom. Between 1995 and 1997, in the BRE test facilities at Cardington, Bedford, a set of full scale tests were performed upon a group of composite structures made of steelwork frames and concrete slabs [18]. The main purpose of these experiments was to trace the global behaviour of the whole structure, emphasizing the effects of restraints and continuity. The tests involved four major experiments, carried out on different parts of the multi-storey structure to study various features of the structural response [18]. In the year 2001, at the same facilities, a full-scale test was carried out upon a cast-in-situ reinforced concrete seven-storey building. During this test an equipment malfunction led to the loss of some important data. However, the surviving results and observations of the post-fire damaged structure contributed to the acknowledgment of both beneficial and detrimental behaviour of the building as a whole [19]. Figure 1.2 illustrates a partial view of the reinforced concrete building tested in Cardington.

Fig.1.2. – The reinforced concrete framed building after the fire tests in Cardington. It is possible to observe the drift in the lower columns imposed by the thermal expansions of the floors (note the black arrows) [19].

More recently, in 2006, three full-scale tests were undertaken on a cast-in-situ concrete building located in Dalmarnock, Glasgow [20]. These experiments provided a complete data set for the structural behaviour and response during the heating and cooling phases of the fire [20].

A noteworthy relationship between full-scale tests and advanced calculation methods has to be mentioned. This relationship relies on the fact that before the application of a numerical tool in fire

resistance assessment, structural engineers must verify its accuracy against full-scale test results [14], considering that until now, most numerical tools available to the application of advanced methods have just been validated against small-scale fire tests (single elements inside furnaces, not accounting for structural induced effects, as mentioned above). So, if engineers are willing to implement advanced methods capable of predicting the global behaviour of concrete structures, there is the need for more full-scale tests in order to assemble useful data related to real structures subjected to fire, focusing on special features such as the thermal restraint induced actions, connections' behaviour and other phenomena originated by the global structural response. Only after this, advanced calculation methods may be used with a high degree of confidence.

Nowadays calculation methods of structural fire safety assessment (especially advanced methods) are gaining an important role within both academic and practicing engineering, because they present the highest correlation between accuracy and labour effort. In other words, with the application of fire calculation methods it is possible to predict the whole structural response without the cost of full-scale tests. At the same time, the often misleading and simplified results of small tests are avoided.

When applying calculation methods, there is one first choice to be made related to level of the analysis accuracy. The possible alternatives are prescriptive and performance-based approaches. The former one considers nominal fires to generate thermal actions, while the latter, using FSE principles, refers to thermal actions based on physical and chemical parameters [4]. Nowadays the prescriptive approach, which represents a non realistic fire, is increasingly being turned apart by the performance-based approach. This one is able to simulate a real compartment fire, thus providing structural engineers with a reliable model of the fire that structures are expected to withstand. This is an important issue, because there are several advantages when considering real fire scenarios than nominal ones, such as:

- More efficient and cost-effective designs, maintaining acceptable standards of fire safety.
- More innovative architectural and structural solutions that would not be approved in the scope of the prescriptive approach.
- Better understanding of the actual fire behaviour, allowing the identification of structural weaknesses and the real amount of fire protection needed.

It is also noteworthy an attitude change in approval authorities towards SFE (especially after WTC's collapse in New York), with specific requests of quantified and justified global structural response during fire hazard, even if the structural design fulfils the prescriptive code requirements [21]. Of course this is only achievable applying a performance-based analysis.

Anyway, it is imperative that a correct match between the fire model and the structural complexity is accounted for. An inappropriate level of complexity and accuracy is often the source of erroneous and misleading results. This subject is further developed in the following sections.

As a concluding remark to this sub-section, the alternative structural fire design procedures of reinforced concrete referred in the EN1992-1-2 are schematically depicted in Figure 1.3.

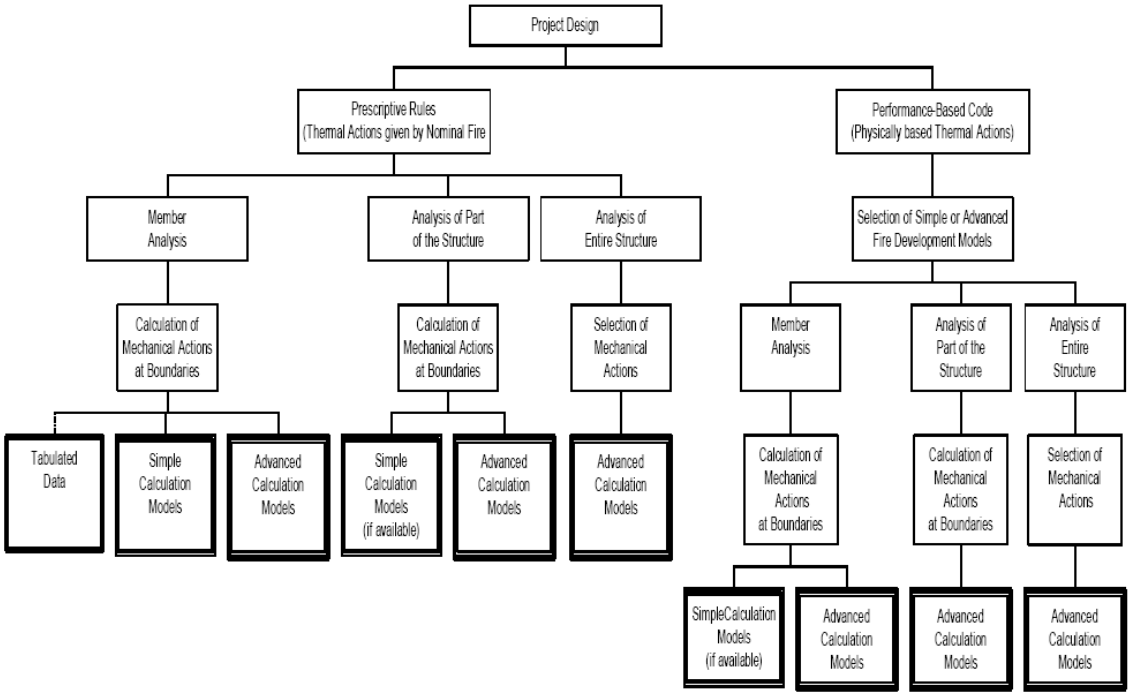

Fig.1.3. – Alternative design procedures, EN 1992-1-2 [4].

It is important to refer that, according to EN 1992-1-2: a) member analysis considers it as isolated from the rest of the structure, and indirect fire actions are not considered, except those resulting from thermal gradients; b) analysis of parts of the structure considers indirect fire actions within the sub-assembly, but no time-dependent interaction with other parts of structure is accounted for; c) global structural analysis involves the entire structure, and indirect fire actions are considered throughout the structure [4].

1.1.2.3 Mechanical actions in fire situation

The design value of actions effects in case of fire should be obtained regarding the accidental design situations prescribed in the Eurocode 0 (EN 1990) [22]:

$$\sum_{j\geq 1} \gamma_{GAj} G_{kj} + \gamma_{PA} P_K + \gamma_A A_k + \psi_{x,1} Q_{k,1} + \sum_{i>1} \psi_{2,i} Q_{k,i} \tag{1.1}$$

where γ_{GA} , γ_A , γ_{PA} = 1, $\psi_{x,1}$ is either $\psi_{1,1}$ or $\psi_{2,1}$ depending on the national annex of each country, G_{kj} is the characteristic value of permanent actions, $Q_{k,1}$ is the characteristic value of the main variable action, $Q_{k,i}$ is the characteristic value of a secondary variable action, P_K is the value representing the effect of pre-stress and A_k is the value of the accidental action, which in case of fire represents the effects of indirect actions due to internal or external restraint to fire induced deformations.

Accordingly to the EN 1992-1-2 it shall be verified for the relevant duration of fire exposure [4]:

$$E_{fi,d} \leq R_{fi,d} \tag{1.2}$$

where $E_{fi,d}$ is the design effect of actions obtained with combination 1.1 and $R_{,fi,d}$ is the corresponding design resistance in the fire situation.

In some cases the EN 1992 1-2 admits the possibility of neglecting the fire induced actions, meaning that the term A_k in combination 1.1 may be disregarded. When this happens, the value of $E_{fi,d}$ may be obtained as the value given by combination 1.1 at ambient temperatures and kept constant along the analysis or by means of the following simplified procedure:

$$E_{fi,d} = \eta_{fi} E_d \tag{1.3}$$

where E_d is the action design value at ambient conditions and η_{fi} is reduction factor given in [4]. In Figure 1.4 a schematic representation of the above procedures to evaluate the fire resistance is plotted.. In Figure 1.4 E_d and R_d refer to the action and resistance values at ambient conditions respectively, and $t_{fi,d}$ is the time requested to failure be achieved, i.e., the fire resistance.

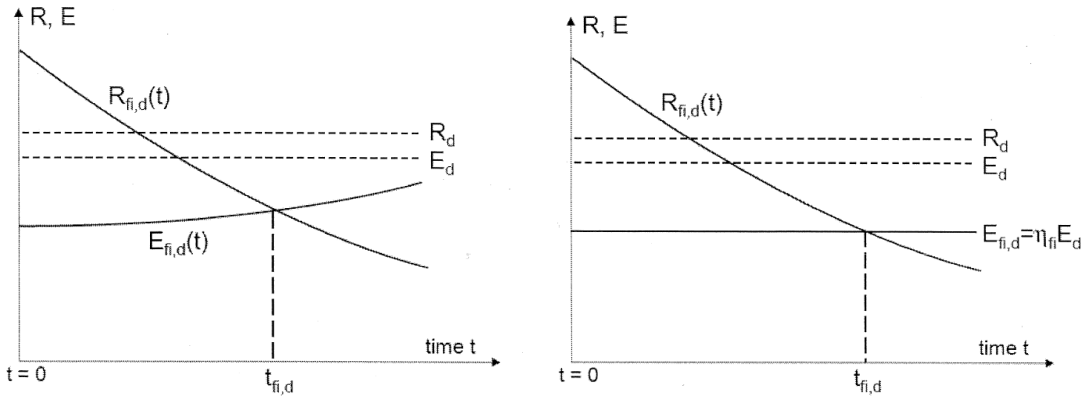

Fig.1.4. – Evaluation of fire resistance according to the EN 1992 1-2: a) considering fire induced effects, b) neglecting fire induced effects [23].

1.1.2.4 Thermal actions for temperature analysis

According to the Eurocode 1 Part 1-2 (EN 1991 1-2) thermal actions in case of fire are given by the net heat flux h_{net} (W/m^2) to the exposed surface of the member [24]. The net heat flux should be determined considering heat transfer by convection and radiation as follows:

$$h_{net} = h_{net,c} + h_{net,r} \tag{1.4}$$

where $h_{net,c}$ is the heat flux by convection and $h_{net,r}$ is the heat flux by radiation given by equations 1.5 and 1.6, respectively.

$$h_{net,c} = \alpha_c (\theta_g - \theta_m) \tag{1.5}$$

where α_c is the coefficient of heat transfer by convection, θ_g (ºC) is the gas temperature in the vicinity of the fire exposed member and θ_m (ºC) is the temperature at the surface of the exposed member.

$$h_{net,r} = \phi \varepsilon_m \varepsilon_f \sigma \left[(\theta_r + 273)^4 - (\theta_m + 273)^4 \right] \tag{1.6}$$

where ϕ is the configuration factor, ε_m is the surface emissivity of the member, ε_f is the emissivity of the fire, σ is the Stephan-Boltzmann constant ($5.67.10^{-8}$ W/m^2K^4), θ_r is the effective radiation temperature of the fire environment (ºC) and θ_m is the temperature of the member's surface (ºC).

In the case of fully fire engulfed members, the radiation temperature θ_r may be represented by the gas temperature θ_g around that member [24]. The gas temperature θ_g may be given by a nominal time-temperature curve or by a natural fire model.

1.1.3. EFFECTS OF FIRE IN REINFORCED CONCRETE STRUCTURES

Fire action in concrete structures can be regarded as a thermal action imposing temperature gradients throughout the structural elements. These temperature gradients have two main consequences upon structural behaviour: on one hand they promote thermal expansions, which in the case of restrained structures may lead to formation of important restraining forces able to cause an anticipated collapse, and on the other hand the temperature has a deteriorating influence in concrete and reinforcement properties, meaning that the higher the temperature is reached the higher is the material load-bearing capacity reduction.

1.1.3.1 Deterioration of the mechanical properties of concrete and steel

The concrete and steel material behaviour when exposed to elevated temperatures is of unquestionable importance to the understanding of the structural fire performance [13].

Concrete does not have a homogeneous composition, being considered a composite and multi-phase material made from the mix of cement paste, water, a combination of fine and coarse aggregates, and in some cases adjuvant products. Each of these components presents different responses of their own to thermal exposures, resulting in a complex reaction of the whole composite system when subjected to fire actions. This is why modelling and predicting concrete behaviour at high temperatures represents a very difficult task [12]. Furthermore, it can be said that concrete performance under fire is mainly controlled by the cement past and the aggregates [25]. When subjected to high temperatures, concrete undergoes on a complex process of physical and chemical transformations. Some of these changes are reversible and others non-reversible upon cooling, meaning that concrete properties shall not remain the same after fire [12].

Deterioration in mechanical properties during fire hazard is mainly attributed to [13]:

- Physicochemical changes in the cement paste;
- Physicochemical changes in the aggregates;
- Thermal incompatibility between aggregates and cement paste.

Furthermore, the properties deterioration is also influenced by [13]:

- Temperature level and heating rate;
- Externally applied loads;
- Sealed or unsealed conditions of concrete, affecting moisture loss from the surface.

Sealed and unsealed concretes present different responses to the hydrothermal reactions, because while the dominant process in unsealed ones is related to the loss of various forms of water (free, chemically bound, adsorbed), in sealed concrete there is a predominance of hydrothermal chemical reactions [13].

An important feature related to cement past is the Calcium oxide – Silicon oxide (C/S) ratio. Low C/S ratio results in low calcium hydroxide content, ensuring a more beneficial hydrothermal reaction, because this component dissociates at about 400ºC into CaO and CO2. Besides that, during cooling CaO rehydrates expansively contributing to the deterioration and exposure of the moisture [13].

As far as the aggregate is concerned, a low thermal expansion improves thermal compatibility with the cement paste, and at the same time a rough angular surface contributes to a higher physical bound with the same paste [13].

Recent experimental studies indicate that strength reduction due to high temperatures is more pronounced in high-strength (HSC) and ultra-high-strength (UHSC) than in normal strength concretes (NSC) [26].

The effect of fire on steel is characterized by a significant loss both in stiffness and in strength. Because of this, an important feature related to the resistance of reinforced concrete structures subjected to fire, is the presence of a sufficient concrete layer providing cover to the reinforcement, in order to slow down the heating process in the steel rebar. When the temperature in reinforcement reaches 700ºC, its load-bearing capacity may be reduced to 20% of the ambient conditions value [3].

1.1.3.2 Spalling

Spalling is the foremost complex phenomenon that occurs when concrete is exposed to rapid temperature rising, such as in a fire scenario, and there is not yet a generally accepted physical and comprehensive model capable of describing it [27]. This phenomenon is often assumed to occur only at very high temperatures, but it has already been noticed in the early stages of a fire and at temperatures as low as 200ºC [12], and even during cooling stages.

Spalling can be concisely characterized as the breaking off of layers and pieces of concrete from the element surface when exposed to fire. The damage extension due to spalling ranges from insignificant surface pitting, to extensive removal of concrete pieces [28]. Figure 1.5 illustrates two cases where the occurrence of spalling lead to a considerable amount of concrete damage. In that figure it is possible to witness the level of reinforcement exposure induced by concrete spalling.

When this phenomenon occurs with some degree of severity it may lead to a significant strength reduction of the reinforced concrete element. The loss of important pieces of concrete due to spalling will promote a reduction of the element cross-section, meaning that the same member forces will be supported by smaller area of concrete [12]. Other deteriorative effect of spalling appears when reinforcing steel bars became directly exposed to fire due to the removal of the concrete layers covering them. This contributes to an increasingly reduction of the element load-bearing capacity because, as above mentioned, steel presents a high temperature sensitive strength loss.

a) b)

Fig.1.5. – Examples of severe spalling: a) spalling on the heated surface of reinforced concrete slab [19]; b) spalling on reinforced concrete column [29]..

Until now, several types of spalling have been noticed: explosive spalling, surface spalling, aggregate splitting, corner separation, sloughing off and post cooling spalling [28]. The most aggressive type is considered to be explosive spalling, and it is generally accepted that it is related to pore pressure in consequence of physically/chemically bound water evaporation within concrete microstructure, and also to thermal dilatation in biaxial compressive stress parallel to the heated surface, leading tensile stresses to appear perpendicular to that surface [27]. This means that the hotter layers of concrete tend to expand, being restrained by the adjacent cooler ones and by the applied loads [28]. Further spalling related effects are stresses due to phase changes of some aggregates, and incompatibilities of strains between hardened cement paste and aggregates [27]. Generally explosive spalling occurs under combined action of pore pressure, compression in the fire exposed region (thermal and load induced stresses) and internal cracking [13]. Recent researches indicate that pore pressure increase within concrete during fire exposure is hardly the only cause of spalling [30] [31] .In Figure 1.6 are illustrated the forces acting near concrete exposed surface, which combined may trigger the occurrence of explosive spalling.

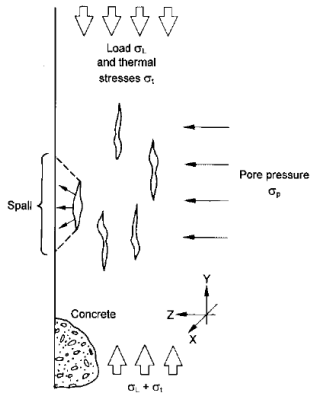

Fig.1.6. – Forces acting in heated concrete inducing explosive spalling [32].

It is important to highlight that to this day spalling prediction is not yet fully reliable, as it is possible that this phenomenon may be stochastic in its nature [26]. Nevertheless, investigations have shown that occurrence of spalling depends on the following factors, taking into account that most of these are inter-related [27] [28]:

- Moisture content: the higher the moisture content, the higher the probability of spalling;
- Permeability, water/cement ratio: lower w/c ratios produces denser concretes, then less permeable ones, increasing the probability of spalling;
- Heating conditions, rate of heating and temperature level: higher rates of heating and fire intensities tend to increase the thermal gradients through the concrete elements, and therefore to raise the risk of spalling;
- Mineral and petrographical composition of the aggregate: the siliceous aggregate concrete generally presents less spalling resistance than the calcareous one;
- Concrete strength: high strength concretes, usually less permeable, tends to be more susceptible to occurrence of spalling;
- Applied load/stress level: the higher the compressive stress applied to the element, the higher the probability of spalling;
- Thermal expansion/restraint: restraint to thermal expansions generates thermal stresses reducing spalling resistance; concretes with high thermal expansion tend to experience higher thermal stresses due to restraint, increasing the possibility of spalling;
- Section size and geometry: thicker elements present more resistance to spalling than thinner ones;
- Reinforcement/cover: the presence of reinforcement bars generally increase spalling resistance; because spalling is often restricted to the unreinforced part of the section, it is possible that higher cover depths increase the risk of spalling.

The importance of spalling increases when HSC and UHSC concretes are used. It is known that these concretes present higher compressive resistance than NSC at ambient temperatures, but they are considerable less porous and moisture absorbent [12]. During heating it is more difficult for water vapour to escape, increasing pressure within concrete microstructure. It is believed that this high pressure generated inside pores makes HSC and UHSC more susceptible to spalling occurrence. However, it has been observed in some experimental research that HSC and UHSC may not suffer for extended explosive spalling, because of their higher tensile strength, which can compensate the increased vapour pressure drawback [12].

Besides spalling, cracking may also be generated during fire. The process leading to cracking is assumed to be the same as in spalling [33]. The dehydration and thermal expansion of concrete may cause cracks to open, rather than explosive spalling. These cracks provide pathways for direct heating of reinforcement bars, and may increase the level of thermal stresses [12]. In some cases cracking development may extend through the element cross-section, providing pathways for fire to spread between adjacent compartments [12]. Recent observations have shown that cracks penetration depth is related to fire temperature, and that cracks generally develop far deep into the concrete element [33].

1.1.3.3 Failure of reinforced concrete structures in fire

Today is generally accepted that fire is capable of inducing collapses in reinforced concrete structures. As stated in [1], from 22 structural fire induced collapses, 7 refer to reinforced concrete, 6 to steel frames, 5 to masonry systems, 2 wood structures and 2 unknown materials[1] [34]. It is possible to learn from these reported collapses that the deterioration of materials strength due to high temperatures cannot be the only responsible for the structural failure. Thermal expansion had a significant influence

on the whole structural performance, as well as on thermal strains and stresses on the individual members [34].

In the end, the structural failure under fire hazard is a function of the loading arrangement, the heating history and the structure's characteristics, and may be categorized into [10]:

- Bending/tension failure;
- Buckling/compression failure;
- Anchorage/bond failure;
- Shear or torsional failure;
- Spalling failure.

Bending, tensile and compressive failures are currently well documented, and codes of practice and standards are providing reliable design guidelines related to these phenomena, while spalling is not yet fully covered for the reasons previously mentioned.

Bending failure is the most common type of failure in horizontal elements, such beams and one-way slabs (it is not so common in two-way slabs), while buckling/compression often represents the failure mode of vertical members (columns and walls) [10]. Anchorage failure occurs when the reinforcement is not capable of developing the needed bond stresses over the embedment length, resulting in a reinforcement pulling out of the concrete element [10]. Some authors consider that spalling is not actually a failure mode, but when it occurs may trigger one of the other 'actual' failure mechanisms [10].

An important failure mechanism of concrete structures, for which there is a lack in regulation and design guidance, is shear failure. This is a considerable drawback in concrete fire design, because real fire events have demonstrated that shear is often the cause of several structural failures [34] [23]. Figure 1.7 illustrates some examples of real structures that displayed shear failure during fire exposure. In 1974 a warehouse in the port of Ghent (Belgium) collapsed during a fire [23]. It was a 3 storey cast-in-situ reinforced concrete building designed to satisfy all prescriptive fire standards (minimum reinforcement cover, etc.). Nevertheless, after approximately 1h20min of fire exposure a part of the building started to collapse. The cause of collapse was found to be related to slabs and beams thermal expansion, promoting excessive drifts at the top of the columns, which then failed due to shear [23]. In 1996, a similar shear failure was observed in the city library of Linköping (Sweden) [35]. Although the building was rated as 60 minutes fire resistant, the excessive thermal expansion of slabs imposed a considerable drift in the critical columns, resulting in shear failure of these latter after 30 minutes of exposure [23] [35]. Another example of shear failure during fire exposure was found in the U.S. Military Personnel Records Centre building, where a thermal induced deformation imposed a drift of approximately 60cm at the top of the columns on the sixth floor, resulting in excessive shear stresses and subsequent failure [1] [34].

Another important feature, often not considered by structural engineers when assessing structural fire safety, is the behaviour of the reinforced concrete buildings during the decay (or cooling) phase of the fire. This subject is not sufficiently studied, especially in terms of material behaviour, but is possible that the contracting strains associated to structural restraint and loss of ductility due to temperature lowering may trigger the failure of the affected elements. This may explain why structural failures (mainly shear failures) have been noticed on buildings that had withstood the heating phase before collapsed during the cooling stage. In Figure 1.7 d) it is possible to witness a shear failure in a reinforced concrete column recorded during the fire decay phase.

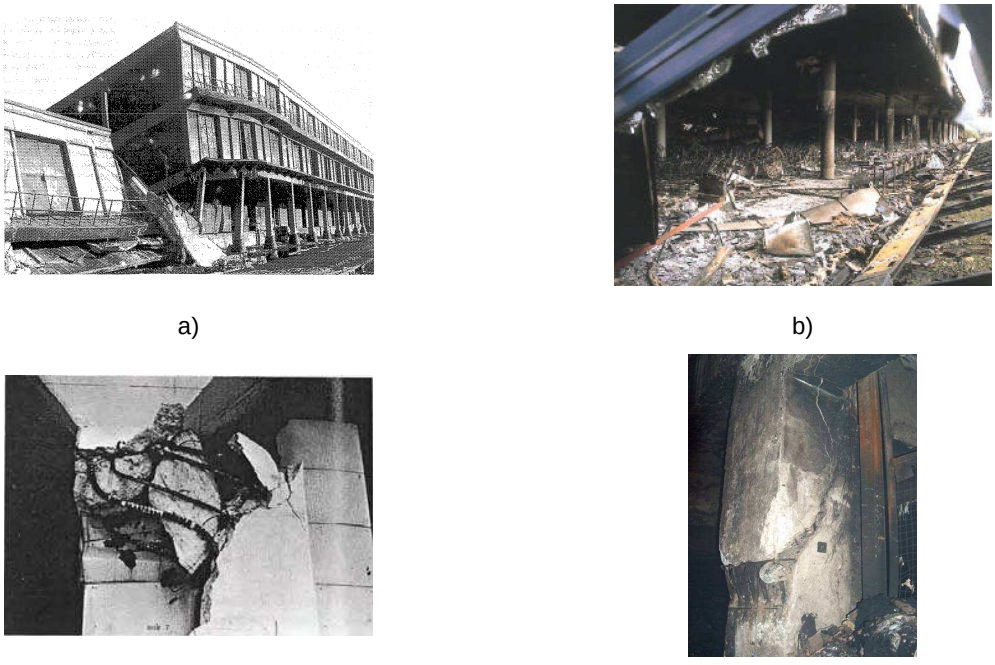

a) b)

c) d)

Fig.1.7. – Examples of structural collapses induced by shear failure due to thermal elongation: a) port of Ghent warehouse [23]]; b) library of Linköping [35]; c) U.S. Military Personnel Records Centre building [34] d) shear failure of a column during cooling [17].

1.2 OBJECTIVES OF THIS WORK

The objective of this work is to evaluate the global response of a 2-D reinforced concrete frame when exposed to fire, based in advanced calculation methods. With the results obtained, the following points are developed:

- Trace the evolution of internal stresses and deformations of the reinforced concrete frame, submitted to different fire scenarios, all of them based in the ISO 834 standard fire curve [36];
- Investigate if the fire assessment based in the EN 1992 1-2 simplified methods (neglecting fire induced actions) lead to non-conservative results compared against the global behaviour response (accounting for fire induced actions);
- Propose a simplified procedure for shear failure assessment of reinforced concrete elements at elevated temperatures, which using the results obtained with the advanced calculation method, indicates if neglecting shear effects may lead to non-conservative results.

1.3 OUTLINE OF THE THESIS CHAPTERS

Chapter 2

Literature Review

This chapter describes the main factors governing the application of advanced calculation methods in the analysis of reinforced concrete structures exposed to fire, as well as a review on their recent developments. The topics covered in this chapter are: i) the concept of advanced calculation method, ii) fire modelling, iii) concrete material models at elevated temperature, iv) steel material models at elevated temperature, v) incorporation of spalling in the calculation models and vi) global analysis of reinforced concrete structures exposed to fire.

Chapter 3

Analysis of Reinforced Concrete Frames Exposed to Fire: Part 1- Global Response Compared to Simplified Methods

This chapter begins with a brief description of the computer code applied to perform the global fire analysis: SAFIR. Next, the thermal and mechanical properties of concrete and steel admitted during the analyses performed are listed.

The first frame analysed in this chapter is the same already investigated by other author, referred in Chapter 2, in order to acknowledge the main features related to computer code hereafter used. After this, the main structure consisting of a three-bay frame, is investigated when exposed to a two simultaneous floor fire. The fire resistance obtained is compared to the resistance displayed by the simplified Zone Method prescribed in the EN 1992 1-2.

Chapter 4

Analysis of Reinforced Concrete Frames Exposed to Fire: Part2- Influence of different fire scenarios

Basically, this chapter follows on the previous one, but here the three-bay frame is subjected to several fire scenarios, in order to investigate the different evolution of internal stresses, deformations and times to failure.

Chapter 5

Simplified Procedure for Shear Failure Assessment at Elevated Temperatures

This chapter contains the proposal for a simplified shear failure assessment procedure based on the recommendations of the Informative Annex D of the EN 1992 1-2. This procedure is intended to be a complementary verification performed as a post-processing investigation to the advanced calculation method results. In this chapter, the frames previously discussed are assessed in order to understand if neglecting shear effects may lead to non-conservative results. To complement this analysis, a case of a frame containing a short-column is also investigated.

Chapter 6

Conclusions and Further Works

In this chapter the general conclusions obtained throughout the work are summarized. The drawbacks in this work are also listed. To conclude, further investigations to complement the work carried out during this thesis are pointed.

2
Literature Review

2.1. INTRODUCTION

This chapter contains a review of the main subjects with implications in the application of advanced calculation methods to the analysis of reinforced concrete structures subjected to fire. Other subjects with relevant importance to the global understanding of the actual behaviour of concrete structures and materials subjected to fire such as *high performance concrete, self compacting concrete, precast concrete, pre-stressed concrete, physical and chemical response to fire, fibre reinforced concrete, assessment after fire exposure, etc.,* are not covered in this review. Further reading on these areas may be found in [37].

Ever since the last few decades, it has been observed an increasing number of research programmes aimed to the understanding of the actual behaviour of reinforced concrete structures at elevated temperatures, although this effort is still far behind the level of work carried out on steel and composite structures. Nevertheless, these researches have already produced some considerable amount of data, which still remain to be fully assimilated by the academic community. In spite of this, there are several features related to structural concrete subjected to fire which are currently sufficiently acknowledged ensuring an acceptable degree of reliability to the application of advanced methods. On the other hand there are several topics where discussion and experimental work is needed.

2.2. THE CONCEPT OF STRUCTURAL FIRE ADVANCED CALCULATION METHOD

The Eurocode 2 Part 1-2 (EN 1992 1-2) [4] states that the advanced calculation methods for structural fire analysis shall provide a realistic analysis of structures subjected to fire, based on fundamental physical behaviour leading to a reliable approximation of the expected behaviour of the relevant structural component exposed to fire. These methods are able to be applied to the whole structure, part of the structure or to single elements analysis.

The advanced calculation methods, also called thermo-mechanical, include two calculation steps: the thermal analysis, dedicated to the evaluation of temperature evolution within structural elements, and the mechanical analysis considering the effects of temperature.

The thermal response analysis shall be based on the acknowledged principles and assumptions of the theory of heat transfer, considering the relevant thermal actions and the materials temperature dependent thermal properties [4]. The mechanical response analysis shall be based on the acknowledged principles and assumptions of the theory of structural mechanics, considering the effects of mechanical properties deterioration with temperature [4].

The great majority of the computer codes available to perform advanced fire analysis are based in the Finite Element Method (FEM). According to [38], three main types of computer programmes are possible to be applied in advanced structural fire analysis:

- Software written to model specific types of elements (beams, columns, etc.) not able to be applied to other elements. Generally, these codes are proprietary programmes established for research purposes;
- Software developed with the objective of modelling the full behaviour of structures in fire. These codes often present a set of material models and different finite elements, which combined, cover a wide range of structural and fire scenarios. Examples of these type of codes are the computer programmes SAFIR [38] , VULCAN [39] and FIRES-RCII [40];
- Software available commercially for general engineering purposes not specifically written for fire analysis. However, the elements comprised in these codes enable their application to the advanced fire analysis of structures. Examples of these codes are ABAQUS [41], DIANA [42] and ANSYS [43]. Besides these commercial programmes, other academic codes not developed specifically for fire analysis may be adapted to perform it, such as the code ADAPTIC [44] initially developed to investigate the non-linear dynamic behaviour of framed structures at ambient temperatures, later extended to include fire and explosion effects [45].

Whatever the computer code applied may be, the EN 1992 1-2 states clearly that, before its application a verification of accuracy shall be made on the basis of relevant tests results, and at the same time the critical parameters shall be checked to ensure that the model complies with sound engineering principles, by means of a sensitivity analysis [4].

2.3. FIRE MODELLING

The Eurocode 1 Part 1-2 (EN 1991 1-2) [24] refers that thermal actions in case of fire are given by the net heat flux to the surface of the exposed member, where the net heat flux should be determined considering heat transfer by convection and radiation.

Generally, for structural analysis purposes the fire action is accounted for by means of a temperature-time curve affecting the structural system to be assessed. This temperature is considered to be the gas temperature around the members exposed to fire. The most basic form to the represent the gas temperature evolution relies in the so called *nominal temperature-time curves*. The nominal curves allowed by the EN 1991 1-2 are the Standard curve, the External fire curve and the Hydrocarbon curve [24]. These fire curves are not dependent of any properties of the structure exposed to fire, such as fire load or ventilation characteristics, thus representing no realistic fire action. The nominal curves present an exponential mathematical formulation schematically plotted in Figure 2.1*a*. A more realistic approach is also allowed by the EN 1991 1-2 based in the natural fire simulation. The *parametric time-temperature curves* are the simpler way to simulate a natural fire, where the temperature evolution is assumed constant in the whole compartment in the same manner it is assumed in the case of nominal fire curves. However, the evolution of temperature in the parametric curves is based on physical parameters of the compartment, thus representing a realistic approach to the real fire evolution. A characteristic feature of the parametric curves is the existence of a *descending branch* representing the cooling (or decay) phase of the fire (which is not accounted for in the nominal curves). Figure 2.1*b* presents a schematic plot of several parametric curves related to different compartment's properties (ventilation, fire load, etc.).

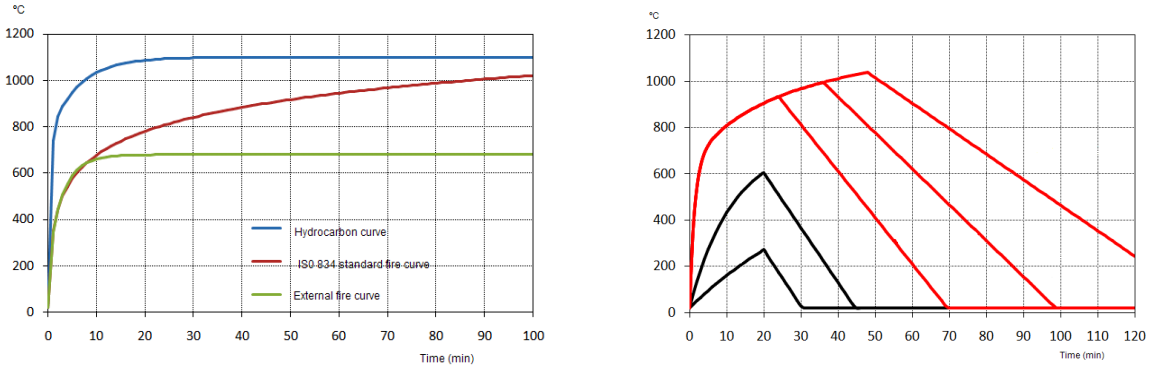

a) b)

Fig.2.1. – Schematic representation of the EN 1991 1-2 fire curves: a) nominal curves, b) examples of parametric curves. Adapted from [46].

One of the drawbacks associated to the application of fire curves representing the compartments gas temperature evolution is the inability to simulate the fire spreading nature from one compartment to another, being only possible to assume simultaneous compartments in fire. Bailey *et al.* [47] presented a procedure to account for compartment fire spread in the scope of natural fire curves. That procedure consists of assuming an initial scenario of compartments in fire, and when the temperature in these compartments reaches its peak value, the fire curve is applied to the adjacent compartments.

When the flash-over, i.e, the simultaneous ignition of all the fire-loads in a compartment, is unlikely to occur, the fire action should be modelled by means of a *localized fire model* [24].

The highest level of accuracy to simulate natural fires in the scope of the EN 1991 1-2 is given by the *advanced fire models*. These models must consider the gas properties, mass exchange and energy exchange. The advanced fire models are possible to be applied in the form of i) *one-zone models*, where a uniform temperature evolution is admitted to the whole compartment, ii) *two-zone models*, assuming an upper layer with time dependent thickness and with time dependent uniform temperature, as well as a lower layer with time dependent uniform and lower temperature, iii) *computational fluid dynamic models (CFD)* giving the temperature evolution in the compartment in a completely time dependent and space dependent manner [24].

The natural fire simulations are applied in the scope of a performance-based approach, as previously discussed in Chapter 1. In spite of this, the application of advanced fire models is not often seen in practicing engineering because these models are too much complex and highly demanding in a computational point of view. In an attempt to erase this drawback, Rein *et al.* [48] developed a procedure to account for the non-uniformity of the fire within the compartment avoiding the complexities of CFD models. The procedure consists of dividing the compartment into a *near field* zone comprising the part of the compartment directly exposed to the flame, and a *far field* zone comprising the rest of the compartment. Figure 2.2 sketches the concept of *far-near* field according to [48]. The structural elements are subjected to different fire action whether they are within the *near* of *far* field zone. The location of the *near field* is not constant during the course of the fire, simulating the *travelling* nature of the fire within the compartment.

The last type of fire modelling raises some problems to application of advanced calculation methods. The main problem relies in the fact that the structural elements are exposed to different thermal actions along their length. Gillie *et al.* [49] analysed the effects of travelling fires in the behaviour of a steel beam, concluding that a wide range of strains and stresses are recorded in the beam depending on the

type of fire input, obtaining remarkably different results when compared against the beam's response subjected to a uniform fire. Because of the travelling nature of the fire, a complex interaction between tensile and compression forces is observed in the beam as heating and cooling are occurring simultaneously in different parts of it [49]. Franssen *et al.* [50] also investigated the effect of localized fires in the structural response, implementing the necessary modifications in the code SAFIR to enable it to deal with this type of fire models. The modification performed in [50] is also suitable to fire analysis when the fire action is given by a CFD model. Taillefer *et al.* [51], using the code SAFIR, investigated the differences obtained regarding the structural response of reinforced concrete beams and 2D frames when exposed to different fire models, identifying the necessity of carefully couple thermal and mechanical models in order to obtain sound results.

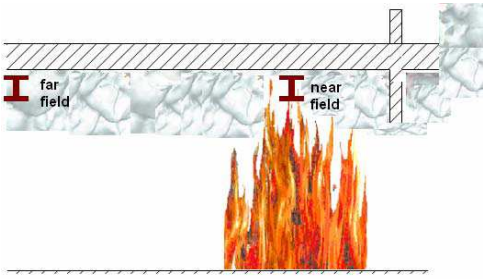

Fig.2.2. – Far and near field for fire modelling [48].

2.4. CONCRETE MATERIAL MODELS AT ELEVATED TEMPERATURES

The mechanical model, or constitutive model, of concrete constitutes perhaps the most fundamental input to the advanced structural fire calculation programmes. Even the most sophisticated Finite Element software packages will produce misleading predictions of the structure´s behaviour if the constitutive model applied does not reflect the true concrete characteristics at elevated temperatures.

According to Anderberg [52], until the mid 1970s the understanding of the mechanical behaviour of concrete at elevated temperatures was very limited, and all attempts to evaluate the stress distribution of a heated concrete member had been based in the elastic theory. This approach had shown itself to be highly inaccurate as it predicts that if a concrete member is unloaded and unrestrained against thermal elongation during heating, the member will fail due to high thermal stresses approximately at 350ºC. As it is commonsense, this prediction is not correct, because unloaded and unrestrained concrete members do not ever fail by themselves [52]. Following the same author, the fundamental phenomenon capable of explaining the true behaviour of concrete members exposed to fire was discovered in the 1970s in Sweden [53] [54] and Germany [55]. During theses researches, an unknown strain component, designated as *transient strain*, was identified. Basically, *transient strain* was defined as a non-recoverable, time independent and dominating compressive strain, which develops during the first heating under simultaneous load [52]. This *transient strain* is believed to considerably contribute to the relaxation and redistribution of thermal stresses in heated concrete members [52].

This strain component was also identified by Khoury [56] [57] in the 1980s. This author refers to it as *Load Induced Thermal Strain* (LITS). LITS is obtained directly from the difference in strain measurement during first heating between one unloaded specimen and another loaded one [10]. Khoury also refers that LITS has three main components: *transient creep, 'basic creep'* and *changes in elastic strain with temperature* [10]. In Figure 2.3 is presented as schematic definition of LITS as well as an analysis of the LITS' three components relative importance obtained from a torsion test.

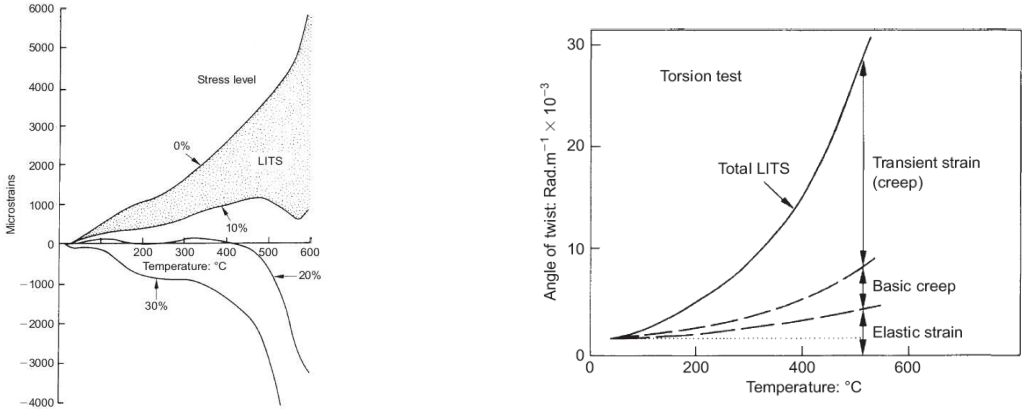

a) b)

Fig.2.3. – LITS: a) definition of LITS [58], b) components of LITS [58].

Whether it is called LITS or transient strain, it is accepted that this transient phenomenon possesses a major role in the behaviour of concrete exposed to fire, and any analysis of heated concrete that ignores transient strain will yield erroneous results, especially for columns [52]. Currently there are two main academic material models which take into account the behaviour under transient conditions [52]: the Anderberg & Thelandersson model and the Khoury *et al.* model. Until this day, several structural analysis of concrete elements subjected to fire have been performed using the two above mentioned models, and it has been concluded by Law *et al.* [59] that one model does not represent structural behaviour more satisfactorily than another.

The Anderberg & Thelandersson model (ATM) considers that total strain of heated concrete is formed as the sum of four strain components derived on a phenomenological basis [52]:

$$\varepsilon_{tot}(T) = \varepsilon_{th}(T) + \varepsilon_{\sigma}(\sigma,T) + \varepsilon_{tr}(\tau,\sigma,T) + \varepsilon_{cr}(t,T,\sigma) \qquad (2.1)$$

where: ε_{tot} (T) is the total strain; ε_{th} (T) the thermal strain; ε_{σ} (σ,T) the instantaneous stress-related strain based on σ-ε relationship; ε_{tr} (τ,σ,T) the transient strain; ε_{cr} (t,T,σ) the creep strain or time dependent strain; T refers to temperature; t time; σ stress; τ stress history.

Anderberg refers that above 100ºC transient strain is essentially a function of temperature and not time [52]. An important feature of the ATM model is the consideration of the load-history in the development of transient strain. As Anderberg states [52] there is a fundamental implication of load-history in the stress-strain relationship of heated concrete. In Figure 2.4 is illustrated the stress-strain curves of concrete at different temperatures, where in Figure 2.4*a* the concrete specimen was heated without any preloading and in Figure 2.4*b* the specimen is stressed with 20% of its strength at ambient temperature. It is possible to verify in Figure 2.4 that if concrete is heated without load it will present a more pronounced loss of stiffness and strength with the increase of temperature than if it had been previously preloaded.

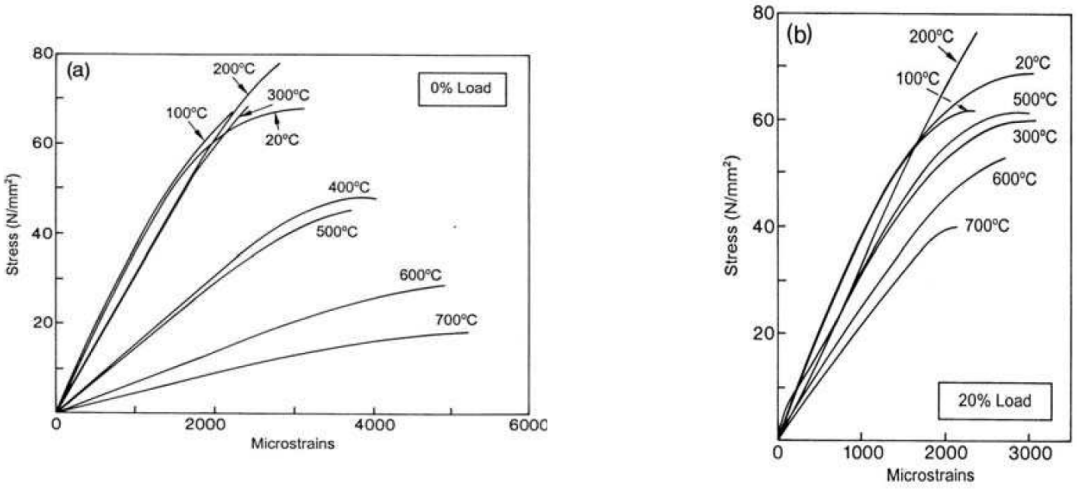

a) b)

Fig.2.4. – Stress-Strain curves for concrete at different temperatures: a) no preloading [52], b) 20% preloading [52].

The importance of load-history is even higher in redundant structures. For instance in a concrete specimen restrained against longitudinal expansion, axial forces will develop during heating making the stress level of the specimen to change during the process. Another example can be found in real structures subjected to fire, where due to the failure of some constituents, alternative load paths are formed imposing new stress states to the other parts of the structure. In Figure 2.5 the measured restraint load (in % to the ultimate load at ambient conditions) as function of temperature with fully restrained specimen and the predicted restraint with the ATM model is compared [52].

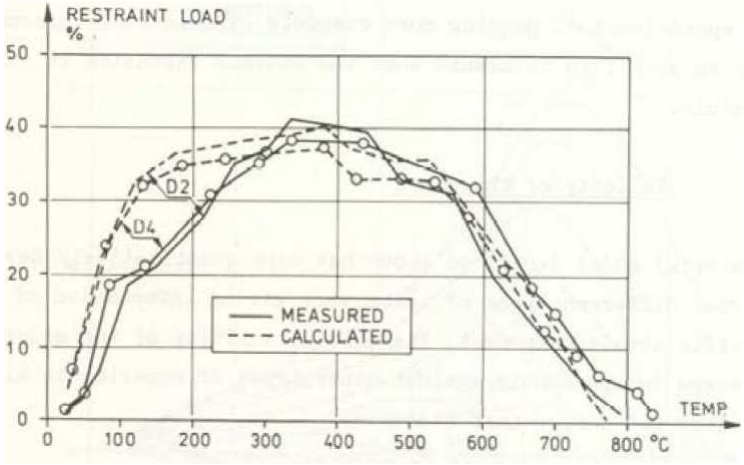

Fig.2.5. – Predicted and measured restraint load [52].

In opposition to the ATM model the concrete model proposed by Khoury *et al.*, does not include explicitly the effect of load-history [52]. The first version of Khoury's model was based on tests up to 600ºC [52], and have been improved since then with respect to the results of a series of experiments of heated concrete during two thermal cycles [58] [60] [61]. These experiments were conducted over several specimens, with sealed, unsealed, loaded and unloaded conditions. The thermal cycle referred

comprises a 14-day period, including first heating, constant temperature phase, cooling stage and subsequent cycle, in order to simulate the environment to which a nuclear reactor's concrete is exposed [58]. Of course, this scenario is different from a fire environment which time scale is much smaller (hours not days), but some of the results obtained are able to be applied to fire concrete analysis. Considering this last comment, the Khoury *et al.* strain model for unsealed and loaded concrete during first heating (the most frequent conditions of structural concrete exposed to fire) is composed of the sum of the following terms [10]:

$$\varepsilon_{tr,tot}^{T,\sigma,d} = \varepsilon_{co,el-pl,i}^{T,\sigma,d} + \varepsilon_{tr,th}^{T,0,d} + \varepsilon_{tr,sh}^{T,0,d} + \varepsilon_{tr,lits}^{T,\sigma,d} + \varepsilon_{tr,crack}^{T,\sigma,d} \qquad (2.2)$$

where: $\varepsilon_{tr,tot}$ means the total strain at transient conditions; $\varepsilon_{co,el\text{-}pl,i}$ refers to the 'initial' elasto-plastic strain determined experimentally during loading prior to heating (the elastic and plastic components may be separated); $\varepsilon_{tr,sh}$ is the shrinkage strain at transient conditions; $\varepsilon_{tr,th}$ is the thermal strain at transient condition; $\varepsilon_{tr,lits}$ is the above mentioned thermal induced thermal strain; $\varepsilon_{tr,crack}$ refers the crack-induced strain which may include excessive thermal strain, cracking of the aggregate and cracking induced by the different thermal expansion/shrinkage between the aggregate and the cement paste [61]. In equation 2.2 *T* is temperature, *σ* stress, *d* drying (unsealed) and *0* zero stress ($\sigma = 0$).

It is an interesting exercise to compare the terms in equation 2.1 and 2.2. The strain terms referring to LIST and transient strain are equivalent. The thermal strain component in 2.1 is equivalent to the sum of the thermal, shrinkage and cracking strains in 2.2. Traditionally, these components have been referred solely as thermal strain because they have been experimentally determined together. In Khoury *et al.* [61] these terms have been separated for the first time and the thermal strain is related to the thermal expansion of non-drying concrete.

Besides the academic models referred, there is also the stress-strain model for concrete at elevated temperatures prescribed in the EN1992 1-2 [4]. This model does not consider any kind of transient strain. Instead, it only comprises a stress-strain curve as function of temperature just like the one shown in Figure 2.6. In other words, in the EN 1992 1-2 model the load-history and the transient strain are not explicitly taken into account [62].

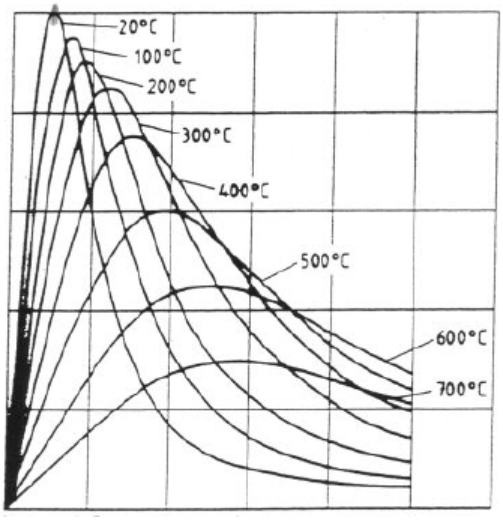

Fig.2.6. – Schematic representation of the EN 1992 1-2's stress-strain curves at different temperatures [16].

Some authors consider [52] [62] that the effect of transient strain in heated concrete is somehow accounted for in the EN 1992 1-2 constitutive model in the way that this model presents excessive large values to the ultimate strain and to the strain-at-pick-stress when compared against those very values published in the literature. In table 2.1 are presented the eurocode's strain values as well some more realistic values (within brackets).

Table 2.1. – Stress-strain values at different temperatures following EN 1992 1-2 for siliceous aggregates' concrete [52].

Temperature (ºC)	$f_{c,T}/f_{c,k}$	$\varepsilon_{c1,T}$ (%)	$\varepsilon_{cu,T}$ (%)
20	1,00	0,25	2,00 (0,35)
300	0,85	0,70 (0,3)	2,75 (0,50)
600	0,45	2,50 (0,5)	3,50 (0,80)
1000	0,04	2,50	4,50 (1,10)

Law *et al.* [59] have studied the implications for structural analysis of LITS. In this study the ATM model, the Khoury's (numerically modelled by Terro) model and de EN 1992 1-2's model have been examined and the results compared. It has been concluded in this study that the correct choice of the modulus of elasticity is critical to the accuracy of the results. As the implementation of the two academic models above referred involves the creation of a stress-strain curve varying with temperature and then modified by the consideration of the transient effects, it has shown to be important to carefully analyse the results considering the actual and the apparent (derived from the initial gradient of stress-strain curve) modulus of elasticity. The results of this study in a simple example (pinned pure concrete beam heated uniformly to 500ºC and cooled back to ambient temperature) are drawn in Figure 2.7. It is observed that the difference between the results considering apparent and actual modulus of elasticity are more pronounced during the cooling phase.

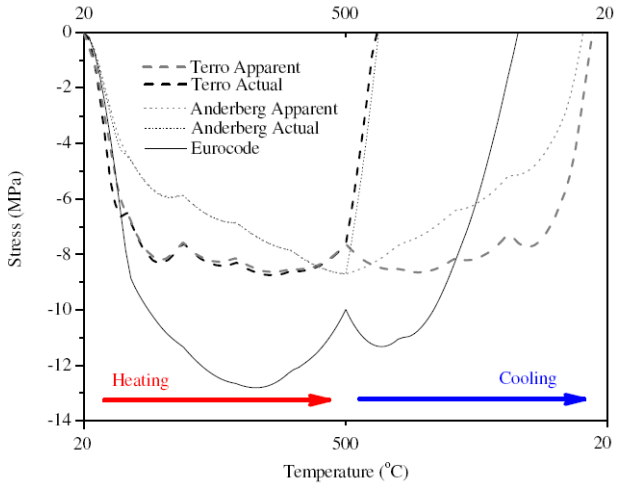

Fig.2.7. – Stresses obtained with different constitutive models [59].

Law *et al.* [63] studied the implications of LITS in multi-dimensional analysis of concrete at elevated temperatures. It was concluded that, in accordance to [59], there are significant differences between a

constitutive curve which include LITS and a full constitutive model accurately representing LITS components. It was also indicated that the inclusion of plastic strains with the above mentioned apparent modulus of elasticity is useful in one dimension analysis, but plastic flow rules case strains to develop laterally when multi-dimension analysis is performed. To solve this problem, Law *et al.* proposed the application of a two step model with an apparent modulus of elasticity and an embedded actual one within the material model. This approach is believed to correctly include the plastic strains originated by LITS equations and at the same time it allows the correct representation of strains in the directions lateral to loading. Gillie *et al.* [64] refers that the consideration of biaxial compression in concrete allows the improvement of its strength approximately to 10 % of the uniaxial value.

Schneider *et al.* [65] proposed an extended model for concrete in compression at elevated temperatures incorporating elastic, plastic and creep strains as function of temperature and load-history, aiming to complete the existing EN 1992 1-2's model. With this model one is able to consider the effect of thermal creep and load-history in all phases of thermal exposure. The different parts of deformation are approximated with discrete equations interacting in concrete model. According to Schneider *et al.* [65] this model is capable of predicting the realistic behaviour of concrete structures, even during the cooling phase of the fire. Considering the load-history during heating up it is possible to obtain an increasing load-bearing capacity due to a higher stiffness. Schneider *et al* [65] also states that, because this model considers the thermal-physical behaviour of material laws, it will lead to a better evaluation of the safety level when applied to EN 1992 1-2 calculation system.

Schneider *et al.* [66] performed an application of the material model presented in [65] (referred as advanced transient concrete model) to the analysis of tunnel cross-section subjected to fire. The results have been compared against the ones obtained with the EN 1992 1-2 constitutive curve. It was concluded that the EN 1992 1-2 curve does not allow the determination of realistic values of structural deformations when compared to the results obtained with the proposed model (which according to Schneider *et al.* is based on measured data). It was stated that the proposed model should be applied if an optimization of concrete is desirable.

Sadaoui *et al.* [67] investigated the effect of transient creep on the behaviour of reinforced concrete columns in fire. Applying a finite element code capable of considering transient creep either explicitly as an additional strain component, or implicitly through the deformation properties of concrete, it has been learned that transient creep induces additional compressive stresses, magnifying bending moment, thus leading to anticipated structural failure.

An important drawback in the knowledge of concrete properties when exposed to fire is the lack of understanding of its behaviour during the cooling phase. Dwaikat *et al.* [68] when analysing a beam exposed to parametric fire simply considered that during the cooling phase concrete does not recover any of its properties loss in the heating process. The mechanisms experimented by the concrete mix during cooling have been analysed by Khoury [60] [61]. From his research it was understood that concrete presents a tendency to expansion at the final stages of cooling from higher temperatures even though the temperature is still decreasing. This expansive phenomenon is believed to be correlated to crack development and chemical rehydration. It is possible that the absorption of moisture from the atmosphere and the rehydration of the lime (CaO) may trigger a cracking mechanism during the last stages of cooling [60]. The EN 1992 1-2 does not present any constitutive model for concrete during cooling [4], although it states that the available stress-strain curve should be altered when considering decay phase of fire. A specific stress-strain concrete curve for natural fires (thus including cooling phase) is possible to be found in the informative Annex C of the Eurocode 4 Part 1-2 (EN 1994 1-2) [69]. At the heating up stage this model follows the EN 1992 1-2 formulation, but after this it admits that concrete does not recover its initial compressive strength when cooling down. In Figure 2.6 is

presented a schematic illustration of the stress-strain curve proposed in EN 1994 1-2 for heating and cooling phase. Figure 2.8 a) shows the evolution of the curve with the temperature and Figure 2.8 b) the evolution of temperature in concrete with time. It is possible to observe that the slope of the descending branch is kept constant during cooling and equal to the slope of the descending branch of the curve correspondent to the maximum temperature achieved. To obtain the curves for the cooling phase EN 1994 1-2 proposes the determination of the residual compressive strength for concrete. Then the compressive strength during the cooling stage may be linearly interpolated between the strength at maximum temperature and the residual strength [69].

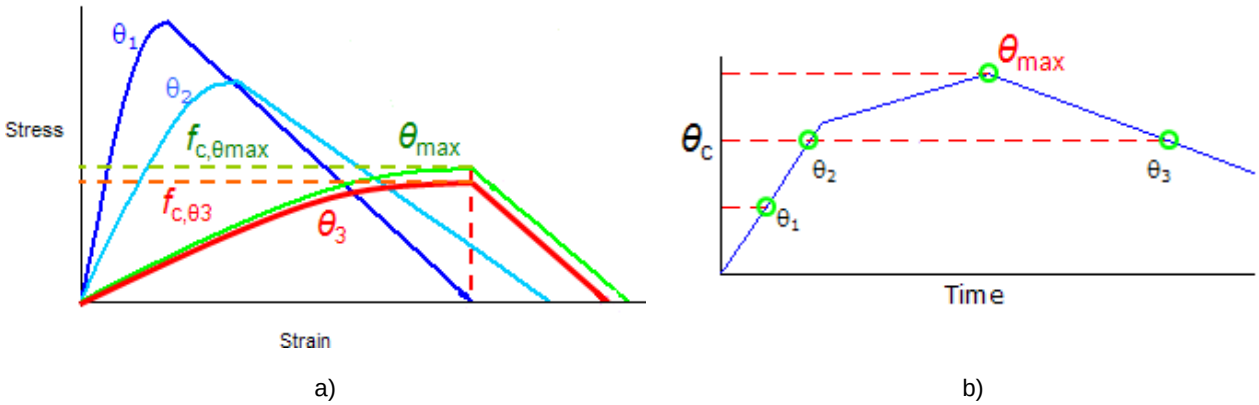

Fig.2.8. – Stress-strain model for concrete exposed to natural fires proposed in EN 1994 1-2, adapted from [2].

The experimental results presented by Klingsch *et al.* [70] during the cooling stage in supersulfated slag cement concrete tends to confirm the trends described by the EN 1994 1-2 model for decay phase. These results have shown a clearly nonlinear material behaviour of concrete when cooling down.

A general overview on the stress-strain relationships of concrete at elevated temperatures is presented by Youssef *et al.* [71]. Here is stated that the existing stress-strain curves are based on fire tests of unconfined specimens, providing different predictions of structural behaviour because of uniqueness of each relationship and the existence of several formulations for calculating the governing parameters. In that analysis the governing parameters are identified as the concrete compressive strength, tensile strength, strain-at-peak-stress, initial modulus of elasticity, transient creep and the reinforcing steel yield stress and bond strength. Youssef *et al.* [71] made recommendations for choosing specific formulations based on accuracy, generality and simplicity.

More complex material models for concrete behaviour at elevated temperatures have been presented by several authors. Luccioni *et al.* [72] proposed a thermo-mechanical model for concrete subjected to high temperatures based on a plastic-damage model extended to consider temperature induced damage. In this model the thermal damage is taken into account through a damage variable that is a measure of the deterioration due to temperature. The concept of irreversibility of damage is presented in this model meaning that the thermal damage variable is irreversible. The application examples of the model have demonstrated this formulation capable of simulating the residual mechanical behaviour of concrete, characterized by the stiffness and strength loss [72].

2.5. STEEL MATERIAL MODELS AT ELEVATED TEMPERATURES

Currently the understanding of the behaviour of steel at elevated temperatures is more advanced than it is in relation to concrete. As Anderberg [52] enunciated, it is generally accepted that the total strain of steel at transient elevated temperatures may be defined as the sum of three components [52]:

$$\varepsilon_{tot} = \varepsilon_{th}(T) + \varepsilon_{\sigma}(\sigma, T) + \varepsilon_{ch}(t, T, \sigma) \qquad (2.3)$$

where: ε_{tot} is the total strain; ε_{th} the thermal strain; ε_{σ} the instantaneous stress-related strain based on stress-strain relationship obtained at constant stabilized temperature; ε_{ch} represents creep strain or time dependent strain. *T*,*t* and σ have the same meaning as in equation 2.1.

As it is explained in [52] steel exposed to fire presents different behaviour whether it appears in the form of reinforcing, pre-stressing, structural, hot-rolled or cold-worked steel. However, as thermal strains are concerned, the results measured experimentally point out small deviations among the different types of steel, indicating that type of steel and its strength characteristics seem to have reduced influence in that strain component [52]. In the same way, experimental results [52] [73] indicate the existence of a similar dimensionless σ-ε relationship for reinforcing and structural steel.

The stress-strain curves of steel may be obtained by several means, being the most common methods the anisothermal and the isothermal ones [74] [75]. In the first procedure a steel specimen is subjected to a known load and then heated at a uniform rate until failure occurs. Throughout the test several strain measurements are performed, and after subtracting the thermal strain (obtained at an unloaded test), the stress-strain curves are drawn. The test is repeated for different loads allowing the production of the different stress-strain curves [76]. For its turn, in the isothermal method, the specimen is heated to a uniform temperature and then strained at constant rate. The stress-strain-temperature curves are derived measuring the stress level at different strains and repeating the test for several temperatures [76]. Anyway, as it was referred in [74] the results obtained from any type of high temperature test is very variable for the same steels and a number of reasons for this fact were presented. In relation to the accuracy of the two procedures above mentioned, it is referred in [76] that the two methods of testing correspond to different load regimes, where the anisothermal simulates the case of steel heated at constant load, and the isothermal corresponds to a situation of constant temperature and varying load. The first scenario is close to a real typical fire situation, while the second is not so common, but possible to be found for instance in a boiler. Nevertheless, in reality a combination of the two loading regimes is present in real structures subjected to fire, as the load in some elements may vary due to P-delta effects and other factors [76].

Creep and relaxation present a difficult challenge in the modelling process as they are unique for every type of steel, thus being hard to establish a common description [52]. The creep strain is just possible to be directly measured in steady state tests, and if the stress level is kept constant it is possible to be separated into two phases (primary and secondary) [52]. On the other side, the evaluation of relaxation is performed at constant strain and temperature and the stress decrease is measured as function of time [52]. In Figure 2.9*a* are presented the results obtained by Anderberg [52] [77] [78] for measured creep at different stress levels, and in Figure 2.9*b* from the same author the results for relaxation of reinforcing steel.

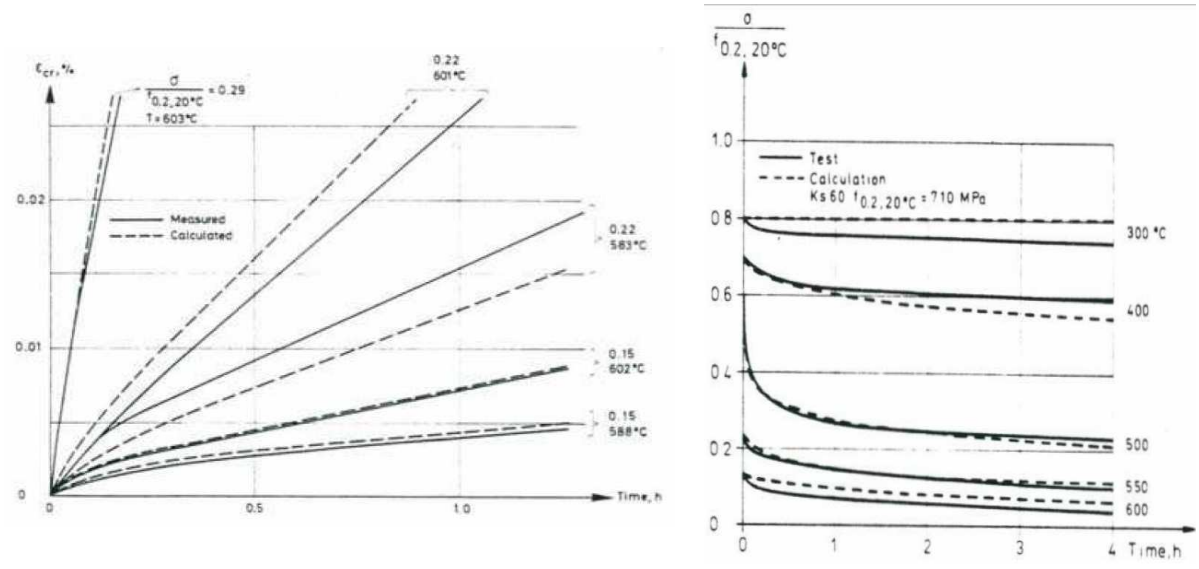

a) b)

Fig.2.9. – a) Measured and predicted creep at different stress levels [77] [78]; b) Measured and predicted relaxation [77] [78].

For design purposes, it is possible to use a simplified model where the creep strain is incorporated in the stress-strain curve, because constitutive models considering a separated creep strain are only important for the prediction of the total behaviour including deformation from creep and relaxation [52]. In a structural fire design process creep may be incorporated in the stress-strain curve, but ensuring that the curve is based on transient tests with a proper rate of temperature in such a way creep influence is accounted for in a safe way [52].

According to [76] there are three main steel material models suitable for design purposes: the bilinear, the multi-linear and Eurocode model.

The bilinear model is the simpler representation of steel mechanical behaviour and is often used at ambient temperature design. This model only requires two input parameters: the yield point and elastic stiffness (both of then temperature-dependant). It is assumed a elastic behaviour until the yield point is reached, and beyond this point the steel is allowed to strain infinitely at constant stress [76]. Some authors states that, although this model presents accurate results at ambient temperatures, it is over simplified for design at elevated temperatures [74] [75].

The multi-linear model constitutes an upgrade version of the bilinear one, where a number of straight lines are fitted to experimental data to approximate the real behaviour. The more lines are considered the more accurate the model will be [76]. Until now, a few number of multi-linear models have been proposed, but in the other hand, as finite element programmes require material constitutive data input in the form of stress-strain pairs, in the end the model applied will be similar to a multi-linear representation, although the initial model introduced in the programme was derived from a more complex algebraic formulation [76].

The Eurocode 3 Parte 1-2 (EN 1993 1-2) [79], and even the EN 1992 1-2 and EN 1994 1-2, presents a detailed mechanical model of steel at elevated temperatures. A difference between the model proposed in the EN 1993 1-2 and in the EN 1992 1-2 is the fact that the former allows the inclusion of strain hardening at temperatures below 400ºC (model presented in the informative annex A of EN 1993 1-2). For temperatures above 400ºC the strain hardening is not considered. In Figure 2.10*a* a schematic

representation of the EN 1993 1-2 stress-strain curve without hardening strain at different temperatures is illustrated. In Figure 2.10*b* the same curves considering strain hardening are also shown.

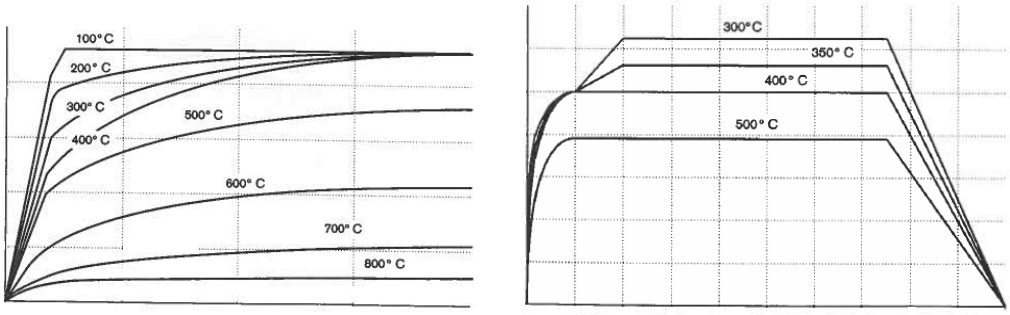

a) b)

2.10. – Schematic stress-strain curves of steel at different temperatures: a) without strain hardening; b) with strain hardening. Adapted from [80].

The Eurocode's steel model presents different strength degradation whether it is hot-rolled or cold-worked [79]. This could be explained with the cold-working fabrication process, during which the steel is stressed beyond the yield strain into the strain hardening. Because of this, the cold-worked steel may present higher effective yield strength than hot-rolled one. However, when exposed to fire, this increase in yield strength is gradually loss at elevated temperatures. This is why the retention factors of the cold-worked steel properties are lower than those in hot-rolled one even though the strength absolute values may be higher [45].

Stainless steel displays a better retention of strength and stiffness than structural carbon steel when exposed to elevated temperatures, due to the beneficial effects of the alloying elements [81]. On the other hand, stainless steel presents a higher thermal expansion than carbon steel, which in the scope of restrained structures may lead to important thermal induced stresses, not covered by the higher strength retention in case of fire [81].

2.6. INCORPORATION OF SPALLING IN THE CALCULATION MODELS

The fundamentals of the spalling phenomenon have already been exposed in sub-section 1.3.2. Although spalling is more susceptible to affect high-performance concrete structures, it has been observed to happen in normal-strength ones. Because of this, and also due to the unpredictability associated to this phenomenon, its incorporation in the calculation models is presented in this literature review.

Dwaikat *et al.* [68] proposed a macroscopic finite element model for the analysis of reinforced concrete structures subjected to fire, where spalling is considered by means of a simplified hydrothermal model through the calculation of pore pressure. This hydrothermal model is based in the principles of mechanics and thermodynamics including the conservation of liquid water and water vapour to predict pore pressure, and the mass transfer of water vapour is driven by [68]:

$$A\frac{dP_V}{dt} = \nabla B \nabla P_V + C \qquad (2.4)$$

where: P_V represents pore pressure, t time; A, B and C are parameters dependent on pore pressure, temperature, rate of heating, permeability of concrete, initial moisture content and the isotherm used in the analysis [68].

The pore pressure obtained with equation 2.4 is then compared against the tensile strength of concrete, meaning that spalling occurs when pore pressure exceeds the mentioned tensile strength. This condition is assessed with the inequality [68]:

$$nP_V \rangle f_{tT} \qquad (2.5)$$

where: n represents the porosity of concrete and f_{tT} the tensile strength at temperature T. Once the occurrence of spalling is detected, the affected area of cross-section is removed and a new boundary surface is considered in the following thermal and mechanical analysis. Applying this model to the analysis of high strength concrete beams (with low permeability), Dwaikat *et al.* concluded that the beam's fire resistance is reduced by more than 50% due to the consideration of spalling [68].

Deeny *et al.* [82] investigated the influence of spalling in the structural analysis of concrete exposed to fire. During this investigation, it was assumed that the occurrence of spalling was certain, i.e., all conditions capable of inducing spalling are considered to be fulfilled. In the study it was analysed when spalling would happen based essentially in the heating rate of concrete [82]. Considering this, spalling is triggered at the moment the fire exposed surface reaches the 375-425ºC interval of temperature, and it is modelled by the removal of the affected area. Deeny *et al.* refers that this abrupt removal of cross-section's layers constitutes an simplified model of a progressive and slower process, thus the same analysis above referred was performed (considering the same temperature criteria) but modelling spalling effects removing only single layers of element at time [82]. The results of the study engaged in [82] yielded that spalling threatens structural stability by exposure of reinforcement to high rates of rising temperature. In figure 2.11 is presented the comparative evolution of reinforcement temperature obtained in [82] considering abrupt, progressive and no spalling situation.

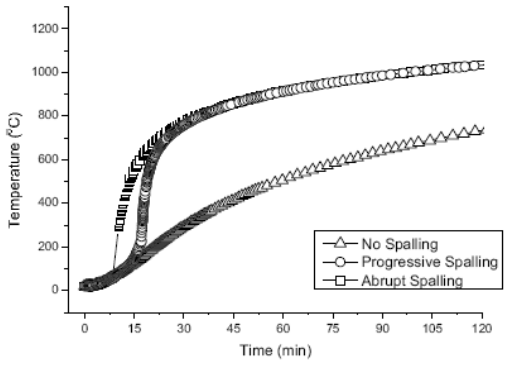

2.11. – Evolution of temperature in reinforcement steel for different spalling modelling [82].

Huang *et al.* [83] presented a finite element model for the analysis of reinforced concrete at elevated temperatures. Besides the inclusion of transient strain, the effect of spalling is possible to be assessed because void segments are allowed. A detailed description of the formulation of this model is presented in reference [84]. Huang *et al.* [83] concluded that the incorporation of spalling on both

thermal and mechanical modelling is very significant in the results obtained for the behaviour of reinforced concrete members exposed to fire.

Franssen *et al.* [85], performed an analysis of the impact of spalling in the fire resistance of a concrete tunnel. For this purpose the effect of spalling was integrated in the non-linear finite element code SAFIR by the successive removal of concrete layers at a constant rate. As SAFIR calculation procedure involves two steps (cross-section thermal analysis and mechanical analysis of the structure considering the information stored during the thermal analysis), for spalling modelling, it is necessary to generate a new file in the thermal analysis every time a concrete layer is removed. When spalling occurs and the concrete elements are removed, the corresponding concrete fibres are replaced by fictitious elements at 1200ºC of temperature (thus with no strength). Franssen *et al.* [85] refers that this process has the advantage of possibly being made automatic, allowing this type of analysis to be performed regularly.

On a different scope of the above mentioned spalling representations, there are other ways to account for the effects of this phenomenon through the application of more complex models, the so called comprehensive hygro-thermo-mechanical models. Accordingly to [86], Khoury *et al.* [86], Gawin *et al.* [86] and Tenchev *et al.* [86] undertook pioneer work in this field.

An example of this sort of formulation is proposed by Schrefler *et al.* [87]. This model considers concrete as a multi-phase porous material at elevated temperatures, accounting for material deterioration, and allows hygro-thermal analysis developing the model equations starting from macroscopic balances of mass, energy and linear momentum of single constituents [87]. Davie *et al.* [86] presented a coupled hydro-thermal-mechanical model to represent the behaviour of concrete at transient elevated temperatures through finite element analysis. With this model it is possible to investigate the relative importance of pore pressure and thermal-induced strains on the mechanical damage of concrete considering different values of material properties such as relative humidity, permeability and tensile strength. Another model, proposed within the NewCon project [88] [89], where concrete is treated as a multi-phase system considering the voids partially filled with liquid and gas phase [90], the influence of polypropylene fibres is possible to be assessed.

An important drawback to the application of the comprehensive hygro-thermo-mechanical models is, notwithstanding its high complexity for practicing engineering purposes, the fact that, as referred in [86], although the coupled hygro-thermo-mechanical behaviour of concrete at elevated temperatures has been well performed so far, the actual causes of spalling are still not fully understood and there is not yet a convincing numerical model for its prediction.

Lim *et al.* [28] presented a different path to the assessment of spalling of concrete exposed to fire. In this risk-based approach the likelihood and extent of spalling for normal-weight and normal-strength concrete structures is assessed by the examination of different factors such as material properties, heating conditions and member layout and configuration. No hygral or thermal calculations, as in the previously presented models, is performed. Lim *et al.* [28] referred that this methodology is able to be applied to existing and new structures, and although it is at an earliest development stage, it may provide a useful guidance for practising engineers.

2.7. GLOBAL ANALYSIS OF REINFORCED CONCRETE STRUCTURES EXPOSED TO FIRE

This section contains a brief summary of the analysis of reinforced concrete structures exposed to fire available in the literature, in order to list the main features related to this kind of procedure, which will be later applied in the following chapters.

Iwankiw [91] indicates two fundamental features that a global analysis shall be able to simulate: i) the effects of thermally-induced strains and restraint forces, ii) the ability to change from pure bending resistance of beams and slabs to combined bending-membrane resistance mode (catenary or membrane action), due to large vertical deflections recorded at elevated temperatures during the course of the fire. Figure 2.12 sketches these two features.

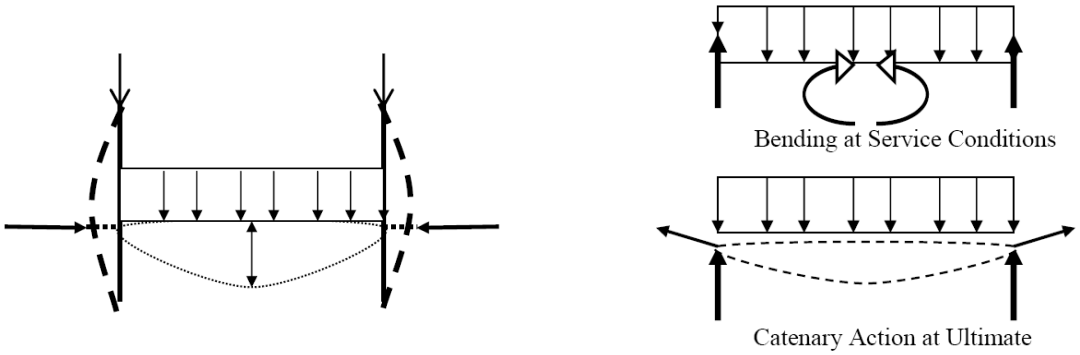

a) b)

2.12. – a) Effect of floor thermal expansion on columns, b) changes in structural resistance of beams from bending to catenary action [91].

Riva [92] investigated the evolution of internal stresses within the elements of a 2D single-bay reinforced concrete frame. In that study, the bay's beam was considered exposed to fire in the lateral and bottom surfaces. As to the column two scenarios were considered: i) exposure only in the inner surface and ii) exposure along three sides. The columns not directly exposed to fire are considered to remain at ambient temperatures during the calculation process. For the sake of simplicity, in this literature review only the case of one side exposed columns is referred. In Figure 2.13 are plotted the results obtained regarding the evolution of displacements and internal stresses in the frame during the exposure to the ISO 834 standard fire curve [36]. Although the frame had been designed to withstand 60 minutes of standard fire exposure according to the tabulated method of assessment, the results obtained displayed a much higher time of fire endurance, confirming how conservative tabulated method is, as already remarked in Chapter 1.

From the analysis of the results illustrated in Figure 2.13 it immediately yields the increase in internal stresses throughout the frame's elements, which is not accounted for in the scope of simplified cross-sectional methods.

Venazi *et al.* [93] performed a global fire analysis regarding a set of two-bay reinforced concrete frames of two and three storeys. The bays span was considered to be 6.0m or 8.0m in order to investigate the effect of different stiffness relations between the beams and the columns. The results obtained in [93] displayed a significant redistribution and increase of internal forces with respect to those for which the frame had been designed, underlining the important role played by global behaviour during the structural response to fire action.

The results obtained in the two previous investigations above reported emphasized the effects of structural continuity in the global fire response. However, they are limited to 2D analyses, which do not account for the slabs membrane action.

Huang *et al.* [94] analysed the behaviour of a reinforced concrete building exposed to fire including the behaviour of floor slabs. The results obtained illustrate that slabs behaviour during fire exposure is highly influenced by both tension and compressive membrane action. In the same study, the presence of adjacent cold slab areas had shown to present a significant influence on the behaviour of the

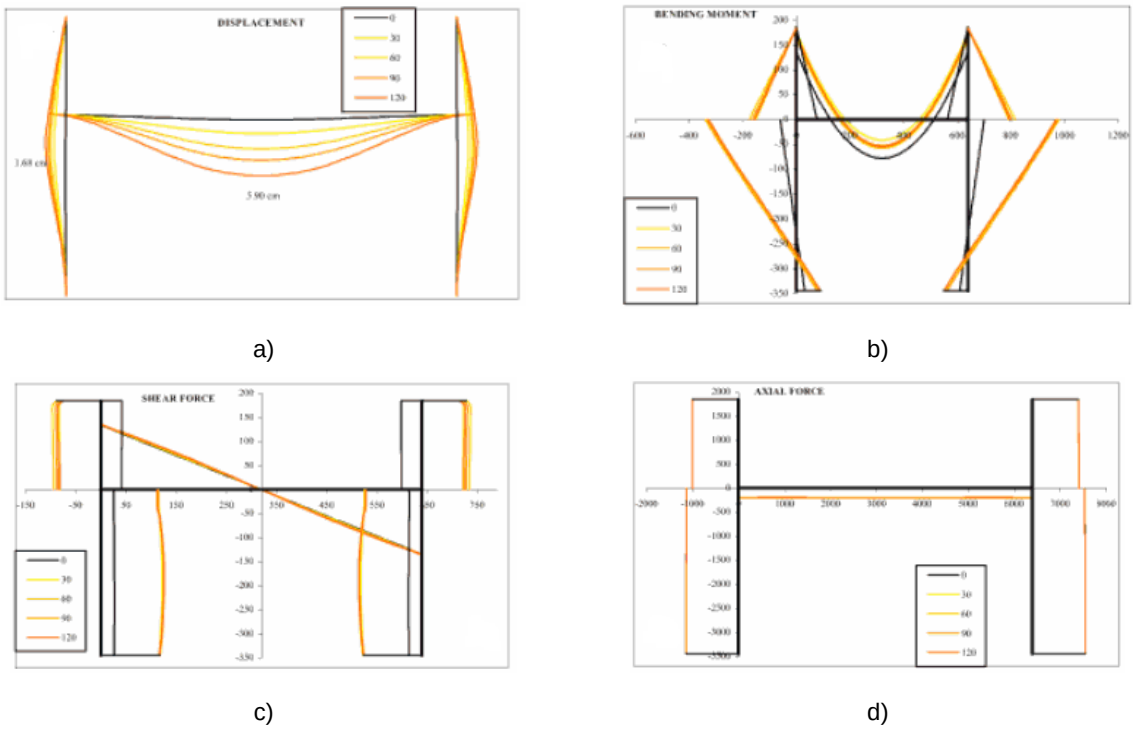

2.13. – results obtained to the case of columns exposed in the inner side: a) displacements, b) bending moment, c) shear force, d) axial force [92].

structure within the fire compartment, because the cold part of the structure provides an increase in the fire endurance of the whole system through structural continuity. The analyses performed in [94] were stopped due to buckling of the fire exposed columns, exposing the importance of designing reinforced concrete columns for high fire resistance periods to prevent columns failures.

According to Moss *et al.* [95] the tensile membrane forces of the slab are limited by the strength loss in the reinforcing steel bars as they heat up and by increasing vertical deflections.

2.8. CONCLUDING REMARKS

The main factors affecting the applications of advanced calculations methods to the fire analysis of reinforced concrete frames have been presented. Several computer codes are currently available to perform this sort of analysis.

The model used to describe the fire action must be carefully coupled with the mechanical model available, in order to obtain sound and realist results.

To simulate the actual behaviour of concrete structures exposed to fire the transient effects must be considered, by means of adequate calculation models and constitutive laws both for concrete and steel

at elevated temperatures. Only the advanced calculation models that consider these features are able to output a rational, safe and cost-effective structural fire assessment.

The inclusion of spalling effects is not very relevant in normal-strength concretes structures, however, when analysing high-strength concrete structures, the calculation model should incorporate this phenomenon.

The global analysis of reinforced concrete structures must be able to display the evolution of displacements and internal forces that actually takes place in structures exposed to fire.

3

Analysis of Reinforced Concrete Frames Exposed to Fire: Part 1

Global Response Compared to Simplified Methods

3.1. INTRODUCTION

This chapter is devoted to the analysis of the global response of 2-D reinforced concrete frames exposed to fire. At first, a brief description of the finite element code applied is performed, followed by the presentation of the thermal and mechanical properties of concrete and steel considered during the analysis.

The first frame analysed here is the same presented in section 2.7 (see Figure 2.13), because of its simplicity and to compare the results obtained with the present calculation model to the one presented in that section.

The second analysis performed in this chapter aims understanding the global behaviour of a three-bay frame. The frame is considered to be exposed to fire in two floors simultaneously, the rest of the building remaining at ambient conditions, including a central concrete core which imposes the floors' thermal expansion towards one single direction, thus imposing significant drifts in the end columns of the frame.

To conclude this chapter, the frame's fire resistance obtained relying in the advanced calculation method is compared against the resistance evaluated based in simplified calculation methods, in order to understand if neglecting structural continuity during the course of the fire may lead to non-conservative results applying the last methods instead of the former.

3.2. NUMERICAL MODELLING

3.2.1. BRIEF SOFTWARE DESCRIPTION

The thermo-mechanical analysis of reinforced concrete frames exposed to fire presented in this work has been performed with the software SAFIR [38]. SAFIR is a non-linear material and geometric finite element program, developed in the University of Liège, intended to the analysis of structures at both elevated and ambient temperatures [38]. As any other finite element program, the structure is divided

into a number of discrete parts, called finite elements, connected by nodes. Further reading about this analysis technique is found in references [3] and [4].

SAFIR includes different finite element types, capable of accommodating several structural idealizations [38]. These elements are the 2-D (two-dimensional) Beam element, 3-D (three dimensional) Beam element, Truss element and the Shell element. There are also the 2-D and 3-D Solid elements related to the thermal analysis. In this work only the 2-D Beam element has been used to model the frames, and as such, just this type of element is detailed in the following text.

The structural fire calculation with SAFIR is composed of two main steps: the thermal and the mechanical analysis. This program also possesses a torsional analysis module, regarding the calculation of 3-D Beam elements having cross-sections subjected to warping, where the torsional stiffness and cross-section's warping function are able to be determined [38].This capability is more related to the analysis of steelwork structures, and thus, it is not further exposed in this work.

The first operation engaged by SAFIR is the thermal analysis, aiming to the evaluation of the temperature distribution in the structure during the whole fire duration. When the temperature distribution is known, then the mechanical analysis module is performed, calculating the behaviour of the structure subjected to mechanical loads, thermal actions and considering the materials' properties changes due to temperature evolution. Although thermal and mechanical analysis are correlated, they are nevertheless, performed separately and subsequently [38]. This presents some implications, such as the fact that thermal analysis deeply influences the mechanical behaviour, but the mechanical analysis does not alter the thermal one (for instance, the cracking of concrete is not considered in the thermal analysis, which is not true, as cracking promotes a variation in the thermal conductivity through concrete material) [38]. An important feature about the application of SAFIR is that the type of thermal analysis depends on the mechanical analysis to be performed. If 2-D (or even 3-D) Beam element is used for mechanical purposes, a 2-D thermal analysis is performed in order to obtain the temperature distribution within the beam's cross-section. A drawback in this procedure is found in the fact that no heat flux is considered along the element's longitudinal axis, i.e., heat transfer is regarded only within cross-section's domain. Generally, as temperature evolution during the fire duration is considered uniform within the fire compartment, this limitation is not very much relevant because the temperature exposure is the same for all structural elements. In the other hand, when non-uniform fire scenarios are analysed, disregarding heat fluxes along the axis may lead to inaccurate results. This may be attenuated by attributing different cross-section temperature histories to the different elements. In Figure 3.1 a schematic representation of the SAFIR's calculation procedure is sketched.

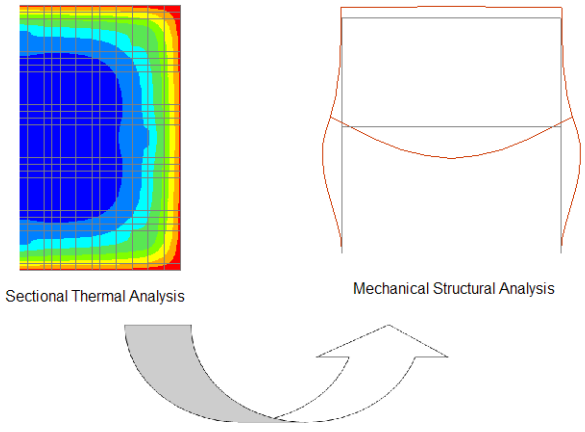

Fig.3.1. – Steps of SAFIR's calculation procedure.

3.2.2. THERMAL ANALYSIS

For the thermal analysis, the Fourier equation may be applied to describe heat transfer by conduction within the concrete element, assuming the hypothesis of a isotropic material, not submitted to movements, not compressible and that no mechanical dissipation happens. In a Cartesian system of co-ordinates *x*, *y*, *z*, it takes the form [38]:

$$k\left(\frac{\partial^2\theta}{\partial x^2}+\frac{\partial^2\theta}{\partial y^2}+\frac{\partial^2\theta}{\partial z^2}\right)+Q=c\rho\frac{\partial\theta}{\partial t} \tag{3.1}$$

where k is the thermal conductivity (W/m.K), θ is the temperature (K), Q is the internally generated heat (W/m^3), c is the specific heat (J/Kg.K), ρ is the specific mass (kg/m$^{3)}$,and t is time (s).

With the SAFIR's thermal analysis code, equation 3.1 is solved numerically by means of finite element method. Classical shape functions, N, are used and temperature is replaced by $T = N_i\, T_i$. Then the equation is multiplied by a weighting function and integrated on the element's volume. This is the weighted residual method, called Galerkin method if the shape functions used for describing the geometry are used as weighting functions [38]. Transforming the first term of equation 3.1 using Green's equation and considering the boundary conditions, equation 3.1 is turned into [38]:

$$\int_{element} k\{\nabla N_i\}\langle\nabla N_j\rangle dv T_i+\int_{element} c\rho N_i N_j dv\dot{T}_i+\int_{element} QN_j dv=-\int_{boundary} N_j q_n ds \tag{3.2}$$

where q_n is the heat flux at element's boundary and ∇ means $\langle\partial/\partial x;\partial/\partial y;\partial/\partial z\rangle$.

Finally, assembling the contributions of all finite elements, the matrix formulation describing the equilibrium of heat fluxes in the structure at any instant is obtained as [38]:

$$[K]\{T\}+[C]\{\dot{T}\}=\{g\} \tag{3.3}$$

where $[K]$ is the conductivity matrix, $[C]$ is the capacity matrix, $\{T\}$ is the node temperature vector and $\{g\}$ is the vector of the heat exchanges at boundary.

Equation 3.3 expresses the thermal equilibrium at a single time instant, thus, in order to analyse the temperature evolution during the fire process SAFIR solves this equation along the time, as fully described in reference [96].

For the thermal analysis associated to 2-D Beam elements, the beam's cross-section is divided into a number of fibres as shown in Figure 3.1, which are linear and may present three or four nodes (triangular or quadrangular elements). In the present work only quadrangular elements have been used.

The 2-D results generated during the thermal analysis are stored for the subsequent mechanical procedure. The 'thermal' finite elements are associated to the cross-section fibres of the beams. This

means that if one beam is exposed to the same thermal flux throughout its length, but it presents different mechanical properties (such as varying reinforcement layout or different geometry), several thermal files have to be produced and attached to the correct position in the beam.

SAFIR thermal analysis may be applied to any material, and to any materials combination, if its physical properties at elevated temperatures are known.

3.2.3. MECHANICAL ANALYSIS

The mechanical analysis performed by SAFIR considers large displacements based in the incremental form of the principle of virtual works [38]. If a total co-rotational configuration is employed, this principle is expressed as in equation 3.4, in which the forces applied on the surface of the structure have not been considered [38]:

$$\int_V (\overline{D}_{ijkl} d\overline{E}_{kl} \delta\overline{E}_{ij} + S_{ij} \delta d\overline{E}_{ij}) dV = \int_V (d\overline{f}_i \delta\overline{u}_i + \overline{f}_i \delta d\overline{u}_i) dV \tag{3.4}$$

where: S_{ij} is the second Piola-Kirchhoff stress tensor, $\overline{f}_i$ represents the volume forces; $\delta\overline{E}_{ij}$ is the Green's strain tensor of the virtual field of displacements, $\overline{D}_{ijkl} = D_{ijkl}$ is the tensor defining the incremental constitutive law of the material, $d\overline{u}_i$ represents the virtual field of displacements from the deformed position of the element and $V = \overline{V}$ is the undeformed volume of the element.

Because the materials constitutive law is dependent of temperature, and temperature is constantly changing during the calculation procedure, the constitutive law is given by[38]:

$$dS_{ij} = D_{ijkl} (dE_{kl} - dE_{kl}^{th}) = D_{ijkl} dE_{kl}^{m} \tag{3.5}$$

where dE_{kl}^{th} is the incremental thermal strain tensor and dE_{kl}^{m} is the tensor of mechanical (stress-related) strains.

In order to solve equation 3.4, applying the finite element methodology based on displacements, the resulting matrix equation that governs the iteration from one position of equilibrium to the next one is written as [38]:

$$\int_V B^T DBdVdp + \int_V S^T \delta ledVdp = (K_u + K_S) dp = f^{ext} - f^{int} \tag{3.6}$$

where K_u comprises the elastic and geometric stiffness matrices, K_S represents the stress generated stiffness matrix, f^{ext} are nodal forces energetically equivalent to the applied forces and f^{int} are the nodal forces obtained from integration of the internal stresses.

During the iteration process, the stiffness matrix is calculated using the Newton-Raphson's method. The method of 'arc-length' is used in order that part of internal stresses in local elements may be redistributed to other parts of the structure when local failure occurs, thus leading to a new equilibrium position. Nevertheless, it has been noticed that this method may fail in many cases [97].

As previously mentioned, in this work only the 2-D Beam element has been used in the mechanical analysis. This element is based in Bernoulli hypothesis, meaning that plane sections remain plane after the deformation and normal to the beam's axis, and no shear deformation is considered. The Beam element is straight in its undeformed position and has a constant cross-section along the longitudinal axis. This cross-section is the same defined during the previous thermal analysis, which is divided into several fibres. During the mechanical analysis, the material behaviour of each fibre is evaluated in the fibre's centre and assumed constant for the whole fibre. Each fibre may present its own material properties.

The element presents two nodes containing three degrees of freedom and an extra node in the centre to accommodate the non-linear component of the axial deformation. A schematic representation of the element is shown in Figure 3.2.a).The different Beam elements that compose the whole structure, are connected, at the level of their cross-sections, through the node-line (Figure 3.2 b)), whose position remains constant during the analysis. In the calculations performed in this work the position of the node-line has been considered in the cross-section's geometric centre.

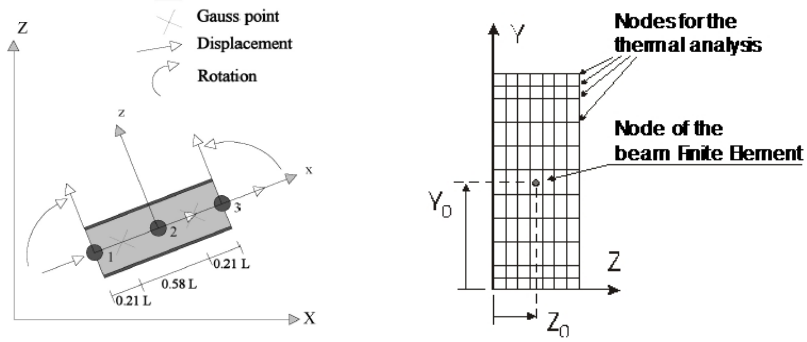

Fig.3.2. – a) 2-D Beam element in SAFIR [97]; definition of node-line or node of the beam finite element [98].

3.3. MATERIALS THERMAL AND MECHANICAL PROPERTIES AT ELEVATED TEMPERATURES

This section describes the thermal and mechanical properties of concrete and steel at elevated temperatures according to Eurocode 2 Part 1-2 (EN 1992 1-2) [4]. The properties are considered as characteristic values, and when the materials properties at ambient temperature are needed, they shall be taken equal to those in Eurocode 2 Part 1-1 (EN 1992 1-1) [99].

3.3.1. THERMAL PROPERTIES

The thermal properties of concrete are exposed in EN 1992 1-2. However, the majority of the thermal properties of steel have to be found in the Eurocode 3 Part 1-2 (EN 1993 1-2) [79]. This fact may be explained because, in EN 1992 1-2 the thermal analysis is oriented to be performed considering solely the concrete cross-section, thus ignoring the presence of reinforcement, which constitutes a satisfactory approximation (only if the ignored reinforcement is the longitudinal one). On a different approach, in the thermal analysis performed in the course of this work, the presence of longitudinal

reinforcing steel bars has not been neglected, and so the steel thermal properties at elevated temperatures have been considered the same as in EN 1993 1-2.

3.3.1.1. Concrete

3.3.1.1.1. Thermal Elongation

The thermal strain of heated concrete (at temperature θ) is defined in relation to its initial length at ambient temperature (20ºC) by equation 3.7 for siliceous aggregates concrete [4]:

$$\varepsilon_c(\theta) = -1{,}8\times10^{-4} + 9\times10^{-6}\theta + 2{,}3\times10^{-11}\theta^3 \quad \text{for } 20ºC \le \theta \le 700ºC$$

$$\varepsilon_c(\theta) = 14\times10^{-3} \quad \text{for } 700ºC \le \theta \le 1200ºC \tag{3.7}$$

Equation 3.8 defines the thermal strain for calcareous aggregates [4]:

$$\varepsilon_c(\theta) = -1{,}2\times10^{-4} + 6\times10^{-6}\theta + 1{,}4\times10^{-11}\theta^3 \quad \text{for } 20ºC \le \theta \le 805ºC$$

$$\varepsilon_c(\theta) = 12\times10^{-3} \quad \text{for } 805ºC \le \theta \le 1200ºC \tag{3.8}$$

The variation of thermal elongation with temperature is drawn in Figure 3.3 for both siliceous and calcareous aggregates concrete.

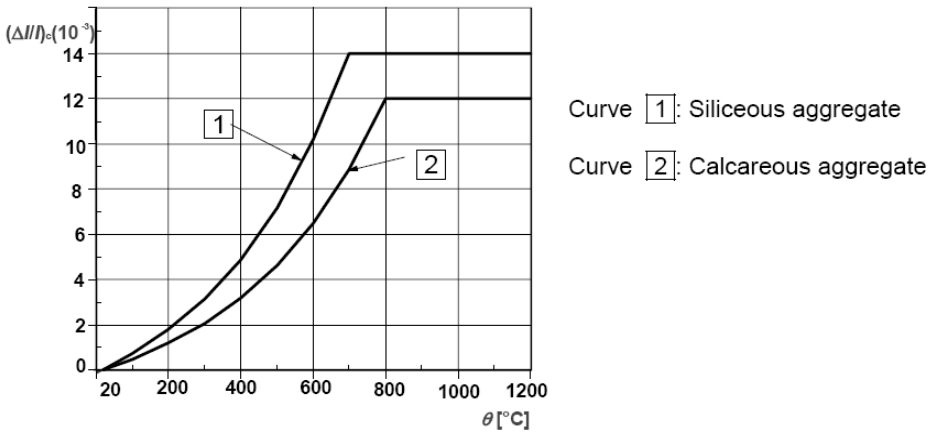

Fig.3.3. – Thermal elongation of concrete with temperature [4].

3.3.1.1.2. Specific Heat

The specific heat of concrete measures the energy required to raise one degree of temperature of one unit volume of concrete. According to EN 1992 1-2 the variation of specific heat of dry concrete as function of temperature may be determined by equation 3.9 (valid for both siliceous and calcareous aggregates concrete) [4]:

$$\begin{aligned} c_p(\theta) &= 900 && \text{for } 20^oC \le \theta \le 100^oC \\ c_p(\theta) &= 900 + (\theta - 100) && \text{for } 100^oC \le \theta \le 200^oC \\ c_p(\theta) &= 1000 + (\theta - 200)/2 && \text{for } 200^oC \le \theta \le 400^oC \\ c_p(\theta) &= 1100 && \text{for } 400^oC \le \theta \le 1200^oc \end{aligned} \qquad (3.9)$$

The evolution of specific heat of dry concrete with temperature is plotted in Figure 3.4. In this plot the peak values for different moisture contents, *u*, are also represented. These peak values are [4]:

$$\begin{aligned} c_{p,peak} &= 900 && \text{for moisture content of 0\% of concrete weight} \\ c_{p,peak} &= 1470 && \text{for moisture content of 1,5\% of concrete weight} \\ c_{p,peak} &= 2020 && \text{for moisture content of 3,0\% of concrete weight} \end{aligned} \qquad (3.10)$$

A linear interpolation between the given values is acceptable for other moisture contents.

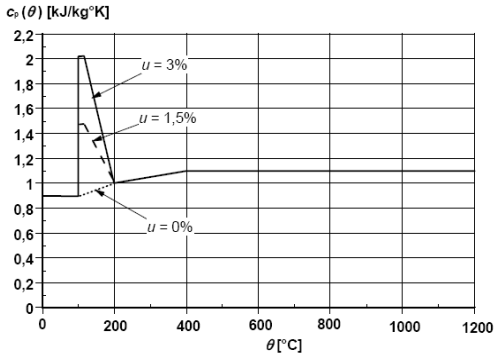

Fig.3.4. – Specific heat of concrete as function of temperature for 3 different moisture contents [4].

3.3.1.1.3. Concrete density

The variation of concrete density with temperature is influenced by water loss and is defined in EN

1992 1-2 as [4]:

$$\begin{aligned}
&\rho(\theta) = \rho(20^{o}C) && \text{for } 20^{o}C \le \theta \le 115^{o}C \\
&\rho(\theta) = \rho(20^{o}C) \times (1 - 0{,}02 \times (\theta - 115)/85) && \text{for } 115^{o}C \le \theta \le 200^{o}C \\
&\rho(\theta) = \rho(20^{o}C) \times (0{,}98 - 0{,}03 \times (\theta - 200)/200) && \text{for } 200^{o}C \le \theta \le 400^{o}C \\
&\rho(\theta) = \rho(20^{o}C) \times (0{,}95 - 0{,}07 \times (\theta - 400)/800) && \text{for } 400^{o}C \le \theta \le 1200^{o}C
\end{aligned} \tag{3.11}$$

3.3.1.1.4. Thermal conductivity

The EN 1992 1-2 defines the concrete's thermal conductivity (λ_c) between two boundary limits. The upper limit as function of temperature is given by [4]:

$$\lambda_c = 2 - 0{,}2451 \times (\theta/100) + 0{,}0107 \times (\theta/100)^2 \quad \text{for } 20^{o}C \le \theta \le 1200^{o}C \tag{3.12}$$

and the lower limit is defined by equation 3.14 [4]:

$$\lambda_c = 1{,}36 - 0{,}136 \times (\theta/100) + 0{,}0057 \times (\theta/100)^2 \quad \text{for } 20^{o}C \le \theta \le 1200^{o}C \tag{3.13}$$

In Figure 3.5 are plotted the evolution of the two limits for thermal conductivity of concrete, as expressed in EN 1992 1-2

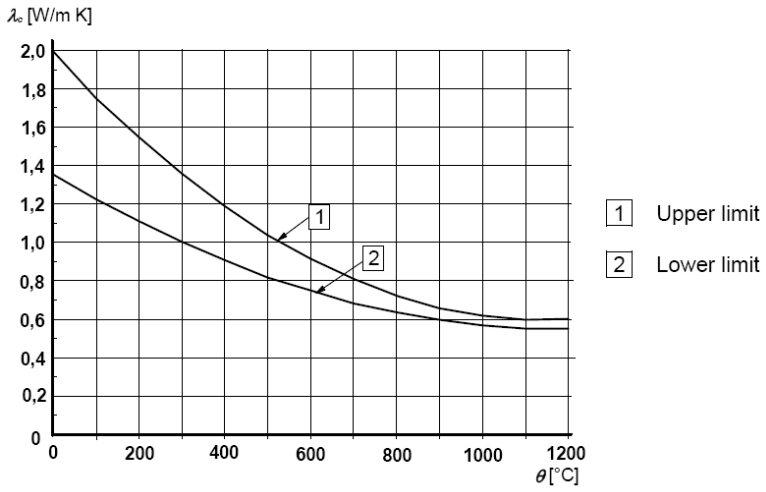

Fig.3.5. – Thermal conductivity of concrete [4].

3.3.1.2. Steel

3.3.1.2.1. Thermal Elongation

The thermal strain of heated steel ($\varepsilon_s(\theta)$) is determine as in equation 3.14, with reference to the initial length at 20ºC [79]; the respective graphical representation is presented in Figure 3.6:

$$\begin{aligned} \varepsilon_s(\theta) &= -2{,}416\times10^{4} + 1{,}2\times10^{-5}\times\theta + 0{,}4\times10^{-8}\times\theta^{2} && \text{for } 20ºC \le\theta\le 750ºC \\ \varepsilon_s(\theta) &= 11\times10^{-3} && \text{for } 750ºC\le\theta\le 860ºC \\ \varepsilon_s(\theta) &= -6{,}2\times10^{-3} + 2\times10^{-5}\times\theta && \text{for } 860ºC\le\theta\le 1200ºC \end{aligned} \qquad (3.14)$$

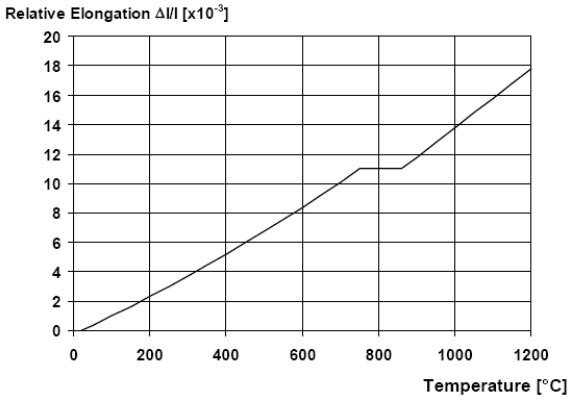

Fig.3.6 – Thermal elongation of steel with temperature [79].

3.3.1.2.2. Specific Heat

The specific heat of steel ($c_a(\theta)$) at elevated temperatures is defined as in EN 1993 1-2 by equation 3.15 [79]. The variation of specific heat with temperature is plotted in Figure 3.7.

$$\begin{aligned} c_a &= 425 + 7{,}73\times10^{-1}\times\theta - 1{,}69\times10^{-3}\times\theta^{2} + 2{,}22\times10^{-6}\times\theta^{3} && \text{for } 20ºC \le\theta\le 600ºC \\ c_a &= 666 + 13002/(738-\theta) && \text{for } 600ºC\le\theta\le 735ºC \\ c_a &= 545 + 17820/(-731+\theta) && \text{for } 735ºC\le\theta\le 900ºC \\ c_a &= 650 && \text{for } 900ºC\le\theta\le 1200ºC \end{aligned} \qquad (3.15)$$

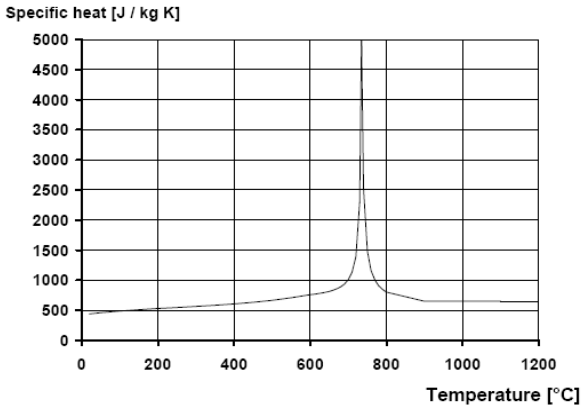

Fig.3.7 – Variation of the specific heat of steel with temperature [79].

3.3.1.2.3. Steel density

The steel density is admitted to remain unchanged during the heating process with the value of ρ_s = 7850 Kg/m^3.

3.3.1.2.4. Thermal Conductivity

Thermal conductivity of steel at elevated temperatures (λ_a (θ)) is determined with equation 3.16 [79], and is represented in Figure 3.8:

$$\lambda_a = 54 - 333 \times 10^{-2} \times \theta \qquad \text{for } 20^{o}C \leq \theta \leq 800^{o}C$$

$$\lambda_a = 27{,}3 \qquad \text{for } 800^{o}C \leq \theta \leq 1200^{o}C \qquad (3.16)$$

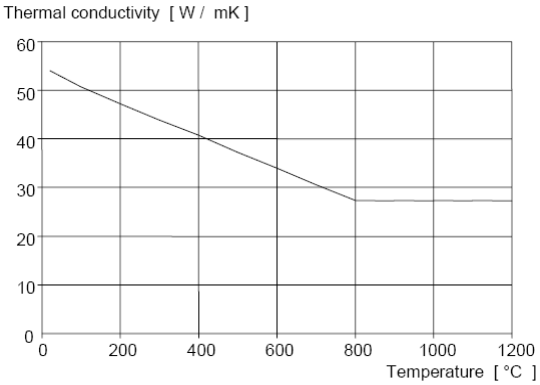

Fig.3.8. – Variation of the thermal conductivity of steel with temperature [79].

3.3.2. MECHANICAL PROPERTIES

The values of mechanical properties indicated in section 3 of EN 1992 1-2 are based on steady and transient states tests, and sometimes a combination of both [4]. The material models presented are valid only for heating rates between 2 and 50 K/min, because creep effects are not considered explicitly [4].

3.3.2.1. Concrete

The mathematical model of the stress-strain relationship for concrete under compression is defined in Figure 3.9. This curve layout is controlled by the compressive strength $f_{c,\theta}$ and the strain-at-peak-stress ($\varepsilon_{c1,\theta}$). For numerical purposes the descending branch shall be considered, limited by the ultimate strain ($\varepsilon_{cu1,\theta}$). The values for the above mentioned parameters, for siliceous aggregates concrete, are shown in Table 3.1.Values for intermediate temperatures may be obtained by linear interpolation. These parameters are valid for normal-weight concrete [4].

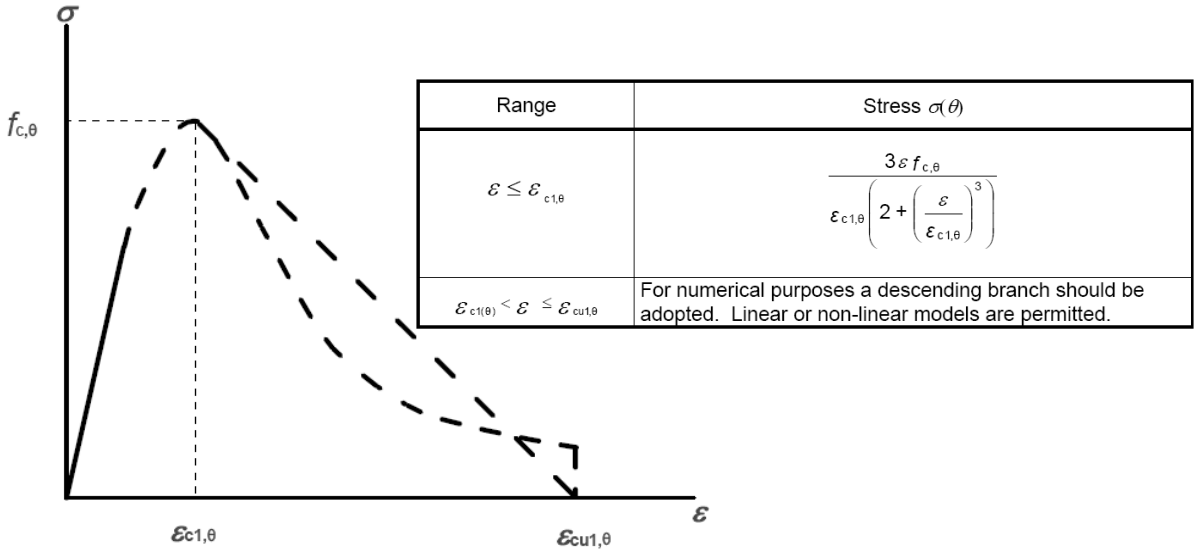

Range	Stress $\sigma(\theta)$
$\varepsilon \le \varepsilon_{c1,\theta}$	$\frac{3\varepsilon f_{c,\theta}}{\varepsilon_{c1,\theta}\left(2+\left(\frac{\varepsilon}{\varepsilon_{c1,\theta}}\right)^3\right)}$
$\varepsilon_{c1(\theta)} < \varepsilon \le \varepsilon_{cu1,\theta}$	For numerical purposes a descending branch should be adopted. Linear or non-linear models are permitted.

Fig.3.9. – Stress-strain mathematical model for concrete under compression at elevated temperatures [4].

When considering natural fires, thus including the cooling phase, the stress-strain model presented in Figure 3.9 should be modified, and possible strength recovery should not be taken into account [4].

The tensile strength of concrete may be conservatively ignored. However, if it is necessary to take this strength into account, its value at ambient temperature must be multiplied by a reduction coefficient, as expressed by [4]:

$$f_{ck,t}(\theta) = k_{c,t}(\theta)\, f_{ck,t} \tag{3.17}$$

Table 3.1. – Values for the main parameters of stress-strain curves of normal weight concrete with siliceous aggregates [4].

Concrete Temperature θ (ºC)	$f_{c,\theta}/f_{ck}$	$\varepsilon_{c1,\theta}$	$\varepsilon_{cu1,\theta}$
20	1,00	0,0025	0,0200
100	1,00	0,0040	0,0225
200	0,95	0,0055	0,0250
300	085	0,0070	0,0275
400	0,75	0,0100	0,0300
500	0,60	0,0150	0,0325
600	0,45	0,0250	0,0375
700	0,30	0,0250	0,0375
800	0,15	0,0250	0,0400
900	0,08	0,0250	0,0425
1000	0,04	0,0250	0,0450
1100	0,01	0,0250	0,0475
1200	0,00	-	-

Figure 3.10 illustrates the mathematical formulation of the tensile strength reduction coefficient as function of the concrete temperature.

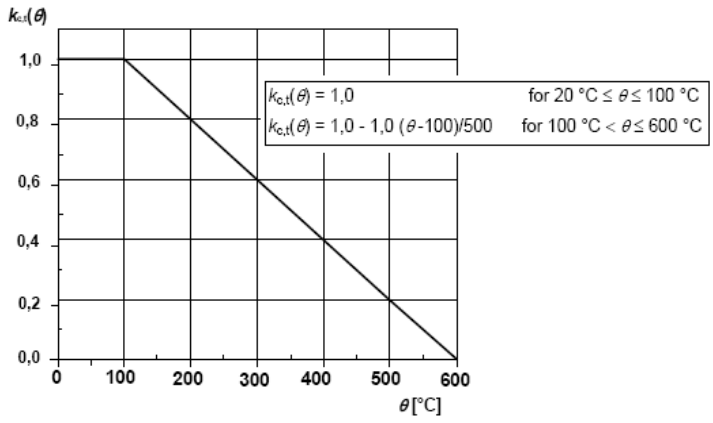

Fig.3.10. – Reduction coefficient to obtain concrete tensile strength at elevated temperatures [4].

3.3.2.2. Steel

The stress-strain relationship for steel at elevated temperatures is represented by the curve drawn in Figure 3.11. This curve is governed by three parameters: the slope of the linear elastic range $E_{s,\theta}$, the proportional limit $f_{sp,\theta}$ and the maximum stress level $f_{sy,\theta}$. Values for these parameters, for hot rolled steel bars, as function of temperature are presented in Table 3.2, where intermediate values may be obtained by linear interpolation. This stress-strain mathematical model is valid for both compression and tension, and is possible to be applied, as a sufficient approximation, in the structural analysis during the cooling stage of the fire [4].

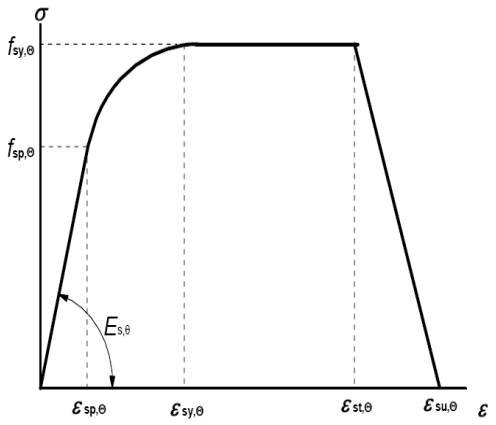

Range	Stress $\sigma(\theta)$	Tangent modulus
$\varepsilon_{sp,\theta}$	$\varepsilon E_{s,\theta}$	$E_{s,\theta}$
$\varepsilon_{sp,\theta} \le \varepsilon \le \varepsilon_{sy,\theta}$	$f_{sp,\theta} - c + (b/a)[a^2 - (\varepsilon_{sy,\theta} - \varepsilon)^2]^{0,5}$	$\frac{b(\varepsilon_{sy,\theta} - \varepsilon)}{a\left[a^2 - (\varepsilon - \varepsilon_{sy,\theta})^2\right]^{0,5}}$
$\varepsilon_{sy,\theta} \le \varepsilon \le \varepsilon_{st,\theta}$	$f_{sy,\theta}$	0
$\varepsilon_{st,\theta} \le \varepsilon \le \varepsilon_{su,\theta}$	$f_{sy,\theta}[1-(\varepsilon - \varepsilon_{st,\theta})/(\varepsilon_{su,\theta} - \varepsilon_{st,\theta})]$	-
$\varepsilon = \varepsilon_{su,\theta}$	0,00	-
Parameter *)	$\varepsilon_{sp,\theta} = f_{sp,\theta} / E_{s,\theta}$ $\varepsilon_{sy,\theta} = 0,02$ $\varepsilon_{st,\theta} = 0,15$ $\varepsilon_{su,\theta} = 0,20$ Class A reinforcement: $\varepsilon_{st,\theta} = 0,05$ $\varepsilon_{su,\theta} = 0,10$	
Functions	$a^2 = (\varepsilon_{sy,\theta} - \varepsilon_{sp,\theta})(\varepsilon_{sy,\theta} - \varepsilon_{sp,\theta} + c/E_{s,\theta})$ $b^2 = c\,(\varepsilon_{sy,\theta} - \varepsilon_{sp,\theta})\,E_{s,\theta} + c^2$ $c = \frac{(f_{sy,\theta} - f_{sp,\theta})^2}{(\varepsilon_{sy,\theta} - \varepsilon_{sp,\theta})E_{s,\theta} - 2(f_{sy,\theta} - f_{sp,\theta})}$	

*) Values for the parameters $\varepsilon_{pt,\theta}$ and $\varepsilon_{pu,\theta}$ for prestressing steel may be taken from Table 3.3. Class A reinforcement is defined in Annex C of EN 1992-1-1.

Fig.3.11. – Stress-strain mathematical model for steel at elevated temperatures [4].

Table 3.2- Values for the main parameters of stress-strain curves for hot rolled steel at elevated temperatures [4].

Steel Temperature θ (ºC)	$f_{sy,\theta}/f_{yk}$	$f_{sp,\theta}/f_{yk}$	$E_{s,\theta}/E_s$
20	1,00	1,00	1,00
100	1,00	1,00	1,00
200	1,00	0,81	0,90
300	1,00	0,61	0,80
400	1,00	0,42	0,70
500	0,78	0,36	0,60
600	0,47	0,18	0,31
700	0,23	0,07	0,13
800	0,11	0,05	0,09
900	0,06	0,04	0,07
1000	0,04	0,02	0,04
1100	0,02	0,01	0,02
1200	0,00	0,00	0,00

3.4. SINGLE-BAY FRAME ANALYSIS BASED ON ADVANCED CALCULATION METHODS

3.4.1. MODEL DESCRIPTION

Before engaging the analysis of a more complex structural system, in this section a single bay reinforced concrete frame is examined, in order to capture the main features related to the structure's behaviour during the course of the fire. With the results achieved hereafter, one is intended to be able to analyse and acknowledge the evolution of structural response of reinforced concrete frames exposed to fire until failure occurs.

The single bay frame modelled in this section is the same presented in the fib bulletin [92], already mentioned in the section 2.7 of this work, whose characteristics are summarized in Figure 3.12.

C30/37 (Siliceous aggregates)	N = 1000 kN, representing the upper floors
S500	G = 36.0 kN/m ; Q = 12.0 kN/m
All Rebar ø20	p = G + 0.5Q

[m]

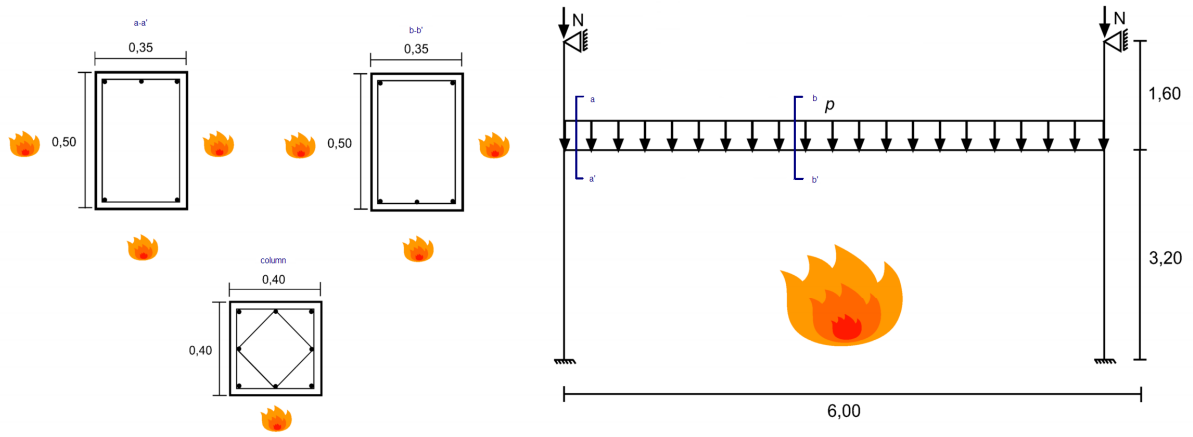

Fig.3.12. – Single-Bay Frame model characteristics.

3.4.2. FIRE INPUT AND THERMAL ANALYSIS

The fire action is considered through the application of the ISO 834 standard fire curve [36] representing the evolution of gas temperature in the compartment delimited by the frame's bay. Figure 3.13 presents the temperature evolution with time. In the same figure are also indicated the convection and emissivity coefficients attributed to concrete elements during the analysis.

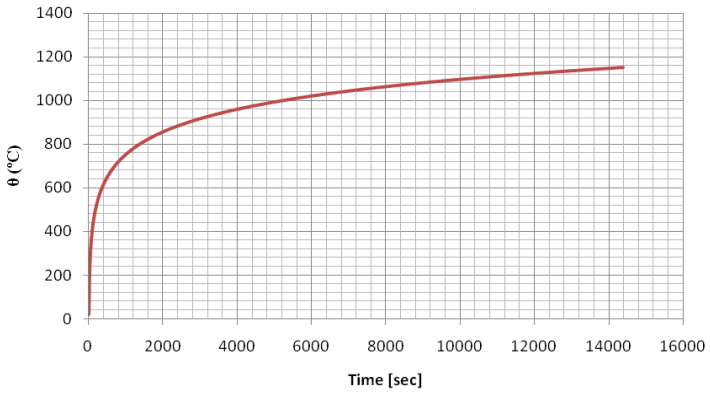

$\theta = \theta_0 + 345.\log_{10}(8t+1)$

$\theta_0 = 20^oC$

Convection coefficient for surfaces exposed to fire $h = 25\ W/m^2$

Convection coefficient for surfaces not exposed to fire $h = 9\ W/m^2$

Emissivity coefficient $\varepsilon_{res} = 0{,}56$

Fig.3.13. – Fire action input.

The results obtained from the thermal analysis are presented in Figure 3.14 for the exposed columns and Figure 3.15 for the beam. The columns outside the compartment fire are assumed to remain at ambient temperature throughout the course of the fire. The fibres that compose the elements' cross-sections are square shaped with 1.0 cm side length. The reinforcing steel bars positions are highlighted by a black contour. There is a 4.0 cm layer of concrete covering the reinforcing steel bars. Due to the problem's symmetry, only half cross-section is presented in both Figures 3.14 and 3.15.

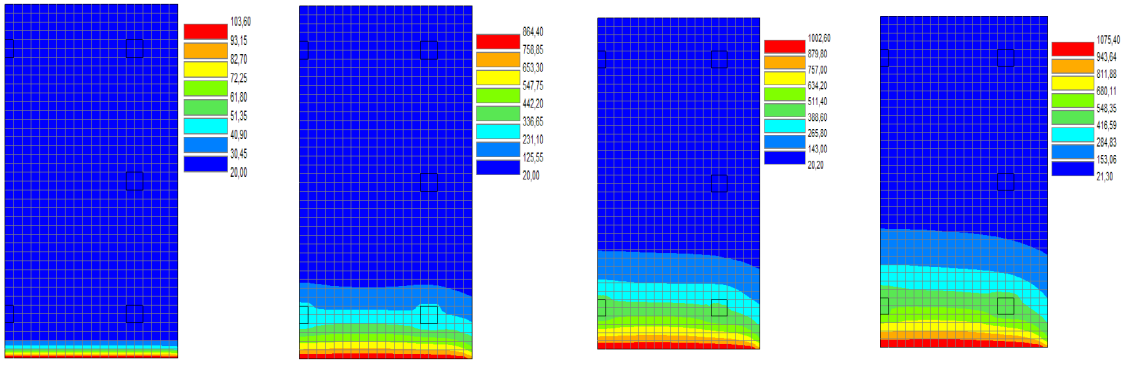

Fig.3.14. – Temperature profiles (ºC) of half column cross-section.

In Figure 3.14 it is possible to observe the evolution of temperature profile of the columns exposed to the ISO 834 fire curve only in the internal side. A careful examination of temperature around the reinforcement yields local disturbance in the concrete, which is explained by the fact that steel presents a greater thermal conductivity than concrete does.

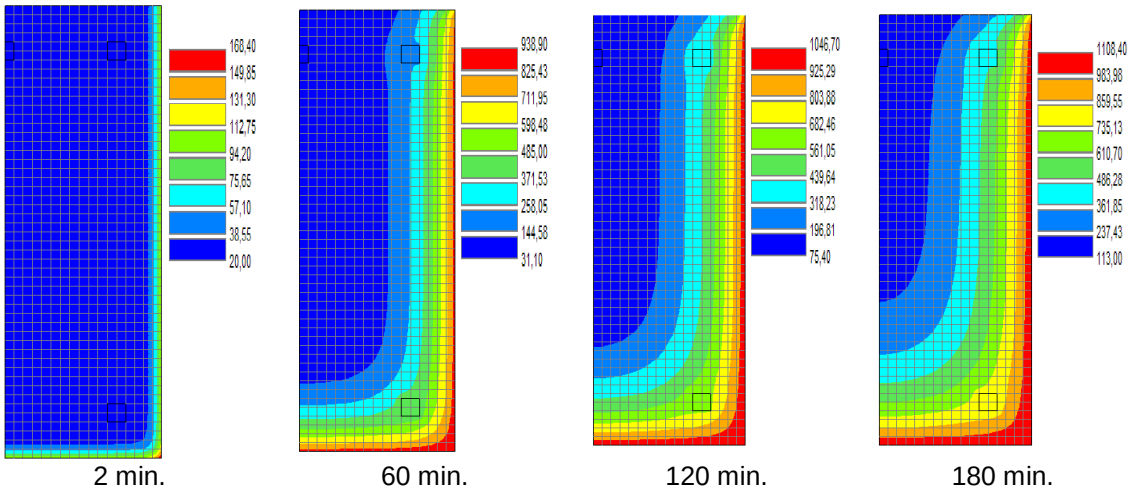

Fig.3.15. – Temperature profiles (ºC) of half beam cross-section.

From the observation of the temperature profiles shown in Figure 3.15 similar conclusions are withdrawn, but in this case, a steeper evolution of cross-section's temperature is remarked, due to the wider exposed surface of the beam in relation to the columns. Figure 3.16 illustrates the evolution of temperature in the exposed column's reinforcement compared against the compartment gas temperature (given by ISO 834 curve). In Figure 3.17 the same analysis is performed in relation to the beam.

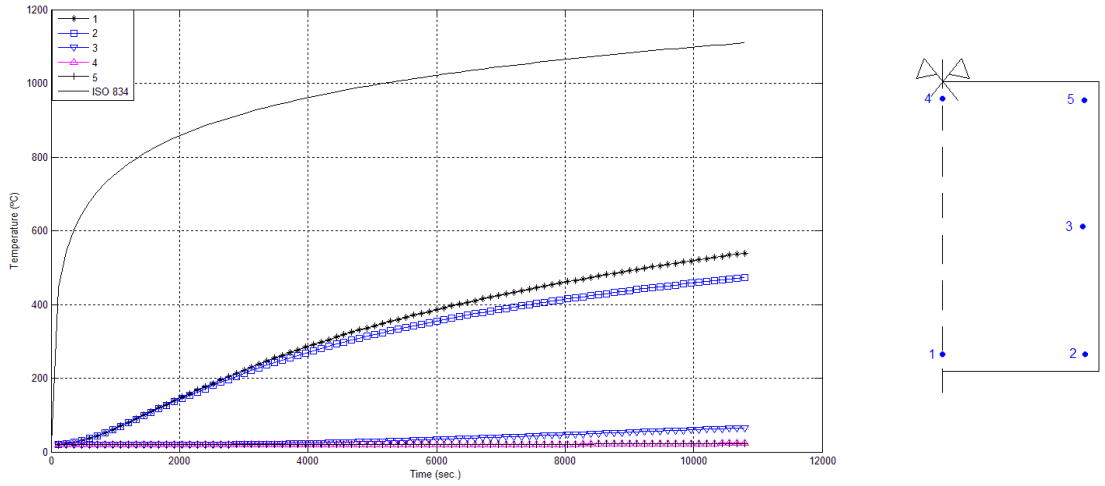

Fig.3.16 –Temperature evolution in the column's reinforcing steel bars.

In Figure 3.18 is plotted the evolution of temperature within the exposed column cross-section. The temperatures are recorded for different depths along the vertical symmetry line. In figure 3.19 the same analysis is performed in relation to the beam.

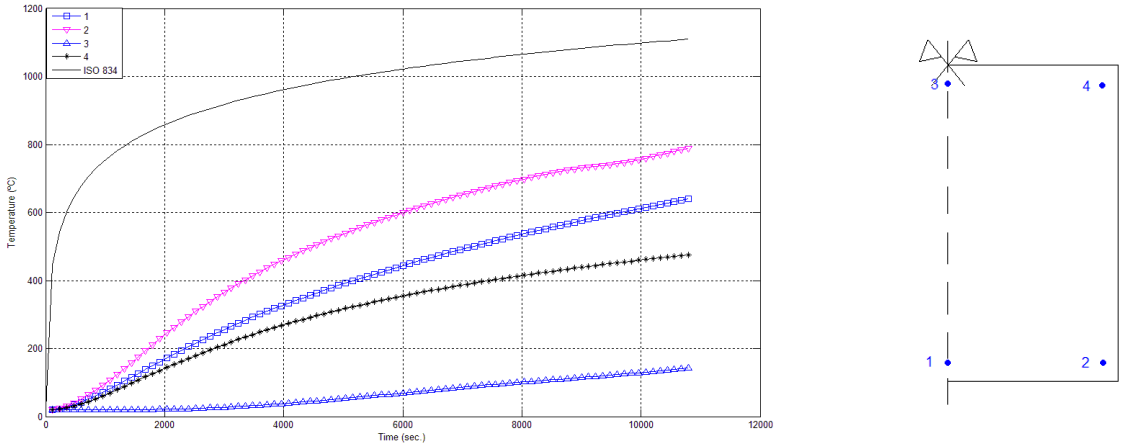

Fig.3.17–Temperature evolution in the beam's reinforcing steel bars.

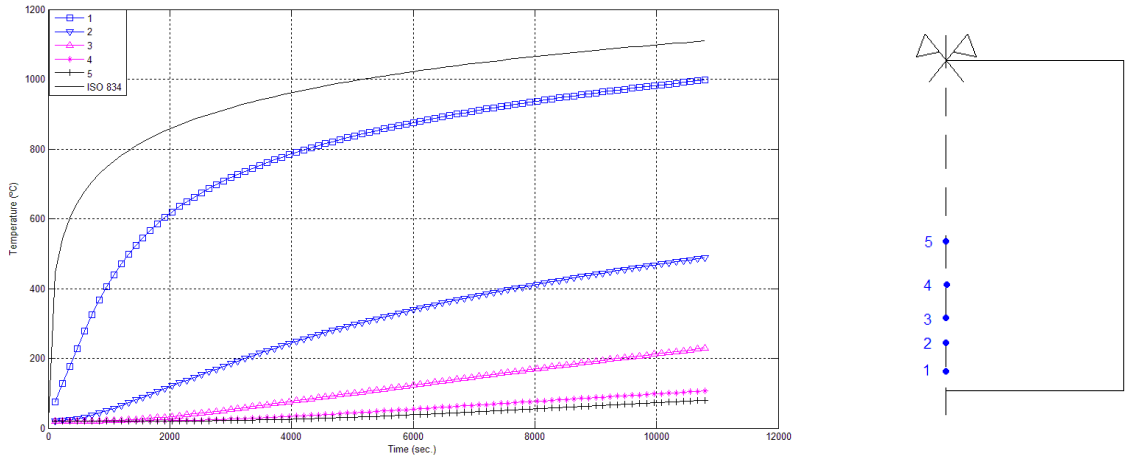

Fig.3.18 –Temperature evolution within column's cross-section.

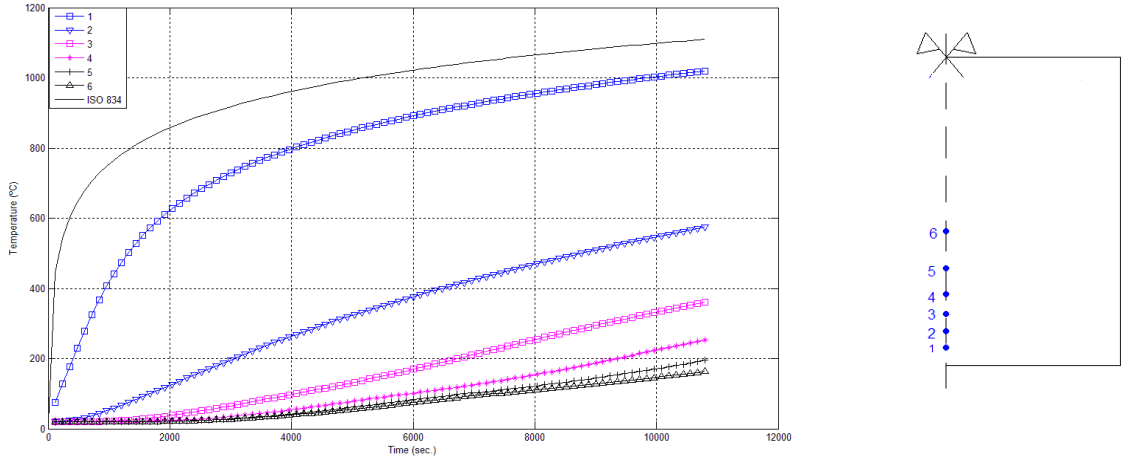

Fig.3.19 –Temperature evolution within beam's cross-section.

3.4.3. STRUCTURAL MECHANICAL RESPONSE

To carry out the structural analysis, considering the problem's symmetry conditions, the mesh illustrated in Figure 3.20 has been used. Elements 1 to 10 are exposed to fire just in the inner side, while elements 16 to 20 present the bottom and lateral sides exposed. Elements 11 to 15 remain at ambient temperatures (20ºC). In the same figure, it is possible to observe the boundary conditions in element 1 (fully fixed), element 15 (simple lateral support) and element 20 to represent the symmetry condition.

The assumptions considered during this structural analysis are:

- No spalling occurs;
- No bond failure between steel and concrete happens;
- No shear failure is considered.

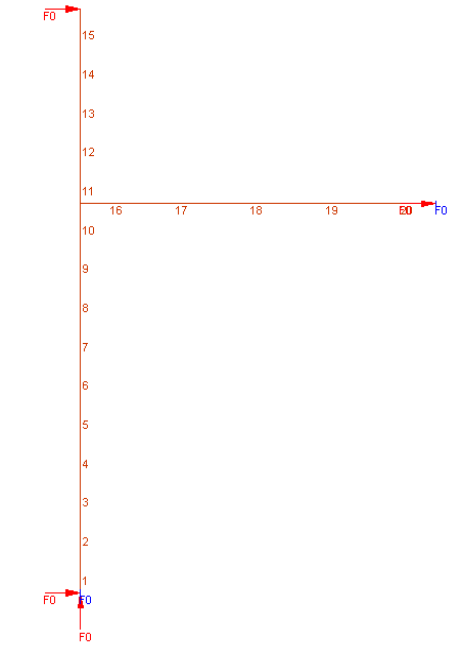

Fig.3.20 – Finite element mesh for mechanical analysis of the single-bay frame.

Although the frame in analysis has reached the final calculation time step without showing any failure, the evolution of internal stresses and displacements obtained is very representative of how redundant structures behave when exposed to fire.

3.4.3.1. Axial Force

Figure 3.21 illustrates the evolution of the axial force in the frame's beam exposed to fire. It is possible to see that prior to fire exposure the beam is, as expected, submitted to tensile force induced by the static loads. When the heating process is initiated, the beam axial force moves from tension to compression in just a few minutes due to thermal action. The heated beam tends to expand as temperature rises, but the columns impose a restraint effect, resulting in a compression force

developed in the beam. The axial force reaches a peak value of approximately 200 kN (compression) 50 minutes after the fire beginning. This highly increasing rate of axial compression is associated to heating rate imposed by the exposure to the ISO 834 standard fire curve.

After 50 minutes of fire exposure the installed axial force starts to decrease, despite the temperature never stops to rise. The main explication to this fact is found at the beam's concrete material degradation, which reduces the axial stiffness, thus, the capability of the installed force. On the other hand, the reduction in the beam's axial force may be also attributed to the degradation of the columns stiffness, which reduces their ability to impose a restraint to the beam's thermal elongation and also to the increasing horizontal displacement of the columns at the connection with the beam, that pulls the beam in the outer direction, thus relieving some part of the axial compression installed.

The variation of the columns axial force during the fire exposure is negligible. The results obtained for the frame axial force follow very closely the ones obtained in [92].

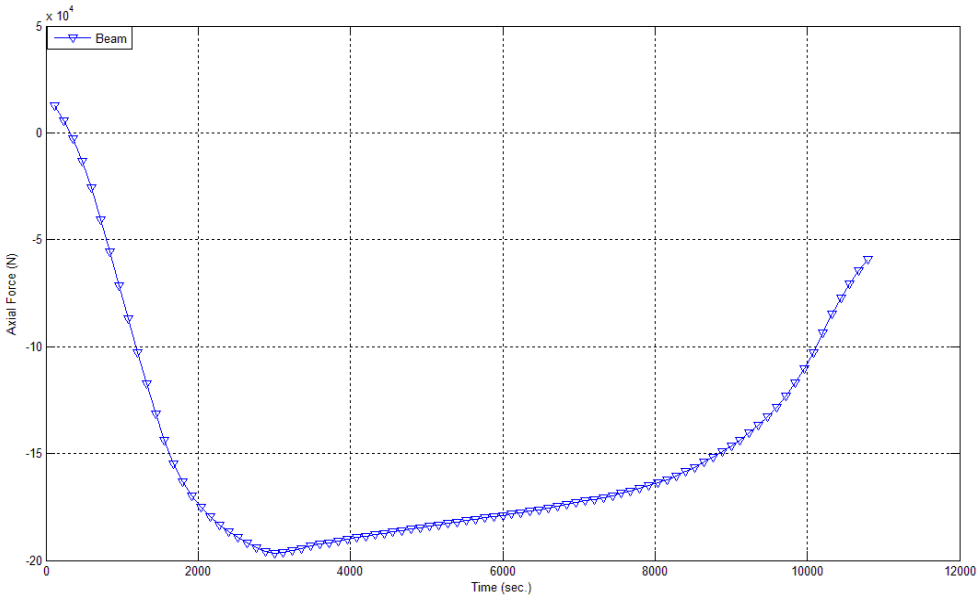

Fig.3.21 – Evolution of axial force in the beam exposed to fire.

3.4.3.2. Bending Moment

The evolution of bending moments during the fire exposure in the key points of the frame is plotted in Figure 3.22. In that figure the points analysed are identified by the corresponding finite element previously represented in the mesh of Figure 3.20. In this way, element 1 refers to the column's support, element 10 to column's top, element 11 to the bottom of the up storey column, element 16 to the beam's connection with the columns and finally element 20 to beam's mid-span.

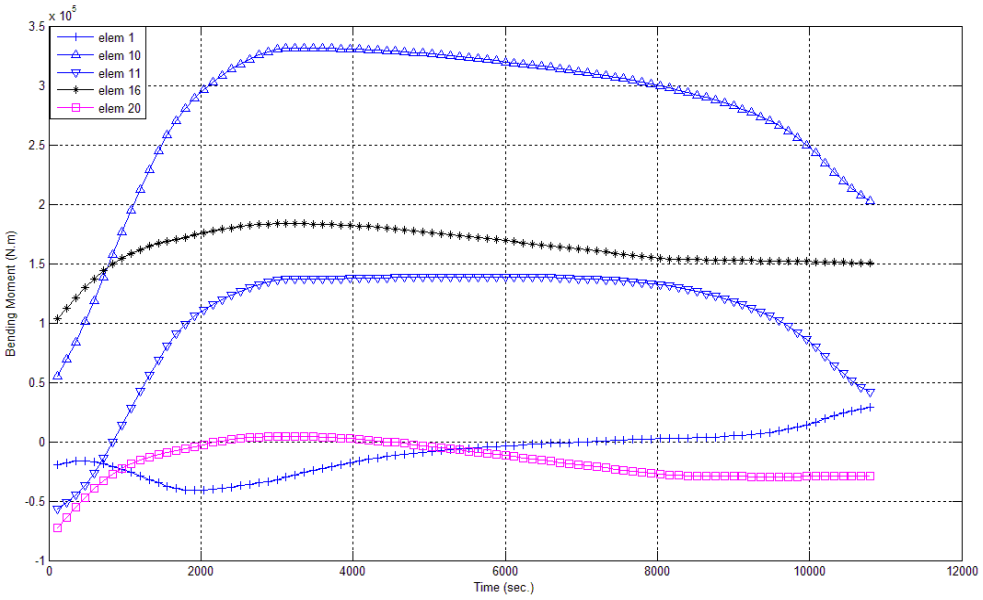

Fig.3.22. – Evolution of bending moments in several points of the frame.

As a first observation to the results obtained in Figure 3.22, it is imperative to acknowledge that the frame's bending moment field changes completely its form since the beginning of the fire, which is impossible to understand relying only in sectional simplified methods of structural fire safety assessment. It is also noteworthy the fact that, the bending moment in some points, such as in the top of the heated column, reaches values seven times greater than the ones at ambient conditions.

When the fire process begins, due to the flexural restraint imposed by the columns, the thermal gradient within the beam's cross-section originates a constant hogging bending moment along the beam. This explains the upward shift observed in the beam's bending moment diagram (see element 16 and 20 in Figure 3.22). In the same manner, a similar process is observed in the fire exposed columns. Nevertheless, looking to the evolution of bending moment in the top of the compartment fire's column (element 10), it yields a much higher increase than the one observed in the beam. This happens because the top of the column is subjected to a drift imposed by the beam's axial expansion, which is capable of introducing elevated bending moments in that point of the structure. The bending moment evolution at the bottom of the upper floor column is also affected by the axial expansion of the beam, resulting in an inversion of the bending moment's signal, achieving values four times higher than the recorded ones at ambient temperatures (element 11 in Figure 3.20).

The bending moments in the columns keep increasing at approximately 50 minutes of fire exposure. At this point, as already referred to the case of the evolution of axial force, the beam's concrete degradation induces a decrease in the axial force, explaining why the bending moment at the top of the exposed columns (element 10) no more increases after that time instant. After the bending moment reaches its peak value, redistribution takes place between the end sections of the beam and the mid-span, promoting a downward shift in the beam's bending moment diagram. This phenomenon is observed in Figure 3.22, comparing the evolution of bending moments in the columns and in the end sections of the beam to the same values in the beam's mi-span.

The evolution of bending moment in the bottom of the fire exposed column (element 1 in Figure 3.20), shows an increase until approximately 30 minutes of fire duration, and then it starts to decrease at a constant rate, when 100 minutes after the beginning of the process it inverts the bending moment signal. After the inversion, the bending moment keeps increasing until the end of the analysis.

3.4.3.3. Shear Force

Figure 3.23 illustrates the shear force evolution during the course of the fire at the bottom of the fire exposed column (element 1), on top of the exposed column (element 10), at bottom of the upper floor column (element 11) and in the end section of the beam (element 16).

The evolutions of shear force at the extremities of the exposed column follow similar trends. The maximum shear value occurs at approximately 50 minutes of fire exposure, corresponding to the bending moment peak value. Element 11 presents an inversion of shear force signal, which is in correspondence with the recorded inversion of the bending moment at that column. The variation of shear in the beam is not important. The results obtained for shear is in accordance to the expected values, as shear evolution is directly related to the variation of bending moment between two points. In the columns, it is observed an increase in the difference between the top and bottom bending moment, to which corresponds an important variation in shear. As to the beam, the difference between end and mid-span sections remains approximately constant (the bending moment diagram only shifts up and downwards), and thus, no appreciable shear variation is recorded.

The shear value observed in the top of the exposed column reaches forces four times higher than the initial value at ambient temperature. This may constitutes a treat to the structure's integrity, but as it has been mentioned above, this model is not capable of predicting shear failure. A simplified procedure to deal with shear failure is presented in Chapter 5 of this work.

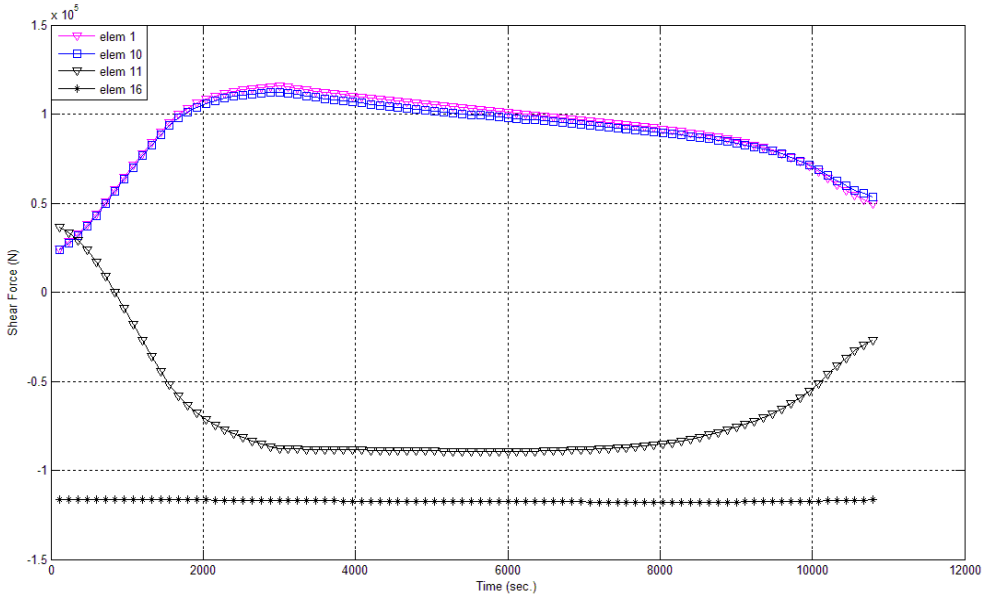

Fig.3.23. – Evolution of shear force in several points of the frame.

3.4.3.4. Structural Displacements

In Figure 3.24 the vertical displacements of the beam's mid-span and of the top of the heated column are drawn. It is possible to observe that the top of the column experiences an upward displacement, induced by the column's thermal elongation. At approximately 100 minutes of fire exposure the

elongation of the column stabilizes because the applied compressive axial load becomes preponderant in relation to the thermal elongation.

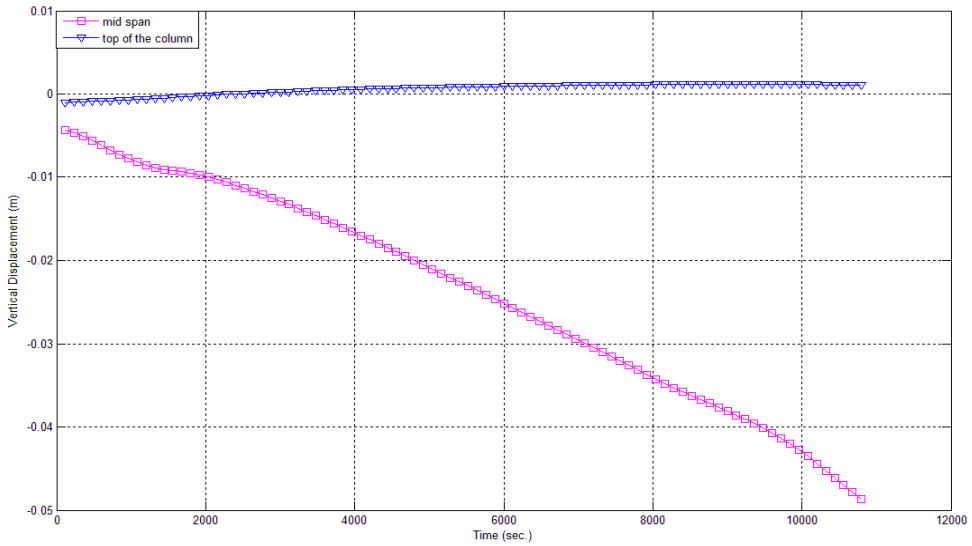

Fig.3.24 – Vertical displacements.

Now, focusing in the displacement of the beam's mid-span, it is observed that it increases very pronouncedly through the heating process, reaching approximately 5cm after three hours of fire exposure. This increase in the vertical deflection may be attributed to the stiffness loss induced by the concrete and reinforcing steel properties degradation at elevated temperatures.

In Figure 3.25 the evolution of the horizontal displacement at the top of the fire exposed column is presented. This drift, imposed by the beam's axial expansion as preciously referred, reaches a maximum value of approximately 2.3cm at the end of the analysis.

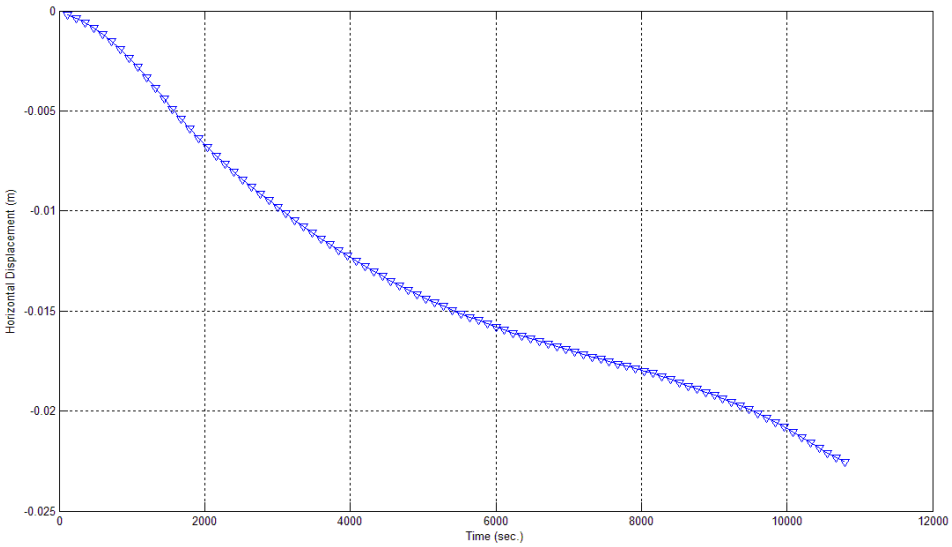

Fig.3.25 – Horizontal displacement (column drift).

3.4.4. CONCLUDING REMARKS

With the analysis above performed it is possible to understand that considering the whole frame behaviour during the course of the fire yields stresses and deformations values that are not considered when applying simplified methods of structural fire design, meaning that these methods may lead to nonconservative results.

It has been observed that the results here obtained present some differences when compared against the values presented in [92]. Although the values of bending moment, shear and axial force are quite similar, the time instant corresponding to the peak values vary from 50 minutes in this work to approximately 30 minutes in results obtained in reference [92]. This may be explained by the fact that the model presented in [92] possibly possesses a smaller reinforcement cover than the one prescribed in this work (4.0 cm). If this is true, the model presented in [92] exhibits a faster material degradation, and thus the peak values occur at earlier instants. This also explains why in the model here presented an inversion of the bending moment in the mid-span of the beam takes place, while it does not in model used in [92]. Another factor contributing to the differences in results may be found in the fact that in this work, due to modelling simplifications, reinforcing bars' cross-section are assumed with squared shape, meaning that in this work a greater effective reinforcement area is being used, compared against the circle shaped bars modelled in [92].

To conclude this section, it is a fair exercise to predict the possible failure mode that this frame would present if the analysis had been carried out for a longer period of time. Regarding Figure 3.26 it is possible to observe the evolution of mechanical strains in the reinforcement of the top of the exposed column (element 10). To understand the strain results, it must be remembered that the steel model at elevated temperatures, admits yielding at a strain of 0.02, independently of the reached temperature. Considering this, it is remarked from Figure 3.24 that both top and bottom reinforcement achieve the yielding branch. This is in conformity with the steeper decrease in bending moment observed 170 minutes after the begining of the heating process (see Figure 3.22). As these sections reach their ultimate capacity, a great amount of bending moment redistribution would occur towards the beam's mid span until a plastic hinge appears in this section.

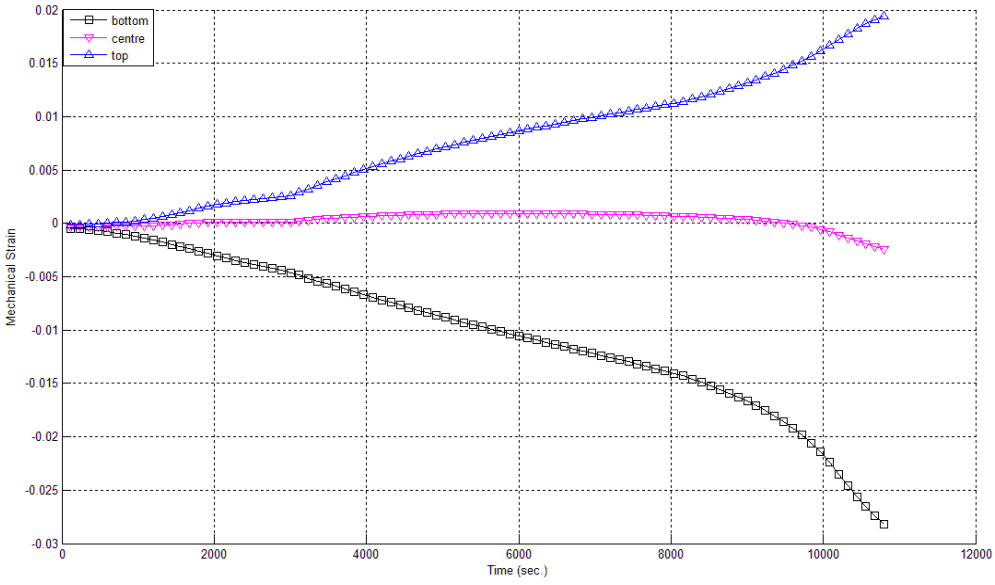

Fig.3.26 – Evolution of mechanical strains in reinforcing steel bars (column, element 10).

3.5. THREE- BAY FRAME ANALYSIS BASED ON ADVANCED CALCULATION METHODS

3.5.1. MODEL DESCRIPTION

This section is dedicated to the presentation of the model to be analysed in the subsequent work. This structural model is an extension of the frame proposed in [92], to which a number of modifications have been applied. Figure 3.27 illustrates the modified frame's model under analysis.
The first modification is related to the number of bays, augmented from one to three. This modification is aimed to evaluate the impact of a larger beams thermal elongation in the columns structural behaviour.

C30/37 (Siliceous aggregates)

S500

All Rebar ø20

1,2,3,4,5,6,7,8,9,10,11,12: number of the columns

1,2,3,4,5,6: number of the beams

N = 880 kN, representing the upper floors

G = 36.0 kN/m ; Q = 12.0 kN/m

p = G + 0.5Q

[m]

I, II, II, IV, V, VI: compartments

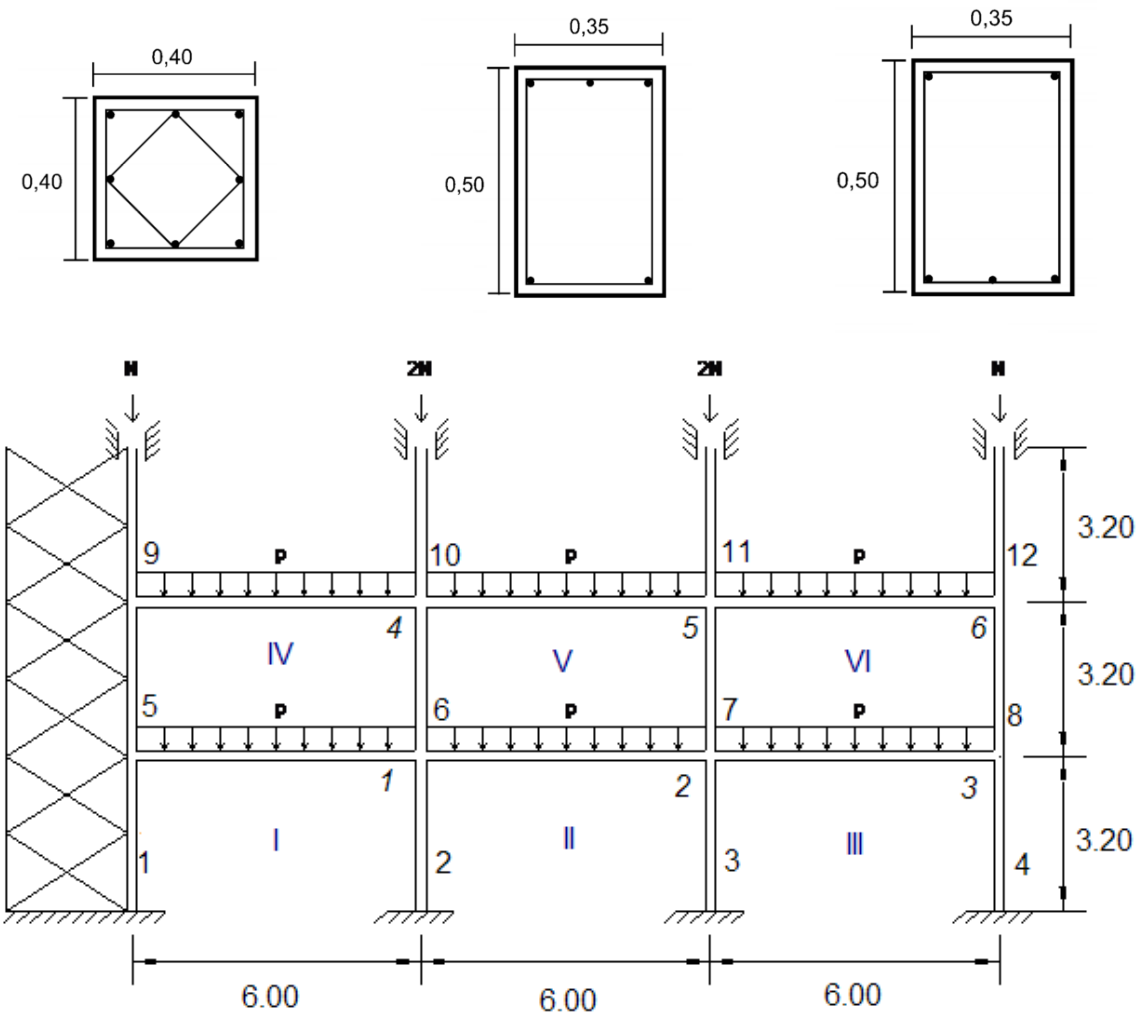

Fig.3.27 – Three-bay frame model.

The second modification is the introduction of a lateral restraint to horizontal displacements at the level of the floors. This characteristic is intended to simulate the presence of a bracing system, such as a central concrete core for the elevator shaft, quite common in real concrete buildings. This restraint is responsible for the fact that the thermal elongation of the beams is directed towards only one direction, in opposition to the expansion recorded in the previous single-bay frame. It is obviously an unfavourable condition to the structure, as it imposes a greater drift in the outer columns. However, as already mentioned, this situation is suitable to real structures, and constitutes a structural condition not often investigated by other authors.
A third modification is added to the structural system, related to the form how the existence of upper floors is modelled. In the frame presented in Figure 3.12 the presence of the upper floors was simulated by the introduction of half columns' length between contiguous floors, assuming that an inflection point exists in the columns mid-height [92]. Then, an axial force representing the load of the upper floors is applied directly at the top of superior columns. It is believed, however, that this structural solution may introduce an excessive horizontal force, by the restraint of the horizontal displacement at mid-height. Although it is reasonable to assume an inflection point at this level, considering no horizontal displacement is not strictly true. For this reason, the influence of the upper "cold" floors is modelled by the introduction of the entire columns length between contiguous floors. These columns are assumed to be fully fixed in rotation at the top and horizontally restrained but allowed to translate vertically, as proposed in [100] and [101] .

3.5.2. FIRE INPUT AND THERMAL ANALYSIS

Fire action is regarded with the evolution of the compartment gas temperature given by the ISO 834 standard fire curve. The values previously presented in Figure 3.13 remain valid to the subsequent analyses. In the next section, the fire scenario summarized in Table 3.3 is considered. The heating process is simultaneous in all fire exposed compartments.

Table 3.3 – Definition of fire scenario.

Fire Scenario	Fire curve	Compartments in fire
1	ISO 834	I, II, III, IV, V, VI

In opposition to the thermal analysis performed in section 3.4.2, the columns are assumed to be exposed to fire along their whole perimeter. This assumption is of course suitable to the interior columns, when the fire is completely spread throughout the entire floor. As to the outer columns this assumption may be too severe, because these columns may keep a part of their surface not directly exposed to fire. However, for the sake of simplicity, and because of the uncertainty related to real surface of exposure, the columns within fire compartments are assumed heated from all sides. The beams' heating conditions remain the same as presented in section 3.4.2, meaning that they are exposed to fire from the bottom and lateral surfaces. Even when the top of the beam is located within the compartment, such as in the fire Scenarios comprising fire in the second floor, thus exposing the top of the first floor's beams, this surface is considered under adiabatic conditions (remaining at ambient temperature - 20ºC). To justify this assumption it may be argued that usually there is a considerable insulation cover on the upper side of the floor, reducing the amount of radiation reaching the actual concrete slabs and beams while convection keeps the hottest gasses away from the floor [100].

Figure 3.28 shows the temperature profiles for different time steps of a whole perimeter exposed column (this profile is valid to all fire exposed columns in this analysis). Comparing these results to the previously obtained in Figure 3.14, it becomes clear how unfavourable this heating condition is.

For the same time steps, the depths of concrete layers with temperatures higher than 500ºC are larger in Figure 3.28 compared against Figure 3.14. In Figure 3.29 the evolution of temperature in reinforcing steel bars as function of time is plotted. In Figure 3.30 is plotted the temperature evolution within the column's cross-section measured along the vertical symmetry line at different depths. The temperature evolution previously given in Figure 3.15, Figure 3.17 and Figure 3.19 regarding the beam's cross-section remain valid for the analysis to be performed hereafter.

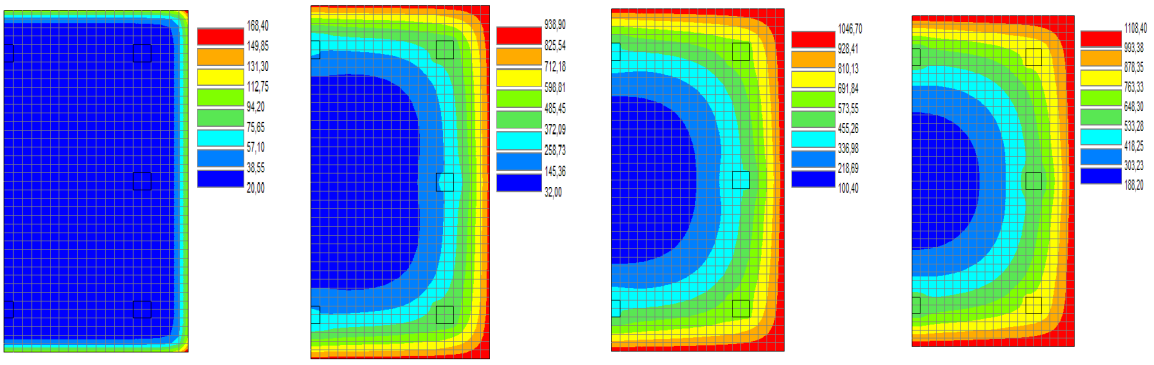

2 min. 60 min. 120 min. 180 min.

Fig.3.28 – Temperature profiles (ºC) of half column cross-section.

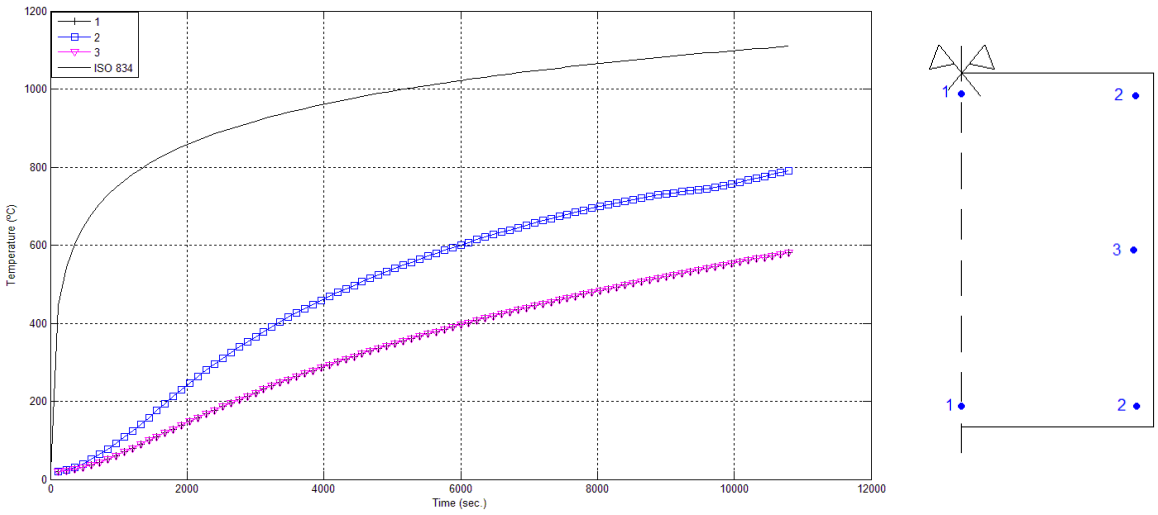

Fig.3.29 –Temperature evolution in the whole perimeter exposed column's reinforcing steel bars.

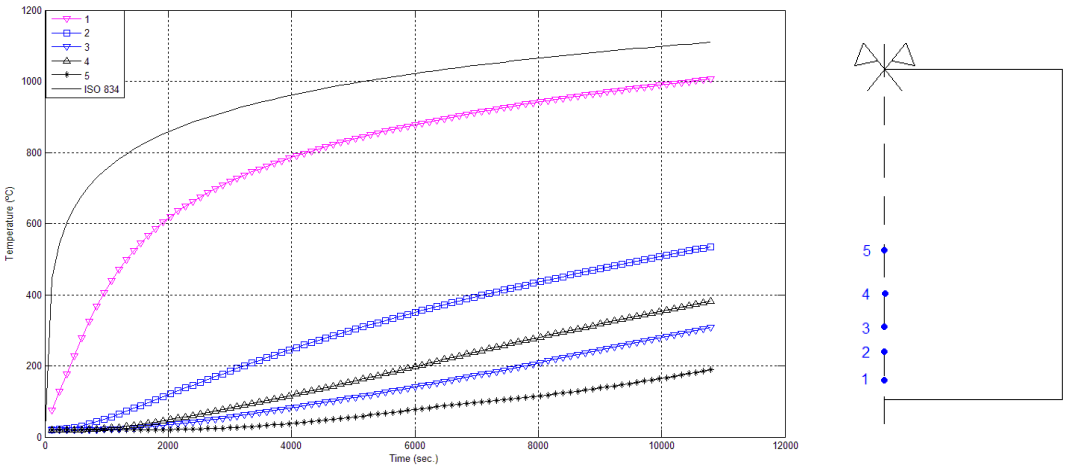

Fig.3.30 –Temperature evolution within the whole perimeter exposed column's cross-section.

3.5.3. FINITE ELEMENT MODEL FOR MECHANICAL ANALYSIS

The structural mechanical analysis of the reinforced concrete frame exposed to the fire scenario mentioned in Table 3.3 is based in the finite element mesh presented in Figure 3.31.

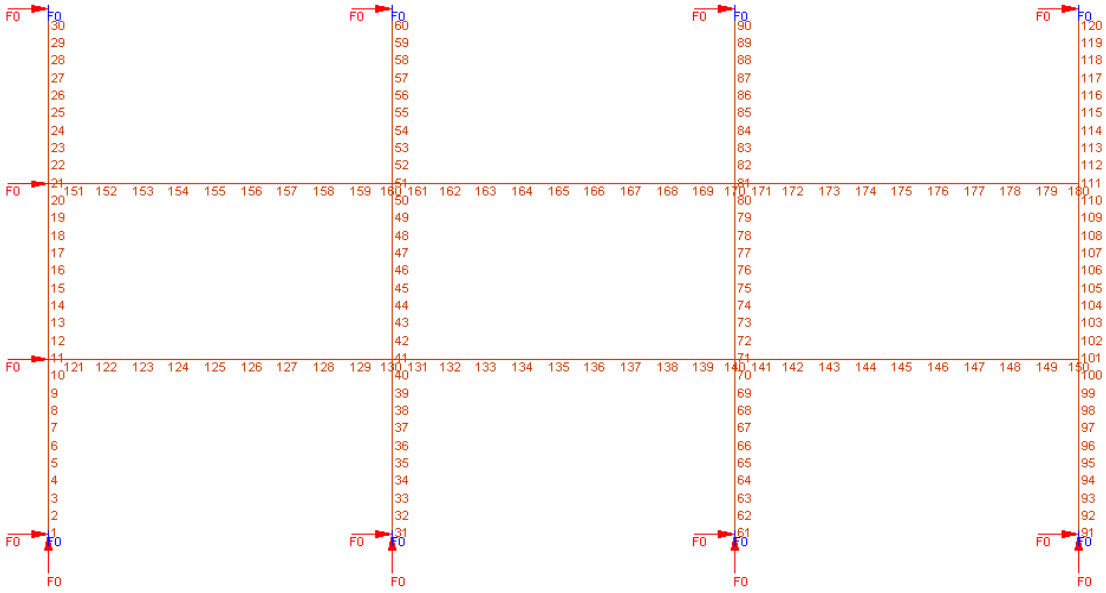

Fig.3.31 – Finite element mesh for structural mechanical analysis.

All structural elements (beams and columns) are divided into 10 finite elements. The columns are modelled with constant reinforcement along their length. The beams are modelled considering a reinforcement layout of three bars in the top and two in the bottom on the three finite elements adjacent to the beam's ends, and two bars in the top and three bars in the bottom on the four finite elements at the span.

The bracing system is simulated by the horizontal restraint applied at the level of the floor (elements 10 and 20). The columns representing the upper floors are fixed at the top, restrained horizontally only.

3.5.4. MECHANICAL ANALYSIS: SCENARIO 1

3.5.4.1. Axial Force

The evolution of the axial force in the beams is illustrated in Figure 3.32. A first remark is made concerning the evolution of axial force in the different beams at the same floor level. In this way, it is possible to observe that the axial compression increases as beams are closer to the bracing system (left end of frame, see Figure 3.31). The reason for this is found in the fact that the closer to the bracing system a beam is located, the greater the horizontal restraint is.

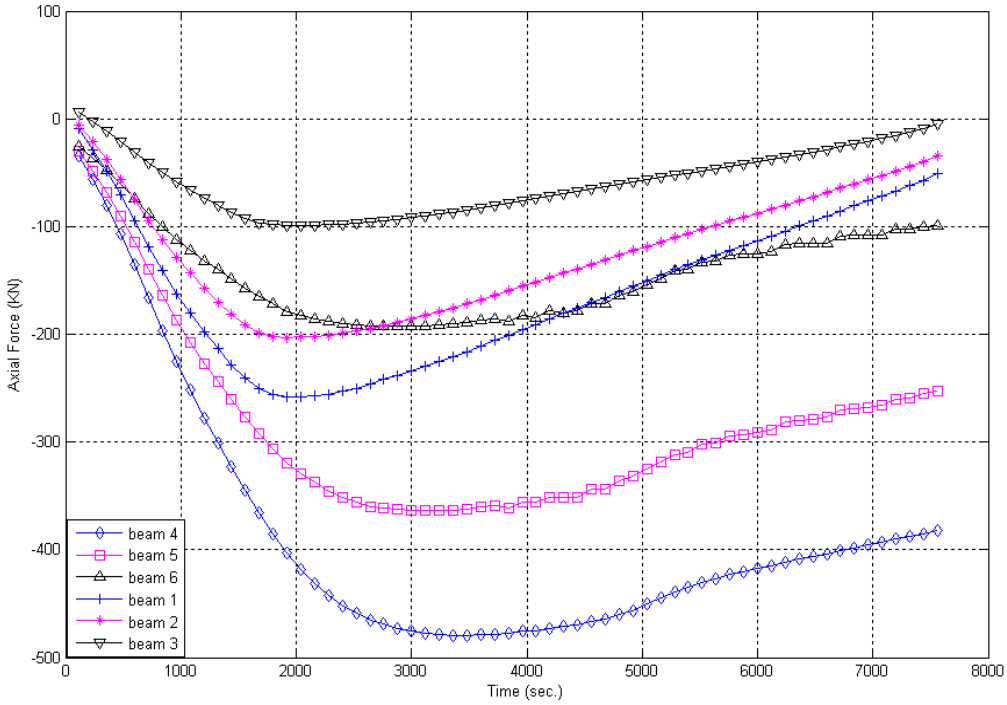

Fig.3.32 – Evolution of axial force in the beams.

A second remark is directed to the fact that the beams of the second floor (beams 4, 5 and 6) present a higher compressive force than the corresponding first floor beams (1, 2 and 3). Once again, the difference in horizontal restraint conditions is the explanation for this effect. Apart of the bracing system, the columns play a role in the horizontal restraint to the beams thermal elongation with its flexural stiffness. It is understandable that the beams in the first floor are linked to columns 1 to 8, which are subjected to fire, while the second floor beams are linked to columns 4 to 12, where half of them (columns 9 to 12) remain at ambient conditions. After these statements, it immediately yields that the first floor beams have less horizontal restraint than the second floor ones. This explains why the axial compression is higher in the second floor, as well as why the maximum value of axial compression is achieved sooner in the first floor beams (approximately after 33 minutes of fire exposition, in opposition to approximately 50 minutes in the second floor), even when the materials deterioration in the two floors beams follows the same process.

3.5.4.2. Bending moment

As it was already observed in the single-bay frame, the bending moment field suffers a considerable change during the course of the fire, including in the cold parts of the frame. Figure 3.33 presents the evolution of bending moments in key points of the frame's columns. The bending moment at the top and bottom of column 4 (elements 100 and 91, respectively) displays a symmetrical path during the course of the fire, as it was expected. The bending moment at these points reaches a peak value approximately after 40 minutes since the beginning of the heating process (250 kNm). It is observed that this is the instant when the maximum axial force in the first floor's beams occurs. After then the bending moment in this column decreases until the structural failure is achieved. Looking now to the elements 101 and 110, respectively the bottom and top of column 8, the bending moment values follow similar trends, not symmetrical. This happens because both first and second floor are imposing a drift to the ends of the column, meaning that the bending moment diagram suffers a shift in one direction.

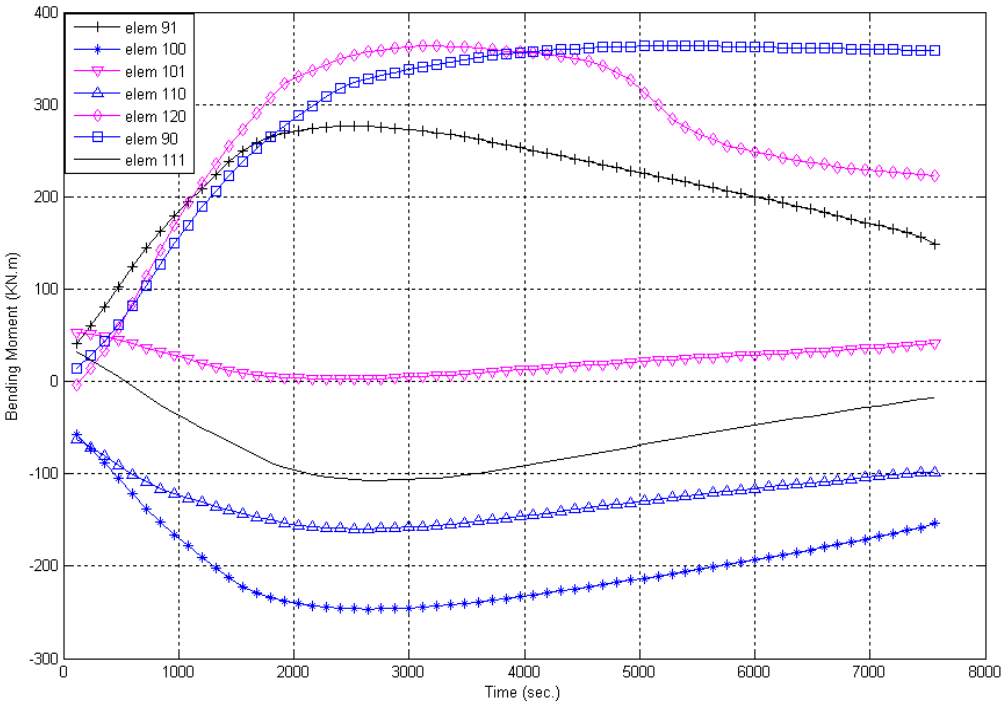

Fig.3.33 – Evolution of bending moment in columns of the frame.

Interesting results are observed in the cold columns of the frame: in Figure 3.33 the evolutions of bending moments in elements 111 and 120 (bottom and top of column 12) show inversion of signs in the earliest stages of the fire. The bending moment at the top of that column suffers a great increase, which stabilizes approximately at 50 minutes of fire exposure, presenting a steeper decrease approximately at 80 minutes. As to element 90, top of column 11, it displays an increase, reaching the value of 470 kNm about 80 minutes since the beginning of the fire, keeping this value throughout the rest of the analysis.

Figure 3.34 illustrates the evolution of bending moments in key points related to the beams. Elements 131 (left end of beam 2) and 135 (mid-span of beam 2) present a variation in the same direction, meaning that the beam's bending moment diagram shift upwards due to the flexural restraint to the rotation induced by the thermal gradient along the beam's cross-section. As a result of this, an inversion of the bending moment sign is recorded 17 minutes of fire exposure at mid-span. The

bending moment diagram keep its shift upwards until 60 minutes of fire duration, when due to materials deterioration it starts redistributing to the mid-span.

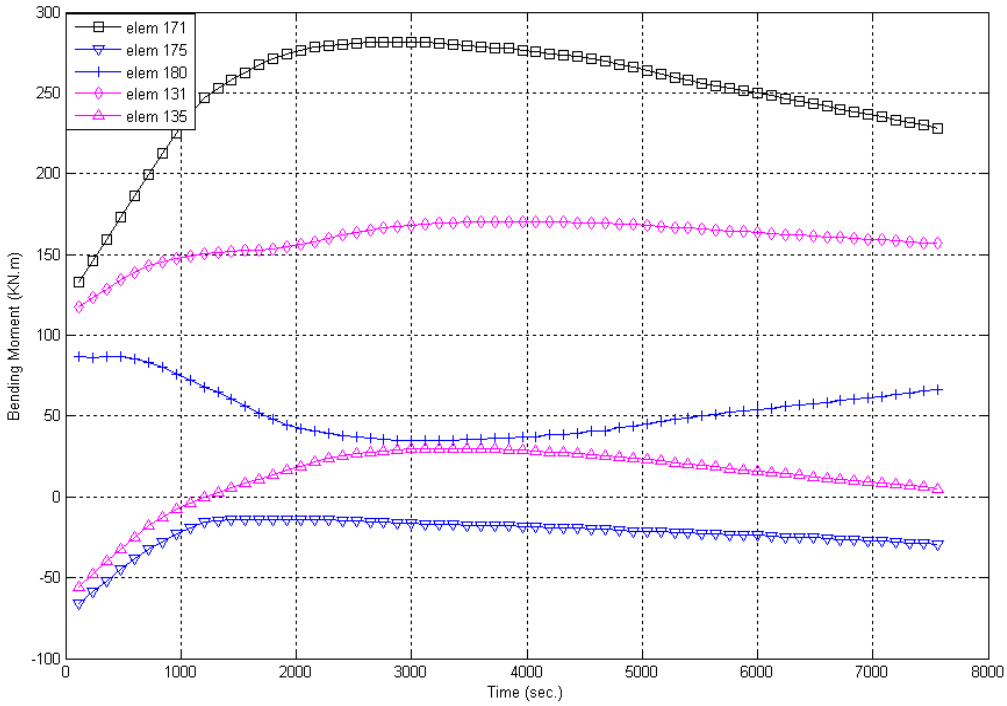

Fig.3.34 – Evolution of bending moment in beams of the frame.

Elements 171 and 175 perform similarly, this time related to beam 6. The first remark is related to the fact that the bending moment in the beam's left end (element 171) reaches values higher than those obtained to the previous beam. This may be explained by the fact that this beam is located in a stiffer part of the frame, possessing a column not exposed to fire, enabling the bending moment in the end of the beam to reach higher values. In opposition to the previous beam, in this case no inversion of bending moment sign is observed in the beam's mid-span. This happens because the beam's right end flexural restraint is imposed by column 8 and 12, which is lesser than compared with the left end restraint, which comprises beam 5 to increase the restraint. Moreover, column 8 is exposed to fire, thus its capacity to impose a restraint decreases with time. This explains why bending moment in element 180 presents a descending branch, and why the bending moment never switches sign. In Figure 3.35 a schematic illustration of the bending moment diagram in the whole frame is presented for three time steps. Figure 3.35*a* corresponds to the static bending moments at the beginning of the process. In Figure 3.35*b*, it is shown the configuration of bending moment diagram at the time step when the maximum bending moment in the top of column 4 is achieved (approximately 40 minutes of fire exposure). At last, Figure 3.35*c* presents the bending moment diagram at the last converged time step (126 minutes) before structural failure. It is possible to observe that, due to the materials deterioration, the bending moment values at the columns has decreased since the time step correspondent to Figure 3.35*b*. Focusing in columns 3, 4 and 8 at Figure 3.35*c*, it immediately yields the non-linear configuration of the bending moment diagram, which is revealing second-order effects in columns exposed to fire, combining axial compression and horizontal drifts, resulting in important P-delta effects.

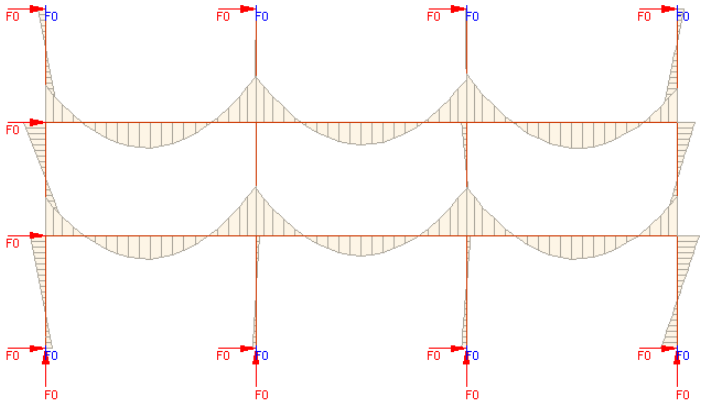

a)

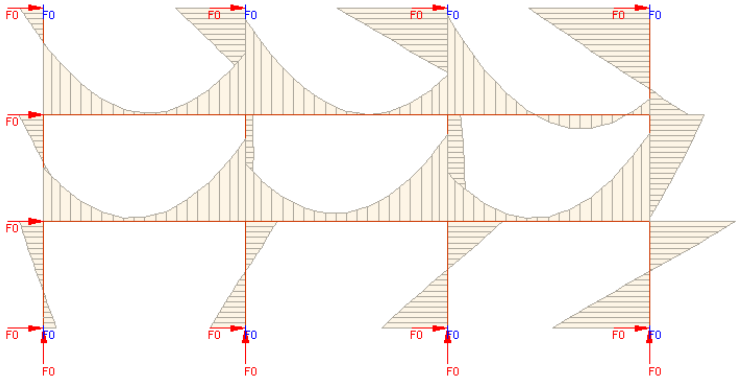

b)

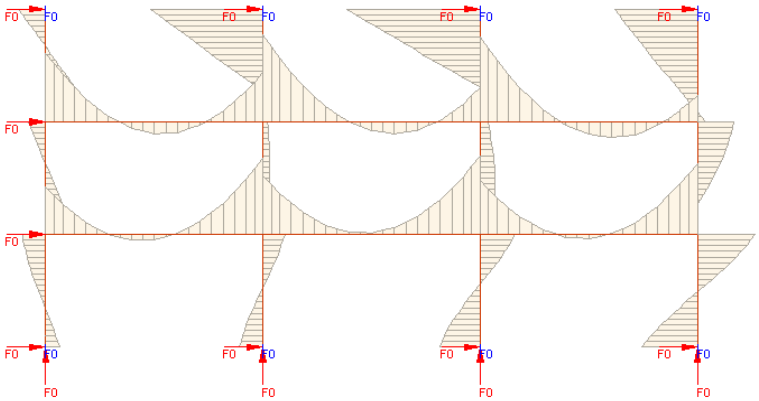

c)

Fig.3.35. – Schematic representation of bending moment diagrams: a) 0 min; b) 40 min; c) 126 min.

3.5.4.3. Shear force

Figure 3.36 presents the evolution of shear force in the representative points of the structure regarding this effort. As it has been previously observed during the single-bay frame analysis, the shear force evolution in beams is not relevant compared against that evolution in the columns. Following the evolution of shear force in element 171, correspondent to the left end of beam 6, the last statement is corroborated.

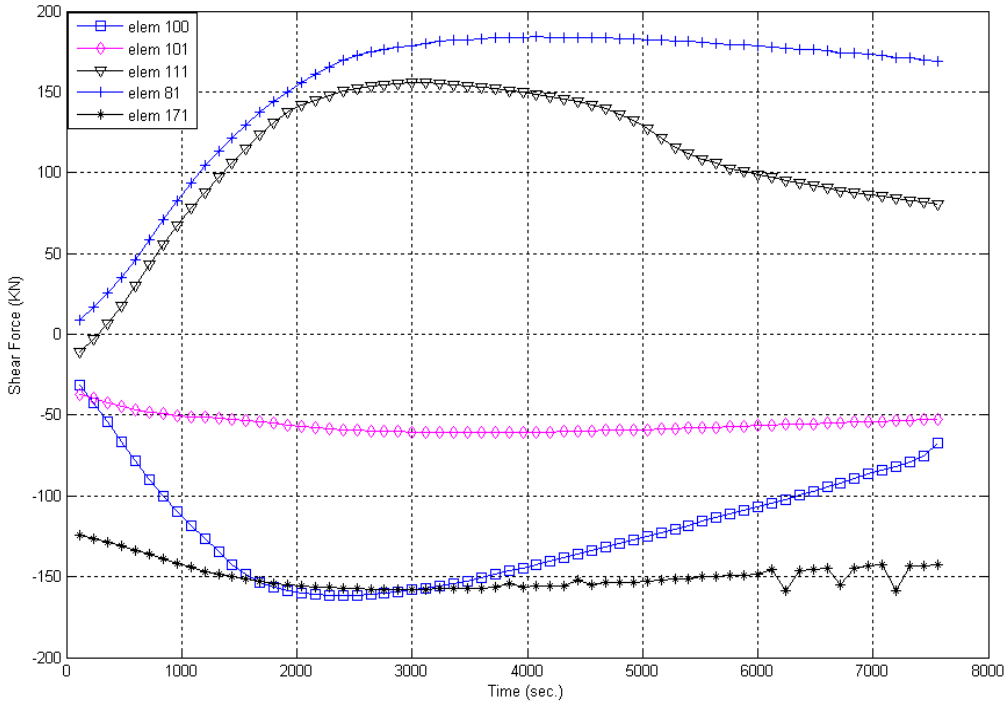

Fig.3.36 – Evolution of shear force.

The evolution of shear force in the top of column 4 (element 100) presents a steeper increase during the initial stages of the fire, which is in conformity with the bending moment evolution in that column. The maximum value obtained is approximately 160 KN. A different conclusion is withdrawn for the shear evolution in column 8, represented by element 101 (bottom of the column). It is observed in Figure 3.36 that the shear variation is almost inexistent in this column. The reason for this, is found in the fact that both ends of the column are subjected to horizontal drifts, meaning that the whole column suffer a similar translation, keeping the same proportion between the ends bending moment, thus presenting no significant shear variation.

An important remark should be made regarding the effects of fire in shear force evolution in the cold parts of the frame. For instance, elements 111 and 81, representing the bottom of columns 11 and 12 respectively, constitute a case where these effects are quite evident. The shear force recorded in these columns outstands completely the initial values before the fire process. As it has already been remarked in the analysis of bending moment of these columns, the shear force in column 11 does not exhibits a decrease during the course of the fire, while column 12 does. This may be an indicative that this last column has failed, even considering that it is not directly exposed to fire. In a similar fashion to the analysis of bending moment evolution, Figure 3.37 displays the shear force diagram for three

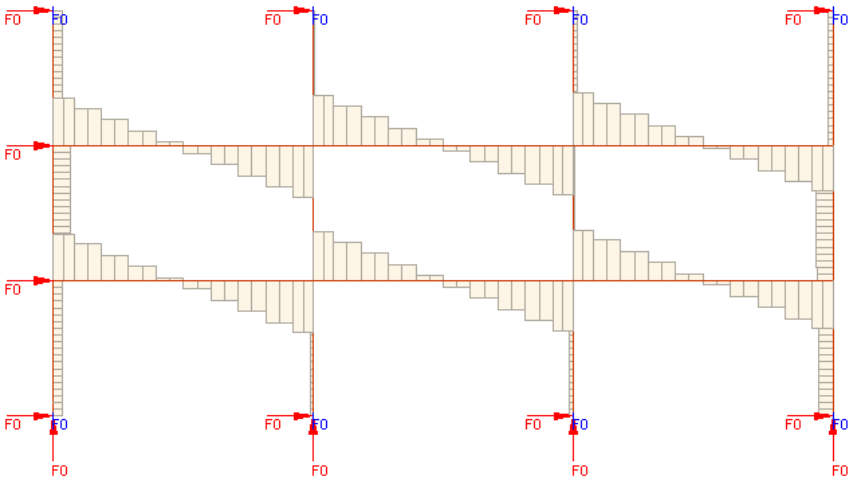

a)

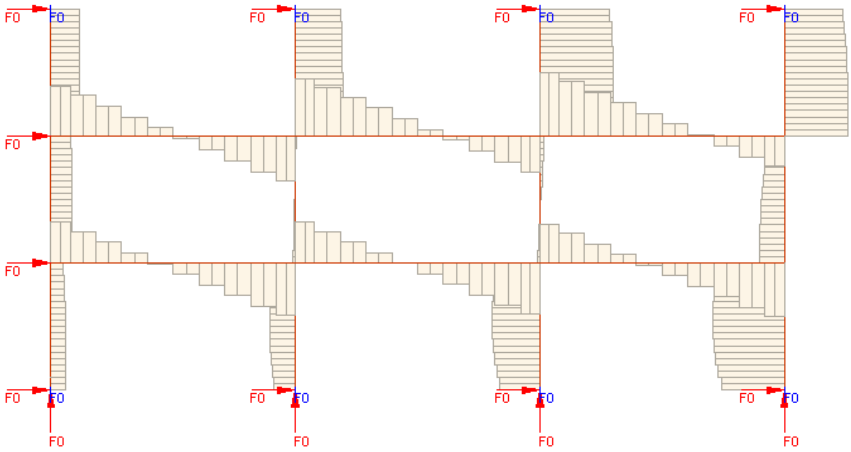

b)

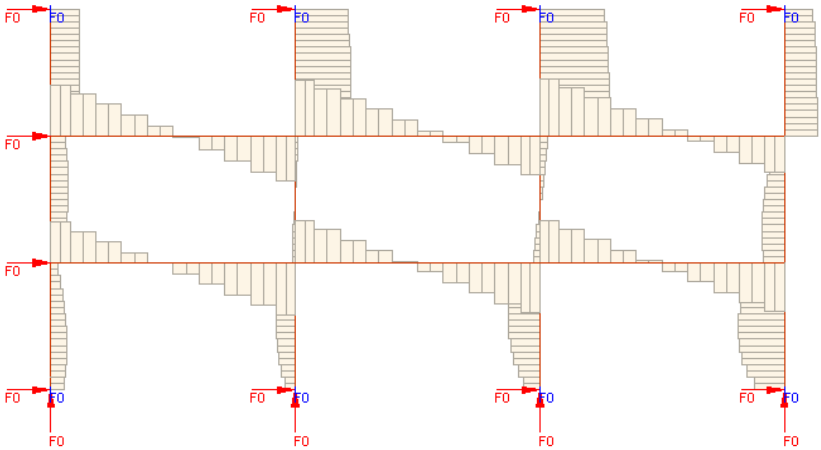

c)

Fig.3.37 – Schematic representation of shear diagrams: a) 0 min; b) 40 min; c) 126 min.

time steps, namely, before the beginning of the fire (Figure 3.37*a*), after 40 minutes of fire exposure (Figure 3.37*b*) and in the last converged iteration 126 minutes after the beginning of the process (Figure 3.37*c*). It is possible to observe in Figure 3.7*c* that the shear force in lower columns is far from being constant, which is related to the non-linearity of the bending moment diagram installed in those elements.

3.5.4.4. Structural displacements

Figure 3.38 illustrates the evolution of horizontal displacements in several points of the frame. The drifts obtained are of considerable importance. The top of column 4 reaches a value of 11,9 cm and the top of column 8 10,3 cm. The reason for this difference relies in the different floor stiffness already discussed when analysing the evolution of axial force. At the mid height of column 12 a horizontal displacement of 4,7 cm is recorded at the last time step, corresponding approximately to half drift at the top of column 8.

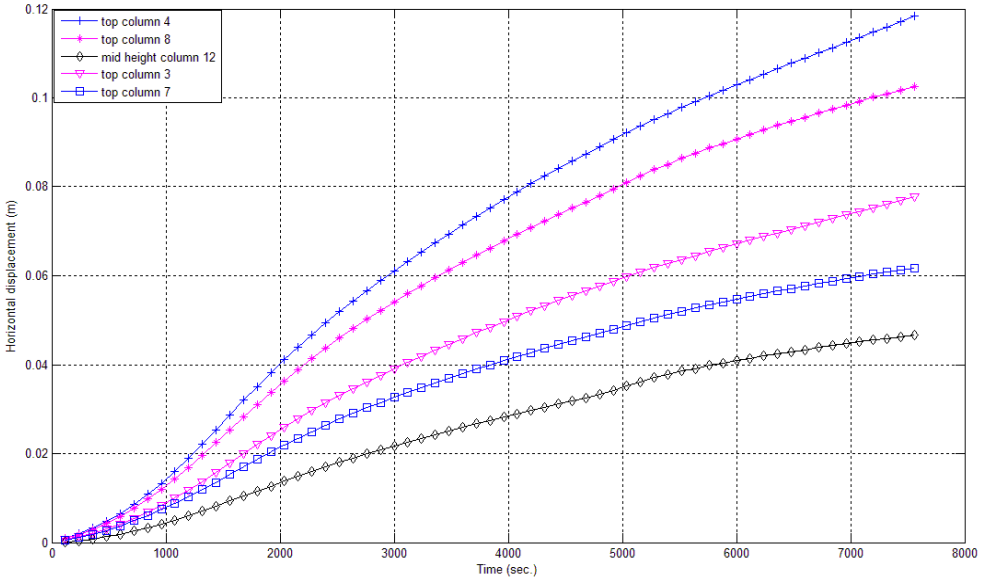

Fig.3.38 – Evolution of horizontal displacements.

The vertical displacements at the mid span of the frame's beams are plotted in Figure 3.39. All beams present a downward displacement in the initial stage of the process due to the static loads. Then, in result of the thermal expansion of the columns an upward displacement is recorded. Finally, the materials deterioration induced by elevated temperatures results in a reduction of the beams stiffness and in a decline of the effects of columns thermal elongation, thus the vertical displacements return to a downward trend. The maximum mid span displacement is achieved in beam 6, with the value of 2.4cm in the final converged time step of the calculation procedure. Figure 3.40 presents the vertical displacements related to the frame's columns. It is possible to observe that, although the initial displacements are negative, induced by static load, during the analysis the displacements recorded are upward directed, as previously stated, because of the columns' thermal expansion. The difference between the values obtained in the top and bottom of the columns are a measure of the thermal expansion of a single column. The vertical displacements of the columns follow similar trends, stabilizing their value in the final stages of the process, due to materials deterioration and to the effect of the axial force installed in the columns. It must be remarked that the vertical displacements obtained

are a consequence of the structural model adopted. It is here remembered that, the top of the columns representing the effect of the cold part of the building are not vertically restrained.

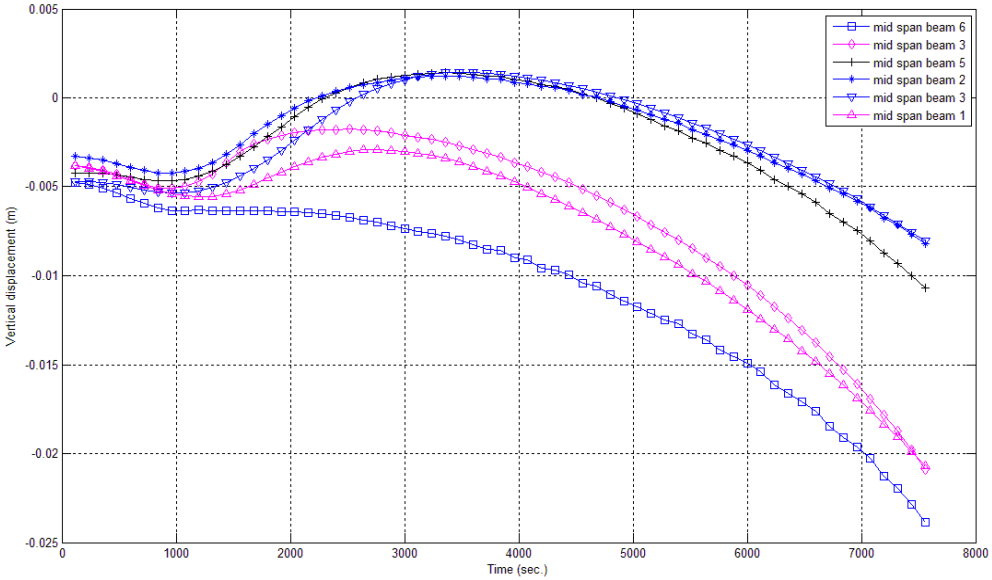

Fig.3.39 – Evolution of vertical displacements in beams' mid-span.

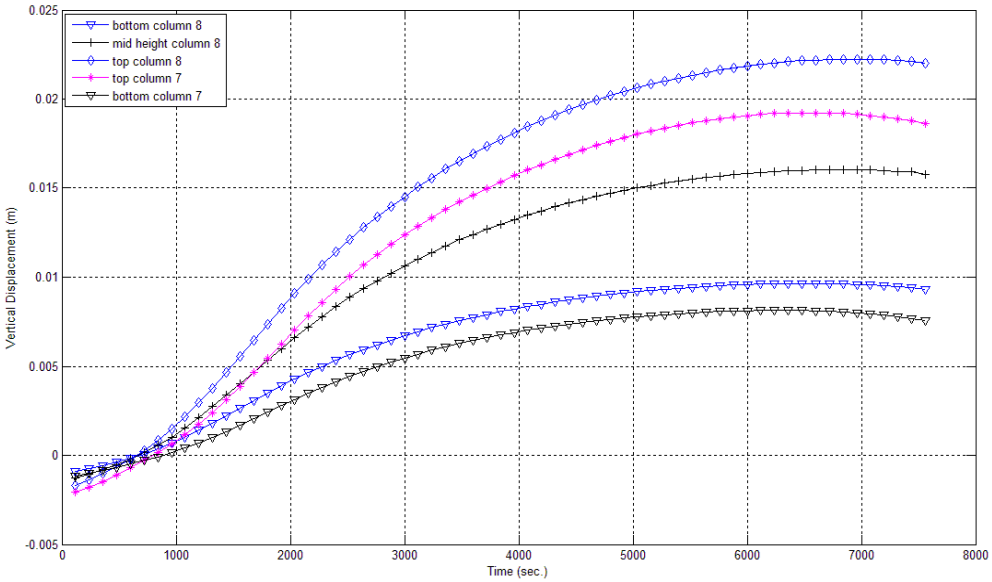

Fig.3.40 – Evolution of vertical displacement in columns.

If a different boundary condition had been considered, the results for vertical displacements would yield differently, with lower vertical displacements and higher axial restraint forces developed in the columns. However, the real restraint in these situations is of difficult quantification, thus, as other authors have proposed [100] [101], no vertical restraint has been considered in the top of the cold columns. To conclude the analysis of the structural displacements, in Figure 3.41, the deformed shape of the structure in the last converged time step of the analysis is compared against the undeformed one.

The displaced shape in Figure 3.41 is scaled 10 times against the initial frame shape, to better highlight the evolution of displacements in the whole frame.

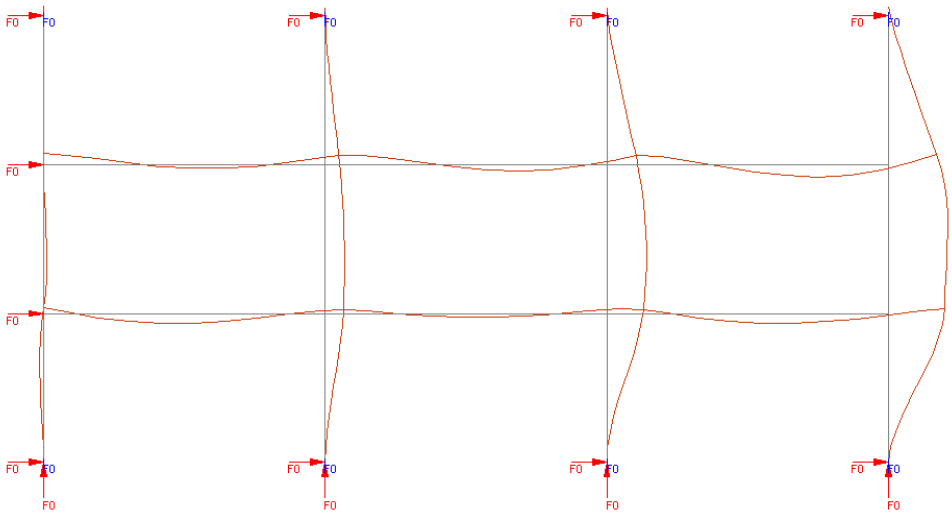

Fig.3.41 – Deformed layout of the frame at the final time step (scaled 10 times).

3.5.5. CONCLUDING REMARKS

Once again, it has been learned that considering the frame's global behaviour, during the course of the fire, outputs an evolution of internal stresses and displacements not possible to foresee relying only in simplified calculation methods that neglect structural continuity.
The analysis of the present frame subjected to the two floor fire scenario reveals another factor not covered by a simplified analysis: the effects of the restraint forces in the cold parts of the building. To clarify this situation an inspection to the mechanical strains installed in reinforcement at the top of column 12 is presented in Figure 3.42. It is observed that the tension reinforcement reaches the yielding strain (0,02 according to the constitutive model adopted) approximately 80 minutes after the beginning of the process. It is recalled that at this instant, the bending moment installed in the top of this column suffers a sudden decay.
A similar strain inspection has been performed to several cross-sections belonging to frame's beams and columns, showing that in other cross-sections no reinforcement yielding is achieved.
Finally, to understand the frame's failure mechanism, Figure 3.43 displays the mechanical strain evolution in reinforcing steel bars at the top of column 4. It is observed that, just as in the former cases, the reinforcing steel bars do not achieve the yielding strain. In spite of this, tracing the evolution of strain in the concrete fibre correspondent to the central cross-section at a 1,0cm depth from the surface, gives an indication that this section reached high compressive strains. Considering this, the structural failure may be attributed to the fact that the ultimate capacity of concrete in column 4 has been achieved.
Regarding Figure 3.43, it is observed that the mechanical strain recorded in the reinforcing steel bars located at the same distance from the neutral axis displays different values. For instance inspecting the tension reinforcement, it is concluded that the mechanical strain measured in rebar 3 is greater than the value recorded for rebar 4. To explain this, it is recalled that SAFIR considers the Bernoulli's hypothesis, where plane sections remain plane after deformation occurs. Because of this, the total strain at the reinforcement level must be constant during the analysis procedure. However, the thermal exposure is not equal to all reinforcement, meaning that the reinforcement exposed to higher temperatures tends to experience higher thermal elongation. This is precisely what happens between

rebar 3 and 4, where rebar 4 is located at the cross-section's corner, thus exposed to higher temperatures (see Figure 3.28). Nevertheless, in order to maintain a constant total strain the higher thermal strain must be compensated by a restraining mechanical strain, as the total strain in SAFIR is given by:

$$\varepsilon_{Tot} = \varepsilon_{mec} + \varepsilon_{th} \tag{3.17}$$

where ε_{Tot} is the total strain, ε_{mec} is the mechanical strain and ε_{th} the thermal strain. Now it is understood that in order to keep ε_{Tot} constant in rebar 3 and 4, and considering a higher ε_{th} in rebar 4, it immediately yields that a compressive ε_{mec} as well as a tension ε_{mec} must be introduced in the strain histories of rebar 4 and 3 respectively. That is why in Figure 3.43 the tension in rebar 3 is always higher than it is in rebar 4. The same line of thought is suitable to explain the difference between the mechanical strains recorded in rebar 1 and 2.

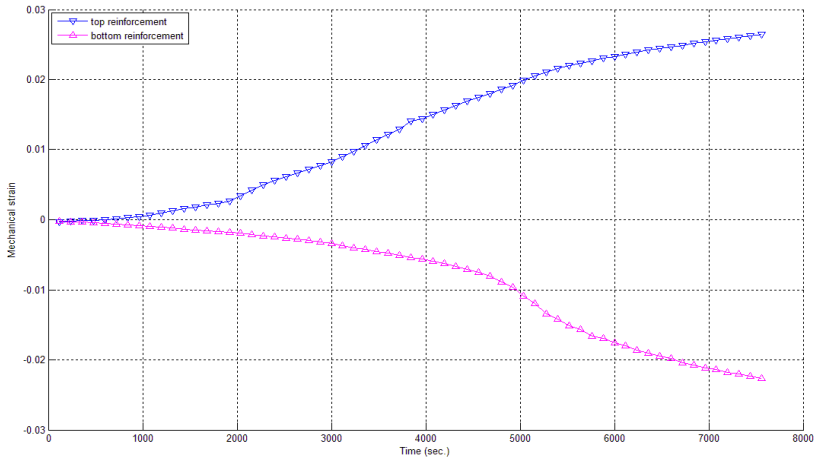

Fig.3.42. – Evolution of mechanical strain in reinforcement at the top of column 12.

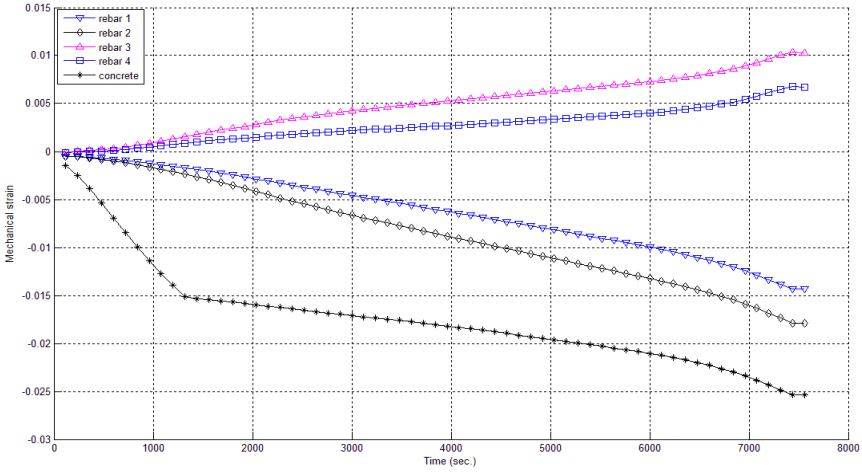

Fig.3.43 – Evolution of mechanical strain in reinforcement and concrete at the top of column 4.

3.6. COMPARISON BETWEEN GLOBAL RESPONSE ANALYSIS AND SIMPLIFIED CALCULATION METHODS

3.6.1. PROBLEM STATEMENT

As previously mentioned in Chapter 1, there are several formulations available to perform structural fire safety analysis. Practicing engineers often apply the so called simplified calculation methods rather advanced ones. This is justified by the fact that advanced calculation methods are extremely laborious, and requires a considerable amount of expertise, usually not part of the structural engineers' training. However, there are some concerns among the structural fire engineering community regarding the range of validity of the simplified calculation methods prescribed in the EN 1992 1-2 [4]. A series of works available in the literature, have shown the accuracy of the simplified calculation methods (the Isotherm of 500ºC and the Zone method) when compared against computational advanced models [15] [16]. From the results presented in the last references, it is possible to understand that, apart from several exceptional cases, the ultimate capacity of reinforce concrete elements obtained with simplified methods is close to the advanced models results, being the former conservative in relation to the last ones.

Nevertheless, these comparative studies have been performed considering a single element analysis, i.e., the simplified method is compared against an advanced calculation method where only a single element is modelled, ignoring any sort of structural continuity. This is precisely the key point in this work. It is not intended here to verify the accuracy of the ultimate capacity obtained from one kind of simpler method and the other more sophisticated, but the validity of applying simple cross-section method (ignoring fire induced actions) compared to a global frame analysis.

3.6.2. THE EUROCODE'S GUIDELINES

In chapter 1 has been referred that the EN 1992 1-2 admits three levels of verification methods: single member, part of the structure and global analysis. The EN 1992 1-2 simplified calculation methods are suitable to single member assessment, where only the effects of thermal deformations resulting from thermal gradients across the cross-section need be considered, while the effects of axial or in-plane thermal expansions may be neglected [4] . This statement may be interpreted by practicing engineers as a permission to ignore the effects of thermal elongations during the course of the fire, which have been proved along this chapter to be a severe factor in the structural performance during the course of the fire.

In spite of this, a review of the Eurocode 1 1-2 (EN 1991 1-2) [24] clarifies the eurocode's philosophy regarding the quantification of mechanical actions on structures exposed to fire. It is referred in section 4 of the EN 1991 Part 1-2 that the effects of imposed and constrained expansions caused by temperature changes due to fire exposure must be considered, except when [24]:

- They may be recognized a priori to be either negligible or favourable;
- They are accounted for by conservatively chosen support models and boundary, and/or implicitly considered by conservatively specified fire safety requirements.

In the assessment of indirect actions, according to EN 1991 1-2, the following should be considered [24]:

- Constrained thermal expansion of the members themselves, e.g. columns in multi-storey frame structures with stiff walls;
- Differing thermal expansion within statically indeterminate members;
- Thermal gradients within cross-sections giving internal stresses;
- Thermal expansion of adjacent members;
- Thermal expansion of members affecting other members outside the fire compartment.

For obtaining the relevant effects of actions during the fire exposure, the mechanical actions shall be combined according to the Eurocode 0 (EN 1990) [22] accidental design situations [24]. For these design situations the value A_k (see equation 1.1) representing the effect of indirect actions due to fire must be determined, considering the thermal and mechanical properties of materials at elevated

temperatures. If the above is taken into consideration during the actions quantification for fire assessment, then the effects of thermal induced actions is covered in the analysis.
The problem rises, when the EN 1992 1-2 (in its sub-section 2.4) states that for member analysis the effects of axial or in-plane thermal elongation need not be considered [4]. Considering this, when a practicing engineer performs a single element assessment based in simplified cross-sectional calculation method, he is driven not to evaluate the effect of thermal elongation in the structural performance. Instead, the structural fire assessment is based in a constant action value obtained from the proper combination of actions given in EN 1991 1-2. This means that the effect of actions should be determined for ambient temperature, using combination factors $\psi_{1,1}$ or $\psi_{1,2}$. Besides this, a simplified procedure for obtaining the fire design value of actions effects (e.g. bending moment) is recommended, which consists of affecting the design value at ambient temperature by a reduction factor for fire situation [4] [24].
As a form of remark to the above discussion, the EN 1991 1-2 refers in its section 4 that indirect actions from adjacent members need not be considered when fire safety requirements refer to members under standard fire conditions [24]. This seems quite contradictory in respect to the rest of section 4 of the EN 1991 1-2, only possible to understand if one considers the standard fire curve a an unrealistic and highly severe way to simulate fire action.
Even considering the previous paragraph, in the following analyses the ISO 834 standard fire curve is applied because it is believed, that in order to identify a possible misleading fire resistance derived from a simplified analysis in opposition to global response, any form of representing the fire action is suitable.

3.6.3. THREE-BAY FRAME ANALYSIS

In this sub-section a comparison between the fire resistance obtained in the previous section relying on a global response analysis and a simplified calculation method analysis is performed. Only the Zone method is applied to represent the simplified calculation methods because between the two simplified procedures recommended in EN 1992 1-2, this one outputs the more accurate values. The formulation steps of the Zone method are summarized in Appendix A.
Table 4.4 presents the results obtained for column 4 (see frame layout presented in Figure 3.27). The calculation of the cross-sectional ultimate capacity based in the Zone method is performed with the spreadsheet available in [17]. However, the current spreadsheet version does not allow the inclusion of reinforcement at the geometrical centre level. For this reason the analysis for column 4 based in the Zone method has neglected the contribution of two reinforcement bars, considering only six. Although this is a considerable drawback of the current spreadsheet version, for the analysis hereafter performed, the error is placed in the safety side, outputting a lower ultimate capacity value to the concrete cross-section. In Table 3.4 $M_{Rd,fi}$ represents the ultimate capacity of cross-section without second-order effects, x is the position of the neutral axis measured in relation to the geometrical centre, $M_{0,fi}$ is the ultimate capacity considering second-order effects, $M_{Ed,fi}$ is bending moment design value and M_{SAFIR} represents the bending moment calculated with SAFIR.
It is recalled here, that the global analysis previously performed with SAFIR yielded a fire resistance of 128 minutes.
A first remark is made in relation to the difference between the values of $M_{Ed,fi}$ and M_{SAFIR}. This difference yields the divergence obtained if one neglects or not the effects of axial thermal elongation in the structure. It is possible to observe that after 30 minutes of fire exposure the bending moment acting at the top of column 4 is approximately 4.3 times higher than the value considered to the safety assessment within the scope of simplified methods.
A second remark is directed to the fact that the analysis performed with the Zone method has shown no failure. It is possible to see in Table 3.4 that the ultimate capacity value (even considering second-order effects) is always higher than the value of $M_{Ed,fi}$. It is recalled that the ultimate capacity would be even higher if the full column's reinforcement had been considered in the simplified calculation.

Table 3.4 – Comparative analysis at the top of column 4.

Time (min)	$M_{Rd,fi}$ (kN.m)	x (m)	$M_{0,fi}$ (kN.m)	$M_{Ed,fi}$ (kN.m)	M_{SAFIR} (kN.m)
0	273.89	0.1359	248.40	57.63	57.63
10	273.89	0.1359	248.40	57.63	121.80
15	273.89	0.1359	248.40	57.63	165.70
30	259.40	0.1371	234.07	57.63	234.40
45	236.96	0.1399	212.20	57.63	246.10
60	219.18	0.1427	194.90	57.63	238.90
75	199.04	0.1465	175.38	57.63	222.40
90	177.00	0.1504	153.96	57.63	205.50
120	132.00	0.1624	110.66	57.63	164.70

Table 3.5 presents the results obtained for the same comparison procedure, this time in order to the cross-section of the left end of beam 6 (see Figure 3.27). Once again it is observed a divergence between the values of bending moment acting during the course of the fire obtained with SAFIR and the design value used to assess the fire safety based in simplified methods. As in the case of column 4, inspecting the results shown in Table 3.5, it is concluded that an analysis based in the Zone method would not predict a cross-section failure at the same instant, or at least, before the failure time achieved with the global analysis (although, in this case the difference is small). A similar comparison procedure has been performed in relation to the beams' mid-span. The conclusions obtained are in the same line as the ones withdrawn regarding the top of column 4 and the left end of beam 6, thus not presented in this work. It is referred that the simplified procedure does not consider the influence of axial force (and second order effects) on the ultimate capacity of the beams.

Table 3.5 – Comparative analysis at the left end of beam 6.

Time (min)	$M_{Rd,fi}$ (kN.m)	x (m)	$M_{Ed,fi}$ (kN.m)	M_{SAFIR} (kN.m)
0	172.55	0.0530	132.70	132.70
10	171.24	0.0569	132.70	186.30
15	169.70	0.0618	132.70	225.4
30	165.79	0.0777	132.70	271.10
45	162.62	0.0957	132.70	281.20
60	160.54	0.1134	132.70	278.70
75	158.60	0.1516	132.70	270.80
90	155.78	0.1896	132.70	258.10
120	146.94	0.3107	132.70	233.30

3.6.4. ANALYSIS OF A DIFFERENT FRAME

The conclusions previously withdrawn are quite significant; however they are related to a specific frame, especially sensitive to the floors' thermal elongation due to the bracing system directing the expansion towards one singe direction. In order to understand if neglecting the thermal elongation effects may lead to non-conservative results in other types of reinforced concrete frames, the frame illustrated in Figure 3.44 has been investigated. This structural layout is representative of the frames commonly analysed by other authors. The frame is exposed to the ISO 834 standard fire in all compartments, with the two inner columns exposed along the whole perimeter, the outer columns exposed in the internal face and the beams exposed in the bottom and lateral surfaces. In opposition to the previous frame, in this case the structure is completely exposed to fire, presenting no cold parts to act as restraining elements. The evolution of the structural behaviour during the course of the fire is illustrated in Appendix B, because, as this frame type is widely found in the literature, there is no point in performing an exhaustive analysis similar to the performed in 3.5.4. The details of the cross-sections belonging to the frame are also displayed in Appendix B. The global response analysis has predicted a structural failure after 151 minutes of fire exposure.

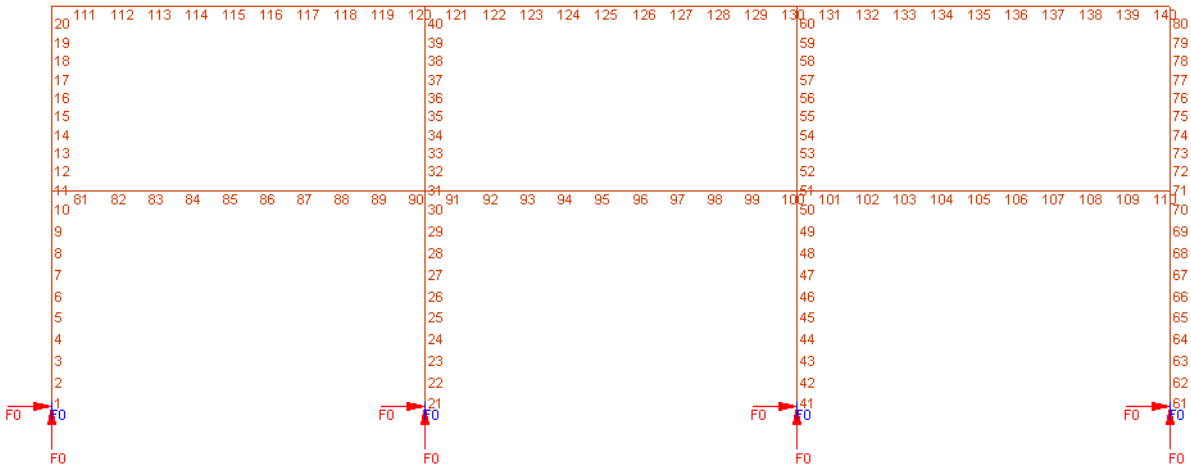

Fig.3.44 – Finite element mesh of a different frame.

Table 3.6 presents the values of the comparative analysis performed in order to the top of the inner column, identified in the finite element mesh drawn if Figure 3.44 as element 50 (which has been identified as the most unfavourable column). In opposition to the previous analysis, in this case the combination of axial force and bending moment in the inner columns has shown to be more unfavourable than in the outer columns. It is recalled that, in the previous frame, the drift at the top of the outer columns had imposed a considerable increase in bending moment, explaining why in that analysis the combination of axial force and bending moment is more severe in the outer columns than it is in the inner ones.

The first conclusion withdrawn from the results listed in Table 3.6 is directed, once again, to the fact that the evolution of bending moment in the top of the column (element 50) displays a variation not at all covered by the simplified approach. It is even possible to observe an inversion of the bending moment sign at the initial stages of the fire.

Now focusing in the comparison of the evolution of the ultimate capacity (considering second-order effects) with the reference bending moment in the scope of simplified method assessment, a failure prediction is made at the last time step (150 minutes). At this time, the Zone method presents an ultimate capacity of -1.42 kN.m (the negative sign is related to the fact that the neutral axis is located outside the cross-section). In this way, the Zone method would yield a failure time somewhere between 120 and 150 minutes of fire exposure. The exact time of failure would be given by the time step where the value of $M_{0,fi}$ equalizes the value of $M_{Ed,fi}$.

Table 3.6 – Comparative analysis at element 50.

Time (min)	$M_{Rd,fi}$ (kN.m)	x (m)	$M_{0,fi}$ (kN.m)	$M_{Ed,fi}$ (kN.m)	M_{SAFIR} (kN.m)
0	105.38	0.1071	86.93	2.635	2.635
10	97.56	0.1042	78.61	2.635	0.332
15	90.19	0.1025	70.92	2.635	-1.996
30	63.94	0.0975	43.68	2.635	-6.718
45	46.77	0.0945	25.87	2.635	-9.190
60	41.24	0.1019	21.86	2.635	-10.460
75	35.84	0.1096	17.81	2.635	-10.930
90	30.46	0.1189	13.85	2.635	-10.800
120	20.94	0.1404	6.87	2.635	-6.031
150	10.28	0.1682	-1.42	2.635	-2.068

Table 3.7 presents the same comparative analysis in order to most unfavourable beam element, which has been proved to be element 130 (see Figure 3.44). This element corresponds to the left end of beam in the central bay of the second floor. It is recorded that an analysis relying upon the assessment of the beam a single element would not predict a structural failure, at least sooner than it has been predicted by the global response analysis. It is possible to conclude in Table 3.7 that the value of $M_{Rd,fi}$ is always higher the value of $M_{Ed,fi}$.

Table 3.7 – Comparative analysis at element 121

Time (min)	$M_{Rd,fi}$ (kN.m)	x (m)	$M_{Ed,fi}$ (kN.m)	M_{SAFIR} (kN.m)
0	213.74	0.0640	127.20	127.20
10	212.14	0.0686	127.20	160.20
15	210.60	0.0736	127.20	176.30
30	205.65	0.0959	127.20	202.40
45	202.13	0.1210	127.20	228.70
60	198.93	0.1558	127.20	238.80
75	195.92	0.2007	127.20	240.60
90	191.31	0.2602	127.20	237.90
120	175.76	0.4380	127.20	225.30
150	154.13	0.6539	127.20	215.70

3.6.5. CONCLUDING REMARKS

The comparisons between global response analyses based in advanced calculation methods and cross-sectional analyses based in simplified calculation methods have indicated that performing a fire safety analysis relying on the last methods may lead to non-conservative results. The main reason for that has been identified as the lack of capacity from the cross-sectional methods to foresee the internal stresses evolution within the structure during the course of the fire. Moreover, it is believed that the clause presented in section 2.4 of EN 1992 Part 1-2 stating that when performing a single member analysis the axial or in-plane thermal elongation effects may be neglected, is possible to induce misleading assessments.

From the two comparative analyses above performed, it has been understood that the frame presenting a higher sensitivity to thermal elongation effects (due to bracing systems, etc.) presents a higher divergence between the results obtained with global response analysis and simplified cross-sectional methods. The reason for this is found in the fact that in restrained structures, there are a much higher development of restraint stresses, leading to an earliest occurrence of collapse.

In the assessment of reinforced concrete beams with simplified methods, the axial force is often neglected because the value of this force related solely to the initial static actions is rather small. However in case of fire the beams axial force displays a considerable increase, being its effects not negligible if a correct assessment of the beams' behaviour is desired.

It is recalled here the results previously presented in Table 3.5, where the time to failure related to the beam computed with the Zone method displayed a close value to the one computed with SAFIR, regarding global structural behaviour. This is considered to be coincidental, as the failure mode obtained with the global analysis is related to the edge columns failure. To prove this, the same analysis has been performed considering that all beams within the frame were reinforced with rebars presenting a yield stress of 800 Mpa at ambient temperature. This calculation presented approximately the same time to failure as the previous one (126 min opposed to 128min). It is obvious, that the time to failure obtained with the Zone method (regarding the beam examined in Table 3.5) is not close to the time to failure computed with SAFIR because of the beams reinforcement higher strength

3.7. FINAL CONSIDERATIONS TO THE CHAPTER

The main conclusions withdrawn during this chapter have been listed in the concluding remarks to the sections where the conclusions have been achieved. For this reason they are not repeated here. In the following chapter the conclusions here obtained are then recalled and the results compared within the scope of the parametric study to be performed.

4

Analysis of Reinforced Concrete Frames Exposed to Fire: Part 2

Influence of Different Fire Scenarios

4.1. INTRODUCTION

This chapter follows on the previous one in the analysis of the reinforced concrete frame presented in Figure 3.27. In chapter 3, the frame has been considered to be exposed to a two floor simultaneous fire scenario (fire scenario 1), aiming to clarify the evolution of internal stresses and structural displacements, considering the interaction between the fire exposed part of the frame with the cold one. With the previous analysis, the main phenomena governing the structural response have been identified, such as the evolution of bending moments at the top of columns and the horizontal drifts measured at the level of the fire exposed floors.

In the following analyses, the reinforced concrete frame is exposed to several fire scenarios to investigate how the structure's response varies with different fire actions.

4.2. FIRE SCENARIOS

The fire scenarios considered to act upon the reinforced concrete frame in analysis are based in the ISO 843 standard fire curve [36] representing the evolution of the compartment gas temperature, meaning that the information comprised in Figure 3.13 remains valid to the analyses performed hereafter. In spite of this, during this chapter, the location of the compartments in fire is changed from one fire scenario to another.

The first group of fire scenarios analysed are intended to cover the behaviour of the structural system when it is exposed to whole floor simultaneous fires. As in the previous chapter, the columns limiting the fire compartments are considered exposed along the entire perimeter, while the beams are admitted exposed in their bottom and lateral surfaces. Table 4.1 summarizes the characteristics of these fire scenarios as well as the time required to the frame's collapse to be achieved. It must be referred that fire scenario 1 has already been analysed in chapter 3, being mentioned here again with comparison purposes.

Table 4.1 – Whole floor fire scenarios characteristics.

Fire Scenario	Compartments in fire	Time to failure (min)
1	I, II, III, IV, V, VI	128
2	I, II, III	32
3	IV, V, VI	122

In the second group of fire scenarios a set of single compartment fires analyses are undertaken. Four fire scenarios are considered with this characteristic, varying the position of the fire exposed compartment, from the central to the lateral one, and from one floor to another. The rest of the structure remains at ambient conditions. Table 4.2 identifies this group's fire scenarios and the time to failure displayed from the analysis based in the advanced calculation method. The analyses are limited to a three hour period, thus if until that time no failure occurs it is considered a *no collapse situation*.

Table 4.2 –Single compartment fire scenarios characteristics.

Fire Scenario	Compartments in fire	Time to failure (min)
4	I	62
5	II	84
6	IV	No collapse
7	V	No collapse

4.3. RESULTS

In this section a comparative analysis of the results obtained for the different fire scenarios is performed. In opposition to the previous chapter, there will not be a fully description of every single fire scenario results individually.

4.3.1. WHOLE FLOOR FIRE SCENARIOS

The fire scenarios considered in this sub-section are the ones where the whole floor is subjected to fire including the case of two floor fire (i.e., fire scenarios 1, 2 and 3). As it has been previously concluded in Chapter 3, for the frame in analysis subjected to a whole floor fire scenario, the behaviour during the course of the fire is mainly characterized by the evolution of stresses and displacements at the outer columns. For this reason, the analysis will be performed regarding these columns.

In Figure 4.1 the drift at the top of column 4 (the outer column of the first floor) obtained in scenario 1, 2 and 3 is plotted. The drift recorded during scenario 3 is of course not significant, as in this case the beams at the first floor are not subjected to any thermal action.

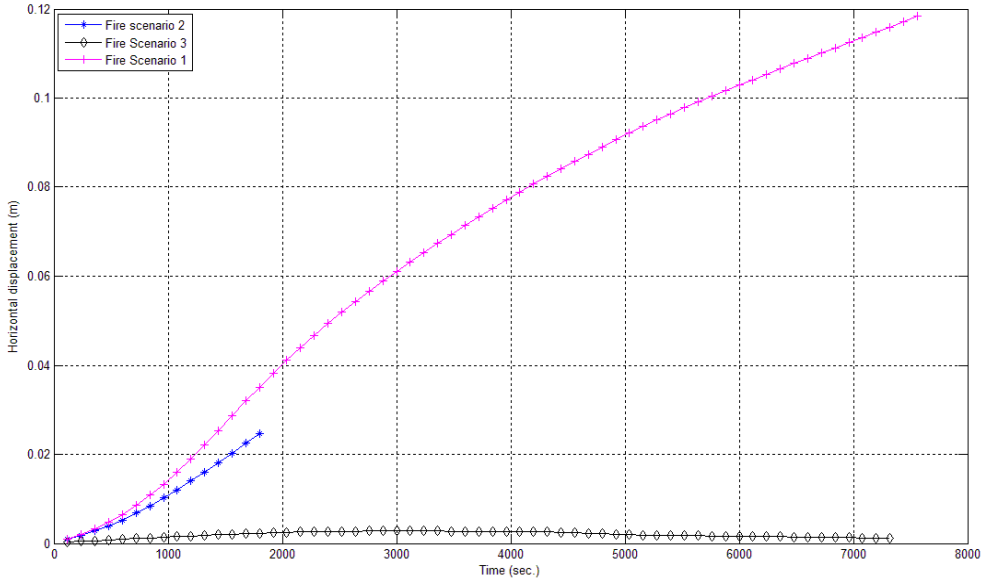

Fig.4.1 – Evolution of horizontal displacement at the top of column 4.

It is possible to observe that the drift displayed in scenario 1 constitutes an upper bound to the several displacements recorded, because in this case the two floors are subjected to the same thermal action, thus being imposed to the first floor a greater cumulated deformation.

A noteworthy remark shall be directed to the fact that in scenario 2 a much smaller time of fire resistance has been achieved in opposition to scenario 1, even when in scenario 1 there is a higher number of structural elements exposed to fire. To understand this, the evolution of bending moment at the top of column 4 regarding these three scenarios is presented in Figure 4.2. The evolution of bending moment in scenario 1 has already been discussed in the Chapter 3. Now focusing in the curve related to scenario 2 it is possible to observe a steeper increase in bending moment is recorded in opposition to scenario 1. The explanation to this is found in the fact that in scenario 2 the thermal expansion of the first floor is restrained by a stiffer structure than in scenario 1, as in scenario 2 there are more parts of the structure at ambient conditions. Because of this, despite the smaller drift, the bending moment at the top of column 4 in scenario 2 increases more, leading to an anticipated failure. This conclusion is of vital relevance as it demonstrates that in the case of restrained structures, more compartments simultaneously exposed to fire do not necessarily mean a more severe fire scenario. On the other hand, these results also enable us to understand how important may be the role played by restrained thermal effects in the whole structural performance, reassuring the conclusion withdrawn in the previous chapter related to the negligence of thermal induced effects within the scope of simplified calculation methods. The evolution of shear force at the top of column 4 is shown in Figure 4.3. The importance of this effort will be recalled ahead in Chapter 5.

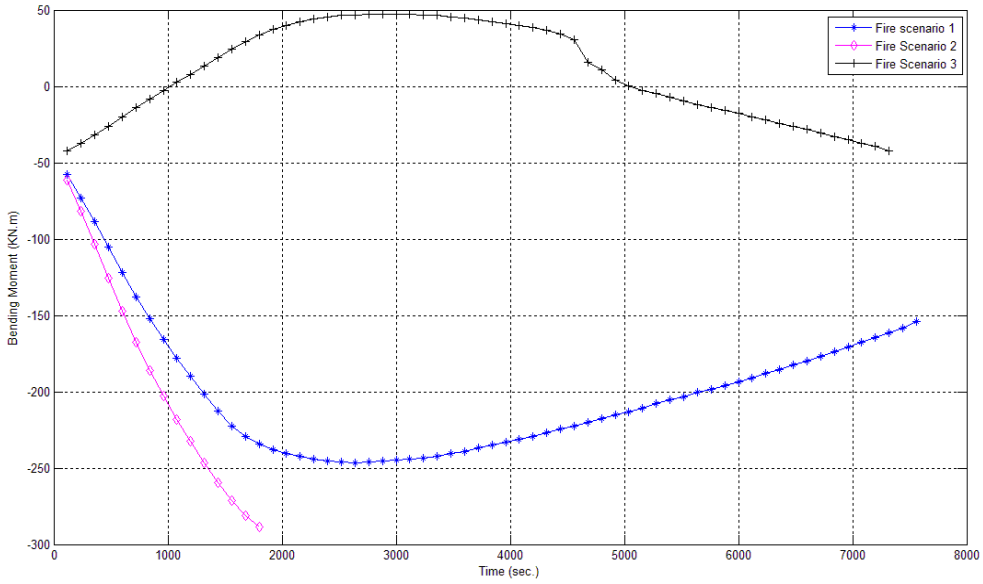

Fig.4.2 – Evolution of bending moment at the top of column 4.

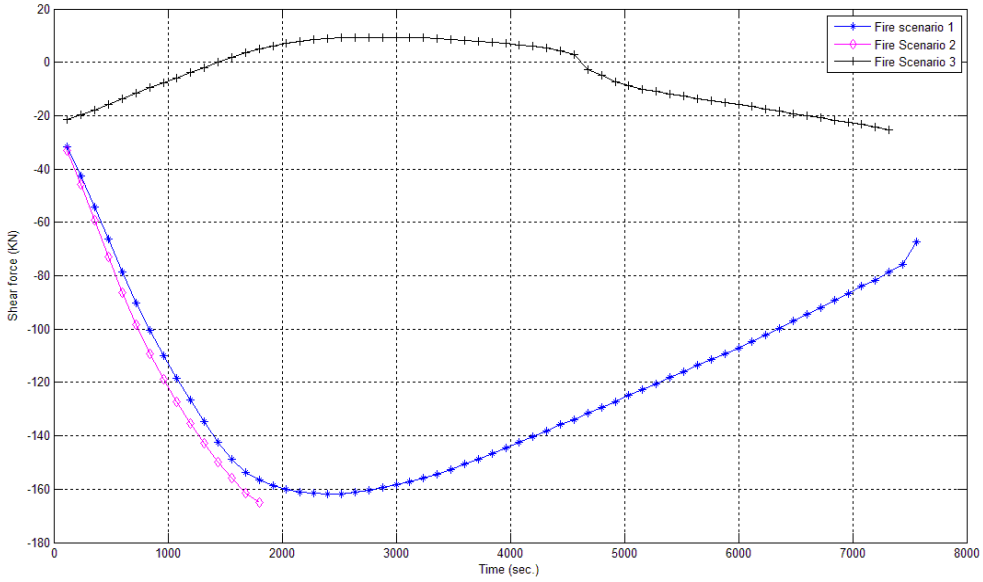

Fig.4.3 – Evolution of shear force at the top of column 4.

In order to easy the understanding of the different structural behaviours obtained regarding these three whole floor fire scenarios, in Figure 4.4 is displayed a schematic representation of the bending moment diagram obtained in the three scenarios after 30 minutes of fire exposure, i.e., immediately before the frame's collapse in scenario 2 (corresponding to the last converged time step in SAFIR regarding scenario 2). From the inspection of the bending moment diagrams presented in Figure 4.4 it is concluded that the bending moment at the top of column 4 in scenario 2 and at the top of column 8 in scenario 3 are quite similar. It is remembered that in scenario 2 only the beams of first floor are imposing a drift at the outer columns and in scenario 3 only the second floor ones are causing this

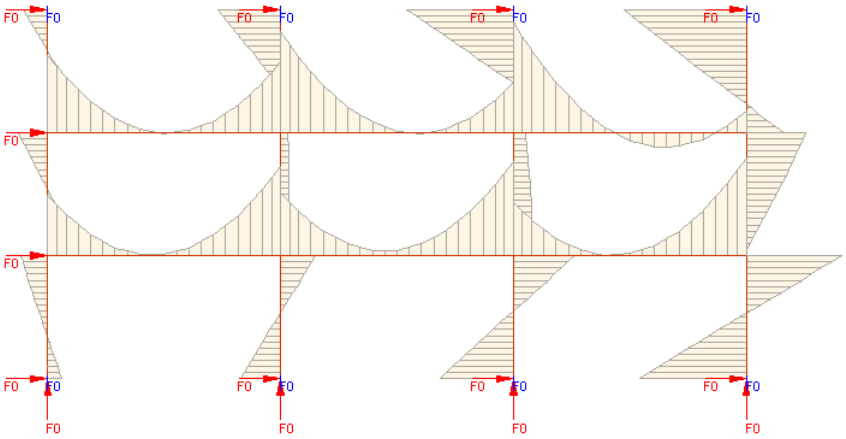

a)

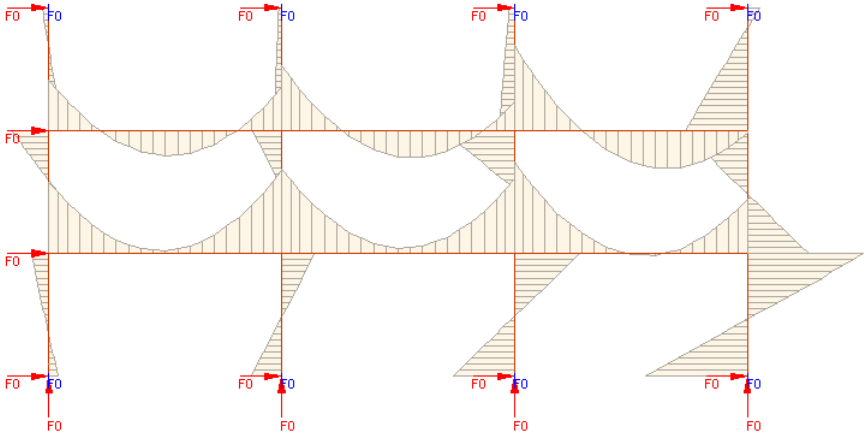

b)

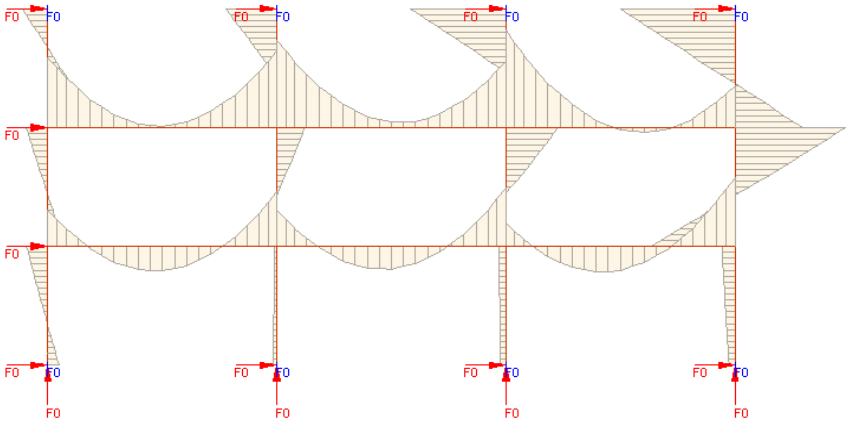

c)

Fig.4.4 – Schematic bending moment diagram after 30 minutes of fire exposure: a) scenario 1, b) scenario 2, c) scenario 3.

effect, thus it was expected that in scenario 3 the same failure mechanism displayed in scenario 2 had occurred, this time concerning column 8. However, in the former case that did not happen, because column 8 was subjected to a lesser axial force (it is located in a upper floor), thus, although the bending moment is quite similar to the one recorded for scenario 2, the combination of axial force and bending moment was not enough to induce the failure of the column exposed to fire.
The frame exposed to scenario 3 eventually presented a failure mode after 122 minutes of fire exposure. Once again, the time to failure presented is smaller than the time obtained regarding the two floor fire scenario, corroborating that the scenario comprising more compartments in fire do not lead to the most severe results. In Figure 4.5 the final deformed shape recorded in scenario 2 and 3 are sketched. The deformed shape regarding scenario 1 has already been analysed in Chapter 3.

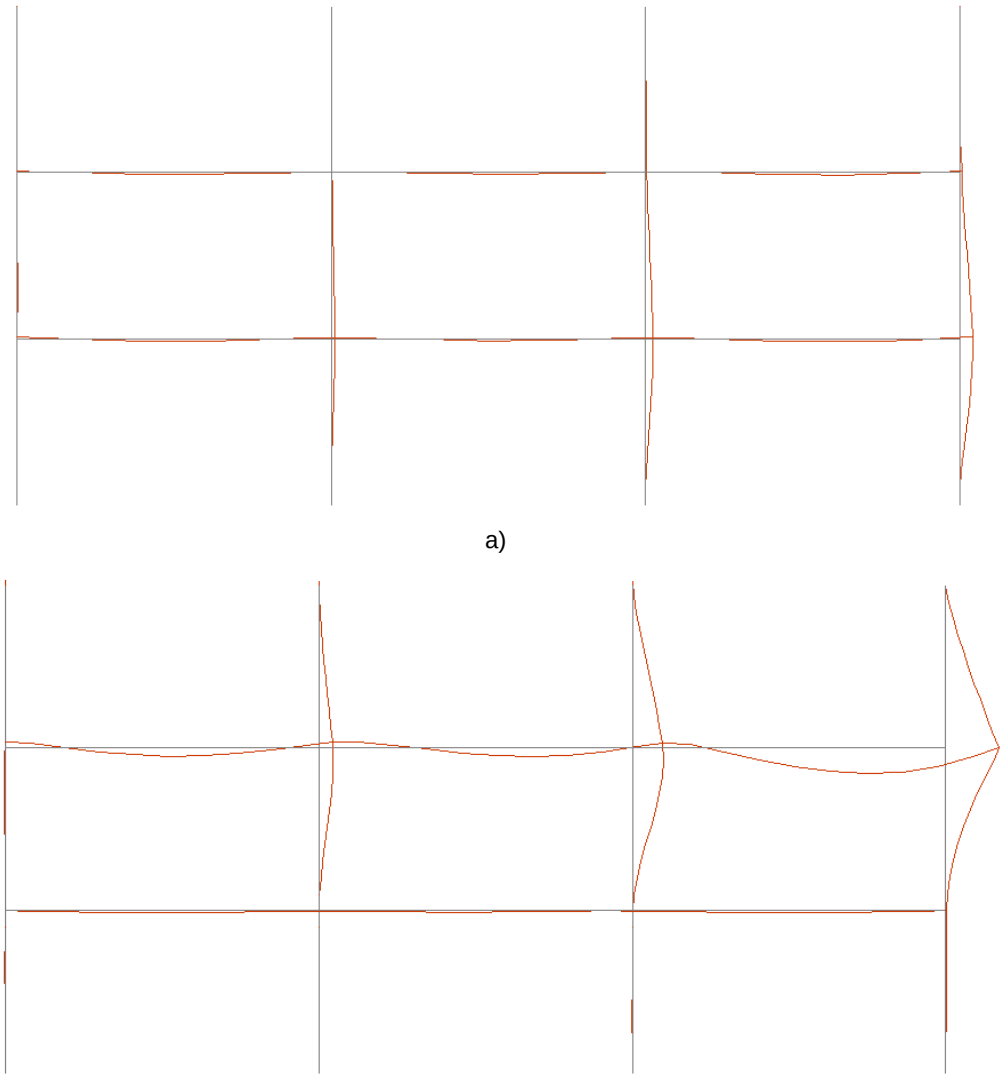

Fig.4.5 – Deformed shape immediately before collapse (scaled 10 times): a) scenario 2 (32 minutes), b) scenario 3 (122 minutes).

The observation of the final deformed shape in scenario 2 clearly indentifies column 4 as the element inducing the collapse, due to the previously mentioned combination of bending moment and axial force. Regarding scenario 3, it is possible to conclude that the failure mechanism comprises an elevated level of deformation in columns 8 and 12, leading to the ultimate strain in the column 12 bottom's reinforcement to be achieved.

4.3.2. SINGLE COMPARTMENT FIRE SCENARIOS

Figures 4.6 and 4.7 present the evolution of the horizontal drift at the top o column 4 and 8, respectively, regarding the single compartment fire scenarios as well as the scenarios comprising the whole floor in fire with comparative purposes.

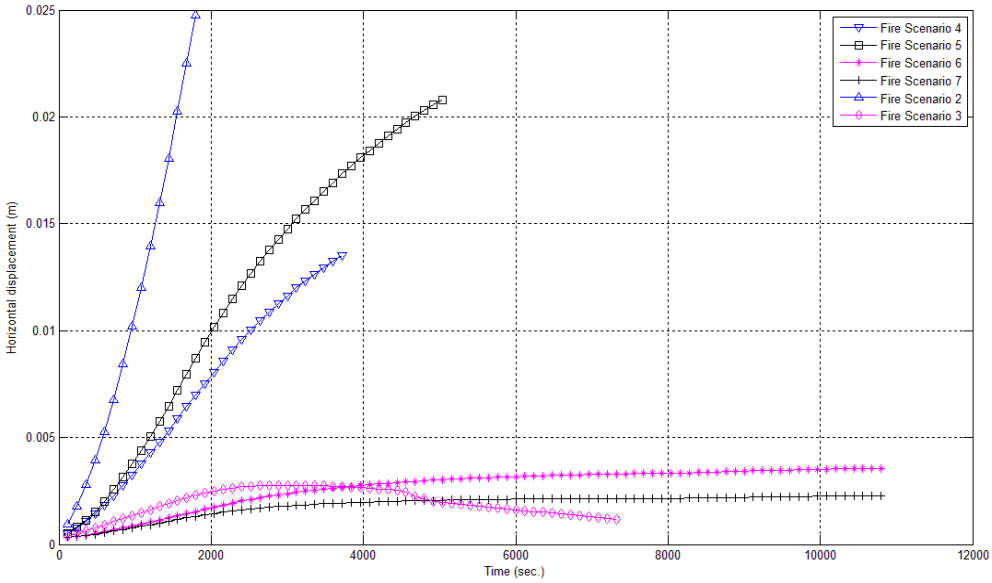

Fig.4.6 – Evolution of horizontal displacement at the top of column 4.

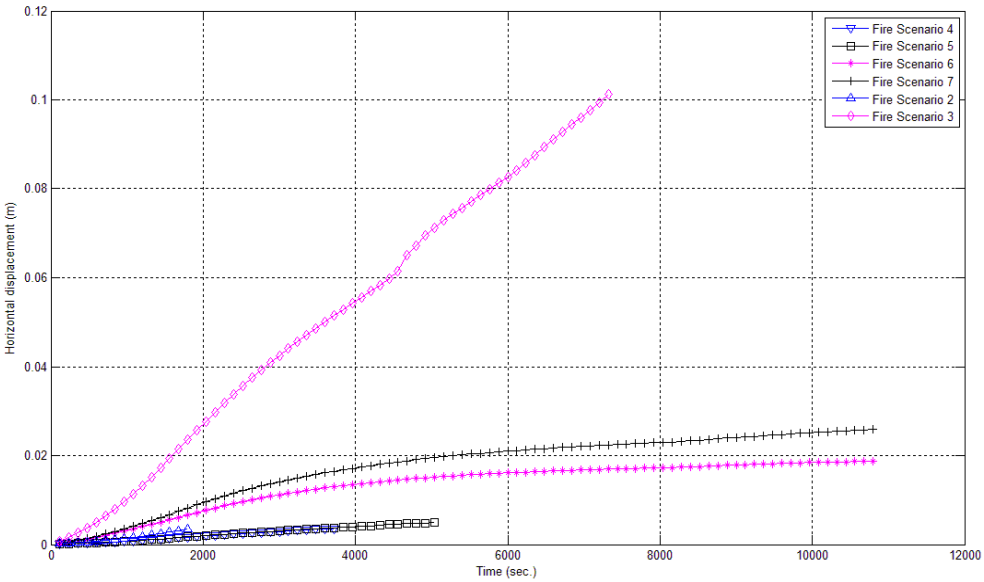

Fig.4.7 – Evolution of horizontal displacement at the top of column 8.

As expected, the drifts at the top of columns 4 and 8 are greater in scenarios 2 and 3 respectively, where a greater thermal elongation is imposed by each floor. As to the drifts recorded in the single compartment fire scenarios, it is observed a greater displacement in the cases where the central compartment is exposed to fire, because in these cases there are fewer elements imposing a restraint the beam thermal elongation in the direction of the outer columns.
In Figure 4.8 the vertical displacements at the central beam's mid-span (beam 2) are illustrated. During the course of fire in scenario 4 the displacement recorded is always upwards due to the curvature imposed by restraining rotation in the adjacent compartment's beam which is subjected to fire. In the case where the beam is directly exposed to fire, such as in scenarios 2 and 5, the displacement is initially directed downwards, followed by an ascending branch due to the imposed curvature as well as to the thermal elongation of the columns. Then, in scenario 5 the downwards trend is resumed as a consequence of the reduction of beam's stiffness due to elevated temperatures.

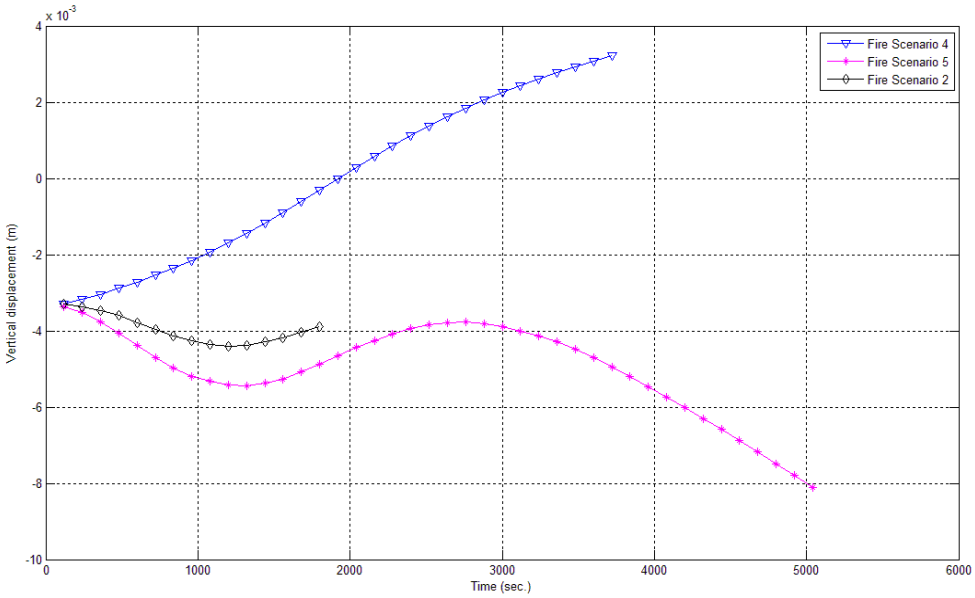

Fig.4.8 – Evolution of vertical displacement at the mid-span of beam 2.

It is noticeable in Figure 4.8 the fact that the vertical displacement at the beam's mid-span is greater in scenario 5 than in scenario 2. In scenario 2 the entire floor is subjected to fire, thus there is a more pronounced degradation in the beams stiffness, reducing the restraint capacity of adjacent compartments. However in scenario 5, where only the central compartment is exposed to fire, although there is a higher restraint imposed by the adjacent cold bays of the frame, a greater rotation at the top of central compartment columns induce a more pronounced vertical displacement at the mid-span.
In Figure 4.9 are plotted the vertical displacements in beam 1 regarding fire scenarios 2, 4 and 5. The conclusions withdrawn for Figure 4.8 are suitable to this case. The previous two displacement analyses have also been performed regarding fire scenarios 3, 6 and 7, i.e., the differences among vertical displacements in the second floor beams considering single bays exposed to fire and the entire floor have been investigated. The results obtained follow closely the ones related to fire scenarios 2, 4 and 5, with a slight variation in the values. However, as only a comparative analysis (investigate the differences between whole floor and single bay fire scenarios) is in the line, there is no point in presenting the results of the second floor, as the trends displayed in that results are similar to the results presented to the first floor. No fire scenario comprising compartments III and VI separately have been considered because the results would not yield any different conclusions in opposition to the several fire scenarios already analysed.

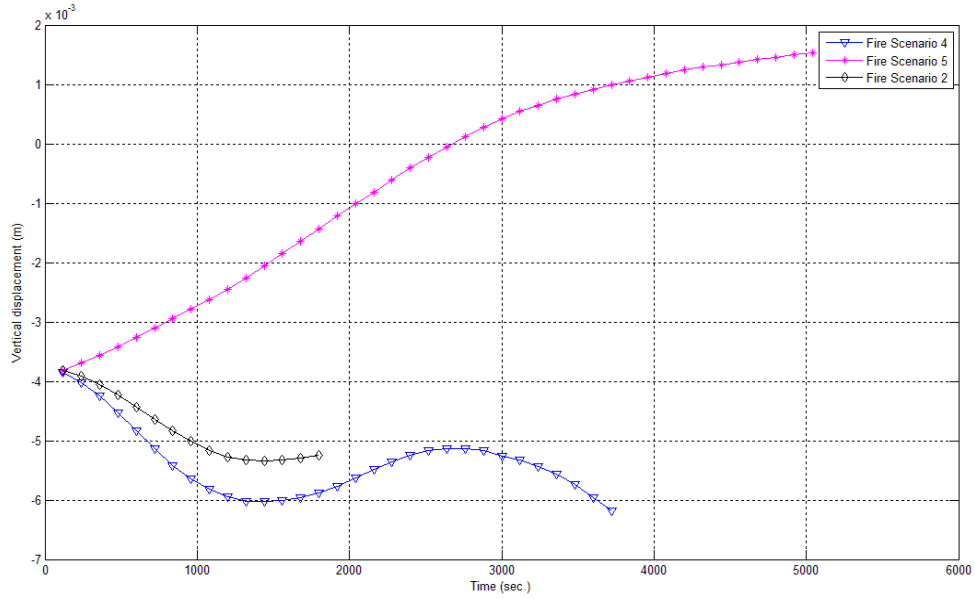

Fig.4.9 – Evolution of vertical displacement at the mid-span of beam 1.

The evolution of bending moment at the top of column 3 is presented in Figure 4.10 regarding fire scenarios 2, 4 and 5. It is remarked that only in scenarios 2 and 5 this column is directly exposed to fire. This explains why in scenario 4 the bending moment presents an ascending trend, while in scenario 5, due to the deterioration of material properties induced by high temperatures, the bending moment decreases after a peak value approximately after 35 minutes of fire exposure.

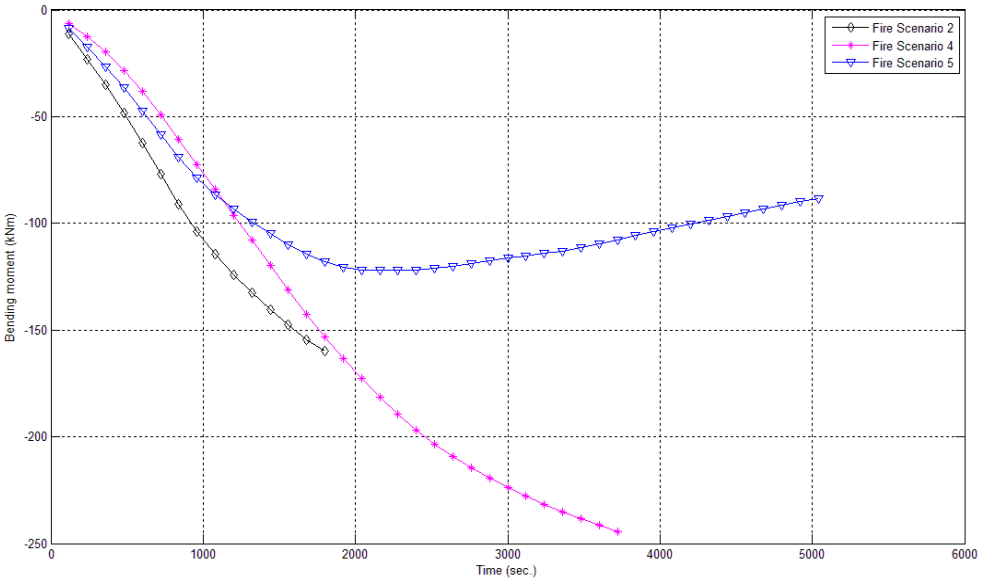

Fig.4.10 – Evolution of bending moment at the top of column 3.

Figure 4.11presents the evolution of bending moment at the top of column 4. Neither in scenario 4 or 5 this column is directly exposed to fire, so in these two cases has the bending moment displayed an

increasing trend. Regarding fire scenario 2, as already discussed, the bending moment value recorded, in association with the axial force, is the cause of structural failure.

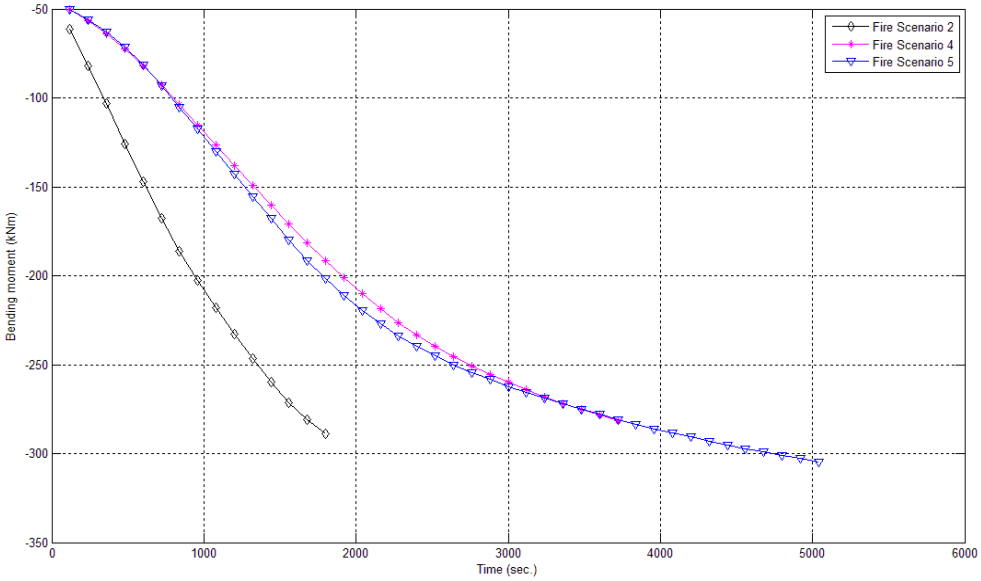

Fig.4.11 – Evolution of bending moment at the top of column 4.

Aiming to understand the collapse mechanism associated to fire scenarios 4 and 5, Figure 4.12 illustrates the evolution of bending moment at the top of the most severe exposed column in each scenario, i.e., the column at the right end of the fire compartment which has to withstand the drift imposed by the beam thermal elongation. Regarding scenario 2, the most unfavourable column is of course the outer one (column 4) as it is the recipient of the cumulative beams thermal elongation.

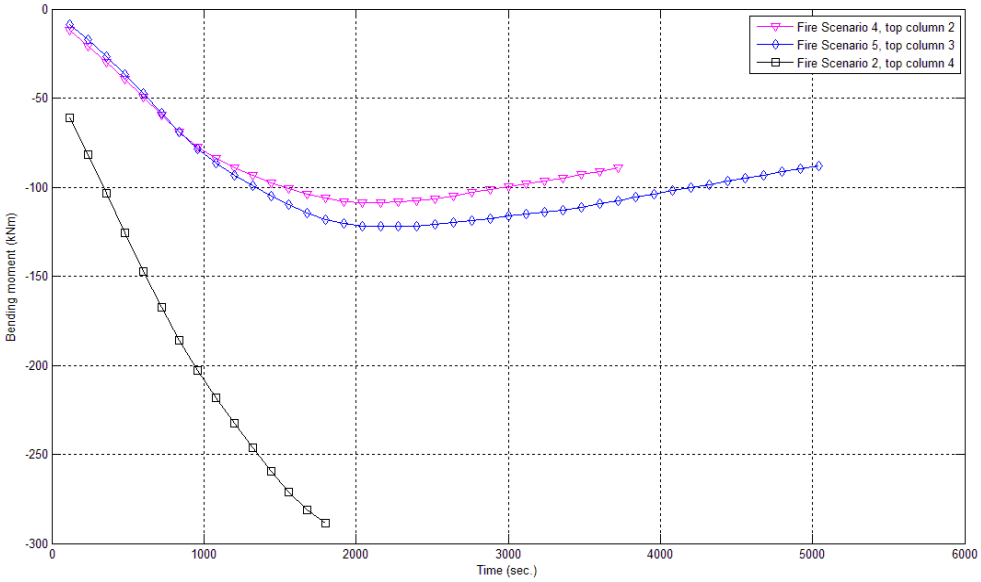

Fig.4.12 – Evolution of bending moment at the top of columns.

From the inspection of Figure 4.12 it is observed that the bending moments at the top of column 2 (in scenario 4) and column 3 (in scenario 5) follows similar trends. However the values recorded for

column 3 tend to became slightly higher because this column is located within a stiffer part of the frame (the central bay is directly surrounded by more cold elements than the lateral bay correspondent to scenario 4). Continuing the inspection of Figure 4.12 it is recorded that a peak bending moment value occurs in both scenario 4 and 5 approximately at the same instant. After this, due to material properties deterioration and to redistribution of stresses within the framed structure, a decrease in bending moment is observed. In spite of this, eventually the combination of bending moment and axial force, associated to the reduction of the columns' strength due to elevated temperatures, leads to the failure of the exposed columns (column 2 in scenario 4 and column 3 in scenario 5). The different stiffness boundary conditions above mentioned regarding the frame's bays associated to scenarios 4 and 5 are also suitable to explain why the frame had withstood more time of fire exposure in scenario 5 than in scenario 4, as in scenario 5 a more effective redistribution takes place, enabling the frame to withstand more time.

A remark shall be made regarding the difference in the values of bending moment at the top of the most unfavourable columns at the instant correspondent to the structural failure. It is observed in Figure 4.12 that the bending moment at top of column 4 in scenario 2 is approximately 3 times higher than the that value recorded in scenarios 4 and 5 (at columns 2 and 3, respectively) at the instant the collapse is achieved. Nevertheless, it must be recalled that columns 2 and 3 are inner columns, thus subjected to a higher axial compressive force than column 4. In result of this, the bending moment required to achieve failure in these last columns is lesser than the one required by column 4.

The comparative analyses performed regarding fire scenarios 2, 4 and 5 have also been performed considering fire scenarios 3, 6 and 7. The results herein obtained displayed similar trends as those obtained in the previous analyses. However, in scenarios 6 and 7 no collapse has been achieved (at least after 3 hours of fire exposure). This is believed to be related to the fact that the axial force in columns 6 and 7 is not enough to induce (combined with the bending moment and deterioration of material strength) the columns failure. To conclude this group of comparative analyses, in Figure 4.13 is presented a schematic draft of the deformed shape the frame has presented immediately prior to collapse in scenario 4. In Figure 4.14 the same schematic draft is shown, this time regarding scenario 5.

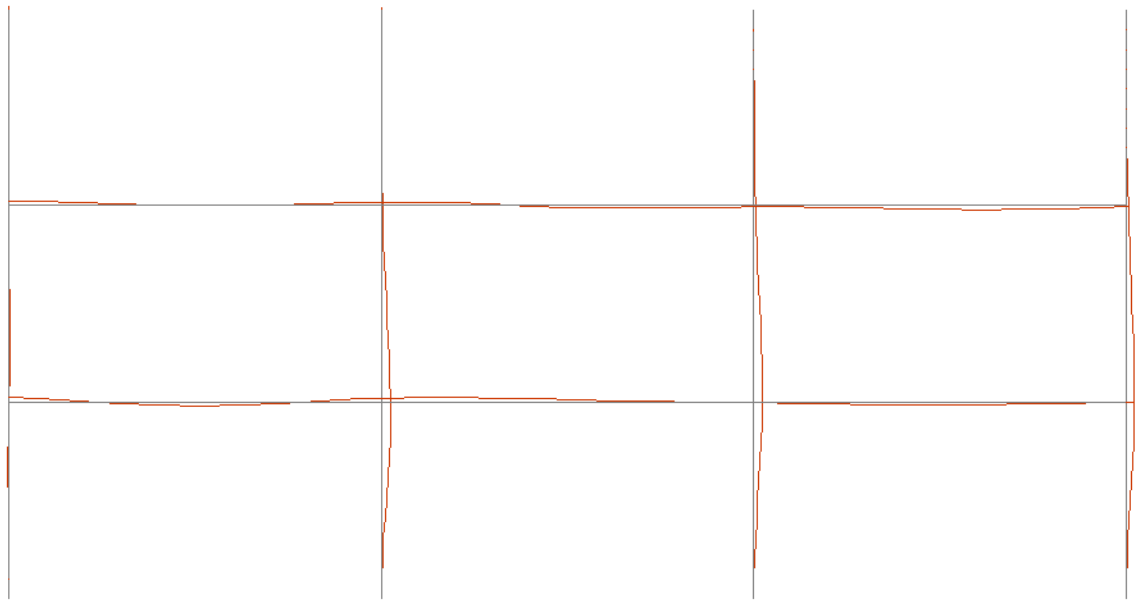

Fig.4.13 – Deformed shape immediately before collapse in scenario 4; 62 minutes (scaled 10 times).

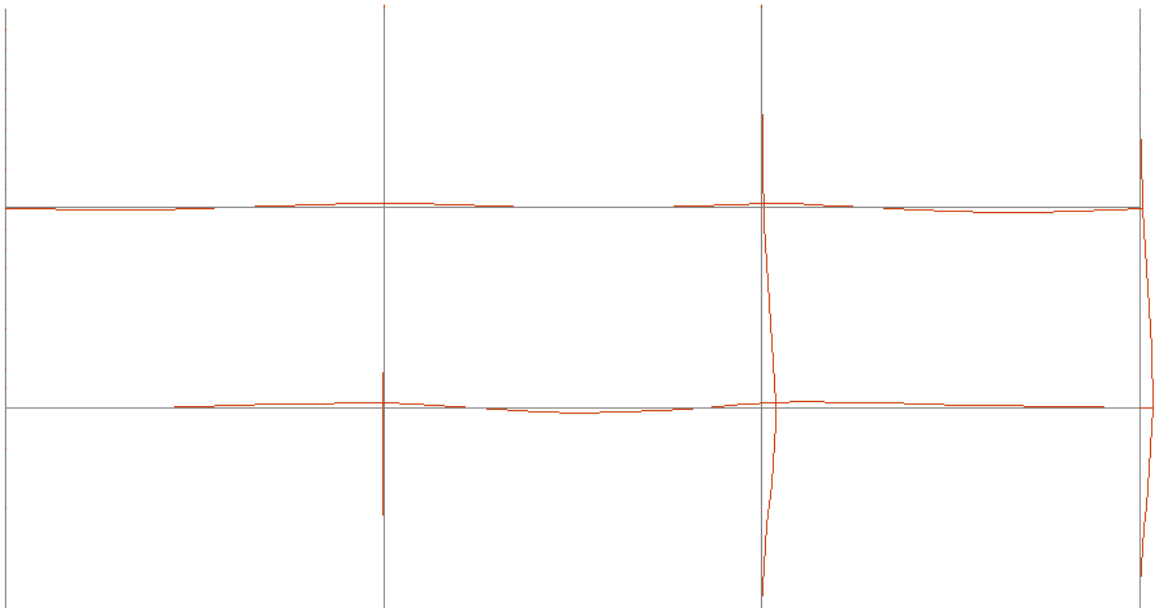

Fig.4.14 – Deformed shape immediately before collapse in scenario 5; 84 minutes (scaled 10 times).

The results related to the comparative analyses among fire scenarios 3, 6 and 7 are not presented in this work, as it would yield repetitive in relation to the analyses comprising scenarios 2, 4 and 6, and at the same time it would not add any further conclusion to ones already withdrawn.

4.4. CONCLUDING REMARKS

During this chapter, the behaviour of the three-bay reinforced concrete frame previously analysed in Chapter 3 has been studied considering different fire scenarios, ranging from whole floor fires to single compartment ones.

The first conclusion herein withdrawn is related to the fact that, in this frame, a fire scenario comprising more parts of the structure simultaneously exposed to fire does not necessarily means the most unfavourable case. It has been concluded that a fire scenario comprising a single frame's bay exposed to fire results in a sooner collapse than a fire scenario where two floors are subjected to fire, as it yields the comparison of the results obtained for scenarios 4 and 5 opposed to scenario 1.

A second conclusion is directed to the fact that for the several fire scenarios, the collapse is related to the columns failure induced by the combination of axial compressive force, bending moment and deterioration of materials strength due to elevated temperatures.

The parametric study performed in this chapter has emphasized the importance of the interaction between the cold and the exposed parts of the structure during the course of the fire, and at the same time, it has underlined the divergence between simplified calculation methods and global response analysis, as the majority of the cases investigated in this chapter have displayed a sooner time to failure compared against the time displayed in the Chapter 3 (scenario1), thus increasing even more the divergence between the two calculation procedures, already comparative analysed in section 3.

5

Simplified Procedure for Shear Failure Assessment at Elevated Temperatures

5.1. INTRODUCTION

During the analyses performed in the previous chapters 3 and 4, it has been noticed an important evolution of the shear force at the top of the columns due to the drift imposed by the beam's thermal expansion. Of course, the advanced thermo-mechanical method previously applied, based in the software SAFIR, is not capable of assess any sort of shear failures, thus, although the shear values obtained are relatively high, they are never the cause of structural collapse. This is considered to be an important drawback in the application of the currently available programmes dedicated to the analysis of structures subjected to fire. As it has been exposed in Chapter 1, several collapses of reinforced concrete buildings induced by columns shear failure were reported, indicating the real severity level this phenomenon represents to structures submitted to fire actions.

Considering the above statements, in this chapter, a simplified calculation method for shear failure assessment is presented. It relies in the results obtained in the previous thermo-mechanical analysis, as it uses the shear forces calculated before, along the course of the fire. On the other hand, the sectional thermal analysis results are applied to evaluate the materials' properties degradation, and calculate the corresponding shear strength capacity. With this method, it is intended to clarify if neglecting the shear effects on columns during the analysis of structures in fire may lead to non-conservative results.

5.2. SHEAR FAILURE ASSESSMENT AT AMBIENT TEMPERATURES

5.2.1. GENERAL OVERVIEW

The structural response of reinforced concrete to shear solicitation is complex and its mechanisms are not fully understood. Despite the research programmes already undertook, it is often found in the literature different models to deal with this type of solicitation, with divergent approaches and analysis criteria. This results in the fact that there is not yet a shear model accepted for the technical community as there are, for instance, regarding bending or axial solicitations [102].

The causes for this lack of understanding are explained in [102]. For one side, as opposed to the normal solicitation analysis, shear behaviour is highly influenced by some concrete phenomena poorly

acknowledged. Cracking of concrete is a remarkable example, as the interaction between the parts of concrete separated by cracks plays a major role in the resistance to shear, and currently its quantification is still rather inaccurate [102]. A schematic representation of a shear induced crack is illustrated in Figure 5.1, where it is compared to a flexural induced one. For the other side, the actual influence of longitudinal reinforcement is not also extensively explained [102].

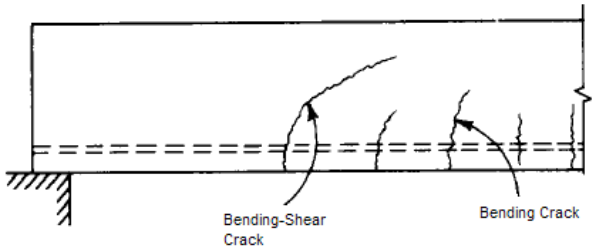

Fig.5.1 – Schematic representation of bending-shear and bending cracks in a reinforced concrete beam [103].

Reinforced concrete elements may present special shear reinforcement, usually in the form of stirrups. Obviously, the presence or not of these elements exert a crucial influence on the structural response to shear. No further development on shear behaviour of reinforced concrete structures is detailed in this work, being recommended references [103] and [104] if more information is desired. In the following text, only the methods of shear capacity assessment proposed in the Eurocode 2 Part 1-1 (EN 1992 Part 1-1) [99], are exposed, in order to present the calculation philosophy inherent to the simplified procedure of shear failure assessment at elevated temperatures ahead proposed.

5.2.2. THE EN 1992 PART 1-1 SHEAR CAPACITY ASSESSMENT METHODS

5.2.2.1. Members not requiring design shear reinforcement

The shear capacity of reinforced concrete members without shear reinforcement is given by equation 5.1:

$$V_{Rd.c} = \left[C_{Rd.c}\, k\left(100\rho f_{ck}\right)^{1/3} + k_1 \sigma_{cp}\right] b_w d \qquad (5.1)$$

with a minimum value given by equation 5.2:

$$V_{Rd.c} = \left(v_{\min} + k_1 \sigma_{cp}\right) b_w d \qquad (5.2)$$

where: $v_{min} = 0.035k^{3/2}f_{ck}$; $\sigma_{cp} = N/A_c$; $k = 1 + (200/d)^{0.5}$; $\rho = A_{sl}/(b_w d) \leq 0.02$; $C_{Rd,c} = 0.18/\gamma_c$; $k_1 = 0.15$., f_{ck} is the characteristic value of concrete compressive strength, A_c is the concrete cross-section area, b_w the minimum cross-section's width, d is the effective cross-section height and N represents the axial force due to loading or prestressing. A_{sl} is the area of tensile reinforcement, which extends for length grater or equal to ($l_{bd} + d$) from the section in analysis, as illustrated in Figure 5.2. In Figure 5.2 A indicates the position of the section in analysis.

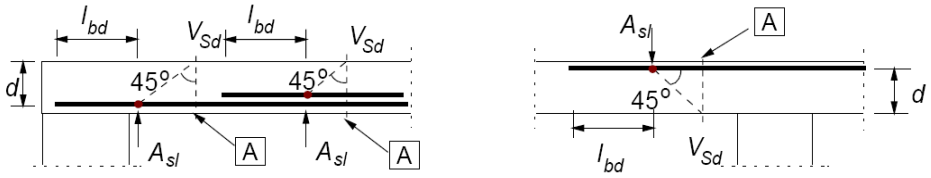

Fig.5.2 – Definition of A_{sl} in Equation 5.1 in accordance with the EN 1992 Part 1-1 [99].

5.2.2.2. Members requiring design shear reinforcement

The EN 1992 Part 1-1 model for shear capacity assessment of elements requiring shear reinforcement is based in a truss model, where the inclination of the concrete struts is limited within the interval that fulfils the condition of $1 \leq cot\theta \leq 2{,}5$. The definition of θ and a schematic representation of the truss model proposed in EN 1992 Part 1-1 is drawn in Figure 5.3. In that figure A represents the compression chord, B the concrete strut, C the tensile chord and D theshear reinforcement.

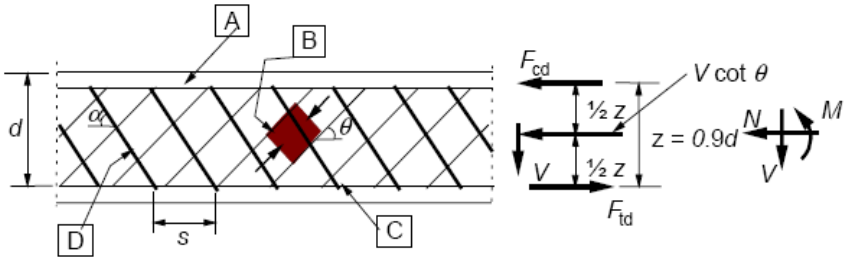

Fig.5.3 – Truss model proposed in EN 1992 Part 1-1 [99].

The shear capacity of a member with shear reinforcement, composed of vertical stirrups, is given by the minimum value between the capacity of the shear reinforcement ($V_{Rd,s}$) and the capacity of the concrete strut ($V_{Rd,max}$), expressed by equation 5.4 and 5.5, respectively.

$$V_{Rd,s} = \frac{A_{sw}}{s} z f_{ywd} \cot\theta \tag{5.4}$$

$$V_{Rd,\max} = \frac{\alpha_{cw} b_w z v_1 f_{cd}}{\cot\theta + \tan\theta} \tag{5.5}$$

where: A_{sw} is the area of transversal shear reinforcement (stirrups), s denotes the spacing between stirrups, f_{ywd} is the design yielding stress of the shear reinforcement and f_{cd} is the design compressive strength of concrete, θ is the inclination of the concrete strut and z the distance between the centre of the compressive and the tensile chords. The value of v_1 is given in equation 5.6 and α_{cw} in equation 5.7.

$$v_1 = 0{,}6\left[1 - \frac{f_{ck}}{250}\right] \qquad (5.6)$$

In equation 5.6 the term f_{ck} is the characteristic value of concrete compressive strength, and shall be introduced in the formula in MPa. In relation to equation 5.7, the term σ_{cp} is the mean compressive stress, measured positive, in the concrete due to the design axial load, obtained by averaging it over the concrete cross-section taking account of the reinforcement.

1	If $\sigma_{cp} = 0$	(5.7)
$(1 + \sigma_{cp}/f_{cd})$	If $0 < \sigma_{cp} \leq 0{,}25 f_{cd}$	
1,25	If $0{,}25 f_{cd} < \sigma_{cp} \leq 0{,}5 f_{cd}$	
$2{,}5\ (1 - \sigma_{cp}/f_{cd})$	If $0{,}5 f_{cd} < \sigma_{cp} \leq 1{,}0 f_{cd}$	

The EN 1992 Part 1-1 also presents a procedure to evaluate the shear capacity of elements presenting inclined shear reinforcement. However, this procedure is not illustrated in this work, because the model proposed is applied only to columns with vertical closed stirrups acting as shear reinforcement.

5.3. SHEAR FAILURE ASSESSMENT AT ELEVATED TEMPERATURES

5.3.1. THE EN 1992 PART 1-2 APPROACH

In section 4.4 of the EN 1992 Part 1-2 [4] it is referred, on one hand that, if minimum cross-sectional dimensions given by the tabulated method data are fulfilled, then no further checks for shear failure are necessary, and on the other hand, when shear failure calculation are used, they shall be supported by experimental data. Nevertheless, a simplified cross-sectional calculation method for shear assessment is presented in the Informative Annex D of the EN 1992 Part 1-2, although, the calculation procedure there proposed is not fully verified.

The main calculation philosophy presented in the above mentioned Informative Annex relies in the fact that shear cross-sectional capacity may be derived from the methods given in the Section 6 of the EN 1992 Part 1-1, considering reduced materials properties due to thermal induced degradation. When the structural fire design is based in the simplified calculation methods prescribed in Section 4.2 of EN 1992 Part 1-2, the shear capacity formulas given in EN 1991 Part 1-1 may be directly applied to the reduced cross-section.

Special considerations are made related to the assessment of shear capacity of reinforced concrete elements without shear reinforcement, or to the cases where shear capacity relies mainly upon the tensile strength of concrete. In these cases the actual shear behaviour of concrete at elevated temperatures must be considered, and if more accurate data related to the reduction of the tensile strength of concrete are not known, the reduction factors presented in Figure 3.4 may be applied. When the simplified calculation methods proposed in section 4.2 of EN 1992 Part1-2 are used, in the case of elements in which shear capacity depends on concrete tensile strength, it is important to evaluate if the source of tensile stresses is found in non-linear temperature distributions (such as in

voided slabs and thick beams). In these cases a reduction in shear strength must be observed in correspondence to the increased tensile stresses [5].

A similar procedure to the one proposed in Annex D of EN 1992 Part 1-2 was applied by Msaad *et al.* [105] to the calculation of the shear capacity of prestressed hollow core concrete slabs under fire conditions. In that study, equation 5.1, for reinforced concrete elements not transversally reinforced, was applied considering materials reduced strength properties. The concrete strength was taken as the average value at web's middle height, because of the fundamental role this zone plays against the horizontal tangential stresses. Experimental results presented a satisfactory correlation between the applied shear load and the shear capacity calculated with that simplified method.

5.3.2. TEMPERATURE EVOLUTION IN SHEAR REINFORCEMENT

As opposed to the cases where there is no shear reinforcement, when the shear capacity is dependent of links and stirrups, the acknowledgment of its properties is vital for the correct shear assessment. The key to understand the changes in shear reinforcement's properties is the determination of the evolution of temperature within it.

It is commonly accepted that for the analysis of longitudinal reinforcement, the steel temperature may be regarded as equal to the temperature of concrete correspondent to the rebar geometrical position, when the cross-sectional temperature profile is determined neglecting the presence of steel elements. However, this simplification is not suitable for the evaluation of temperature evolution of steel in transversal reinforcement. As referred in Annex D of EN 1992 Part 1-2, the transversal reinforcement, or links, pass through zones with different temperatures, and contribute to the distribution of heat from the warmer to the cooler zones. Thanks to this, the link's temperature is lower than that of the surrounding concrete, and tends to become uniform along its whole length [4]. In spite of this favourable effect, the link is not uniformly strained in its length, and in fact, the maximum stress occurs near a shear crack [4]. To solve this problem, in Annex D of EN 1992 Part 1-2 a reference point within the concrete cross-section to quantify the link's temperature is proposed. Figure 5.4 illustrates schematically the location of this point, identified by P. The point P is determined by the intersection of the links and the line a-a, which constitutes the upper boundary of the effective tension area A.

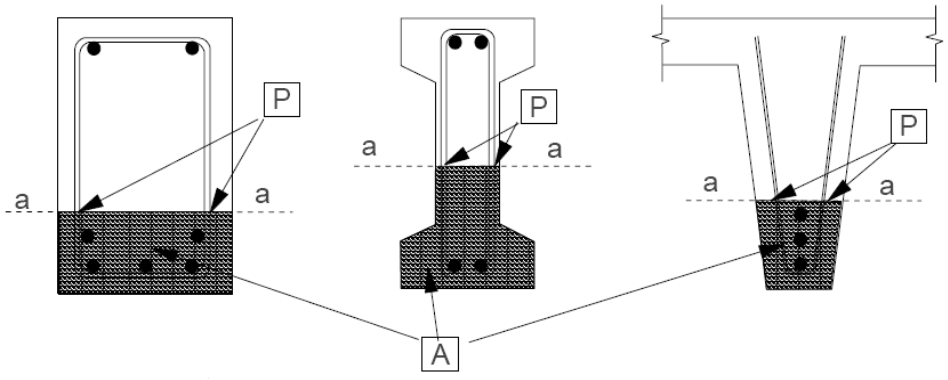

Fig.5.4 – Points to evaluate the reference temperature for links according to EN 1992 Part 1-2, [4].

The effective tension area is defined in Section 7. 3 of the EN 1992 Part 1-1, as the effective tensioned concrete section surrounding the tensile longitudinal reinforcement, delimited by the height $h_{c,ef}$. The value of $h_{c,ef}$ shall be taken as the minimum among the values of 2,5(h-d), (h-x)/3 and h/2. Figure 5.5 provides a definition of the terms *h*, *d* and *x*, as well a representation of the effective tension area

according to EN 1992 Part 1-1. In that figure B means the effective tension area and A the level of the reinforcing steel bars centroid.

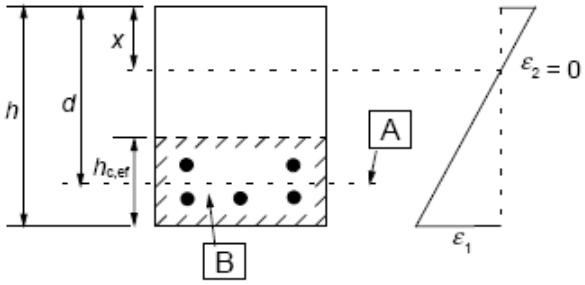

Fig.5.5 – Definition of effective tension area according to EN 1992 Part 1-1, [99].

Aiming to understand the evolution of temperature within the concrete cross-section including the presence of links, a 2-D thermal analysis has been carried out applying the thermal module of SAFIR. It must be remarked that this 2-D thermal analysis neglected heat transfer between the links and the surrounding concrete along the longitudinal axis of the reinforced concrete element. However, as only a qualitative evaluation of the links temperature is desired, the 2-D thermal analysis is acceptable. The results are drawn in Figure 5.6, regarding only 1/4 cross-section due to symmetry conditions of the problem, which represents one of the columns exposed to fire along the whole perimeter, previously illustrated in Figure 3.26. In Figure 5.6 the links and the longitudinal reinforcement are highlighted by a black contour. It is possible to observe in Figure 5.6 that the temperature in the link tends to become uniform during the process, although in initial time steps, due to the great thermal gradient imposed by the steeper initial branch of the ISO 834 standard curve [36], an important difference of temperature in several points corresponding to the link is observed.

Figure 5.7 illustrates a comparative analysis of the evolution of temperature in some key points considering the thermal calculation with links (Figure 5.6) and without links (Figure 3.28). The key points selected are the centre of the corner longitudinal reinforcing steel bar (point 2), the bottom of the link intersecting the corner reinforcing bar (point 1), the central reinforcing steel bar (point 6), the point of the link passing aside the central steel bar (point 5), and the point corresponding to position P (point 3 and 4, the first with link and second without) identified above in Figure 5.4.

The temperature evolution analysis for points 1, 3 and 6 has considered the presence of links, while the analysis for 2, 4 and 6 has not. A good correlation between the temperature in points 1 and 2 is recorded, meaning that if it is expected to determine the temperature profile in the bottom of the link, an accurate approximation is made if the temperature values are obtained from the thermal analysis of the concrete cross-section without transversal reinforcement, taking the temperature values from the position of the longitudinal steel bars (admitting that the presence of longitudinal bars has been considered, as in the analysis performed in Chapter 3).

Looking to evolution of temperature at points 3 and 4, it is possible to conclude that the results obtained are very similar considering or not the presence of links. This is an important observation, as this is the point the Annex D of EN 1992 Part 1-2 indicates as representative of the temperature of links.

In opposition to the previous two comparative analysis performed, the evolution of temperature in points 5 and 6 presents a considerable variation between each other. This may be explained by the fact that, the presence of the steel link constitutes a 'channel' of considerable higher thermal conductivity within the concrete cross-section, enabling temperature redistribution between points with higher thermal exposure (like point 1) and the cooler parts (point 5). When the links are not considered in the thermal analysis, the whole heat conduction has to be calculated through concrete elements. This difference explains why temperature evolution in point 5 (with links) follows more closely the same evolution in point 1 than the evolution obtained in the analysis of point 6 (no links).

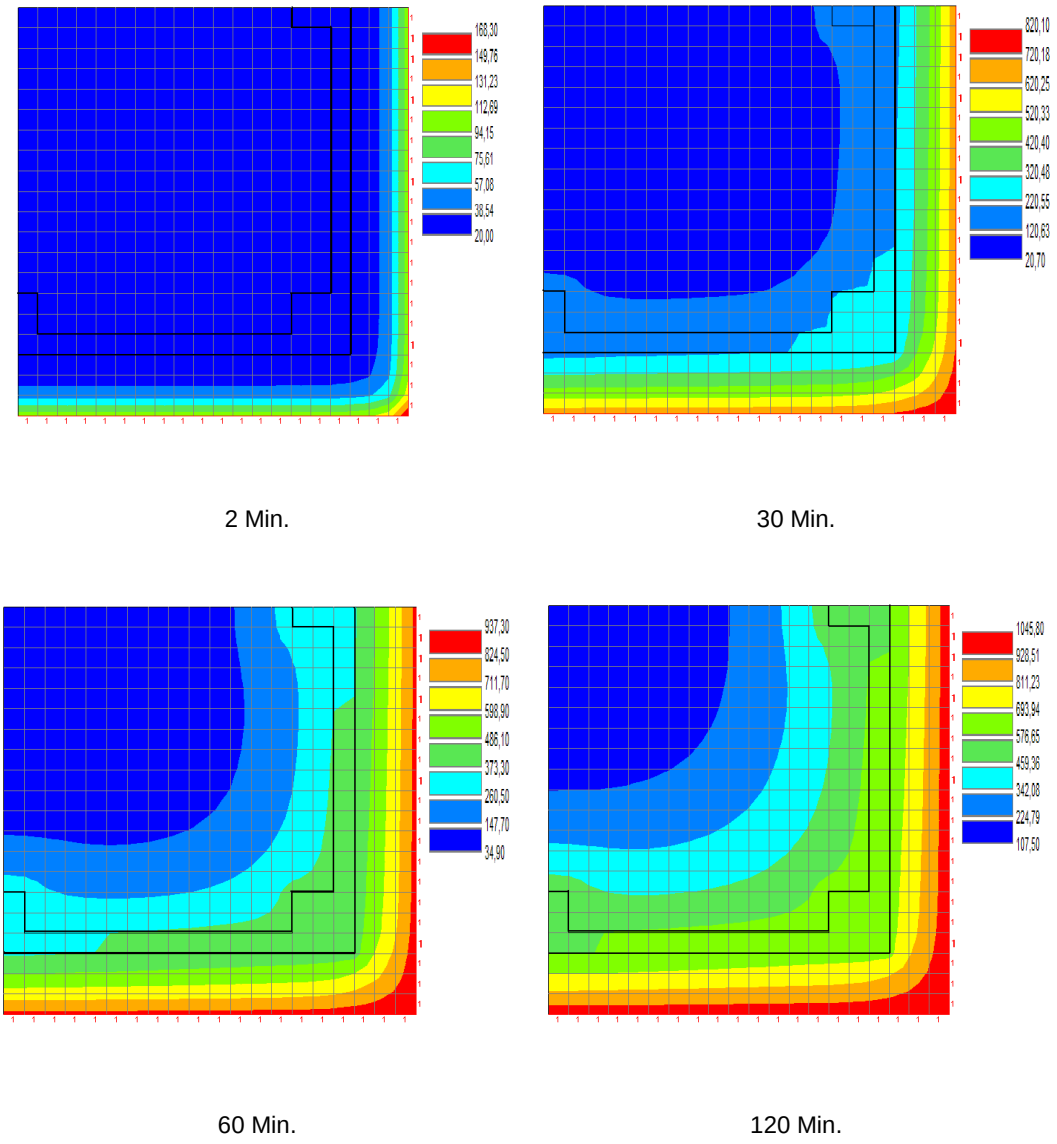

2 Min. 30 Min.

60 Min. 120 Min.

Fig.5.6 – Evolution of temperature (ºC) in the link obtained with a 2-D thermal analysis.

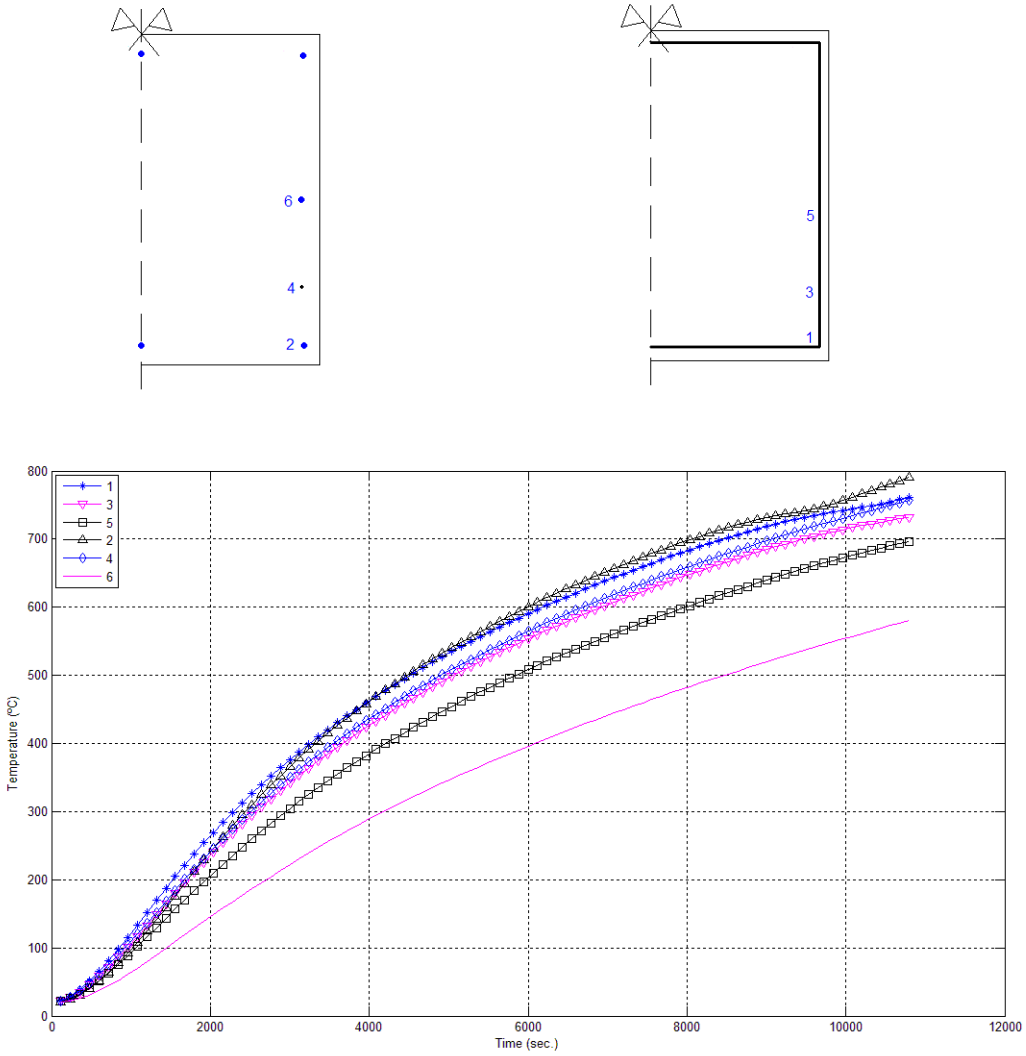

Fig.5.7 – Comparative analysis of the evolution of temperature in key points of cross-section with and without links.

In conclusion to this sub-section, it is referred that for the shear failure assessment to be performed hereafter, only the thermal calculations which have not considered the presence of links are going to be used, because this method is intended to be a complementary analysis to the advanced calculations previously performed, thus, no further thermal files are going to be created. The results obtained in Figure 5.6 and 5.7, must be carefully analysed because they are originated from a 2-D thermal analysis rather than from a 3-D analysis, meaning that heat transfer between the links and the surrounding concrete in the longitudinal axis of the concrete element has not been modelled. Because of this, in the following calculation two reference temperatures are going to be considered: the temperature in the corner reinforcement (point 2) and the temperature in the mid height cross-section (point 6). These two temperature histories constitute an upper and lower limit for the temperatures in links, and so, the lower and upper limit for their strengths, respectively. Furthermore, the temperature for links recommended in the EN 1992 1-2 lies within these two limits. This is important because the value of $h_{c,ef}$ is not constant during the course of the fire, meaning that an extra computational effort is required to define the point to read the links temperature recommended in EN 1992 1-2. In the procedure here

proposed this is not necessary as the there are two reference temperatures covering the recommended value. In this way the cross-section points where the reference temperatures are read remain constant during the analysis.

5.3.3. PROCEDURE FOR SHEAR CAPACITY ASSESSMENT OF REINFORCED CONCRETE ELEMENTS

The first step in the simplified procedure for shear capacity assessment of reinforced concrete elements is to compute the concrete reduced cross-section. In this work, the geometry reduction is performed similarly to the Isotherm of 500 ºC method proposed in the EN1992 1-2. It is acknowledged that the Zone method is more suitable to the analysis of fire exposed columns, regarding bending and axial compression (that is why this method was applied in Chapter 3). However, for shear capacity assessment this consideration is of reduced importance, so, for the sake of simplicity, the isotherm of 500ºC is applied to determine the reduced concrete cross-section, even in the analysis of columns. For every single time step, the sectional thermal file is read, and the cross-section geometry is updated, considering the fibres with temperatures lower than 500ºC. Inside the updated cross-section, the concrete is considered to keep its strength at ambient temperature.

The next step is to evaluate the strength of the steel in transversal reinforcement. For this purpose, the two reference temperatures mentioned in paragraph 5.3.2 are read from the sectional thermal files. The reduction of steel strength as function of temperature is made in accordance to the values proposed in EN 1992 1-2, presented in section 3.3 of this work.

Considering the reduced concrete cross-section and steel strength, the formulas presented in the EN 1992 1-1 are applied, considering the following features:

- The value of α_{cw} is determined at every time step considering σ_{cp} as the axial force dived by the reduced area of concrete;
- Equations 5.4 and 5.5 are equalized and solved in order to *cot(θ)* at every time step. The value of *cot(θ)* obtained in this way is the most unfavourable to the shear capacity. The final value of *cot(θ)* is compared against the reference interval referred in EN 1992 Part 1-1 ([1,0;2,5]) and corrected if needed at every time step;
- After the determination of *cot(θ)*, the values of $V_{Rd,s}$ and $V_{Rd,max}$ are computed and compared against de shear force acting in the concrete element at every time step. The values of $V_{Rd.s}$ and $V_{Rd,max}$ are attached to the number 1 and 2, if they are determined based in the temperature evolution of the corner or the mid height section rebar, respectively.

5.4. APPLICATION OF THE SIMPLIFIED PROCEDURE TO THE FRAME ANALYSED IN CHAPTERS 3 AND 4

In this section, the frame analysed in the previous chapters in the scope of the advanced calculation methods, are assessed regarding the shear failure of their columns. As to the shear failure assessment of beams, calculations performed, yet not presented in this work, have shown that for these structural elements shear forces are always below the level of shear capacity during the course of the fire.

In the following text, the number and position of finite elements and structural compartments of the frames are the same as exposed in Figure 3.27 and 3.31. The shear reinforcement for all the columns is considered constant throughout the whole structure with the value A_{sw}/s = 5,03 cm^2/m (ø8//200 mm, closed stirrups).

5.4.1. FRAMES WITH UNIFORM FIRE IN THE WHOLE FLOOR

5.4.1.1. Scenario 2: ISO 834 fire in compartments I, II and III

Figure 5.8 and 5.9 illustrate the application of the simplified shear failure assessment procedure above proposed. Figure 5.8 shows the evolution of shear capacity and shear force in the top of column 4 (the column with the greatest drift) when only the first floor is subjected to fire. It is possible to see that a shear failure due to lack of capacity of shear reinforcement is recorded approximately 23 minutes after the beginning of the heating process considering reference temperature 1, and 25 minutes if reference temperature 2 is chosen. From the same figure it is also possible to observe that shear failure due to crushing of concrete is far from being the cause of possible shear failure.

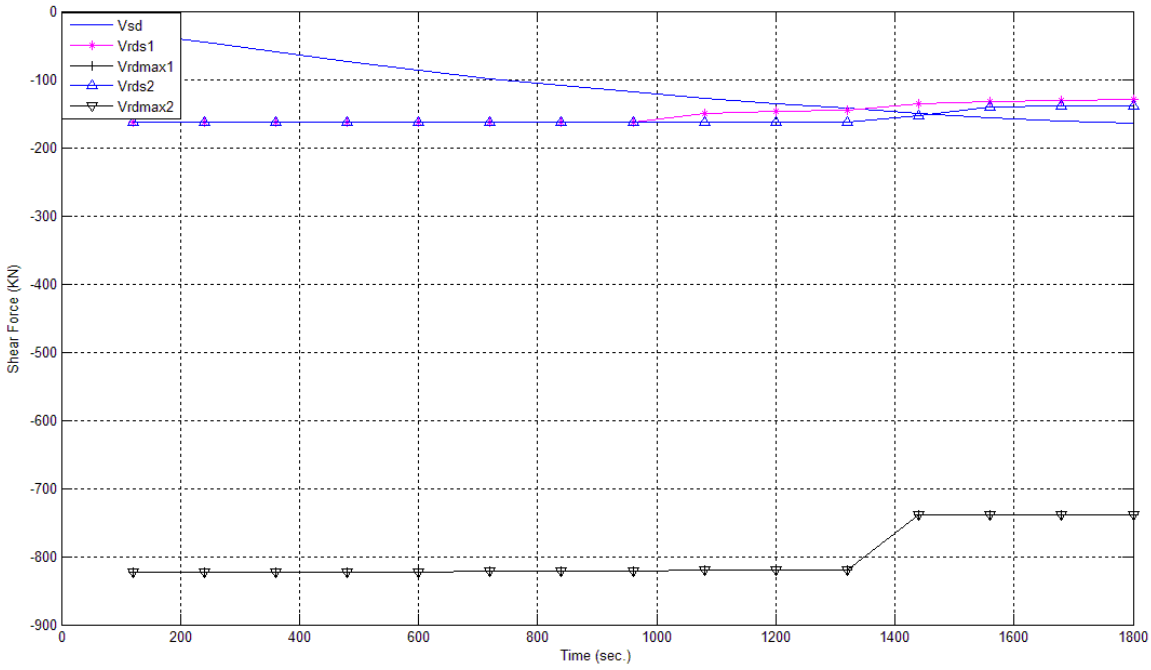

Fig.5.8 – Evolution of shear force and shear capacity in the top of column 4, scenario 2.

Figure 5.9 presents the evolution of shear capacity and shear force in the top of the column 8. Because this column is not exposed to fire, its shear capacity remains constant during the process. It is observed that, although an important increase of shear force is recorded, no shear failure is expected.

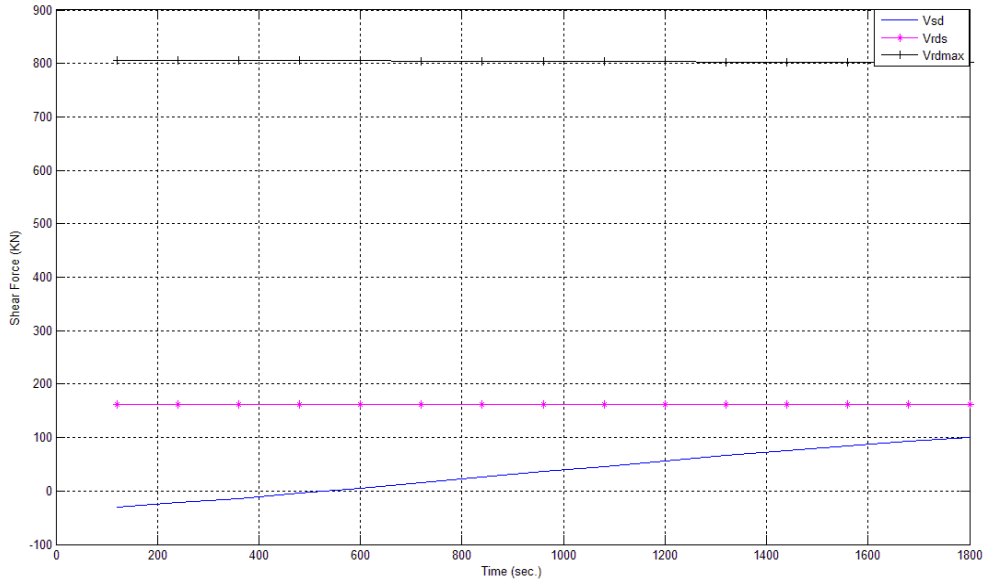

Fig.5.9 – Evolution of shear force and shear capacity in the top of column 8, scenario 2.

5.4.1.2. Scenario 3: ISO 834 fire in compartments IV, V and VI

In this case, it is observed in Figure 5.10 that a shear failure may occur in the top of column 8 after 25 minutes of fire exposure. The instant of shear failure in this case is approximately the same with the two links reference temperatures.

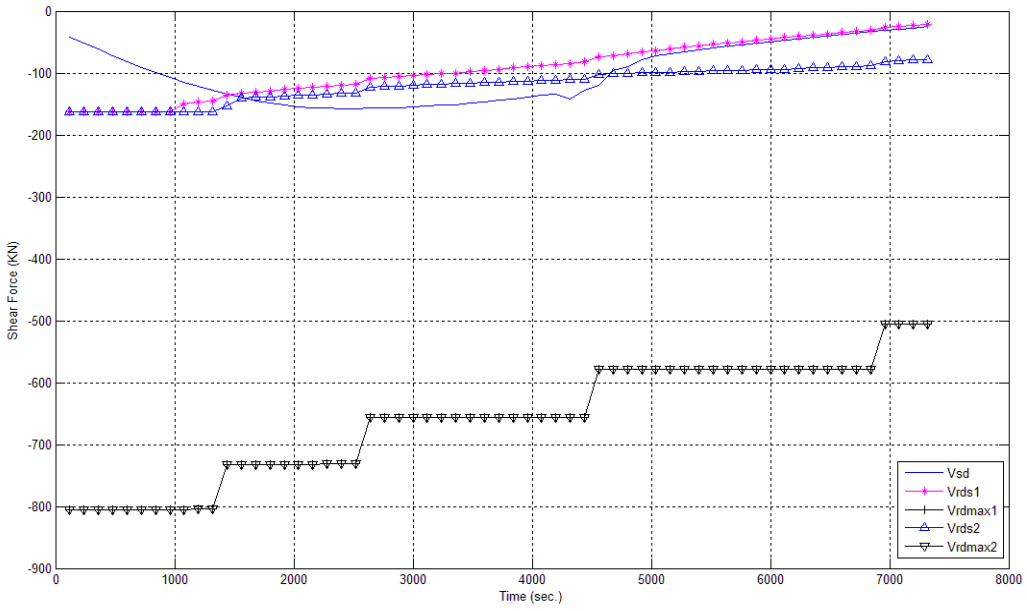

Fig.5.10 – Evolution of shear force and shear capacity in the top of column 8, scenario 3.

In Figure 5.11, the evolution of shear capacity and shear force in column 11 is plotted. This column is not exposed to fire, and corresponds to the column where the maximum shear forces have been recorded during the course of the fire. In opposition to the previous case, where the fire compartments were located in the first floor, here a shear failure is observed in the cold part of the building. This shall be taken just as an indicative reference of the possible anomalies that the cold part of the structure may suffer due to indirect restraint fire actions, because if shear failure could control the evolution of structural results, the analysis would have been stopped before column 11 suffered any hazard, due to the shear failure in column 8 which happens just 25 minutes after the fire initiates.

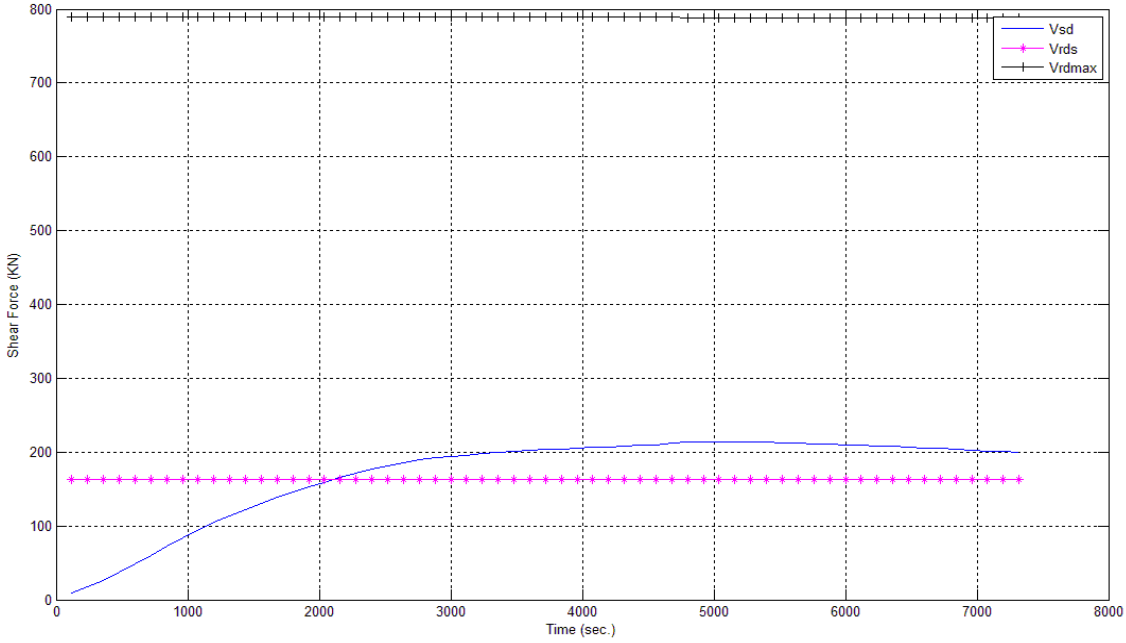

Fig.5.11 – Evolution of shear force and shear capacity in the top of column 11, scenario 3.

5.4.1.3. Scenario 1: ISO 834 fire in compartments I, II, III, IV, V and V

Figure 5.12 presents the evolution of shear capacity and shear force installed in column 4, when a simultaneous fire occurs in the first and second floor. A shear failure, due to lack of links capacity is observed at about 25 minutes of fire exposure considering both reference temperatures. For its turn, in Figure 5.13 it is possible to observe the evolution of shear capacity and shear force in column 8. In this case, only if the most unfavourable links reference temperature is considered, a shear failure is expected at final stages of the fire, meaning that for this column, shear failure is not limitative if compared to the analysis performed in Chapter 3. This was expected, because in this column no relevant shear force increase is recorded, as both top and bottom of this column suffer approximately the same drift during the course of the fire.

To conclude the analysis of the influence of shear failure in this fire scenario, in Figure 5.14 the comparative evolution of shear capacity and shear force is plotted, in reference to the cold part of the structure, more precisely column 12. It is possible to see that no shear failure is expected, although the links capacity is almost reached at about 50 minutes of fire duration. Once again, this indicates that indirect restraint fire actions may play an important role in the structural response to fire, even in the cold parts of the building.

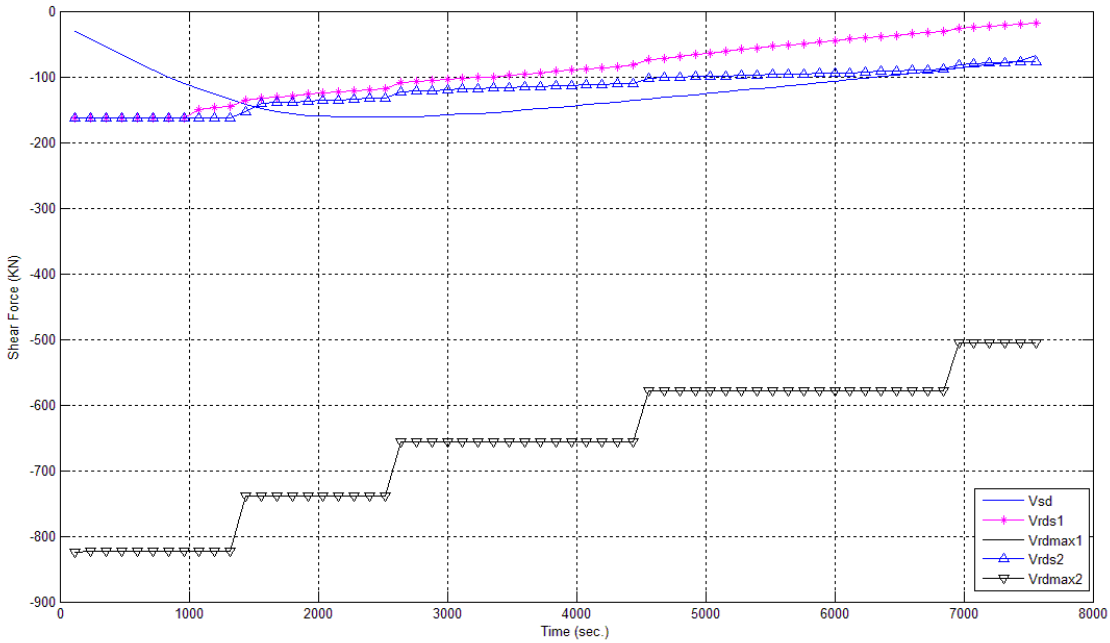

Fig.5.12 – Evolution of shear force and shear capacity in the top of column 4, scenario 1.

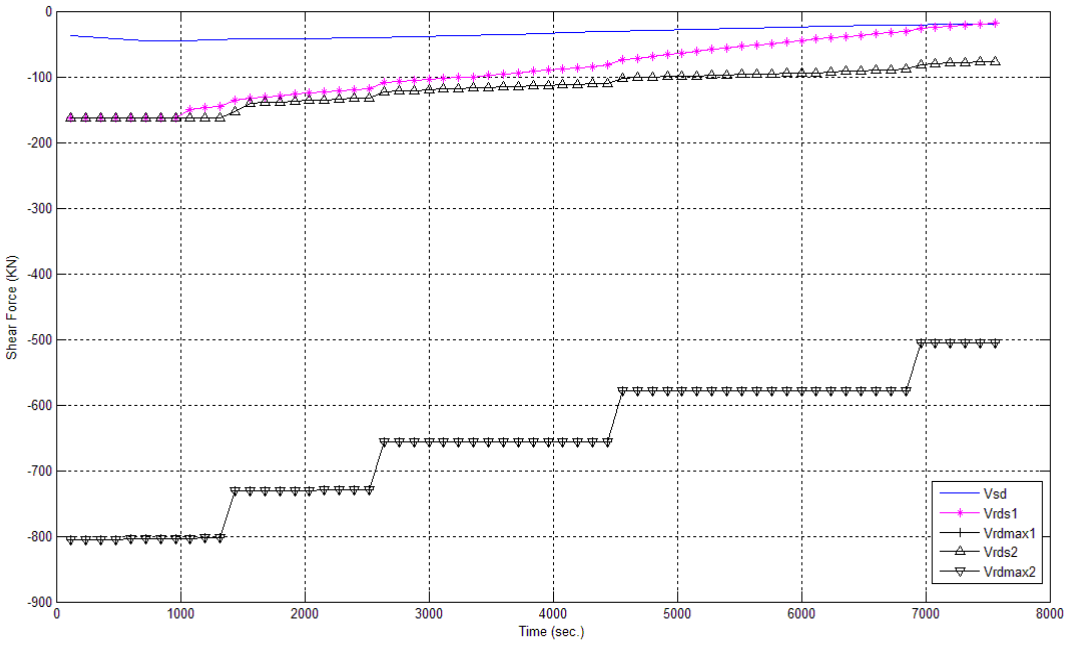

Fig.5.13 – Evolution of shear force and shear capacity in the top of column 8, scenario 1.

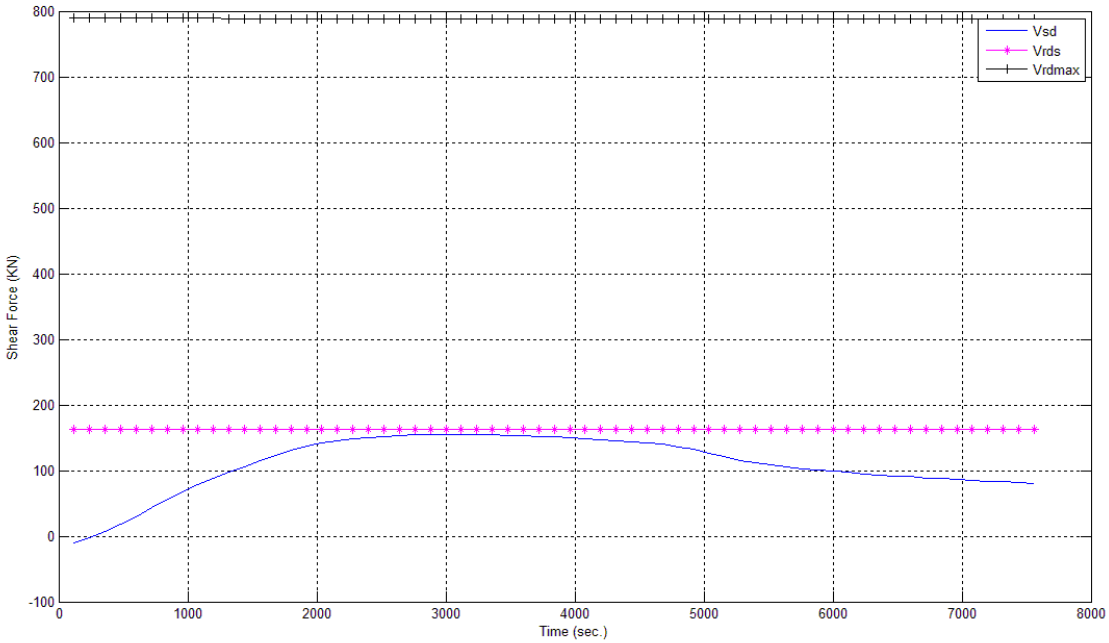

Fig.5.14 – Evolution of shear force and shear capacity in the top of column 12, scenario 1.

5.4.2. FRAMES SUBJECTED TO SINGLE COMPARTMENT FIRES

In this sub-section, the frames exposed to compartment fires are evaluated with the simplified procedure for shear failure assessment proposed. In opposition to the cases previously analysed, in these fire scenarios smaller drifts are observed, thanks to the fact that a lesser part of the structure is exposed to fire, thus a minor floor thermal expansion is expected. Nevertheless, as a considerable part of the structure remains at ambient temperatures, important restraint efforts are developed, enabling shear failures in the columns at the cold parts of the frame to happen.

5.4.2.1. Scenario 5: ISO 834 fire in compartment II

This fire scenario corresponds to case of a fire in the central compartment of the first floor, keeping the rest of the structure at ambient temperatures.

It is possible to observe in Figure 5.15 that, although the degradation of shear capacity induced by temperature rising, no shear failure is expected in column 3, because the shear force increase is not sufficient to promote it.

Different conclusions are withdrawn from the analysis of Figure 5.16 relative to the evolution of shear capacity and shear force in the top of column 4. This column is not exposed to fire, thus its shear capacity remains the same during the analysis. As expected, when compartment fires are modelled, the cold parts of the frame are subjected to great thermal restraint forces, and because of this a shear failure induced by lack of capacity of links is observed in column 4 approximately 46 minutes after the fire starts

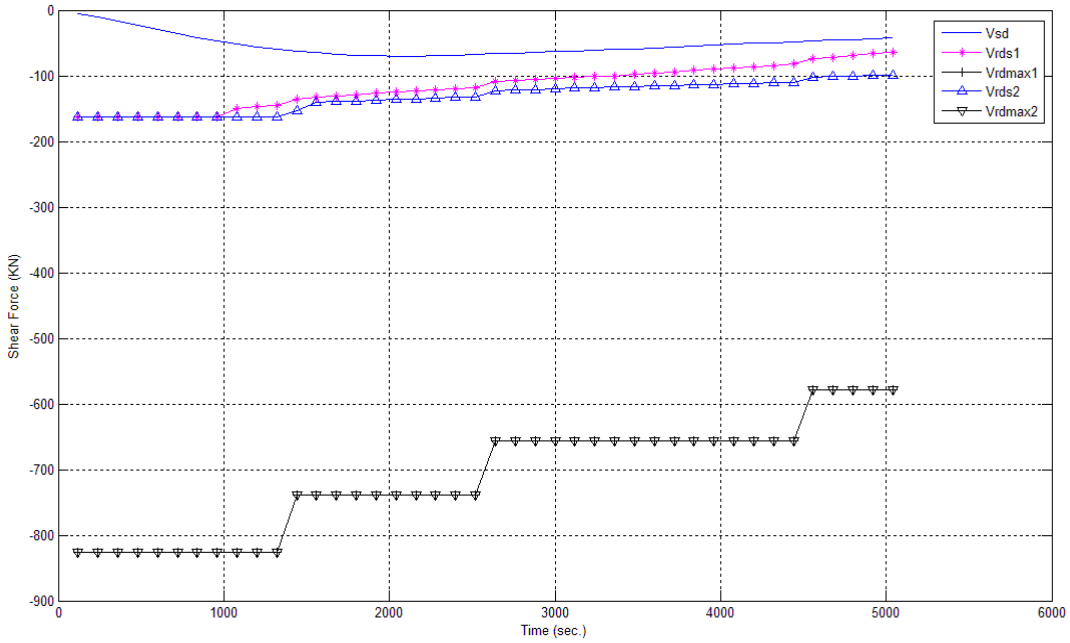

Fig.5.15 – Evolution of shear force and shear capacity in the top of column 3, scenario 5.

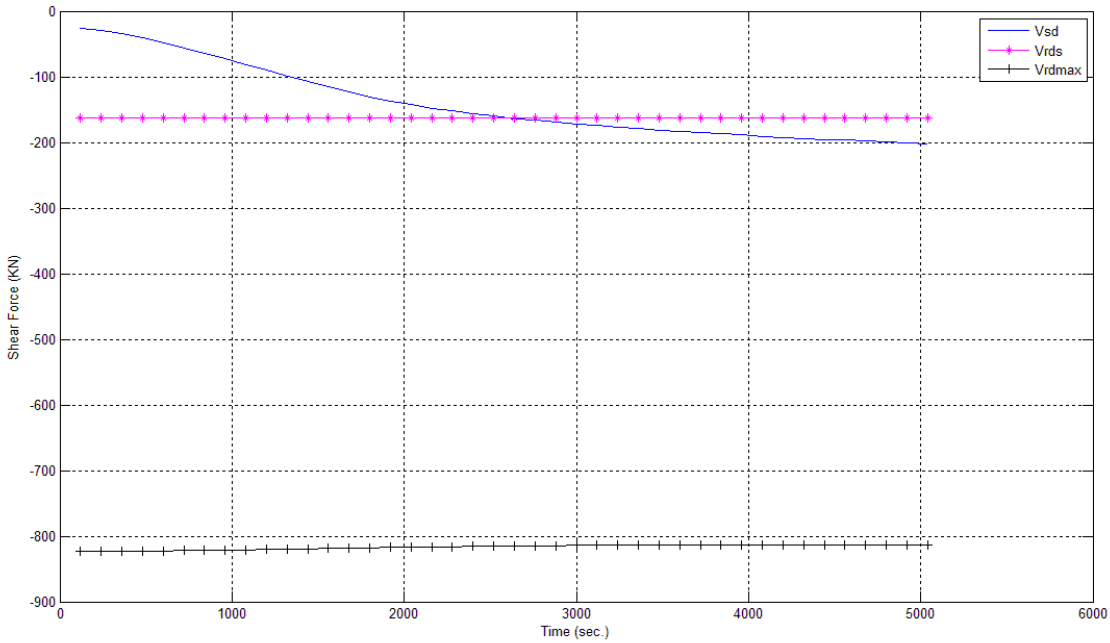

Fig.5.16 – Evolution of shear force and shear capacity in the top of column 4, scenario 5.

5.4.2.2. Scenario 7: ISO 834 fire in compartment V

In this case only the central compartment of the second floor is exposed to fire, and it is reminded that the thermo-mechanical analysis performed in Chapter 3 has presented no failure mechanism for this fire scenario during the three hours analysis. The observation of Figure 5.17 indicates that a possible shear failure may happens in column 7, which is located within the fire compartment, after 120 minutes of fire action.

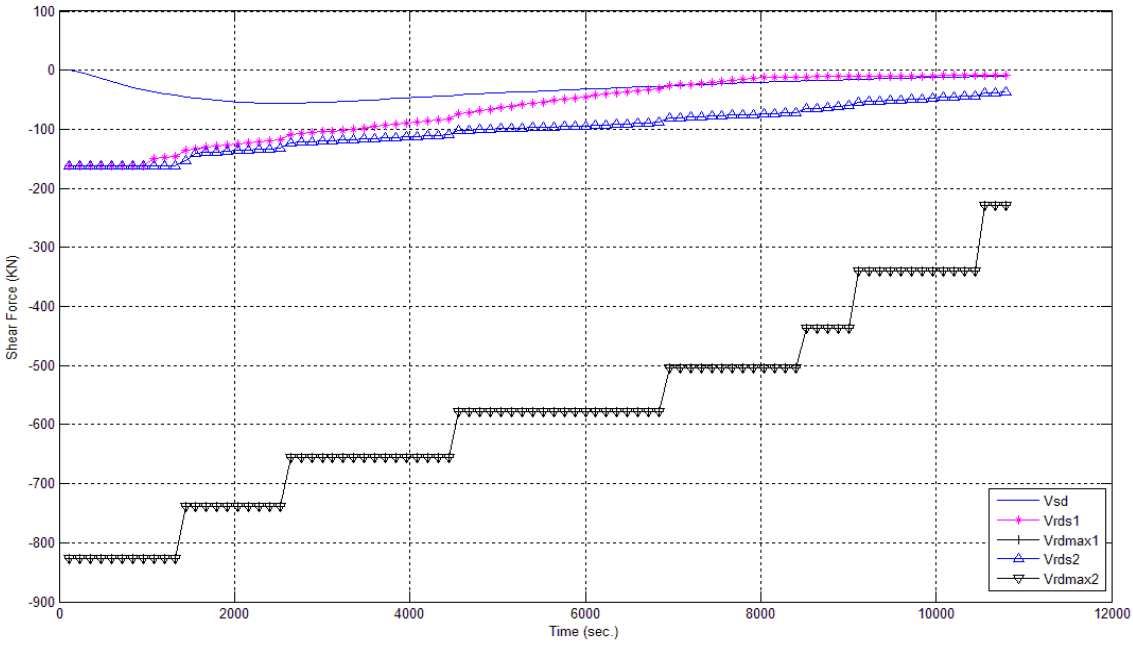

Fig.5.17 – Evolution of shear force and shear capacity in the top of column 7, scenario 7.

The prediction of shear failure by links rupture is indicated only regarding the most unfavourable reference temperature. Anyway, this is indicative, because in the previous analysis, where only compartment II is subjected to fire, the advanced calculation method stopped the analysis before the three hour limit, while in this case no stop is made, meaning that the shear capacity is much more deteriorated due to the longer thermal exposure. Notwithstanding that, this shear failure is of lesser importance when compared with the results presented in Figure 5.18. In this figure the evolution of shear force is compared against the shear capacity of column 8 (at ambient temperature). It is possible to see that after approximately 80 minutes of fire duration, a shear failure due to lack of links capacity occurs in that column. Once more, it is shown here, that when compartment fires are analysed, shear failures present higher importance in the colder parts of the structure that are subjected to high restraint forces. Because of this, the possible shear failure recorded in Figure 5.17 becomes secondary in relation to the failure observed in Figure 5.18.

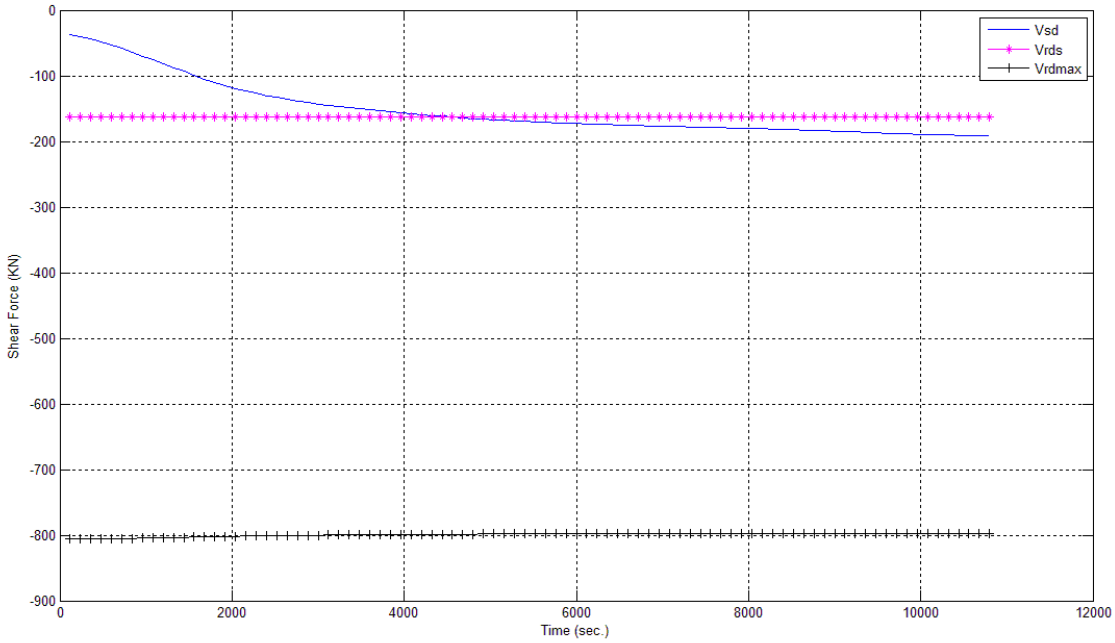

Fig.5.18 – Evolution of shear force and shear capacity in the top of column 8, scenario 7.

5.4.2.3. Scenario 4: ISO 834 fire in compartment I

The conclusions withdrawn for this fire scenario are similar to those in Scenario 5, meaning that no shear failure is predicted for the fire exposed column, and on the other hand, a shear failure induced by links lack of capacity is expected to occur in column 4 (at ambient temperature) approximately after 48 minutes of fire exposure. Because the evolution of shear efforts and capacities is similar to the ones presented for Scenario 5, the evolution for Scenario 5 is not plotted in this work.

5.4.2.4. Scenario 6: ISO 834 fire in compartment IV

The application of the simplified procedure of shear failure assessment to this fire Scenario presented similar results to the ones obtained in relation to Scenario 7. For this reason the results are not shown in this work.

5.5. APPLICATION OF THE SIMPLIFIED PROCEDURE TO DIFFERENT REINFORCED CONCRETE FRAMES

In the previous section, it has been pointed out that neglecting shear failure assessment in columns of frames exposed to fire may lead to non conservative results, meaning the structure is able to present a failure mechanism sooner than it was predicted applying advanced calculation methods regarding only normal stresses effects, such as bending moments and axial forces. However, those results are related to a particular structural layout, composed of a braced 3-bay reinforced concrete frame. Considering this, the present section is devoted to the application of the proposed simplified procedure for shear failure assessment to different types of reinforced concrete frames, and then to understand if

neglecting shear failure in advanced calculation methods leads, as in the previous sections, to non conservative structural fire performance predictions.

5.5.1. 3-BAY, 2 STOREYS UNBRACED FRAME

This frame consists of 2 storey high and 3 bay building, with 6,0 m long beams and 3,5 m long columns in the first floor and 3,0 m long in the second. This is the same frame previously presented in Figure 3.44. The structural fire analysis has been carried out based in the software SAFIR, but in this case, because only the shear failure prediction is in the line, no exhaustive study on the failure mechanism is shown in this work. However, the evolution of axial force, shear force, bending moment and structural displacements, as well as the cross-section and reinforcement layout of beams and columns are possible to be found in Appendix B. The shear reinforcement in the columns is composed of closed stirrups (ø6//150 mm).

In the analysis of this frame, in opposition to the previous calculations, exterior columns (elements 1 to 20 and 61 to 80 in Figure 3.44) are heated only in three faces, remaining the outer face at ambient temperatures. This assumption was made, to guarantee that the simplified shear failure procedure here proposed is applied to a full variety of frames and heating conditions. Figure 5.19 presents the results relative to element 80, which is the one that has shown the most relevant shear force evolution during the course of the fire. It is observed that no shear failure is predicted. In this particular analysis only the reference temperature related to the cross-section corner rebar has been considered, because the column of this frame present no mid-height rebar (as it is possible to very in Appendix B). Nevertheless, even considering only the most unfavourable reference link temperature, no shear failure is expected.

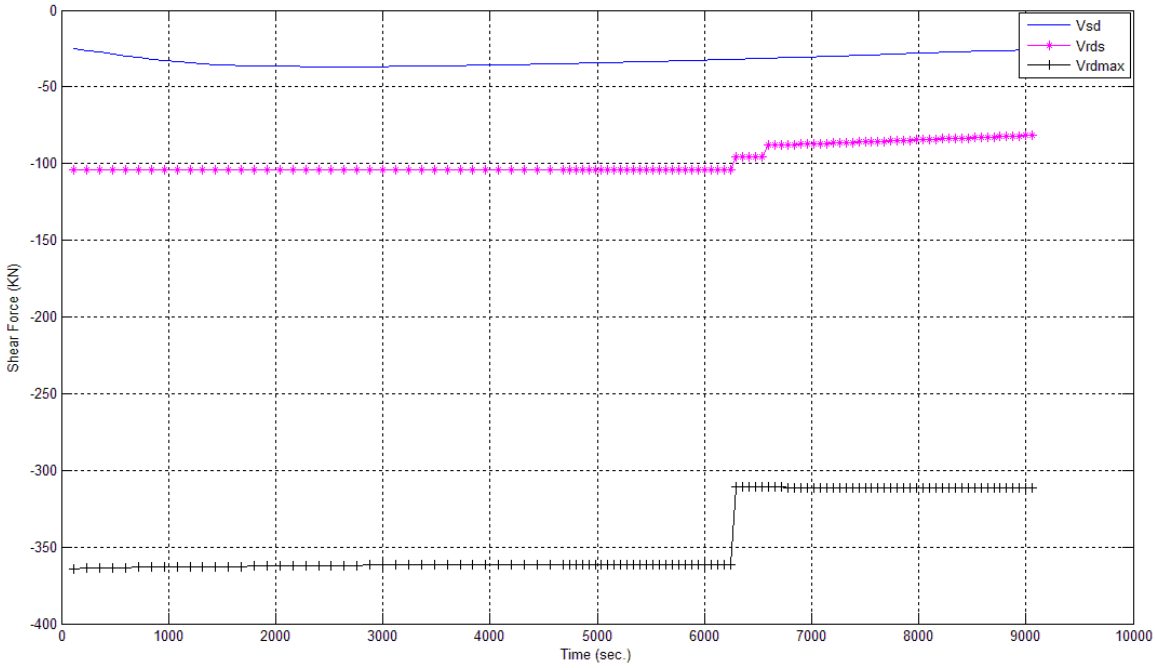

Fig.5.19 – Evolution of shear force and shear capacity in element 80.

5.5.2. 3-BAY, 2 STOREYS BRACED FRAME

The geometrical properties of the last frame remain valid to this one, with the difference that in this case, the frame is braced by means of a horizontal restraint located at the level of the floors in the left side (elements 10 and 20 in Figure 3.44). This means that the thermal expansion is directed integrally towards the right side, imposing a drift in the outer columns greater than in the previous case. Looking to Figure 5.20, it is concluded that, even with this unfavourable effect, no shear failure is expected.

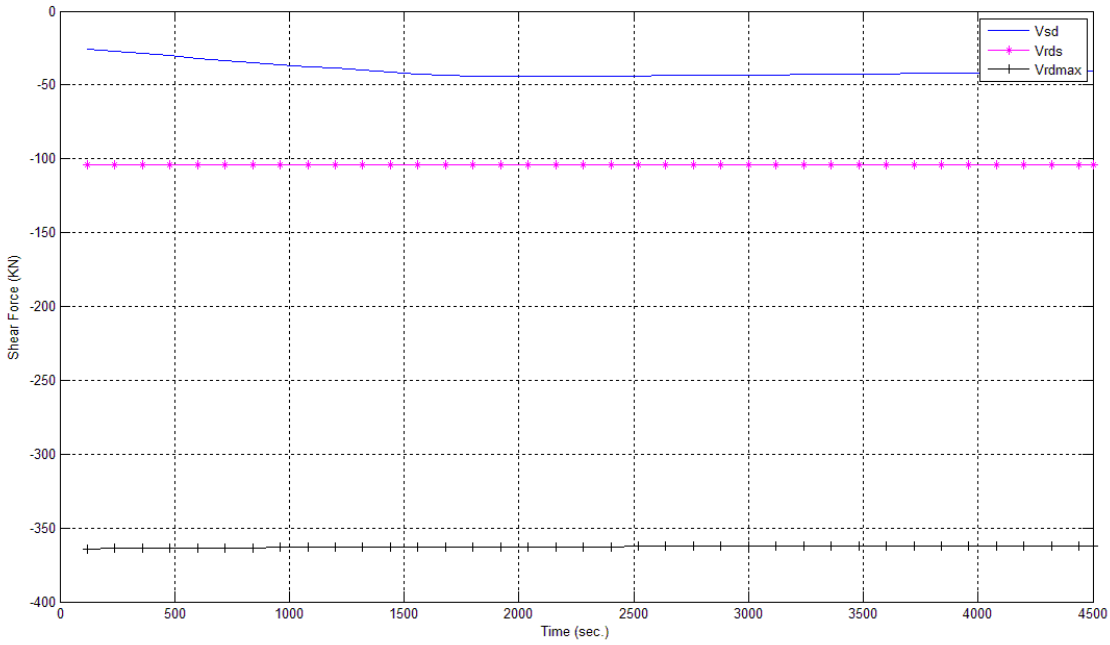

Fig.5.20 – Evolution of shear force and shear capacity in element 80.

Considering the results obtained for the last two frames, it is understood that when the frame is composed of columns with low stiffness compared to the beam's stiffness, no important shear force increase is observed and thus no shear failure is expected. It is possible to conclude, from the observation of the evolution of internal forces in these frames, presented in Appendix B, that the failure mode is related to the formation of plastic hinges in the ends and in the mid span of the beams until the stability of the structure is no more possible to be achieved. The heating conditions in the outer columns seem to have no special implications. It is believed that if the outer columns were fully heated in their perimeter, the results would remain similar to the ones obtained, because in this case, relative stiffness between columns and beams is in charge of the global structural behaviour.

5.5.3. FRAMES CONTAINING A SHORT COLUMN

Reinforced concrete frames containing short columns often constitute the structural solution for many buildings. It is generally accepted that these short columns, because of their higher stiffness compared against the 'normal' length ones, are subjected to an important share of the horizontal actions applied to the structure. Considering this, and keeping in mind that the effect of floors' thermal elongation results in horizontal forces within the structure, it immediately yields that these sort of columns may be particularly susceptible to shear failure during the course of the fire. To investigate these two frames containing a short column have been analysed with the simplified procedure here proposed.
The first frame is similar to the one analysed regarding fire scenario 1, replacing column 4 for a short column of 1,0m length. The new structural model is illustrated in Figure 5.21, considering shear

reinforcement in the top of this element composed of closed stirrups (ø8//100 mm). The longitudinal reinforcement in the beams and columns is the same as in Figure 3.27.

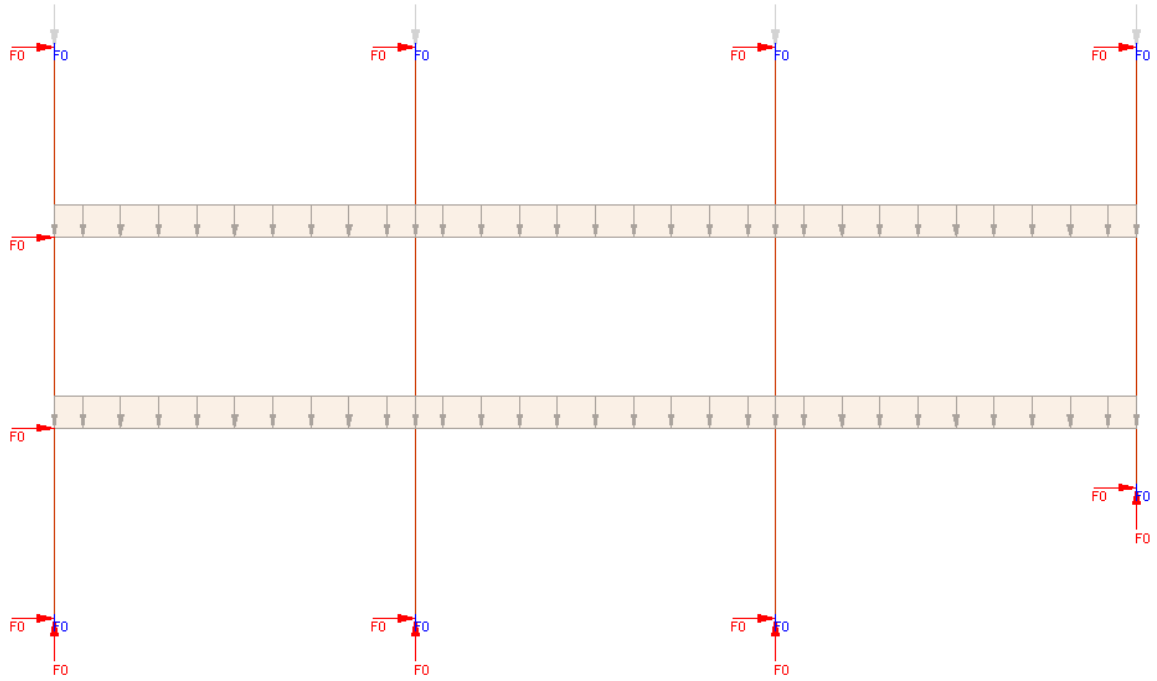

Fig.5.21 – Structural model containing a short column (column 4).

The shear force and shear capacity evolution in column 4 is plotted in Figure 5.22. The first conclusion withdrawn from that figure is that the global fire resistance of the frame is reduced by the inclusion of the short column. In the second place, it is observed that the possible shear failure is highlighted in comparison to the frame without this particular element. The shear failure due to lack transversal reinforcement capacity is recorded after approximately 7 minutes of fire exposure. This possible failure occurs at a very initial stage of the fire, explaining why the values of $V_{Rd,s}$ and $V_{Rd,max}$ keep their ambient conditions capacity (the temperature evolution in cross-section is steal limited, see Figure 3.28). Furthermore, in Figure 5.22 it is observed that the intersection between the shear capacity and shear force curves is more pronounced than it is the previous cases where no short columns had been considered, underlining the severity that shear effects may have in short column within structures submitted to fire actions.

The second frame containing a short column analysed in this sub-section is a variation of the frame previously presented in sub-section 5.5.2, where the right end column of the first floor has been replaced by a 1,0m length column, as it is schematically represented in the model of Figure 5.23. The transversal reinforcement at the top of the short column is considered to be composed of closed stirrups (ø6//80 mm).for the same reasons referred regarding the analysis the results presented in Figure 5.19 and Figure 5.20, only one reference temperature has been considered.

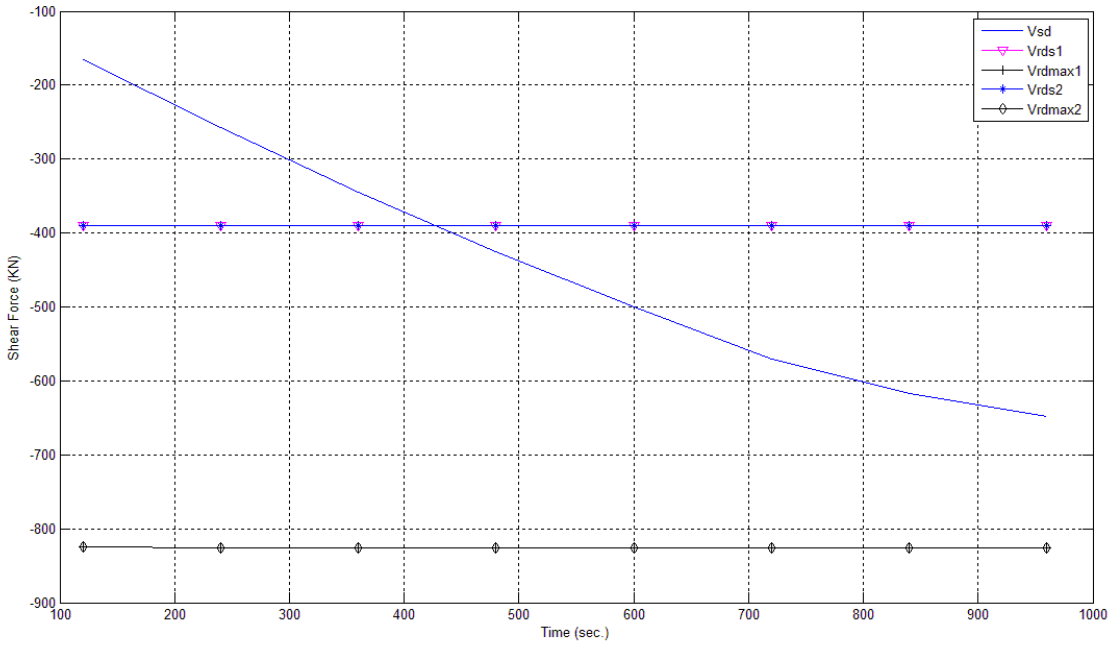

Fig.5.22 – Evolution of shear force and capacity at the top of the short column (column 4).

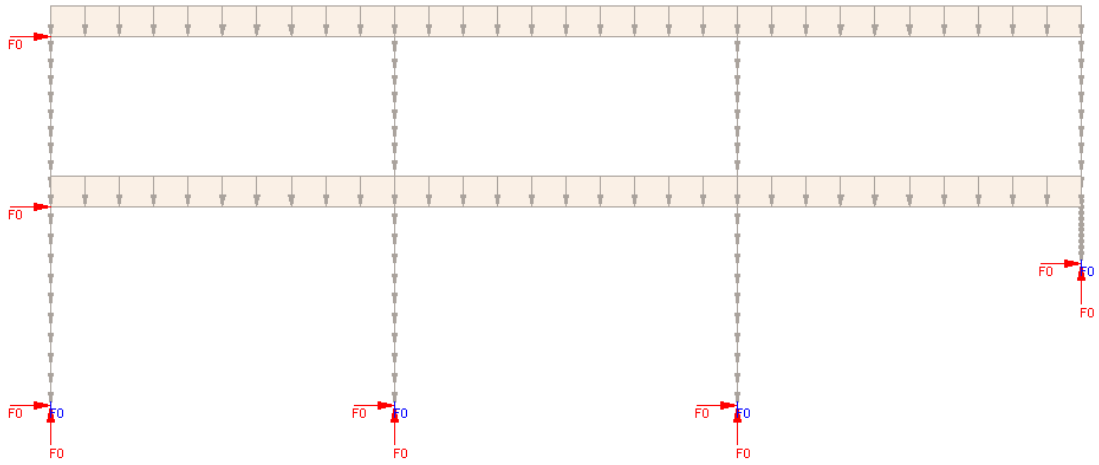

Fig.5.23 – Structural model.

In Figure 5.24 it is plotted the evolution of shear force in the top of the short column against the evolution of shear capacity in accordance with the simplified assessment procedure proposed. Once again, the inclusion of a short column in the frame's structural layout, promoted an earlier fire induced collapse compared to the final time achieved in the frame without this element (frame presented in 5.5.2). In opposition to the results obtained for the same frame without the presence of a short column, a shear failure is predicted for the section located at the top of the referred column approximately 10 minutes after the beginning of the heating process. The reason why in Figure 5.24 the shear capacity maintains the initial value is the same mentioned for the analysis of Figure 5.22.

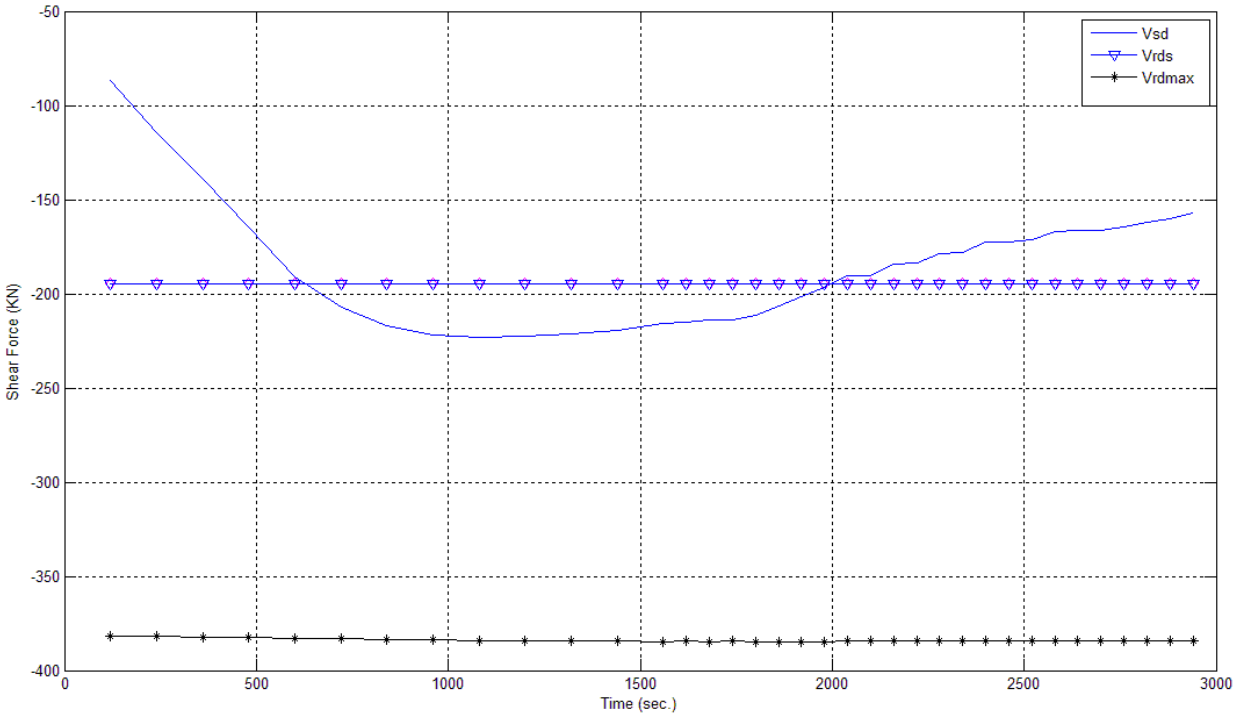

Fig.5.24 – Evolution of shear force and shear capacity at the top of the short column.

5.6. CONCLUDING REMARKS

A simplified procedure for shear failure assessment at elevated temperatures has been proposed in this chapter. The calculation procedure is based in the recommendations of EN 1992 Part 1-2, and applies the results obtained for a previous analysis based in advanced calculation methods.
The application of the simplified shear assessment procedure has revealed that the effects of shear in concrete columns exposed to fire may play a decisive role in the structural performance. However, the fact that in the analyses above presented the shear force installed in the columns intersects the curve representing the shear capacity shall not be interpreted as an effective shear failure, meaning that the previous structural results from SAFIR are misleading, and an anticipated collapse is expected. It is obvious that the simplified procedure proposed is in its initial development stages, still lacking of experimental validation. Furthermore, even at ambient temperatures, shear calculation models have shown to be of limited accuracy, thus their extrapolation to fire conditions shall be carefully considered.

Notwithstanding that, the conclusions withdrawn from this chapter analyses may be summarized as:

- Shear failure may occur in columns exposed to fire due to excessive horizontal expansion of floors;
- If shear failure occurs in columns, lesser times of fire resistance may be displayed by the whole frame;
- It is possible to quantify the risk of shear failure by means of simplified calculation procedure, that uses the results obtained in the advanced models calculations;
- The shear failure of columns is controlled by the shear reinforcement exhaustion, at least in the results outputted by the proposed model;
- The point where the links reference temperature has no significant influence in the results obtained. However, for long times of fire exposure, different links temperature may lead to divergent situations. While the recommendations of the EN 1992 1-2 are not clarified, it is believed that the most severe reference temperature to the links should be considered.

- The inclusion of short columns in the structural layout increases the risk of shear failure, because these elements present a higher stiffness in relation to horizontal actions than the 'normal' length columns, thus retaining a higher level of shear force. The existence of short columns shall be carefully examined when assessing the structural fire behaviour of a reinforced concrete building**.**

6
Conclusions and Further Works

6.1. FINAL REMARKS TO THE WORK

This section is directed to summarize the main conclusions which have been withdrawn during the course of the work.

In Chapter 3 the global behaviour of a three-bay reinforced concrete 2D frame has been traced during the course of a fire, acting simultaneously on two floors. Because the frame has been modelled comprising a bracing system, the beams thermal elongation have been directed towards one single side, imposing a considerable drift at the outer columns. As a result, the failure mechanism of the frame is characterized by the failure of the outer column, due to a combination of strength loss and increase of bending moment imposed by the floors expansion. Besides that, it is also noteworthy to recall that during the course of the fire a plastic hinge has appeared in a column not exposed to the fire, emphasizing the importance of the interaction between the exposed and the cold parts of the building during the fire.

The conclusions from the study performed in Chapter 4, contributed to understand that the complexity of the interaction between the exposed and the cold parts of frame increases with the consideration of compartment fires, due to the high level of restraint displayed by the analysed frame. This means that a great deal of stresses redistribution takes place throughout the frame.

It is precisely the redistribution of stresses within the structure that lead to the conclusions concerning the fire safety assessment neglecting fire induced effects. As it has been demonstrated in this work, applying the Zone method (the most accurate simplified calculation method prescribed in the EN 1992 1-2) neglecting fire induced effects outputs fire resistances higher than the ones obtained relying on the global response analysis based in advanced calculation methods. It must be emphasized this conclusion is based in results obtained using the standard fire curve as fire model, when the EN 1991 1-2 states that when fire safety relies in this fire curve, no fire induced effects need to be considered. The possible reason for this assumption may be related to the fact that this fire curve is too severe and unrealistic. However, even considering this drawback, the results obtained clearly yield that a global response analysis outputs an evolution of stresses not at all possible to assess with simplified cross-sectional methods, thus, as the calculation have shown, a non-conservative assessment is performed applying the last methods.

Another conclusion withdrawn from this work is related to the effects of shear on the safety of reinforced concrete structures exposed to fire. Although the EN 1992 1-2 indicates that shear failure is uncommon in fire situations, the simplified procedure here developed based in the very recommendations given in the EN 1992 1-2 has shown a significant number of situations where shear failure may lead to an earlier structural collapse than it is output by the advanced model. Of course the procedure here proposed is still in its earliest stages of development, therefore the results obtained shall not be understood as definitive ones. In spite of this, the results shall at least bring to discussion if neglecting shear is a reasonable procedure in structural fire safety assessment of reinforced concrete structures.

The effects of shear failure are more visible when the frame comprises a short column, because this element possesses a great stiffness when compared to the 'normal' length columns, thus receiving the greatest amount of shear when horizontal actions act on the structure. Furthermore, the existence of a short-column has proven itself to present a deteriorative effect also when only bending moment and axial force are considered, as it has been illustrated by the fact that in chapter 5 the frames comprising a short-column displayed a lesser time of fire endurance than the time previously when no column of this sort was added to the structure.

To conclude, in the case of highly restrained structures, fire action is above all manifested as a horizontal action, increasing remarkably the internal stresses in the frame's columns, thus these elements should be carefully assessed in order to obtain the necessary fire resistance.

6.2. FURTHER WORKS

To continue the work here carried out, several paths may be followed. At first, the comparison between the global response analysis and the simplified cross-sectional methods should be extended to other frame layouts and to different cross-section shapes, dimensions and reinforcement ratios. Only after this is complete, the results may be generalised to the great majority of actual reinforced concrete buildings. It is now appropriate to refer that this work has been developed within a timeline of one semester, thus imposing a considerable time restraint to the development of the necessary wide range of case studies, in order to generalise the results obtained.

The second possible improvement to this work relies in the application of different fire models, especially natural fire simulations. If natural fires are analysed, the results would be extended to more realistic fire scenarios, thus raising the degree of their validity in the scope of the performance-based approach to fire analysis. Of course this will only be possible when appropriate concrete constitutive models became available within the computer codes, enabling the correct simulation of reinforced concrete members during the cooling phase of the fire.

Another upgrade to the analyses here performed would be found in the fire analysis considering 3D structures. Only with a 3D analysis it is possible to consider the whole structural behaviour including the slabs membrane action. As this membrane action involves the development of considerable forces in the slabs plane (tensile or compressive), these forces are restrained by the beams, and through them, by the columns. This may result in a change of the stresses installed in the columns and increase even more the divergence of the fire resistance obtained with the advanced method and the simplified one (that neglects fire induced effects).

As to the simplified shear failure assessment procedure here proposed, it is believed that no further numerical work is needed until any sort of experimental data results are obtained indicating the factors governing shear failure at elevated temperatures.

REFERENCES

1. Beitel, J., Iwankiw, N., *Analysis of Needs and Existing Capabilities for Full-Scale Fire resistance testing, National Institute of Standards and Technology* NIST GCR 02-843, 2002.

2. *One Stop Shop in Structural Fire Engineering, http://www.mace.manchester.ac.uk/project/research/structures/strucfire/default.htm, accessed in 2009/04/11*.

3. Fletcher, I., Borg, A., Hitchen, N., Welch, S., *Performance of concrete in fire: a review of the state of the art, with a case study of the Windsor tower fire*, in *Proceedings of the fourth international workshop Structures in Fire*. 2006: Aveiro. p. 779-790.

4. European committee for standardisation, *Design of concrete structures: General rules: - Structural Fire Design, EN 1992-1-2, Eurocode 2, Part 1-2*: Brussels, 2004.

5. Purkiss, J.A., *Fire Safety Engineering - Design of Structures*. Second ed. 2007, Oxford: Butterworth-Heinemann.

6. Coelho, A.L., *Segurança contra incêndio em edifícios de habitação 0008*. 1998, Amadora: Edições Orion.

7. Hasofer, A.M., Beck, V.R., Bennetts, I.D., *Risk Analysis in Building Fire Safety Engineering*. First ed. 2007, Oxford: Butterworth-Heinemann.

8. Lataille, J.I., *Fire Protection Engineering in Building Design*. 2003, Burlington: Butterworth-Heinemann.

9. Office of the Deputy Prime Minister, *The Building Regulations 2000. Ammendments 2002 to Approved Document B*. 2002: ODPM, London.

10. Khoury, G.A., *Fire and Concrete: From Materials Behaviour to Application*, in *Proceeding of the International workshop "Fire Design of Concrete Structures - From Materials Modelling to Structural Performance"*. 2007: Coimbra. p. 3-24.

11. Bailey, C., *Structural Fire Design: core or specialist subject?* The Structural Engineer, 2004. **available at http://www.mace.manchester.ac.uk/project/research/structures/strucfire/DataBase/References/defaultOther.htm**.

12. Fletcher, I.A., Welch, S., Torero, J.L., Carvel, R.O., Usmani, A., *The Behaviour of Concrete structures in fire.* Journal of Thermal Science .2007. **11**(2): p. 37-52.

13. Gabriel Alexander, K., *Effect of fire on concrete and concrete structures.* Progress in Structural Engineering and Materials, 2000: p. 429-447.

14. Lennon, T., *The need for large-scale fire tests*, in *Proceedings of the International workshop "Fire Design of Concrete Structures - From Materials Modelling to Structural Performance"*. 2007: Coimbra. p. 541-549.

15. Gonçalves, M.J.C.R., *Fire Behaviour of Structural Concrete Elements - Numerical Analysis and Methodology (in Portuguese), Ph.D thesis*. 2007 University of Porto.

16. Rigberth, J., *Simplified Design of Fire Exposed Concrete Beams and Columns - An evaluation of Eurocode and Swedish Building Code Against Advanced Computer Models.* Department of Fire Safety Engineering, Report 5063, Lund, Sweden, 2002.

17. Fermandes, M., *Verificação da Resistência ao Fogo de Estruturas de Betão com Base nos Métodos Simplificados do EC2 - Parte 1-2, Mestrado Integrado em Engenharia Civil - 2008/2009 - Departamento de Engenharia Civil, Faculdade de Engenharia da Universidade do Porto, Porto, Portugal, 2008.*

18. *The Cardington Tests, http://en.wikipedia.org/wiki/Cardington_test, accessed in 2009/04/05.*

19. Bailey, C., *Holistic Behaviour of Concrete Buildings in Fire.* Structures & Buildings, 2002. **152**(3): p. 199-212.

20. Deeny, S., Empis, C. A., Stratford, T., Gillie, M., Torero, J.L., *The Dalmarnock fire tests on a cast insitu concrete structure*, in *Proceedings of the International workshop "Fire Design of Concrete Structures - From Materials Modelling to Structural Performance"*. 2007: Coimbra. p. 559-570.

21. Lane, B., Lamont, S., *Arup Fire's presentation regarding tall buildings and the events of 9/11, available at http://www.arup.com/_assets/_download/download353.pdf.* London, 2005.

22. European committee for standardisation, *Basis of structural design, EN 1990, Eurocode 0*: Brussels, 2002.

23. Taerwe, L., *From Member Design to Global Structural Behaviour*, in *Proceedings of the International workshop "Fire Design of Concrete Structures - From Materials Modelling o Structural Performance"*. 2007: Coimbra. p. 253-270.

24. Lennon, T., et al., *Designer's guide to EN 1991-1-2, 1992-1-2, 1993-1-2 and 1994-1-2 handbook for the fire design of steel, composite and concrete structures to the eurocodes 0008*. Designer' s guides to the eurocodes 0011, London: Thomas Telford.

25. Kodur, V.K.R., Phan, L., *Factors governing the fire performance of high strength concrete systems*, in *Proceedings of the fourth international workshop Structures in Fire*. 2006: Aveiro. p. 573-586.

26. Schneider, U., Horvath, J., *Explosive Spalling of Concrete Under Fire Conditions*, in *Proceedings of the International workshop "Fire Design of Concrete Structures - From Materials Modelling to Structural Performance"*. 2007: Coimbra. p. 161-176.

27. Lim, L., Lamont, S., Lane, B., Yin, R., Heise, A., *A New Risk-Based Approach to Predict Spalling of Ordinary Strength Concrete Walls Subjected to Fire*, in *Proceedings of the International workshop "Fire Design of Concrete Structures - From Materials Modelling to Structural Performance*. 2007: Coimbra. p. 379-392.

28. Kodur, V.K.R., *Strategies for improving the performance of high-strength concrete columns under fire hazard.* Structural Control and Health Monitoring, 2008: p. 921-938.

29. Jansson, R., *Liquid/Steam Pressure Measurement Inside Concrete Exposed to Fire*, in *Proceedings of the fourth international workshop Structures in Fire*. 2006: Aveiro. p. 747-756.

30. Jansson, R., Boström, L., *The influence of pressure in the pore system on fire spalling of concrete*, in *Proceedings of the fifth international workshop Structures in Fire*. 2008: Singapore. p. 418-429.

31. Sertmehmetoglu, Y., *On a mechanism of spalling of concrete under fire conditions, Ph.D Thesis, King's College, London, 1977*.

32. Georgali, B., Tsakiridis, P. E. , *Microstructure of Fire-Damaged Concrete, A Case Study.* Cement and Concrete Composites, 2005. **27**(2): p. 255-259.

33. Mostafaei, H., Sultan, M.A., Bénichou, N., *Performance of Structural Systems in Fire*, in *Proceedings of the International Conference Applications of Structural Fire Engineering*. 2009: Prague. p. 604-609.

34. Anderberg, Y., Bernander, K., *Biblioteksbranden I Linköping den 21 september 1996: studium av orsaken till tidigt ras*, Fire Safety Design AB (FSD): Lund.

35. ISO 834., *Essais de Résistance au Feu*: Organisation Internationale de Normalisation. Norme Internationale. Genève, 1975.

36. International Workshop Fire Design of Concrete Structures - from Materials Modelling to Structural, P., *Fib Workshop Proceedings of the International Workshop*. 2008, Coimbra: Universidade de Coimbra. XVI, 597 p.-XVI, 597 p.

37. Franssen, J.-M., *SAFIR a thermal/structural program modeling structures under fire*, in *NASCC Proceedings*. 2003: Baltimore, MD. p. Session D5 Pag.1-22.

38. *Vulcan Solutions Limted, http://www.vulcan-solutions.com/software.html, accessed in 2009/06/25*.

39. Iding, R., Bresler, B. & Nizamuddin, Z, *FIRES-RCII, a computer program for the fire response of structures - Reinforced concrete frames.*: Report UCB FRG 77-8, Univ. of California, Berkeley, 1977.

40. Hibbet Karlsson SorensonInc., *ABAQUS v6.4 & v6.5 Manuals*: ABAQUS Manual Set, 2003-2005.

41. *TNO DIANA, http://www.tnodiana.com/, accessed in 2009/06/25.*

42. *ANSYS, http://www.ansys.com/products/default.asp, accessed in 2009/06/25.*

43. Izzuddin, B.A., *Nonlinear dynamic analysis of framed structures*: PhD thesis, Imperial College, London. 1991

44. Wang, Y.C., *Steel and Composite Structures - Behaviour and Design for Fire Safety*. 2002, London: Spon Press.

45. European committee for standardisation, *Actions on Structures: General rules: - Actions on structures exposed to fire, EN 1991-1-2, Eurocode 1, Part 1-2*: Brussels, 2002.

46. Gonçalves, T.F.D., *Resitência ao Fogo de Estruturas de Betão: Comportamento Global de Estruturas em Situação de Incêndio* Tese de Mestrado em Engenharia Civil, Instituto Superior Técnico, Universidade Técnica de Lisboa, Lisboa, 2008.

47. Bailey C.G., B.I.W., Plank R.J., *Analyses of the Effects of Cooling and Fire Spread on Steel-framed Buildings* Fire Safety Journal, 1996. **26**(4): p. 273-293.

48. Rein, G., Zhang, X., Williams, P., Heise, A., Jowsey, A., Lane, B., Torero, J.L., *Multi-Story Fire Analysis for High-Rise Buildings*, in *11th Interflam*. 2007: London. p. 605-616.

49. Gillie, M., Röben, C., Irvine, A., Kirkpatrick, S. , *The Effects of Non-Uniform Fires on Structural Behaviour*, in *Proceedings of the fifth International workshop Structures in Fire*. 2008: Singapore. p. 771-777.

50. Franssen, J.-M., Pintea, D., Dotreppe, J-C., *Numerical Evaluation of the Effect of Localised Fires on Composite Steel Concrete Buildings*, in *Proceedings of the fourth International workshop Structures in Fire*. 2006: Aveiro. p. 885-896.

51. Taillefer, N., Muller, A., Fromy, P., Demouge, F., *Case Study: Concrete Beam Submitted to Natural Fire*, in *Proceedings of the International workshop "Fire Design of Concrete Structures - From Materials Modelling to Structural Performance"*. 2007: Coimbra. p. 583-593.

52. Anderberg, Y., *The impact of various material models on structural fire behaviour prediction*, in *Proceedings of the fifth international workshop Structures in Fire*. 2008: Singapore. p. 253-265.

53. Thelanderson, S., *Mechanical Behaviour of Heated Concrete Under Torsional Loading at Transient High Temperature Conditions*, Bulletin No. 46, Lund Institute of Technology: Sweden, 1974.

54. Anderberg, Y., Thelanderson, S. , *Stress and Deformation Characteristics of Concrete at High Temperatures: Experimental Investigation and Material Behaviour Model*, Bulletin 54, Lund Institute of Technology: Sweden, 1976.

55. Schneider, U., *Loss of strength due to kinetic reactions of normal concretes up to 1000ºC*: Ph.D. thesis, Technical University, 1973, Braunschweig, Germany.

56. Khoury, G.A., *Transient Thermal Creep of Nuclear Reactor Pressure Vessel Type Concretes*: Ph.D. Thesis, at Civil Engineering Department, Imperial College of Science and Technology, University of London, London, 1983.

57. Khoury, G.A., Sullivan, P. J. E., Grainger, B. N., *Strain of Concrete During First Heating to 600ºC under Load.* Magazine of Concrete Research, 1985. **37**(133): p. 195-215.

58. Khoury, G.A., *Strain of concrete during two thermal cycles. Part 1: strain over two cycles, during first heating and at subsequent constant temperature.* Magazine of Concrete Research, 2006. **58**(6): p. 367-385.

59. Law, A., Gillie, M., *Load Induced Thermal Strain: Implications for Structural Behaviour*, in *Proceedings of the fifth International workshop Structures in Fire*. 2008: Singapore. p. 488-496.

60. Khoury, G.A., *Strain of heated concrete during two thermal cycles: Part 2: strain during first cooling and subsequent thermal cycle.* Magazine of Concrete Research, 2006. **58**(6): p. 387-400.

61. Khoury, G.A., *Strain of heated concrete during two thermal cycles. Part 3: isolation of strain components and strain model development.* Magazine of Concrete Research, 2006. **58**(7): p. 421-435.

62. Franssen, J.-M., *"Plastic Analysis of Concrete Structures Subjected to Fire", Fire Design Of Concrete Structures: What now? What next? "*. 2004: fib Task Group 4.3, Politecnico di Milano, Dipartimento di Ingegneria Structurale, December 2-4, Milano, Italy, pp.133-146.

.

63. law, A., Gillie, M., Pankaj, P., *Incorporation of load induced thermal strain in finite element models*, in *Proceedings of the International Conference Applications of Structural Fire Engineering*. 2009: Prague. p. 592-597.

64. Gillie, M.U.A.e.R., M., *Bending and Membrane Action in Concrete Slabs.* Fire and Materials, 2004. **28**: p. 139-157.

65. Schneider, U., Schneider, M., Franssen, J-M., *Consideration of Nonlinear Creep Strain of Siliceous Concrete on Calculation of Mechanical Strain Under Transient Temperatures as a Function of Load History*, in *Proceedings of the fifth International workshop Structures in Fire*. 2008: Singapore. p. 463-476.

66. Schneider, U., Schneider, M., Franssen, J-M., *Numerical Evaluation of Load Induced Thermal Strain in Restraint Structures, Calculation of a Tunnel Cross Section Subjected to Fire* in

Proceedings of the International Conference Applications of Structural Fire Engineering. 2009: Prague. p. 289-294.

67. Sadaoui, A. and A. Khennane, *Effect of transient creep on the behaviour of reinforced concrete columns in fire.* Engineering Structures, 2009. **In Press, Corrected Proof**.

68. Dwaikat, M., B., Kodur, V. K. R., *Effect of fire scenario, restraint conditions, and spalling on the behaviour of RC beams*, in *Proceeding of the fifth International workshop Structures in Fire*. 2008: Singapore. p. 369-379.

69. European committee for standardisation, *Design of composite steel and concrete structures: General rules: - Structural Fire Design, EN 1994-1-2, Eurocode 4, Part 1-2*: Brussels, 2005.

70. Klingsch, E., Frangi, A., Fontana, M., *Experimental analysis of concrete strength at high temperatures and after cooling*, in *Proceedings of the International Conference Applications of Structural Fire Engineering*. 2009: Prague. p. 216-221.

71. Youssef, M.A. and M. Moftah, *General stress-strain relationship for concrete at elevated temperatures.* Engineering Structures, 2007. **29**(10): p. 2618-2634.

72. Luccioni, B.M., M.I. Figueroa, and R.F. Danesi, *Thermo-mechanic model for concrete exposed to elevated temperatures.* Engineering Structures, 2003. **25**(6): p. 729-742.

73. Anderberg, Y., *Mechanical properties of reinforcing steel at elevated temperatures*: Tekniska Meddelanden Nr. 36, Halmstad Järnverk AB, Lund, 1978.

74. Cooke, G.M.E., *An introduction to the mechanical properties of structural steel at elevated temperatures.* Fire Safety Journal, 1988. **13**(1): p. 45-54.

75. Kirby, B.R., Preston, R. R., *High temperature properties of hot-rolled structural steels for use in fire design studies.* Fire Safety Journal, 1988. **13**(1): p. 27-37.

76. Gillie, M., *The Behaviour of Steel-Framed Composite Structures in Fire Conditions*: Ph.D. Thesis, The University of Edinburgh, Edinburgh, 2002.

77. Anderberg, Y., *Behaviour of steel at high temperatures*: RILEM 44-PHT, February 1983.

78. Anderberg, Y., *Predicted Fire Behaviour of Steels and Concrete Structures*: Division of Building Fire Safety Design and Technology, Lund Institute of Technology, Lund 1982.

79. European committee for standardisation, *Design of steel structures: General rules: - Structural Fire Design, EN 1993-1-2, Eurocode 3, Part 1-2*: Brussels, 2005.

80. Vila Real, P.M.M., *Incêndio em estruturas metálicas cálculo estrutural 0008*. 2003, Amadora: Edições Orion.

81. Gardner, L., *Stainless Steel Structures in Fire*, in *Proceedings of the fourth International workshop Structures in Fire*. 2006: Aveiro. p. 247-258.

82. Deeny, S., Stratford, T., Dhakal, R., Moss, P., Buchanan, A., *Spalling of concrete, implications for structural performance in fire*, in *Proceedings of the International Conference Applications of Structural Fire Engineering*. 2009: Prague. p. 202-207.

83. Huang, Z., Burgess, I. W., Plank, R. J., *Effects of Spalling on the behaviour of reinforced concrete structures in fire*, in *Proceedings of the International workshop "Fire Design of Concrete Structures - From Materials Modelling to Structural Performance"* 2007: Coimbra. p. 199-210.

84. Huang, Z., Burgess, I. W., Plank, R. J., *A Non-Linear Beam-Column Element for 3 D Modelling of General Cross-Sections in Fire*: Research Report, DCSE/03/F/1, Department of Civil & Structural Engineering, The University of Sheffield, 2003

85. Franssen, J.-M., Hanus, F., Dotreppe, J-C., *Numerical Evaluation of the Fire Behaviour of a Concrete Tunnel Integrating the Effects of Spalling*, in *Proceedings of the International workshop "Fire Design of Concrete Structures - From Materials Modelling to Structural Performance"*. 2007: Coimbra. p. 359-367.

86. Davie, C.T., Zhang, H., Pearce, C.J., Bicanic, N., *Computational Modelling of Concrete Exposed to Fire: The Effects of Coupled Hygro-Thermal-Mechanical Behaviour on the Development of Spalling in Concrete Structures* in *Proceedings of the fifth International workshop Structures in Fire*. 2008: Singapore. p. 357-368.

87. Gawin, D., F. Pesavento, and B.A. Schrefler, *Modelling of hygro-thermal behaviour of concrete at high temperature with thermo-chemical and mechanical material degradation.* Computer Methods in Applied Mechanics and Engineering, 2003. **192**(13-14): p. 1731-1771.

88. Khoury, G.A., Majorana, C. E., *Polypropylene Fibres and Explosive Spalling*, in *Proceedings of the International workshop "Fire Design of Concrete Structures - From Materials Modelling to Structural Performance"* 2007: Coimbra. p. 211-224.

89. Khoury, G.A., *NewCon project.* Concrete Engineering International, Tunnels and Tunnelling, Spring 2006. **10**(1): p. 6-11.

90. Majorana, C.E., Salomoni, V. A., Khoury, G. A., *Micro-Structural Modelling of Concrete Under Fire Conditions*, in *Proceedings of the International workshop "Fire Design of Concrete Structures - From Materials Modelling to Structural Performance"*. 2007: Coimbra. p. 81-94.

91. Iwankiw, N., *Segmentation of Analysis/Design Levels for Structural Fire Engineering*, in *Proceedings of the fourth International workshop Structures in Fire*. 2006: Aveiro. p. 933-1003.

92. Riva, P., *Structural behaviour of continuous beams and frames*, in *fib bulletin 46: Fire design of concrete structures - structural behaviour and assessment*. 2008.

93. Venanzi, I., Breccoloti, M, *Analytical Safety Assessment of R.C. Frames Exposed to Fire*, in *Proceedings of the International workshop "Fire Design of Concrete Structures - From Materials Modelling to Structural Performance"*. 2007: Coimbra. p. 289-298.

94. Huang, Z., Burgess, I. W., Plank, R. J., *Behaviour of Reinforced Concrete Structures in Fire*, in *Proceedings of the fourth International workshop Structures in Fire*. 2006: Aveiro. p. 561-572.

95. Moss, P.J., et al., *The fire behaviour of multi-bay, two-way reinforced concrete slabs.* Engineering Structures, 2008. **30**(12): p. 3566-3573.

96. Franssen, J.-M., Kodur, V. K. R., Mason, J., *Elements of theory for SAFIR 2002 A Computer Program for Analysis of Structures Submitted to Fire*: University of Liege, 2002.

97. Lopes, N.F.F.B., *Behaviour of stainless steel structures in case of fire*: Ph.D. thesis, University of Aveiro, Aveiro, 2009.

98. *SAFIR ,http://www.argenco.ulg.ac.be/logiciels/SAFIR/what.html, assessed in 2009/04/20*.

99. European committee for standardisation, *Design of concrete structures: General Rules and Rules for Buildings, EN 1992-1-1, Eurocode 2, Part 1-1*: Brussels, 2004.

100. Flint, G., Usmani, A., Lamont, S., Lane, B., Torero, J., *Fire Induced Collapse of Tall Buildings*, in *Proceedings of the fourth International workshop Structures in Fire*. 2006: Aveiro. p. 415-426.

101. Lamont, S., Lane, B., Flint, G., Usmani, A., *Behaviour of Structures in Fire and Real Design - A Case Study* Journal of Fire Protection Engineering, 2006. **16**: p. 5-35.

102. Faria, R., Vila Pouca, N., *Esforço Transverso. Torção. Punçoamento.*: Faculdade de Engenharia da Universidade do Porto, Porto, Março 1997.

103. Nilson, A.H. and D. Darwin, *Design of Concrete Structures with contributions by David Darwin 0008*. 1997, New York [etc]: McGraw-Hill Companies.

104. Jiménez Montoya, P., Á. García Meseguer, and F. Morán Cabré, *Hormigón Armado ajustada al código modelo y al Eurocódigo 0008*. 2000, Barcelona: Editorial Gustavo Gili.

105. Msaad, Y., Chefdebien, A., *Temperature and Shear Capacity Calculation for Prestressed Hollow Core Slabs Under Fire Conditions*, in *Proceedings of the International workshop "Fire Design of Concrete Structures - From Materials Modelling to Structural Performance"*. 2007: Coimbra. p. 351-357.

Appendix A

This appendix contains the exact transcription of Section B2 and Section B3 of Informative Annex B the EN 1992 1-2 [1]. Section B2 describes the Zone Method and Section B3 identifies the procedure to quantify second order effects.

B.2 Zone method

(1) The method of subdividing the cross-section into several zones is described below. This method, although more laborious, provides a more accurate method than the 500°C isotherm method especially for columns. The method is applicable to the standard temperature-time curve only.

(2) The cross-section is divided into a number ($n \geq 3$) of parallel zones of equal thickness (rectangular elements) where the mean temperature and the corresponding mean compressive strength $f_{cd}(\theta)$ and modulus of elasticity (if applicable) of each zone is assessed.

(3) The fire damaged cross-section is represented by a reduced cross-section ignoring a damaged zone of thickness a_z at the fire exposed sides, see Figure B.3. Reference is made to an equivalent wall (see Figure B.3 (a) and (d)). The point M is an arbitrary point on the centre-line of the equivalent wall used to determine the reduced compressive strength for the whole of the reduced cross section. When two opposite sides are exposed to fire the width is assumed to be $2w$ (see Figure B.3 (a)). For a rectangular cross-section exposed to fire on one face only, the width is assumed to be w (see Figure B.3 (c)). This is represented by a wall with a width

equal to $2w$ (see Figure B.3 (d)). The flange of Figure B.3 (f) is related to the equivalent wall in Figure B.3 (d), and the web to the equivalent wall in Figure B.3 (a).

(4) For the bottom and ends of rectangular members exposed to fire, where the width is less than the height, the value of a_z is assumed to be the same as the calculated values for the sides, Figure B.3 (b), (e), (f).

The reduction of the cross-section is based on a damaged zone of thickness a_z at the fire exposed surfaces which is calculated as follows:

(5) The damaged zone, a_z, is estimated as follows for an equivalent wall exposed on both sides:

a) The half thickness of the wall is divided into n parallel zones of equal thickness, where n ≥ 3 (see Figure B.4),

b) The temperature is calculated for the middle of each zone.

c) The corresponding reduction factor for compressive strength, $k_c(\theta)$ is determined (see Figure B.5).

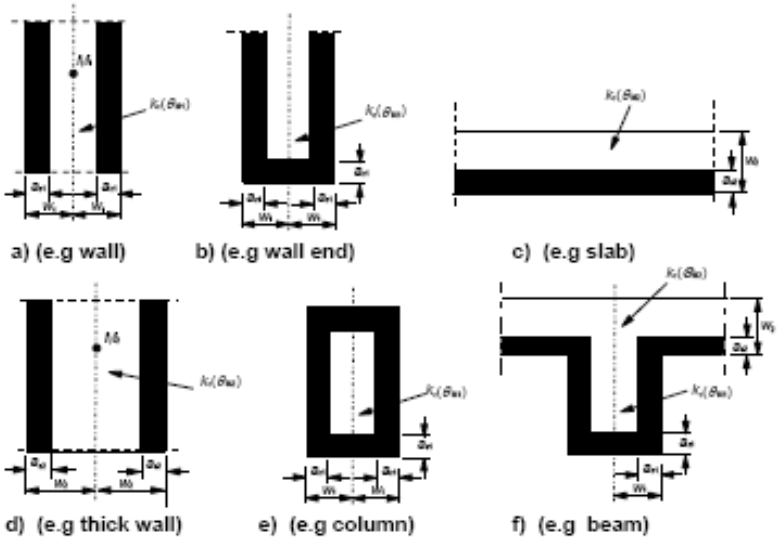

Figure B.3. Reduction of strength and cross-section for sections exposed to fire

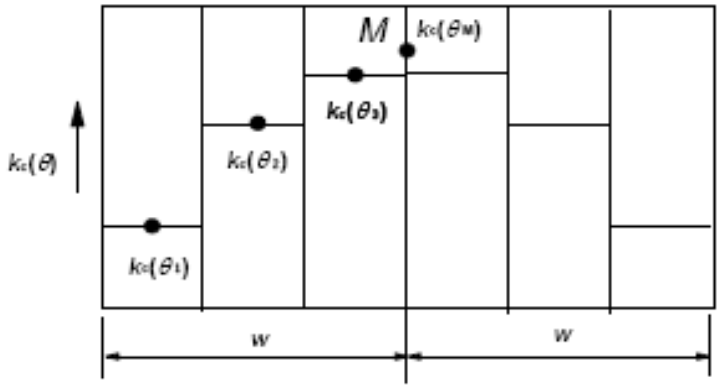

Figure B.4. Division of a wall, with both sides exposed to fire, into zones for use in calculation of strength reduction and a_z values

(6) The mean reduction coefficient for a particular section, incorporating a factor (1- 0,2/*n*) which allows for the variation in temperature within each zone, may be calculated by Expression (B.11)

$$k_{c,m} = \frac{(1-0,2/n)}{n} \sum_{i=1}^{n} k_c(\theta_i) \qquad \text{(B.11)}$$

where

n is the number of parallel zones in width *w*
w is half the total width
m is the zone number

(7) The width of the damaged zone for beams, slabs or members in plane shear may be calculated using Expression

$$a_z = w\left[1-\frac{k_{c,m}}{k_c(\theta_M)}\right] \qquad \text{(B.12)}$$

Where $k_c(\theta_M)$ denotes the reduction coefficient for concrete at point *M*.

(8) For columns, walls and other constructions where second order effects may be calculated using Expression (B.13).

$$a_z = w\left[1-\left(\frac{k_{c,m}}{k_c(\theta_M)}\right)^{1,3}\right] \qquad \text{(B.13)}$$

(9) When the reduced cross-section is found and the strength and modulus of elasticity are determined for the fire situation, the fire design follows the normal temperature design procedure similar to that shown in Figure B.2 by using $\gamma_{M,fi}$ values.

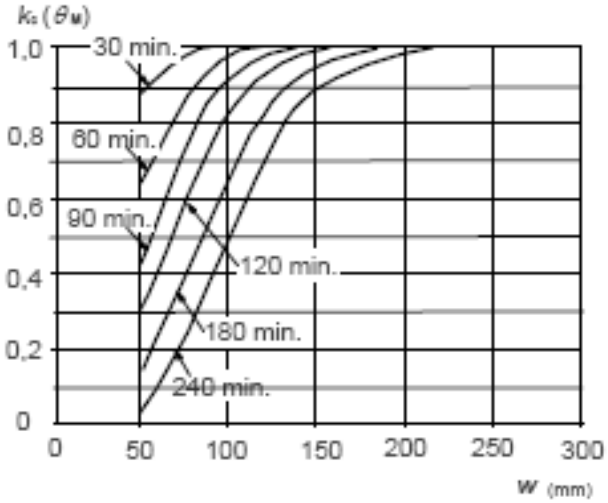

w is assessed as:
- The thickness of a slab,
- The thickness of a one sided exposed wall or column,
- Half the thickness of the web of a beam,
- Half the thickness of a two sided exposed wall or column or
- Half the smallest dimension of a four sided exposed column.

a) Reduction of compression strength for a reduced cross-section using siliceous aggregate concrete.

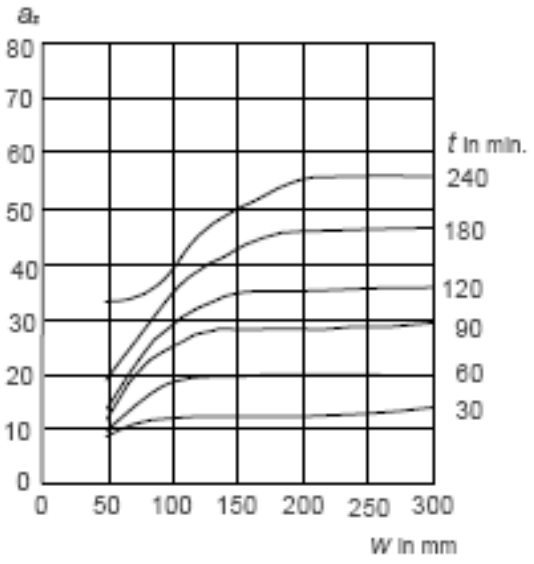

b) Reduction in cross-section a_z, of a beam or slab using siliceous aggregate concrete.

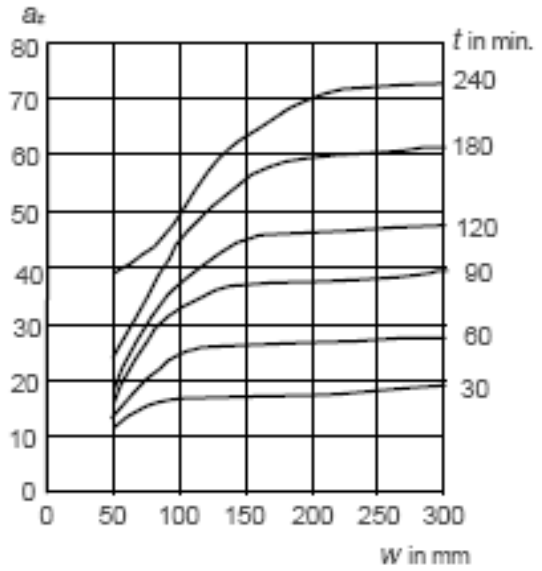

c) Reduction in cross section a_z, of a column or wall using siliceous aggregate concrete.

Note: The value for siliceous aggregate concrete are conservative for most other aggregates

Figure B.5: Reduction in cross section and concrete strength assuming standard temperature-time curve

B.3 Assessment of a reinforced concrete cross-section exposed to bending moment and axial load by the method based on estimation of curvature.

B.3.1 Buckling of columns under fire conditions

(1) This clause deals with columns in which the structural behaviour is significantly influenced by *second order effects* under fire conditions.

(2) Under fire conditions, the damage of the outer layers of the member due to high temperatures, combined with the drop of the elasticity modulus at the inner layers, results in a decrease of the stiffness of structural members under fire conditions. Because of this, second order effects can be significant for columns in the fire situation although at ambient temperature conditions their effect is negligible.

(3) The assessment of a column under fire conditions as an isolated member may be made by using a method based on the estimation of curvature (see Section 5 of EN 1992-1) if the following rules are applied.

(4) For braced building structures, indirect fire actions need not be considered if the decrease of the first order moments due to the decrease of stiffness of the column is not taken into account.

(5) The effective length under fire conditions, $l_{0,fi}$, may be taken as equal to l_0 at normal temperature as a safe simplification. For a more accurate estimation the increase of the relative reaction at the ends of the column, due to the decrease of its stiffness can be taken into account. For this purpose a reduced cross-section of the column given by B.2 may be used. It should be noted that the equivalent stiffness of the reduced concrete section in this case should be:

$$(EI)_z = [k_c(\theta_M)]^2 \cdot E_c \cdot I_z$$

where

$k_c(\theta_M)$ is a reduction coefficient for concrete at point M (see B.2)
E_c is the elastic modulus of the concrete at normal temperature
I_z is the 2nd moment of area of the reduced section

The elastic modulus of the reinforcement is $E_{s,\theta}$ (see Table 3.2)

B.3.2 Procedure for assessing fire resistance of column sections

(1) This method is valid only for the assessment of columns in braced structures.

(2) Determine the isotherm curves for the specified fire exposure, standard fire or parametric fire.

(3) Divide the cross section into zones with approximate mean temperature of 20ºC, 100ºC, 200ºC, 300ºC ... up to 1100ºC (See Figure B6).

(4) Determine the width w_i, area A_{ci} and co-ordinates x_i y_i of the centre of each zone.

(5) Determine the temperature of reinforcing bars. The temperature of the individual reinforcing bar can be evaluated from the temperature profiles in Annex A or handbooks and is taken as the temperature in the centre of the bar.

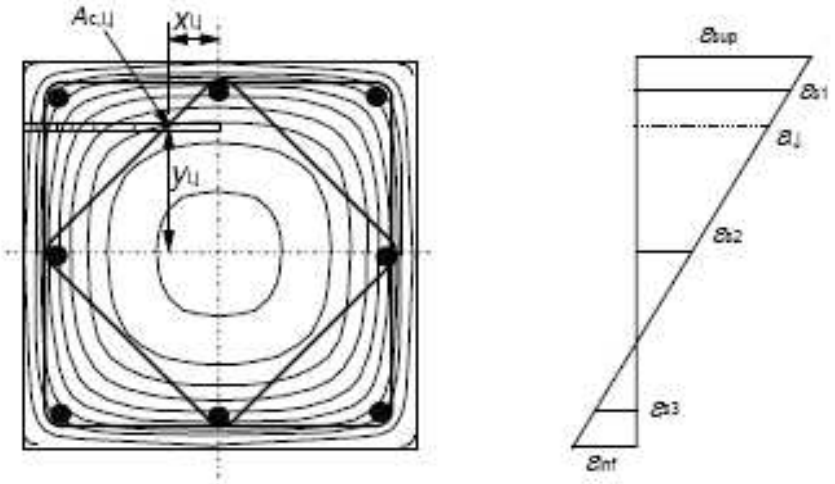

Figure B6: Dividing cross-section of column into zones with approximate uniform temperature

(6) Determine the moment-curvature diagram for $N_{Ed,fi}$ using, for each reinforcing bar and for each concrete zone, the relevant stress-strain diagram according to 3.2.2.1 (Figure 3.1 and Table 3.1), 3.2.3 (Figure 3.3 and Table 3.2) and where appropriate 3.2.4 (Table 3.3) and 3.2.2.2.

(7) Use conventional calculation methods to determine the ultimate moment capacity, $M_{Rd,fi}$ for $N_{Ed,fi}$ and the nominal second order moment, $M_{2,fi}$, for the corresponding curvature.

(8) Determine the remaining ultimate first order moment capacity, $M_{0Rd,fi}$, for the specified fire exposure and $N_{Ed,fi}$ as the difference between ultimate moment capacity, $M_{Rd,fi}$, and nominal second order moment, $M_{2,fi}$, so calculated. See Figure B7.

(9) Compare the ultimate first order moment capacity, $M_{0Rd,fi}$, with the design first order bending moment for fire conditions $M_{0Ed,fi}$.

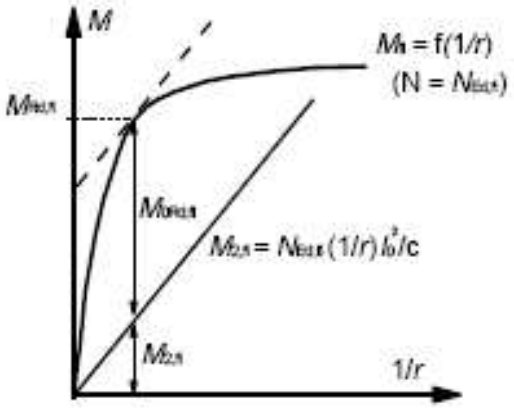

Where c is a factor(≈ 10) depending on the curvature distribution (see EN 1992-1-1, Cl 5.8).
$M_{0Rd,fi} \geq M_{0Ed,fi}$

Figure B7: Determination of ultimate moment capacity ($M_{Rd,fi}$), second order moment ($M_{2,fi}$) and ultimate first order moment capacity ($M_{0Rd,fi}$)

References

1. Europeancommitteeforstandardisation, *Design of concrete structures: General rules: - Structural Fire Design, EN 1992-1-2, Eurocode 2, Part 1-2*: Brussels, 2004.

Appendix B

This appendix contains the details of the frame considered in chapter 3 and 5 with comparison purposes regarding the main frame analysed in those chapters. Figure B1 presents the frame's geometric description. The dimensions are given in meters.

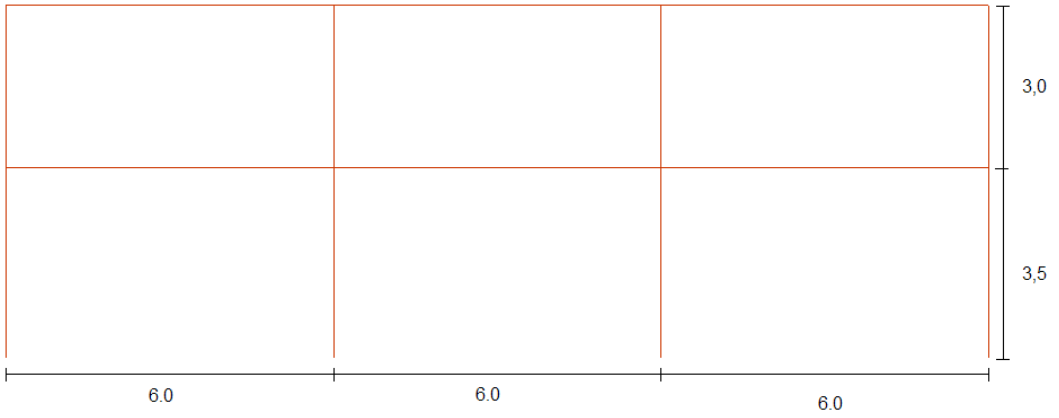

Fig.B1 – Frame's geometry model.

The cross-sections are illustrated in Figure B2. The reinforcement concrete cover is 5.0cm.

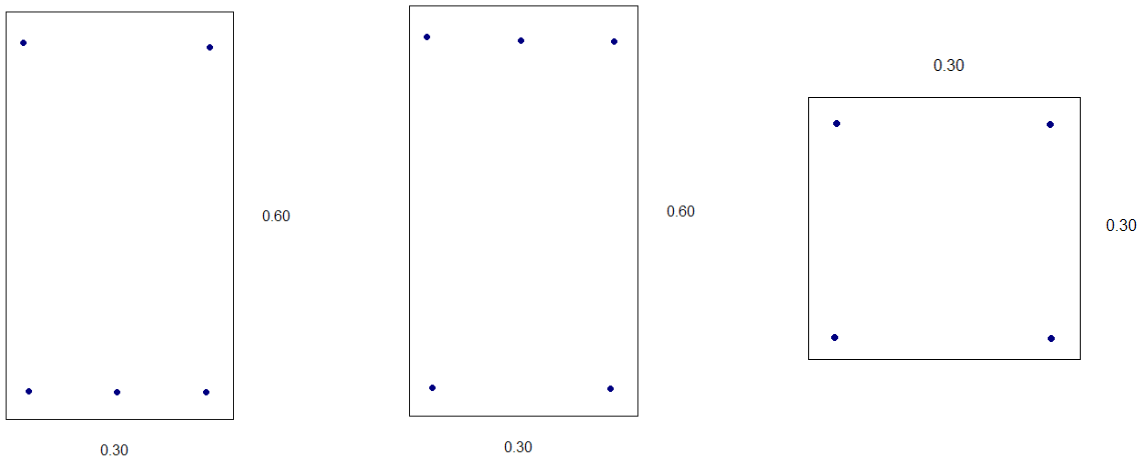

Fig.B2 – Cross-sections: a) beam at mid-span, b) beam at the end, c) column.

Each column is divided into 10 finite elements with constant cross-section, equal to the one shown in Figure B2*c*. The beams are also composed of 10 elements. The three elements at the ends are admitted with the cross-section presented in Figure B2*b* and the four elements in the span have a cross-section equal to the one presented in Figure B2*a*.
All bays in the frame are exposed to the ISO 834 standard fire curve simultaneously.
A schematic representation of the bending moment diagram at different time steps is presented in Figure B3. In the same manner, a schematic draft of shear force diagram is displayed in Figure B4. The deformed shape is sketched in Figure B5. The time to failure in this case is 151 minutes. From Figure B6 to B8 the same analyses are performed this time regarding the braced frame (75 minutes to failure).

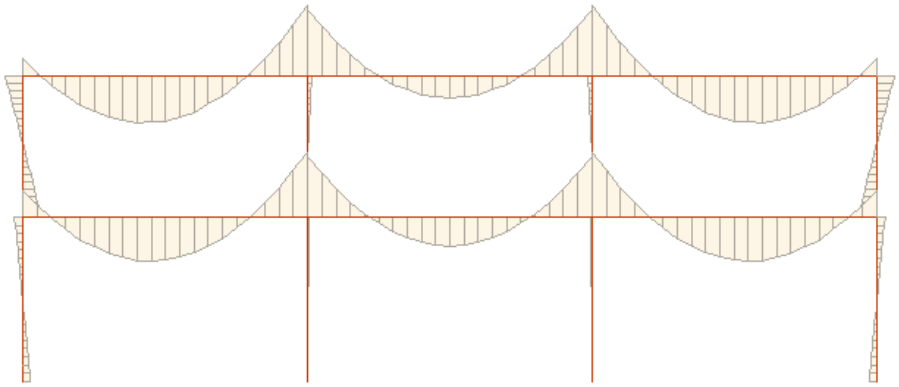

a)

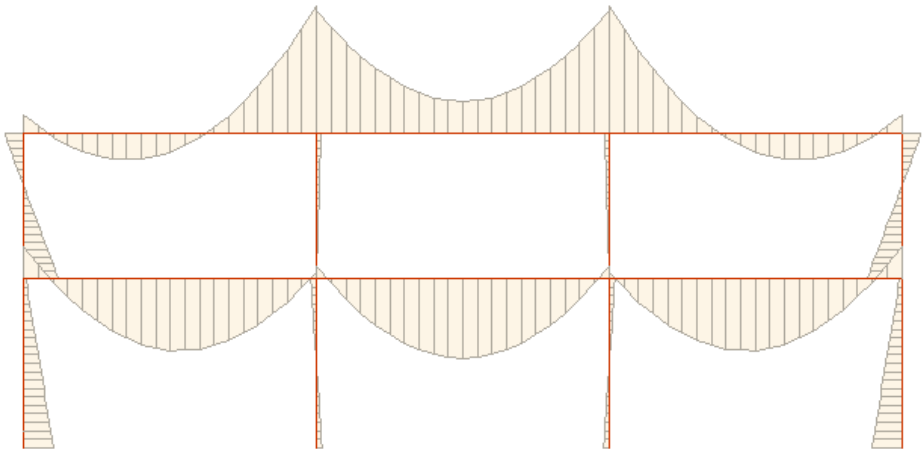

b)

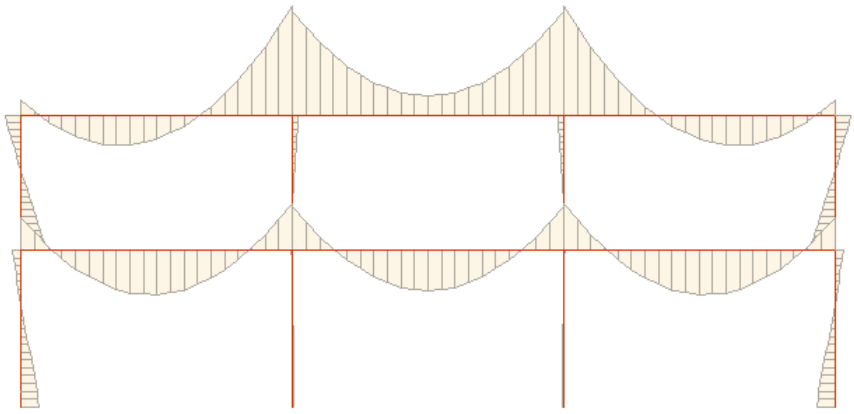

c)

Fig.B3 – Schematic bending moment diagram: a) 0 minutes, b) 80 minutes, c) 151 minutes.

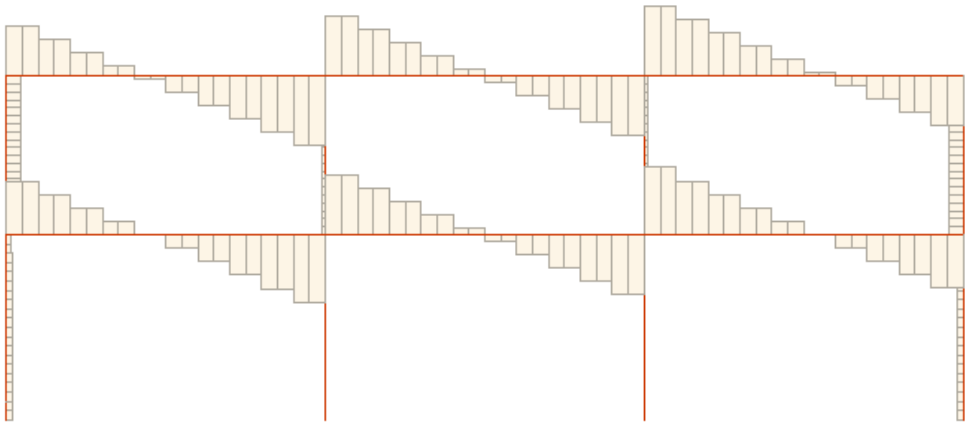

a)

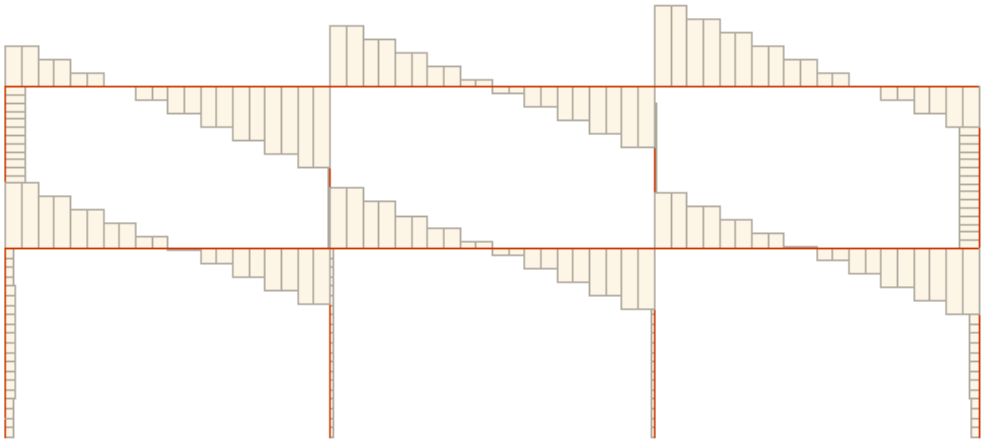

b)

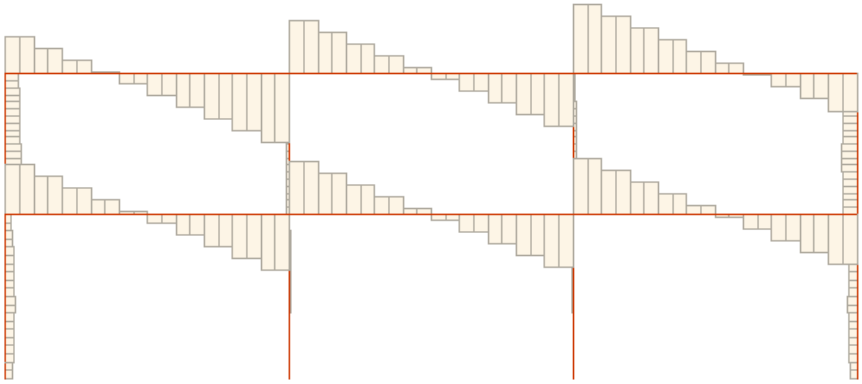

c)

Fig.B4 – Schematic shear force diagram: a) 0 minutes, b) 80 minutes, c) 151 minutes.

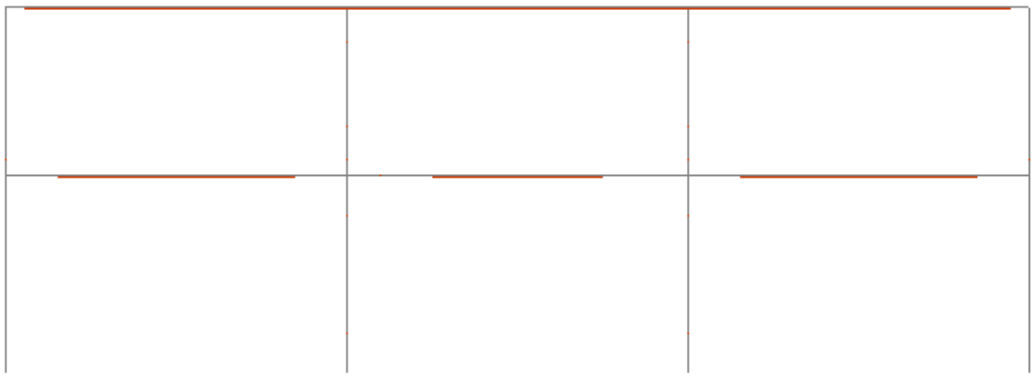

a)

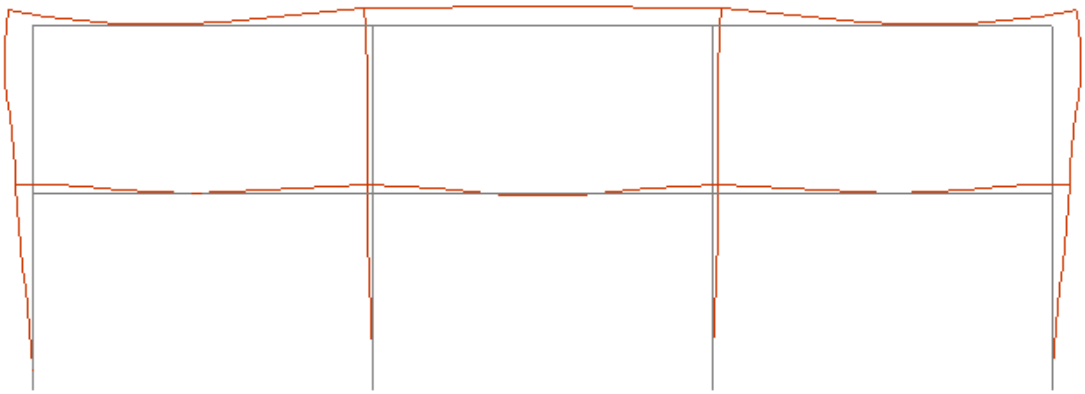

b)

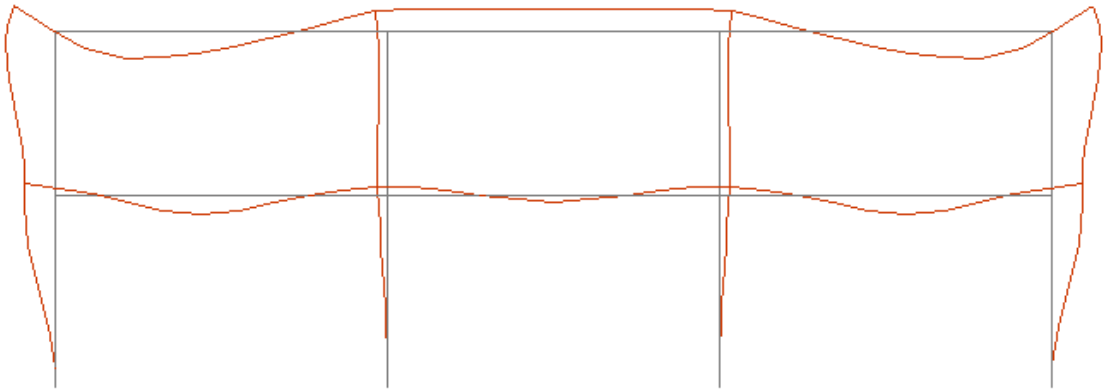

c)

Fig.B5 –Deformed shape (scaled 10 times): a) 0 minutes, b) 80 minutes, c) 151 minutes.

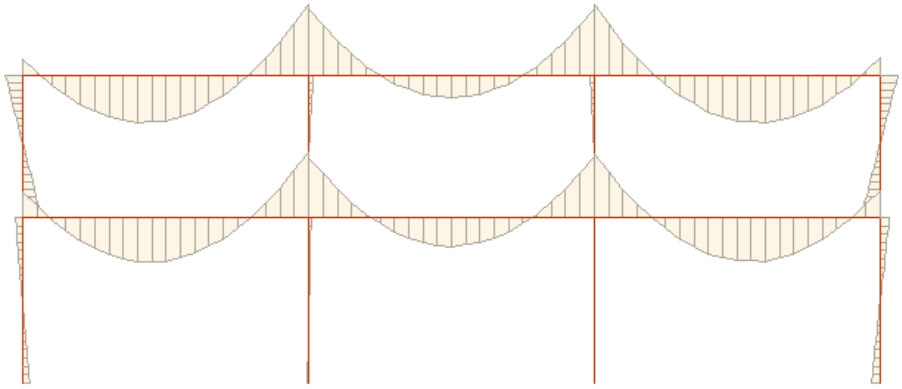

a)

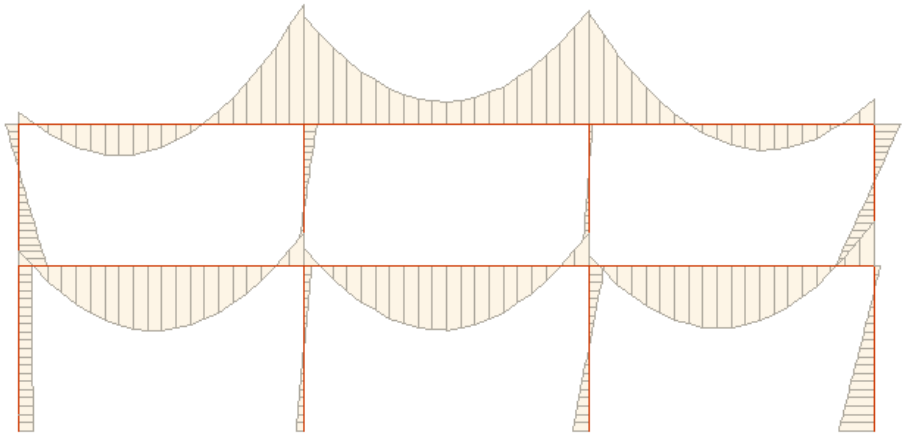

b)

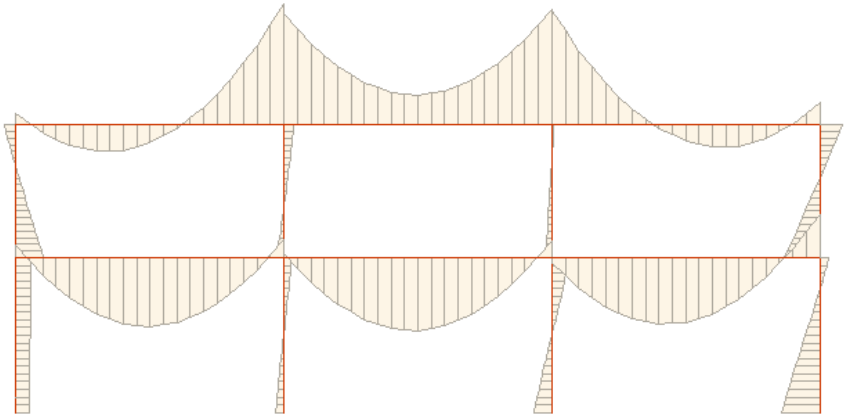

c)

Fig.B6 – Schematic bending moment diagram: a) 0 minutes, b) 40 minutes, c) 75 minutes.

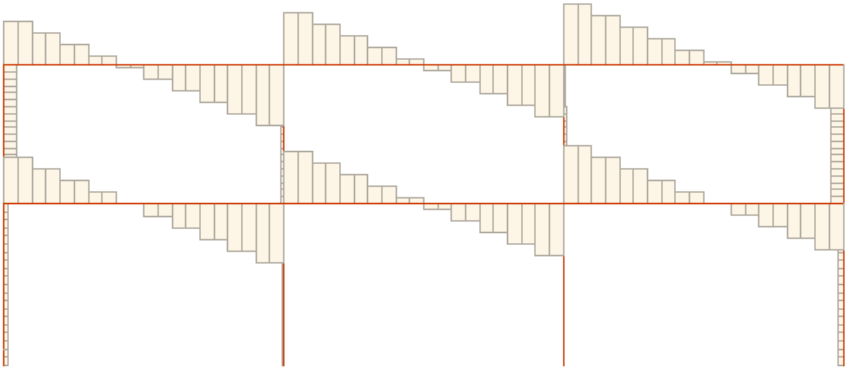

a)

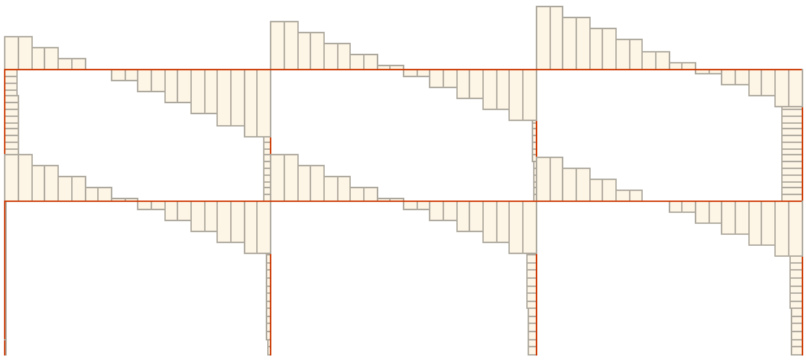

b)

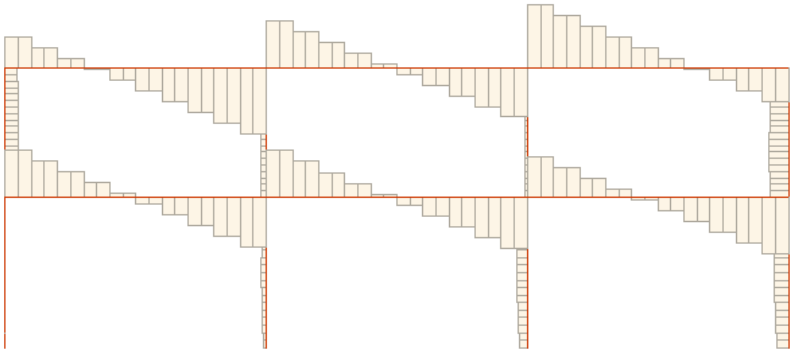

c)

Fig.B7 – Schematic shear force diagram: a) 0 minutes, b) 40 minutes, c) 75 minutes

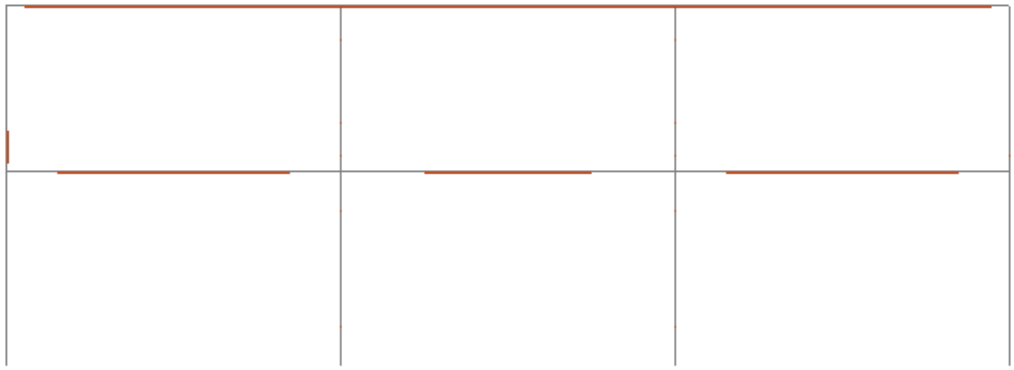

a)

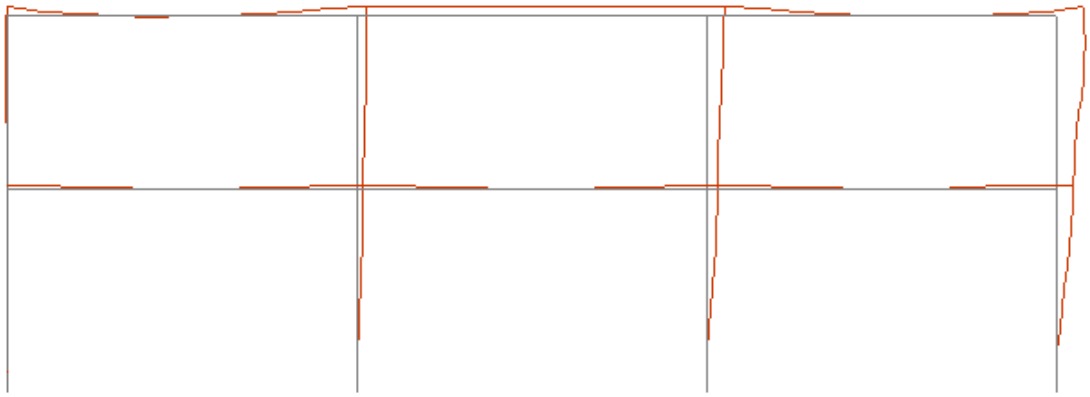

b)

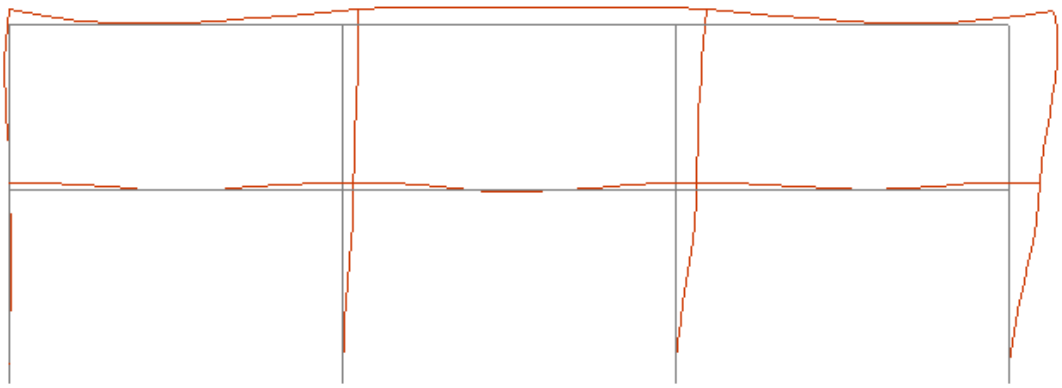

c)

Fig.B8 –Deformed shape (scaled 10 times): a) 0 minutes, b) 40 minutes, c) 75 minutes